STUDIES OF THE DIFFUSION CHARACTERISTICS AND MECHANICAL PROPERTIES OF NiGa

Thesis

Submitted for

The Degree of Doctor of Philosophy

by

Andrew T. Donaldson

MAY 1974

Department of Metallurgy

Imperial College of Science & Technology

University of London

CONTENTS

CHAPTER 1: Synopsis

1.1 Abstract

The constitutional defect structure in NiGa has been examined by X-ray and density techniques and has been found to vary continuously throughout the phase field of the compound. An empirical constitution defect model has been derived which shows no abrupt change in defect mechanism at the stoichiometric composition.

The tracer diffusion coefficients of nickel-63 and gallium-67 have been measured in alloys in the composition range 47·18 to 52·4 atomic % nickel over the temperature ranges 978°K to 1380°K and 1084°K to 1384°K respectively. The results for both species, have been interpreted in terms of linear Arrhenius dependences and the activation energies of diffusion (of both species) compared with diffusion data reported previously in similar compounds.

Compression creep experiments have been conducted in alloys in the composition range 48·96 to 52·27 atomic % nickel over two separate temperature ranges, namely 732° to 887°K and 953° to 1077°K. Stress exponents and creep activation energies have been evaluated, from variable stress tests and variable temperature tests respectively, in each temperature range.

The diffusion activation energies and the creep activation energies have been compared and discussed in the light of the proposed constitutional defect model.

CHAPTER 2: Introduction and Literature Survey

2.1 Intermetallic Compounds - a General Introduction

Engineering advances, in recent years, have resulted in an increasing demand for materials suitable for use under extreme service conditions, such as high stresses coupled with high temperatures. As a consequence increasing attention has been paid to intermetallic compounds. These are attractive for structural applications for three broad reasons.

(1) Their mechanical properties; a general characteristic of many intermetallics is a high intrinsic yield strength at high fractions of the melting point often coupled with a high strain hardening. Furthermore, many intermetallics have good deformability at low homologous temperatures, although this often cannot be easily realised because of their susceptibility to grain boundary embrittlement.

(2) Diffusion properties; diffusion rates in ordered materials tend to be lower than for disordered alloys of the same composition. This is important in high temperature applications because it contributes to microstructural stability with respect to both grain growth and to the dissolution and agglomeration of dispersed phases. It also helps with respect to oxidation and corrosion behaviour in the unprotected condition by slowing the kinetics of the process of attack, and in coated parts by slowing the degradation of the coating by interdiffusion with the substrate. Furthermore, low diffusion rates improve high temperature mechanical properties by retarding those atomistic deformation processes

which are diffusion controlled (e.g., dislocation climb).

(3) Intermetallic compounds generally show a high degree of compatability with the matrix in two-phase alloys. This is because most multi-phase alloys incorporating intermetallic compounds are equilibrium or quasi-equilibrium structures and therefore do not tend to degrade by interaction with the matrix. Thus alloys may be so designed that the composition of the matrix is either very similar or very different from that of the dispersed intermetallic with different attendant advantages in each case. Finally a large contribution to the strength of alloys for long time moderate temperature service, may be attained by dispersing ordered intermetallics with an optimised degree of coherency of the intermetallic with the matrix by control of both composition and heat treatment.

Intermetallic compounds have found applications is such diverse fields as gas turbines (superalloys which contain Ni_3Al), semiconductors (GaAs), superconductors (Nb_3 Sn) and supermagnets ($SmCo_5$). Other applications may arise from such phenomena as superelasticity (AuCd) and mechanical memory - the return to original shape, after deformation, by a low temperature phase transformation - as in NiTi.

Many of the unusual properties of intermetallic compounds arise from the fact that they exhibit an ordered crystal structure, which is often retained to very high hologous temperatures. Furthermore, although typified as compounds and assigned specific formulae (e.g., Ni_3Al, Fe_2Nb, GaAs) they can often exist at compositions other than the stoichiometric proportions defined by their respective formulae.

Non-stoichiometric compositions are achieved by the introduction of composition dependent (constitutional) defects. The compound AgMg, for example, at stoichiometry, has a structure which consists of two interpenetrating simple cubic lattices (called sub-lattices), one exclusively occupied silver atoms and the other by magnesium atoms. Silver rich alloys are achieved by the excess silver atoms replacing some magnesium atoms on the magnesium sublattice. In magnesium rich alloys the reverse substitution occurs. [61, 33]

The history of the development of alloys which contain or are based upon intermetallic compounds, together with a review of their physical properties, structural applications and future development potential has been compiled by Westbrook (1969) [154] .

2.2 The Phase Diagram of the Nickel-Gallium System

The phase diagram of the nickel-gallium system, shown in Fig. 2.1, is that due to Hansen (1958) [66] . The diagram was constructed largely from the data of Hellner & Laves (1947) [68] and Hellner (1950) [67] .

Several intermetallic compounds have been identified in the system. The compound centred about the equi-atomic composition and characterised by the formula NiGa has a CsCl (B2) structure. It is stable over a wide range of composition, on either side of stoichiometry, at high temperatures. The phase field extends from approximately 40 to 65 atomic % nickel at some 800°C. The phase range at room temperature is more restricted, extending from about 45 to 53 atomic % nickel.

The compound NiGa has a congruent melting point, near the nickel rich limit of its stability range, at ~ 64 atomic % nickel and a temperature of 1220°C. The melting temperature of the compound falls with decreasing nickel content. The solidus curve falls more rapidly than the liquidus so that alloys solidify over an increasing temperature

FIG 2.1. NICKEL - GALLIUM PHASE DIAGRAM

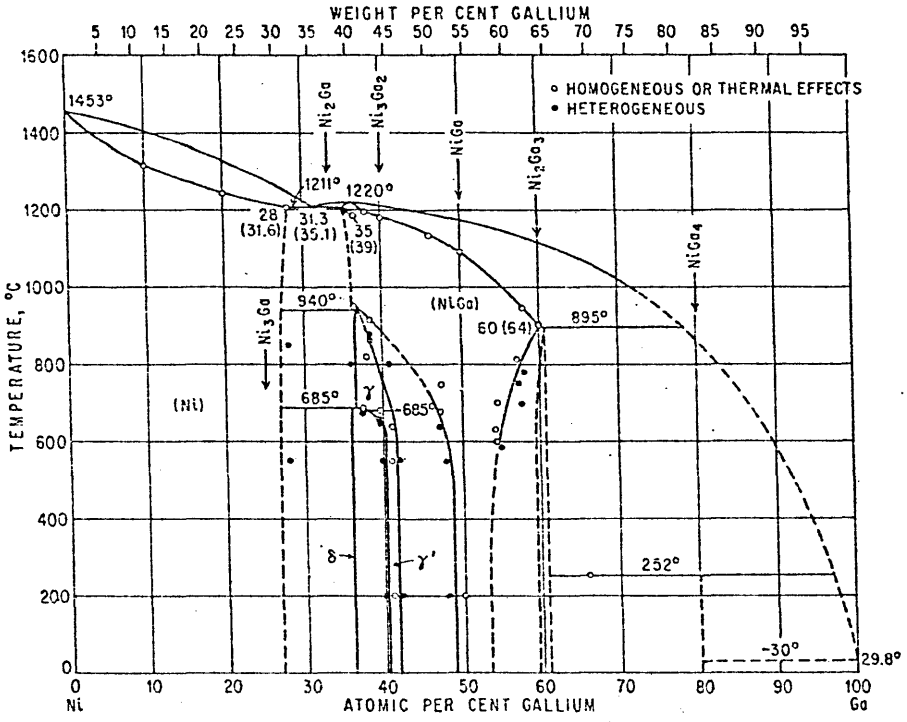

from ref. 66

interval as compositions move to lower nickel content. For example, the 55 atomic % nickel composition solidifies between ~ 1180° and 1160°C while an alloy containing 45% nickel solidifies over the interval ~ 1140 - 1050°C.

2.3 Intermetallic Compounds with the CsCl Structure

2.3.1 The CsCl Structure

The CsCl (B2) structure consists of two interpenetrating simple cubic lattices with the lattice points of one lattice lying at the cube centres of the second lattice. In intermetallic compounds of the type AB which exhibit the CsCl structure, at stoichiometry the A atoms exclusively occupy the lattice sites of one simple cubic lattice (henceforth the A-sublattice), while the B atoms occupy the lattice sites of the second simple cubic lattice (the B-sublattice). The resultant structure is ordered body centred cubic with one species (A atoms) occupying the cube corners and the other species (B atoms) occupying the cube centres [Fig. 2.2] .

2.3.2 Order-Disorder in Intermetallics with the CsCl Structure

The most widely used and powerful technique in elucidating the crystal structure of materials is that of X-ray diffraction. X-ray studies on the compound AgMg have shown that it has the CsCl structure at low temperatures and that this ordered structure is retained up to its melting point at about 820°C [155, 14] . Similar investigations on the compounds AuCd [148] and NiAl [13] have indicated that these too remain ordered (CsCl) up to their respective melting temperatures.

Diffusion studies on AgMg [61, 33] have shown no discontinuity in the Arrhenius curve for the activation energy of diffusion which

FIG.2.2.
THE CsCl STRUCTURE

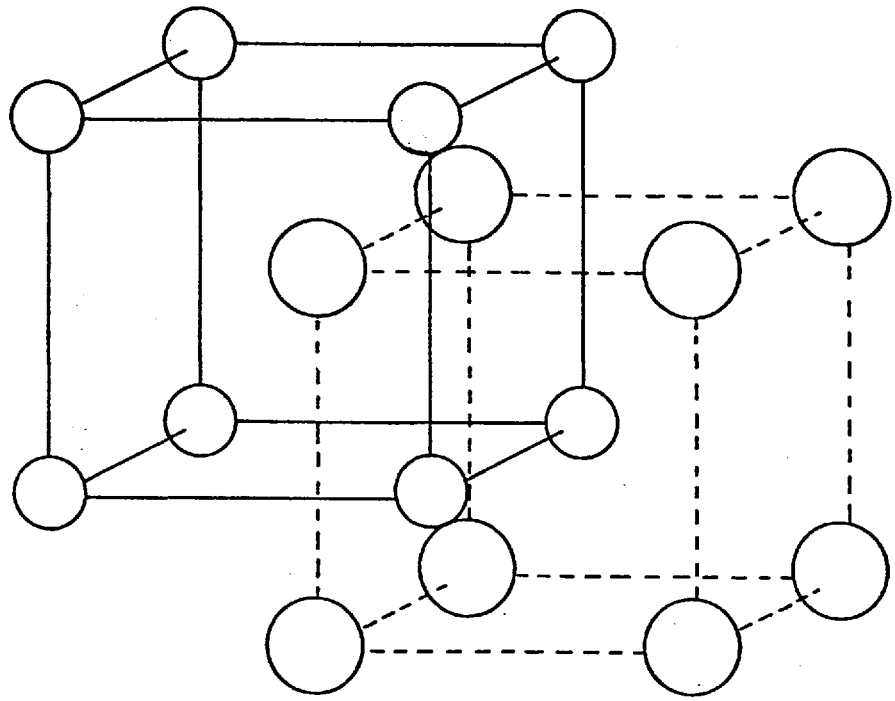

= A ATOMS (NICKEL)

= B ATOMS (GALLIUM)

could be attributable to an order-disorder transformation, thereby supporting the results of X-ray studies. Similar diffusion data in AuCd [57] also indicate that the compound remains ordered up to its melting temperature.

The compound FeCo is found to undergo an order-disorder transformation at about 730°C [111] while the compound CuZn becomes disordered above 470°C [5, 121] . Diffusion studies on the latter compound [95, 86] have shown that below the critical ordering temperature T_c, diffusivities were considerably lower than diffusion rates in the disordered structure. Furthermore the activation energy of diffusion was higher below T_c, in the ordered structure, than above T_c where the structure is disordered [37] .

Investigations into the effect of order on creep deformation rates in CuZn [16] have revealed a discontinuity in the temperature dependence of the strain rate near T_c. In the compound FeCo the ductility of the material is found to change rapidly with the degree of order, with material quenched from above T_c and hence retaining a disordered structure, showing a far greater ductility than material quenched from just below T_c which has an ordered structure [81] .

Studies on many intermetallics with the CsCl structure have shown that in general they remain ordered up to high homologous temperatures often close to the melting temperature. The order-disorder transformations observed in both CuZn and FeCo illustrate the considerable effect of order on material properties.

2.3.3 Order-Disorder in NiAl and NiGa

The compounds NiAl and NiGa may most usefully be compared for the purpose of assessing the likely ordering behaviour of the latter because both have the A element (nickel) in common while their B elements,

aluminium and gallium respectively are chemically very similar. X-ray diffraction studies on NiAl [13] and NiGa [145] have shown that both of these compounds exhibit the ordered CsCl (B2) structure at room temperature. Other work on density measurements and lattice parameters has indicated that the two compounds maintain their stability over their respective phase fields by similar constitutional defect mechanisms [see section on constitutional defects] .

More recent investigations into the temperature stability of the ordered structure of NiAl [75] have shown that long range order remains complete up to 1000°C ($\sim 0{\cdot}7\ T_M$) and is substantial right up to the melting temperature (T_M). Bradley (1951) [12] studied the ternary system Ni-Fe-Al metallographically and found two β-phases, one ordered (B2) and the other disordered (A2), were present in some ternary alloys. However the binary compound NiAl was found to be single phase and ordered (B2) for all temperatures investigated.

A number of physical properties of NiAl, which are affected by the degree of long range order, have been investigated as a function of temperature but no discontinuities attributable to an order-disorder transformation have been reported. The properties studied include elastic constants up to 800°C [142] , slip systems up to 800°C [3] , resistivity up to 1200°C [59] , diffusion coefficients up to 1350°C [8, 65] and elevated temperature deformation mechanisms (creep) up to 1475°C [140] . All these studies suggest that the compound NiAl remains ordered to very high temperatures close to its melting point.

Data on the degree of order in NiGa at high temperatures is less plentiful. However X-ray studies [145] on the intensity of the first superlattice line $\{100\}$ of the ordered CsCl (B2) structure in NiGa indicated that the relative intensity ratio of this first superlattice line to the first fundamental line $\{110\}$, [I_{100}/I_{110}] did not vary

appreciably between room temperature and the highest temperature studied, 860°C ($\sim 0.7\ T_M$). It was concluded that the degree of long range order in NiGa did not vary significantly between room temperature and 860°C and that the compound probably remained ordered to temperatures close to its melting point.

In conclusion, the close similarity of NiGa and NiAl together with the evidence that the latter compound remains ordered up to its melting temperature, support the view that NiGa too is ordered to temperatures close to its melting point.

2.4 Structure Defects in CsCl Intermetallic Compounds

2.4.1 Composition Dependent Defects

Many CsCl intermetallic compounds exist over a wide composition range, usually centred about the ideal (1:1) stoichiometric composition. Non-stoichiometric compositions are maintained by the introduction of composition dependent (constitutional) defects. Although the overall symmetry is retained and the crystal structure remains the same, the lattice perfection is strongly affected by the presence of defects.

The compound AgMg, for example, exists in silver rich compositions by the excess silver atoms substituting for magnesium atoms onto the Mg-sublattice, while in magnesium rich alloys excess magnesium substitutes for silver onto the Ag-sublattice [61, 33]. This type of defect structure is known as the substitution or anti-structure (order/disorder) defect mechanism.

Other B2 compounds maintain off-stoichiometric compositions by the introduction of vacancy defects. The compounds NiAl [13], NiGa [145] and AuCd [144] are all thought to contain constitutional vacancies on one side of the stoichiometric composition (in the compound

AB, vacancies occur in B-rich alloys), and substitutional (anti-structure) defects on the other side of stoichiometry (A-rich alloys).

In NiAl, the ideal structure is realised only at stoichiometry. The introduction of excess nickel, which has a smaller atomic size and greater atomic weight than aluminium, results in a contraction of the lattice parameter and a rise in the density of the compound [13].

The difference in the X-ray atomic scattering factor between nickel and aluminium allows the manner in which nickel replaces aluminium in nickel-rich alloys, to be determined quantitatively from diffraction line intensitites. It has been found that the Ni-sublattice is entirely filled by nickel atoms while the Al-sublattice is filled as far as possible by aluminium atoms and the remaining sites are occupied by the excess nickel atoms [13].

In aluminium rich alloys, direct substitution of nickel by the larger, lighter aluminium atoms should result in an increase in the lattice parameter and a fall in density. In fact the lattice parameter does increase and the density fall as expected up to a composition of $\sim$ 51 atomic % aluminium. Thereafter, with increasing excess of aluminium the lattice parameter falls while the density decreases more rapidly than before [13, 23].

The theoretical density, calculated from the lattice parameter, may be correlated with the observed density and the compositional dependence of the lattice parameter (in Al-rich alloys) may be explained if the unit cell is supposed to contain fewer than two atoms. Between stoichiometry and a composition containing about 51 atomic % aluminium the number of atoms per unit cell is very close to 2·00, indicating direct substitution of nickel by aluminium. In more aluminium rich compositions the number of atoms per cell falls continuously to a minimum of 1·84 near the phase boundary. This suggests that constitutional vacancies occur on the

Ni-sublattice in compositions containing more than 51 atomic % aluminium.

X-ray diffraction line intensities have confirmed the presence of nickel anti-structure atoms in nickel rich alloys and some limited substitution of nickel by aluminium between 50 and 51 atomic % aluminium followed by nickel vacancies in still more aluminium rich alloys [13].

Lattice parameter and density studies on NiGa [145,129] have been interpreted as indicating a NiAl type of defect structure. However, unlike NiAl, the calculated number of atoms per unit cell does not reach 2·00 at the stoichiometric composition nor at some gallium rich composition. In fact the average number of atoms per unit cell is only 1·98 in the 52·4 atomic % nickel alloy, and 1·89 in the 47·4 atomic % nickel composition [145]. At the stoichiometric composition the number of atoms per unit cell is about 1·96. These results suggest that the stoichiometric composition and even nickel-rich alloys may contain constitutional vacancies, as well as gallium-rich alloys.

The presence of consititional defects at the stoichiometric composition has been reported in Fe_2Nb where iron substitutional atoms have been identified (in the stoichiometric alloy) by Mössbauer techniques [132].

It would seem then that while constitutional vacancies and anti-structure atoms probably occur in NiGa [145] there is no clearly defined change, in the type of defect present, at the stoichiometric composition. Rather that nickel vacancies, present in gallium-rich alloys, decrease in number with increasing nickel content, and that in nickel-rich alloys, nickel anti-structure atoms begin to occur. Thus constitutional defect mixing may take place. Theoretical considerations [143] and experimental studies on AuCd [144] have already indicated that constitutional and thermal defects may interact to result in defect equilibria and mixed defect structures.

It has been found that two effects control the ordering and hence the likely constitutional defect structure in CsCl compounds, namely the atomic size factor and the electron to unit cell ratio [104]. In NiAl and NiGa, which are β-phases, the electron to atom ratio corresponding to Hume-Rothery's rule [77] is 1·5; the ratio for which the Fermi surface is first expected to touch the Brillouin zone is 1·48, but in practice it is found that β-phases are stable with respect to other structures for an electron to atom ratio up to 1·5 or even higher [122]. According to Hume-Rothery's rule for phases containing transition metal atoms (in this case Ni), the transition metal is assumed to make no electronic contribution and an electron to atom ratio of 1·5 is achieved at stoichiometry. This corresponds to 3·0 electrons per unit cell and consequently if this value is not to be exceeded in B-rich (aluminium in NiAl, gallium in NiGa) alloys it is necessary for nickel atoms to be replaced by vacant sites and not by B atoms.

In fact the limiting value of the electron to unit cell ratio has been found to be 3·00 for CoAl and 3·04 for NiAl, suggesting that only in the latter compound is there some limited substitution of the transition metal by aluminium [23]. No similar data is available for NiGa.

Studies of electric and magnetic properties in NiAl and CoAl have indicated that limited substitution of nickel by aluminium occurs [18], in accordance with earlier predictions based on lattice parameter measurements [13, 23].

2.4.2 Complex Constitutional Defects in NiAl

The compositional dependence of the defect structure in NiAl may be summarised as follows: nickel-rich compositions contain exclusively nickel anti-structure atom defects, the stoichiometric composition

contains no defects, aluminium-rich alloys contain a limited number of aluminium anti-structure atoms and nickel vacancies [13, 23].

It has been suggested that the constitutional nickel vacancies, in aluminium-rich alloys, may form clusters. Defects observed in aluminium rich NiAl with the electron microscope have been interpreted as platelets of aluminium atoms between layers of nickel vacancies. This aggregation of vacancies was thought to be preparatory to the formation of the compound δ- Ni_2Al_3 [2].

Evidence has been reported for the existence of an ordered defect structure, where nickel vacancies ($\square$) occur on a regular array, resulting in compounds such as $Ni_{48}\,\square_{16}\,Al_{64}$ [31]. Additionally there is some evidence that local microscopic regions of δ-Ni_2Al_3 occur in aluminium rich compositions of β-NiAl, nominally considered to be the single phase B2 structure [94]. These data illustrate the difficulty in specifying the true nature of the compound (NiAl) and locating the limit of the phase field, at least in Al-rich compositions.

While no similar observations have been carried out on NiGa it is apparent that the constitutional defect structure may be complex and that a number of different constitutional defect types, whose concentration and distribution varies as a function of composition, may occur across the phase field.

2.4.3 Temperature Dependent Defects

It is now generally established that in pure metals and random solid solutions, with close packed structures, mono-vacancies are the predominant thermally formed defects. But investigations on a number of B2 intermetallic compounds have shown that the activation energy of vacancy formation E_F is very low when based on the assumption that mono-vacancies can form independently on either sub-lattice. For example the value of E_F in copper is ~83·9 kj/mole (0·87 eV per atom)

while in the compound AuCd the vacancy formation energy E_F lies between 38·6 and 57·9 kj/mole (0·4 to 0·6 eV/atom) [148, 146, 118] .

Furthermore the activation energy of motion E_M in B2 compounds has been found to be rather low and to depend upon the conditions under which it was determined. Among other factors E_M appears to be a function of temperature. For example, in quenching experiments on Au-49% Cd E_M varied between 33·8 and 56·90 kj/mole (0·35 to 0·59 eV) depending upon the quench temperature [120] .

In monatomic lattices there is good agreement between data for the sum $(E_F + E_M)$ and the activation energy of self-diffusion Q. This suggests that the random motion of thermally formed mono-vacancies by nearest neighbour jumps is the predominant rate controlling diffusion mechanism in pure metals (and probably random solutions). In an ordered (B2) intermetallic compound such a diffusion mechanism ignores several constraining factors inherent to the structure. It assumes that the energy of formation of a vacancy is the same on either sub-lattice and that nearest neighbour motion can occur irrespective of the resultant disordering. Furthermore it does not consider the correlation between the diffusivities of the two species, necessary to maintain the structure.

There is little reason to expect that the sum $(E_F + E_M)$ should equal Q in B2 compounds unless account is taken of such factors as the possible change in E_F as a function of the type of lattice site, the dependence of E_M on defect type and the particular diffusion mechanism which Q represents. Furthermore the various factors affecting E_F, E_M and Q are likely to vary as a function of composition and temperature, still further complicating the relationship between the three energies.

Again taking the compound AuCd as an example, the sum $(E_F + E_M)$ has been reported with values of 92·6 kj/mole (0·96 eV) [148] and between 70·4 and 93·5 kj/mole (0·73 to 0·97 eV) [146, 120] for an Au-49%Cd alloy. The activation energies of diffusion for the two species Cd^{115} and Au^{198}

have been reported as 117·7 kj/mole and 117·7 kj/mole respectively in the stoichiometric alloy [78] and 130·2 and 125·3 kj/mole for the species Cd^{109} and Au^{195} respectively in an Au-49%Cd alloy [56]. These data illustrate the discrepancy between the sum $(E_F + E_M)$, determined on the assumption of monovacancy formation and motion, and the diffusion activation energy Q.

A number of thermal defect types, which would comply to the constraints of structure symmetry, have been proposed for an ordered (B2) intermetallic of the type AB [93]

(i) An interstitial atom A_i together with an A-sublattice vacancy $\square_A$ to give the defect $(A_i + \square_A)$

(ii) An interstitial atom B_i together with a B-sublattice vacancy $\square_B$ to give the defect $(B_i + \square_B)$

(iii) Interstitial atoms A_i and an equivalent number of interstitial atoms B_i $(A_i + B_i)$

(iv) A atoms substituted onto the B-sublattice (A_B) plus an equivalent number of B atoms on the A-sublattice (B_A) to give the order/disorder defect $(A_B + B_A)$

(v) Vacant sites on the A-sublattice $(\square_A)$ and an equivalent number of vacant sites on the B-sublattice $(\square_B)$ giving the two vacancy defect $(\square_A + \square_B)$.

The activation energy of formation of interstitial atom defect is large in close packed structures and consequently the probability of thermal defects containing interstitial atoms being formed is low. Interstitial defects will not be considered in the following analysis.

The order/disorder defect $(A_B + B_A)$ does not involve the formation

of new lattice sites while the two vacancy defect ($\square_A + \square_B$) involves the formation of one new lattice site on each of the sublattices. The free energy and entropy of these two defect types may change both as a function of composition and temperature thus so too might their relative concentrations. For example the order/disorder defect may occur to a significant extent when the ordering energy is low relative to the vacancy formation energy. Furthermore, thermal defects may interact with other thermal defects or constitutional defects to produce more complex defect types [143] . This leads to the question of defect mixing and defect equilibria which will now be considered.

2.4.4 Thermal Defects in the Stoichiometric Compound AB

If at absolute zero the stoichiometric composition is perfectly ordered (contains no defects), then for a total of N lattice sites there are $^N/_2$ A-sublattice sites exclusively occupied by A atoms and $^N/_2$ B-sublattice sites exclusively occupied by B atoms. As the temperature is increased thermal defects are progressively introduced into the lattice; their type and number depends on their formation energy. From structure symmetry any defect involving lattice sites on one sublattice must be balanced by an equivalent number of sites on the other sublattice. There is no constraint that the type of defect (anti-structure atom or vacancy) must be the same on each sublattice.

When n_1 defects of the order/disorder type are formed, n_1 anti-structure atoms occur on each sublattice. For small deviations from perfect order ($n_1 \ll N$) at the equilibrium temperature T the additional configurational entropy S_1, due to the defects, is given by:-

$$S_1 = 2kn_1 \ln (N/2n_1)$$

where k is Boltzmann's constant.

Also the concentration of these defects (n_1/N) is given by:

$$\frac{n_1}{N} = \frac{1}{2} \exp\left(\frac{\Delta S_1}{2k}\right) \exp\left(-\frac{E_1}{2kT}\right)$$

where E_1 is the energy of formation of the $(A_B + B_A)$ defect and S_1 is the vibrational entropy factor (arising from the change in lattice vibration frequencies caused by the anti-structure atoms).

A similar line of reasoning for the case of the two vacancy defect ($\square_A + \square_B$) yields:

$$S_2 = 2k\, n_2 \ln(N/2n_2)$$

and $$\frac{n_2}{N} = \tfrac{1}{2} \exp\left(\frac{\Delta S_2}{2k}\right) \exp\left(-\frac{E_2}{2kT}\right)$$

where n_2/N, S_2, ΔS_2 and E_2 are the defect fraction, the configurational and vibrational entropies and the energy of formation of the ($\square_A + \square_B$) defect respectively.

The two vacancy defect results in the introduction of one new site on each of the two sublattices, each site being vacant. However, the same balance may be achieved if a vacancy on the A-sublattice is accompanied by an A atom moving into a new B-sublattice site. One new lattice site has been formed on each sublattice but the nature of the defect type is different on either sublattice.

This situation is effectively the case of a B-sublattice vacancy combining with an A atom. Thus if the energy of formation of the two vacancy defect E_2 is considered to be the sum of the energy of formation of a vacancy on the A-sublattice $E_{\square A}$ and the energy of formation of a vacancy on the B-sublattice $E_{\square B}$ then the vacancy $\square_B$ may degenerate into a vacancy $\square_A$ plus an A antistructure atom if:

$$\square_B + A_A \rightarrow \square_A + \square_B \qquad \text{if: } E_{\square B} > E_{\square A} + E_{AB}$$

where E_{AB} is the energy of formation of an antistructure atom A_B on the B-sublattice.

The two vacancy defect thus degenerates into a new triple (lattice site) defect according to:

$$(\square_A + \square_B) + A_A \longrightarrow 2\square_A + A_B$$

if $$E_2 > 2E_{\square A} + E_{AB}$$

The structure balance of the lattice is preserved, since each sublattice has acquired a new site; but instead of one vacancy on each sublattice there are two vacancies on the A-sublattice and an anti-structure atom A_B on the B-sublattice. Such a triple defect would be favoured by a large difference in the energy of vacancy formation on each of the sublattices. This is thought to be the case, as evidenced by the compositional variation in the nature of the constitutional defect structure, in both NiAl and NiGa [143, 145].

As a result of the above analysis the existence of a third type of thermal defect, namely an asymmetrical triple (lattice point) defect of the type $(2\square_A + \square_B)$ has been proposed for B2 compounds [143]. The configurational entropy of this defect (S_3) and its concentration (n_3/N) can be evaluated in the same way as the other two thermal defect types already considered. Again assuming small deviations from perfect order:

$$S_3 = 3k\, n_3 \ln N/n_3$$

and

$$\frac{n_3}{N} = \exp\left(\frac{\Delta S_3}{3k}\right) \exp\left(-\frac{E_3}{3kT}\right)$$

where n_3/N, S_3, ΔS_3 and E_3 are the defect fraction, configurational and vibrational entropy contributions and the energy of formation of the triple defect respectively.

If the vibrational entropy factors (S values) for the three defect types are of the same order as in monatomic lattices, and approximately equal, then the relative concentrations of the three types can be evaluated [101] . The ratios of the concentrations of the three defect types can be expressed in terms of their energies of formation and as a function of temperature (assuming $S_1 = S_2 = S_3$ [101]) according to the equations:

$$n_1/n_2 = \exp\left[(E_2-E_1)/2kT \right] \qquad 2.1$$

$$n_1/n_3 = \tfrac{1}{2} \exp {}^3/_2 \exp\left[({}^{E_3}/_{3kT}) - ({}^{E_1}/_{2kT}) \right] \qquad 2.2$$

$$n_2/n_3 = \tfrac{1}{2} \exp {}^3/_2 \exp\left[({}^{E_3}/_{3kT}) - ({}^{E_2}/_{2kT}) \right] \qquad 2.3$$

Using equations 2.1 to 2.3 shows which type of thermal defect will predominate in the structure as a function of temperature and how these relative defect fractions are affected by the energies of formation of the three defect types.

On the assumption that $E_1 \ll E_2 \ll E_3$ it has been shown that the order/disorder defect is predominant at low temperatures and that the ratio n_1/n_2 is always greater than unity except for the limiting case $E_1 = E_2$ (see equation 2.1) [143] . Also the relative importance of the triple defect increases steeply with temperature because both the ratios n_1/n_3 and n_2/n_3 fall with increasing temperature (see equations 2.2 and 2.3).

A point of interest is that if $E_1 + E_2 \lesssim E_3$ the triple defect becomes the most stable because of the energy gain from the reaction:

$$(\square_A + \square_B) + (A_B + B_A) \longrightarrow (2\square_A + A_B) + B_B$$

It also follows that whenever $2E_3 < 3E_1$, $2E_3 < 3E_2$ or $E_3 < E_1 + E_2$, significant defect mixing takes place, although the absolute number of defects may be quite small. Finally, because equilibrium conditions are more readily reached at high temperatures - where the triple defect is favoured - it has been suggested that a higher proportion of triple defects may be retained at lower temperatures than required by equilibrium conditions. The triple defect may effectively be quenched in and hence present in larger concentrations than expected at low temperatures [143].

This entire analysis of thermal defect types and equilibria is based on the assumption of small deviations from perfect order and consequently small defect fractions. When a significant amount of disordering occurs, at high temperatures, defect formation energies become dependent upon the degree of order rather than constant [55].

In conclusion, since CsCl type intermetallic compounds can exist at non-stoichiometric compositions where constitutional defects occur, the effect of defect interaction in non-stoichiometric compositions on defect equilibria must be considered.

2.4.5 Thermal Defects in Off-Stoichiometric Compositions.

Non-stoichiometric compositions contain constitutional defects which may significantly affect the energies of formation and equilibria of thermal defects. In an AB compound, in which the predominant constitutional defects are assumed to be A-sublattice vacancies ($\square_A$) in B-rich alloys and A_B anti-structure atoms in A-rich alloys (the defect structure proposed for NiAl and NiGa) the two constitutional defect types may be expected to have different effects.

On the B-rich side of stoichiometry the fraction ($^{n2}/_N$) of the two vacancy defect ($\square_A + \square_B$) may be reduced because of the consti-

tutional vacancies ($\square_A$) already present. This is likely because the energy of formation E_2 of the two vacancy defect should rise with increasing B content and departure from stoichiometry (where $\square_B$ vacancies are not constitutionally favoured). Furthermore the triple defect ($2\square_A + A_B$) might be favoured (relative to stoichiometry) in view of the apparent high energy of formation of B_A anti-structure atoms (not favoured constitutionally) [143].

The high energy of formation of B_A anti-structure atoms means that the energy of formation E_1 of the order/disorder defect will also be high in B-rich alloys. Thus both E_1 and E_2 are likely to rise with increasing excess of B and the triple defect ($2\square_A + A_B$) may be favoured because of the reaction

$$(A_B + B_A) + (\square_A + \square_B) \longrightarrow (2\square_A + A_B) + B_B$$

if $E_1 + E_2 > E_3$

However it has been suggested that while E_2 may be raised, E_3 should be lowered, relative to stoichiometry, with increasing excess of B [143]. But, on the assumption that the introduction of thermal vacancies onto a lattice already containing large numbers of constitutional vacancies would be difficult, the formation energies E_2 and E_3 may both be expected to rise, although the triple defect may be favoured.

The only means by which the energy of formation of the triple defect E_3 could fall, in B-rich alloys, would be if the energy of formation of an anti-structure atom A_B falls more rapidly with increasing B than the energy of formation of two A-sublattice vacancies ($\square_A$) is expected to rise. In such a case the sum energy of formation of two vacancies ($2\square_A$) and one anti-structure atom (A_B), that is E_3 the energy

of formation of the triple defect ($2\square_A + A_B$) may fall with excess of B. However the suggestion that the formation of A_B defects becomes progressively easier in alloys deficient in A seems unlikely.

On the A-rich side of stoichiometry, anti-structure atoms A_B are the predominant constitituional defect. The lattice is full and the introduction of thermal vacancies into a defective but full lattice is likely to be easy [143]. Thus the defect formation energies E_2 and E_3 are both decreased relative to the stoichiometric composition, while E_1 may be raised in view of the fact that the introduction of additional anti-structure atoms may be difficult.

In summary, it can be seen that thermal defect formation energies vary as a function of alloy composition. The two vacancy defect and possibly the triple defect are favoured by the presence of anti-structure atoms and full site occupancy (as in A-rich alloys); in B-rich alloys only the triple defect may be favoured, relative to the other two, by the presence of constitutional vacancies.

2.4.6 Thermal Defects - a Summary

As a result of the analysis of thermal defects in the preceeding two section (2.4.4 and 2.4.5) a number of conclusions may be drawn:

(i) In AB compounds, structural symmetry requires that thermal defects occur in pairs rather than as point defects. In some compounds asymmetrical triple defects, consisting of two vacancies on one sublattice and an anti-structure atom on the other, may be stable.

(ii) Defect formation energies as conventionally determined on the assumption of monovacancy defects are low by a factor of two or three. The energy of formation E_F may vary with composition

within the range of stability of the structure and will depend on the types of defect formed.

(iii) The conventionally determined mobility energies E_M may be strongly dependent on both composition and quenching temperature (since defect equilibria are probably a function of both composition and temperature). The temperature effect might itself be composition dependent.

2.5 Defects in NiGa

2.5.1 Composition Dependent Defects

Lattice parameter measurements on NiGa have indicated a lattice spacing maximum in the 52·0 atomic % nickel alloy at 970°C and in the 51·8 atomic % nickel alloy at 870°C [108]. The composition at which the lattice spacing maximum occurs can be seen to vary with temperature (due to thermal defects) and it has been suggested that this composition tends towards stoichiometry with decreasing temperatures [145].

Nevertheless, unlike NiAl [13], in NiGa the composition of the lattice parameter maximum occurs on the nickel-rich side of stoichiometry. This suggests that no gallium substitution (for nickel) occurs in gallium-rich alloys but that vacancies, on the nickel sublattice, occur directly in such non-stoichiometric alloys.

Lattice parameter and density measurements on NiGa [145,129] have confirmed nickel sublattice vacancies as the constitutional defects present in gallium rich alloys and indicated that nickel anti-structure atoms may be the predominant defects in nickel-rich alloys.

2.5.2 Thermal Defects

Density measurements on quenched and slowly cooled NiGa alloys have indicated that very high thermal vacancy concentrations may easily be quenched-in. Thermal vacancy formation has been found to occur to a significant extent for temperatures above 500°C. The thermal vacancy fraction is of the order of 1 atomic % for a quench temperature of 850°C [145].

The thermal vacancy fraction has been found to vary with composition, with the largest concentrations occuring in the stoichiometric and nickel-rich alloys while nickel deficient alloys, where large numbers of constitutional vacancies are already present, contain fewer thermal vacancies.

Lattice parameter measurements have shown that the composition at which the maximum lattice spacing occurs varies with temperature [108]. This suggests that the compositional dependence of the thermal vacancy concentration also varies with temperature; effectively that the activation energy of vacancy formation varies with composition and that defect mixing and equilibria occur (which has already been proposed on theoretical grounds, sections 2.4.4 and 2.4.5).

It has been suggested that with increasing temperature nickel atoms fill some or most of the thermal vacancies on the gallium sublattice [145] giving rise to a new nickel anti-structure atom and an additional nickel sublattice vacancy. This is in fact the reaction proposed in the formation of the triple defect ($2\square_A\ A_B$) [143].

The energy of formation (E_F) of thermal vacancies has been computed by assuming that the lattice parameter contraction due to vacancies is linearly proportional to their concentration ($^n/_N$) and that the quench retains the high temperature concentration of vacancies. Then:

$$(a_o - a)/a_o \approx {}^{n}/_{N} \approx \exp(-{}^{E_F}/_{2RT})$$

where a_o is the equilibrium room temperature lattice parameter, a is the parameter actually measured at room temperature after quenching from the temperature T(°K). The factor 2 in the exponential is required in the B2 structure because each defect formed consists of two vacancies.

Vacancy formation energies computed from this equation, for NiGa, are found to increase with nickel content from 63·2 kj/mole (15·1 kcal/mole) in the 47·4 atomic % nickel alloy to a maximum of 71·1 kj/mole (17·0 kcal/mole) at stoichiometry and thereafter to decrease again to 63·2 kj/mole (15·1 kcal/mole) in the 52·4 atomic % nickel composition [145].

The variation in the energy of defect formation with composition in NiGa has been accounted for as follows:

(i) In the stoichiometric composition the initial thermal defects may be either two vacancy defects or order/disorder defects. The stable constitutional defects in NiGa are known to be nickel vacancies $\square_{Ni}$ and nickel anti-structure atoms Ni_{Ga}, while gallium vacancies and anti-structure atoms are thought to have high energies of formation. This may lead to the formation of triple defects ($2\square_{Ni} + Ni_{Ga}$). The equilibrium defect structure, at elevated temperatures, should consist of nickel sublattice vacancies, a small number of gallium sublattice vacancies and some nickel antistructure atoms. In effect a mixture of the two vacancy defect and triple defects, whose relative proportions would vary with temperature.

The experimental activation energy of formation E_F, based on the assumption of two vacancy defects would only be an

approximation. The true value would depend on the extent of the interaction between, and the activation energies of the various defect types.

(ii) In nickel rich compositions nickel anti-structure atoms are the predominant constitutional defects; the full but defective lattice is thought to favour thermal vacancy formation [143]. Both the two vacancy and triple defects may occur, but the constitutional anti-structure atoms may impede the introduction of still further nickel anti-structure atoms and depress the formation of the usual triple defects ($2\square_{Ni} + Ni_{Ga}$). In fact the introduction of nickel anti-structure atoms may be so restricted that they may react with the nickel vacancies (of the two vacancy defects), to result in the formation of a nickel atom on the nickel sublattice and a gallium sublattice vacancy, thereby lowering the total defect energy. The normally high energy gallium vacancy is stabilised and a new triple defect ($Ni_{Ni} + 2\square_{Ga}$) is formed which is not stable at stoichiometry nor at low temperatures [145].

The probability and extent of formation of such a defect is directly related to the change in the energies of formation of gallium sublattice vacancies and nickel antistructure atoms relative to each other as a function of composition and temperature. Thus again the overall defect formation energy is seen to depend on defect equilibria.

(iii) In gallium rich compositions nickel sublattice vacancies are the predominant constitutional defects and these tend to favour the triple defect ($2\square_{Ni} + Ni_{Ga}$) formation [see section 2.4.5]. Once again defect mixing is likely and the defect formation energy will depend on defect equilibria.

It is clear that throughout the phase field of the compound NiGa, conventionally determined values of the energy of defect formation E_F will depend upon the proportions and interaction between the defects formed. Defect interaction is likely to be most marked in off-stoichiometric compositions where large concentrations of constitutional defects occur. In consequence the apparent vacancy formation energies observed experimentally are likely to be low throughout the phase field and most markedly so in non-stoichiometric compositions. Finally the maximum in E_F need not occur at stoichiometry but at that composition in which minimum defect interaction occurs. This composition is likely to be temperature dependent and in NiGa is thought to lie on the nickel rich side of stoichiometry, where only small numbers of triple defects are possible [145] .

The activation energy of motion E_M of thermal defects in NiGa has been found to depend upon the fraction of defects remaining ($f = n(t)/n(o)$) at some time t during the annealing out of quenched-in defects. In the stoichiometric material values of E_M were 179·9 kj/mole (43·0 kcal/mole), 146·4 kj/mole (35·0 kcal/mole) and 125·5 kj/mole (30·0 kcal/mole) for remaining defect fractions (f) of 0·8, 0·5 and 0·2 respectively [145] .

The change in E_M with defect fraction suggests that more than one defect type is involved in the relaxation mechanism and that defect mobility varies with defect fraction indicating that different defects are annealed out at different rates. Similar behaviour has been reported in AuCd [120, 56] and in both this compound and NiGa defect equilibria are likely to be responsible.

In conclusion it is evident that thermal defect mixing and defect equilibria in NiGa may account for the fact that energies of formation and motion can be composition dependent and also temperature dependent.

2.6 Diffusion

2.6.1 Diffusion Mechanisms in Solids

Crystalline solids have a regular array of lattice sites which are energetically favoured positions for atoms. Atoms diffusing through a crystal thus tend to jump between lattice sites, although jumps may occur in more or less random directions. The type of lattice sites involved in such jumps and the nature of the jumps themselves define the particular diffusion mechanism.

It is known that the regularity of the lattice structure breaks down in the vicinity of line defects (dislocations) and surface defects (grain boundaries and free surfaces) with the consequence that atomic packing is not as dense as in the bulk material. Thus while the particular mechanisms by which atoms move within the field of such defects may be the same as in the bulk material the more open, less regular nature of the matrix may allow diffusion to occur more rapidly. This leads to the conclusion that distinct regions can exist within a solid where diffusion may occur by similar mechanisms but be restricted by different boundary conditions.

There are several such diffusion 'classes', namely diffusion along line defects called dislocation pipe diffusion, diffusion at surfaces (both internal and external) called grain boundary and surface diffusion and diffusion in the bulk material called volume. Diffusion rates in the first three classes are less temperature sensitive than volume diffusivities, and in general their diffusivities are high but activation energies low. Thus dislocation pipe, grain boundary and surface diffusion are important at low temperatures but less so at high temperatures where volume diffusion predominates.

A number of diffusion mechanisms, applicable particularly to volume diffusion, have been distinguished in solids. They are characterised by the type of elementary jump which takes the atom from one equilibrium lattice site to another. These diffusion mechanisms will be outlined briefly in

the following sections.

2.6.2. Interchange and Ring Mechanisms

In these mechanisms the diffusing atom moves by interchanging its position with that of another lattice atom by a correlated rotation of two (direct interchange) or more (ring mechanism) atoms about a common centre [See FIG. 2.3, A & B] .

Both of these mechanisms have high activation energies but in the ring mechanism the energy is minimised for either 4 or 6 atoms participating in the ring, depending upon crystal structure [160] . Values calculated for copper are 964·4 kj/mole (10 eV) for the pair interchange and 385·8 kj/mole (4 eV) for a ring involving 4 atoms [97] .

The ring mechanism has been invoked to explain certain anomalies of diffusion behaviour in some b.c.c. transition metals [123] .

2.6.3 Interstitial Mechanisms

In interstitial mechanisms the diffusing atom may move by jumping between two adjacent interstitial positions (the direct interstitial mechanism), bu pushing a neighbouring atom from a normal lattice site into an interstitial position (interstitialcy mechanism) or by a correlated motion of a line of displaced atoms (the crowdion mechanism) [see FIG. 2.3, C, D & E].

The direct interstitial mechanism is thought to be restricted to the movement of atoms which are small relative to the lattice atoms. Carbon and nitrogen diffuse in iron by this mechanism [163, 11, 46] . If the interstitial atoms are comparable in size to the lattice atoms the interstitialcy or crowdion mechanisms are preferred.

The calculated activation energy for an interstitialcy mechanism in copper is 482·2 - 964·4 kj/mole (5 to 10eV) [97] which is still high in comparison to the observed activation energy for self-diffusion. In fact in most cases where the diffusing species is similar in size

FIG. 2.3
DIFFUSION MECHANISMS

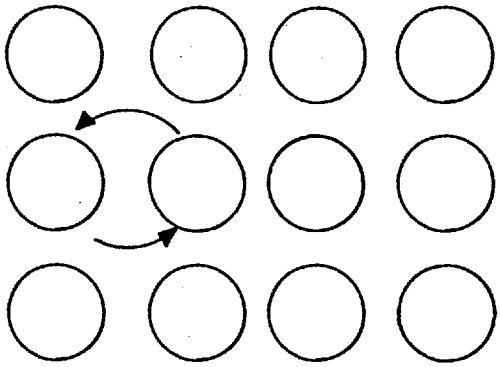

A. INTERCHANGE MECHANISM

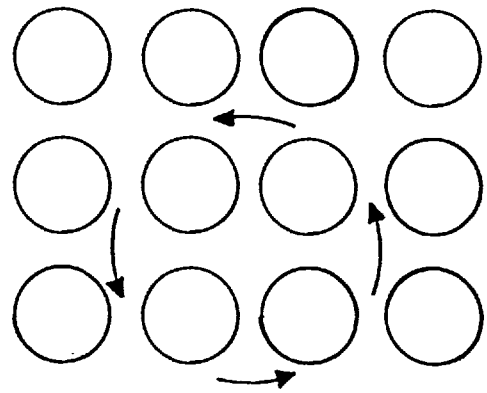

B. RING MECHANISM

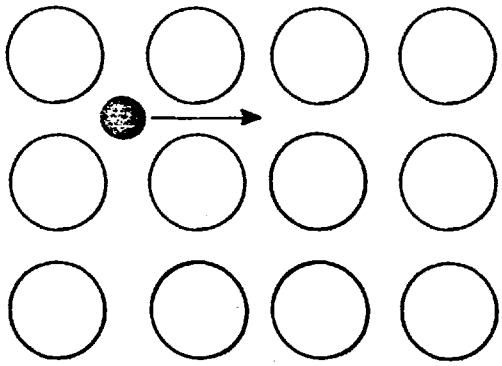

C. INTERSTITIAL MECHANISM

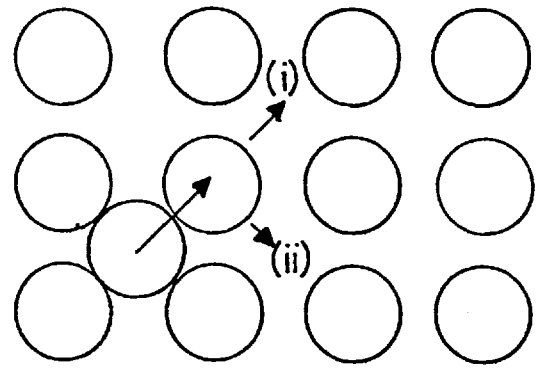

D. INTERSTITIALCY MECHANISM
(i) COLINEAR
(ii) NON-COLINEAR

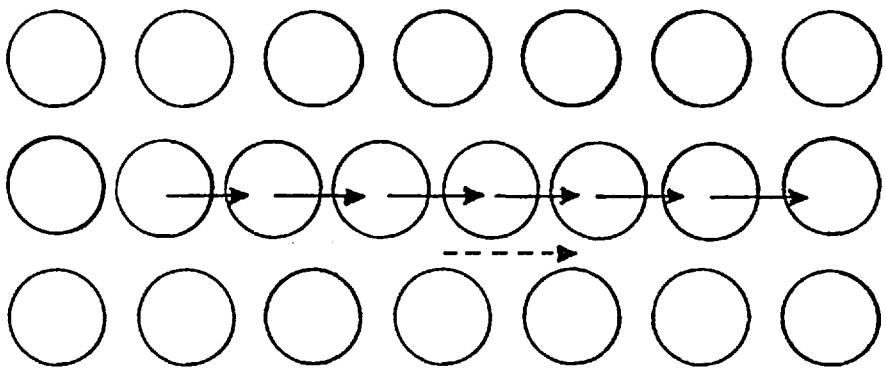

E. THE CROWDION MECHANISM

FIG 2.3
DIFFUSION MECHANISMS

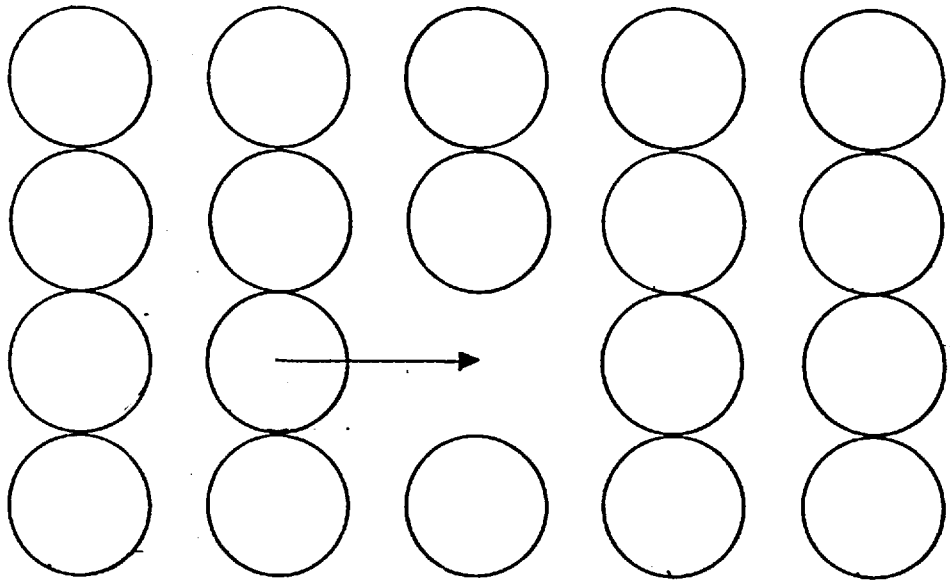

F. THE VACANCY MECHANISM

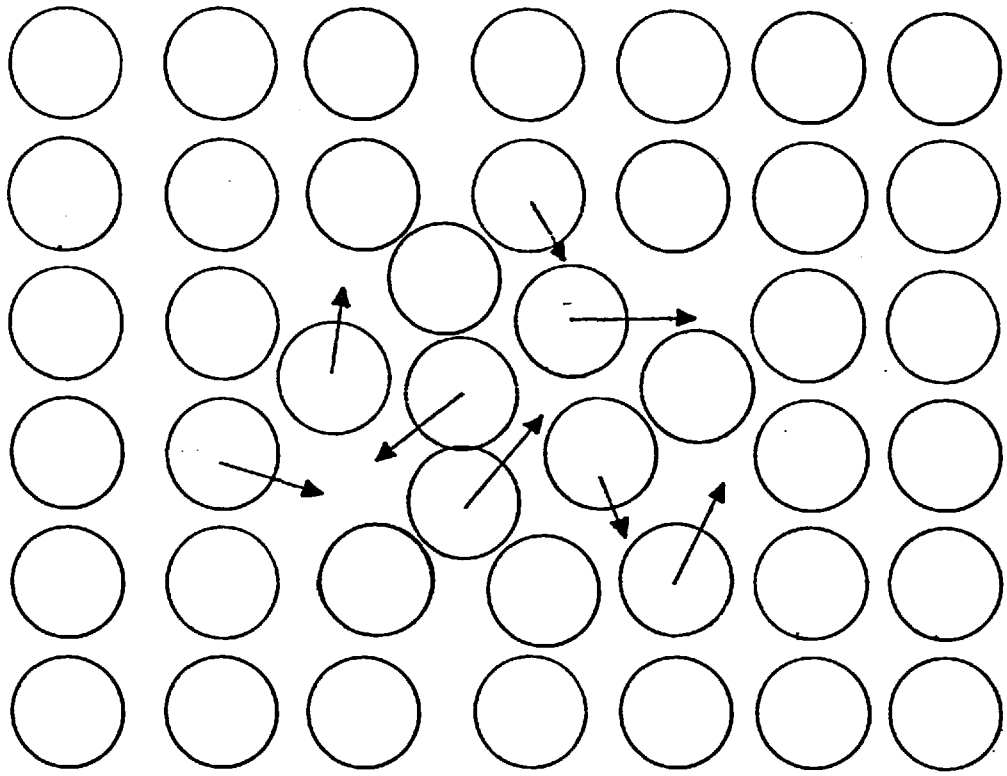

G. RELAXION MECHANISM
ATOMS ENTER & LEAVE RELAXION REGION WHERE MOVEMENT OCCURS BY IRREGULAR JOSTLING (AS IN A LIQUID)

to the matrix atoms vacancy mechanisms are prefered to any of the interstitial mechanisms.

2.6.4 Vacancy Mechanisms

The simple (single) vacancy mechanism involves the exchange of positions between the diffusing atom and an adjacent vacancy [see Fig. 2.3, F] . If there is a binding energy between vacancies, diffusion may involve the movement of vacancy complexes containing two or more vacancies. However vacancy complexes lack the symmetry of monovacancies and are more restricted in their movement, although di-vacancies may be important in diffusion at very high temperatures.

A further modified vacancy mechanism is the relaxion mechanism [see Fig. 2.3, G] where the atoms surrounding a vacancy are sufficiently displaced from their equilibrium positions to be comparable with a region of localised melting. Atoms in a relaxion can diffuse by an irregular jostling motion similar to that for atoms in a liquid.

In general, in close packed lattices, with all atomic species of about the same size the single vacancy diffusion mechanism has the lowest activation energy and is predominant. The calculated energy for a vacancy mechanism in copper is 144·7 to 270·0 kj/mole (1·5 to 2·8 eV) [97] .

2.7 Diffusion Equations

Lattice defects are known to play an important role in the transport of matter through crystals, but in some mechanisms (e.g. the interchange mechanism) the influence of lattice defects may be ignored while in others (e.g. the vacancy mechanism) the diffusion rate constant is a function of the concentration of lattice defects. The effect on the

diffusion equations derived for the two groups of mechanisms has been reviewed by Compaan and Haven (1957) [123] .

In general, diffusion equations have been developed to describe mathematically a particular diffusion mechanism. Usually such equations are applicable only to volume diffusion where the regularity of the lattice allows such factors as the type and number of defects, the jump frequency and the size and shape of the potential energy barrier that the diffusing species must cross in the course of a jump, to be evaluated.

2.7.1 Fick's Laws

By an analogy with heat transport, Fick (1855) [45] developed two general relationships to describe mass flow in solids.

Under steady state conditions of unidirectional mass flow in a solid, the concentration (c_i) of a species i at any given point is independent of time (t). The mass flux (j_i) of the species i passing through a unit area of plane (perpendicular to the flow direction) in unit time is given by Fick's first law as:

$$j_{ix} = -D_{ix} \left(\frac{\partial c_i}{\partial x}\right) \qquad 2.4$$

Where x is the distance in the flow direction and D_{ix} is the diffusivity of the species i in the direction x and has the dimensions ($L^2\ T^{-1}$) usually cm^2/sec.

Similar equations may be written to describe the steady state flow of species i in the directions y and z yielding two more diffusion coefficients D_{iy} and D_{iz}. The three diffusion coefficients are usually assumed equal in cubic materials.

Under conditions of non-steady state equation 2.4 can be differentiated with respect to time to give Fick's second law:

$$\frac{\partial c_i}{\partial t} = \frac{\partial}{\partial x}\left(D_{ix} \frac{\partial c_i}{\partial x}\right) \qquad 2.5$$

In the special condition that the diffusion coefficient D_{ix} is indpendent of position equation 2·5 reduces to:

$$\frac{\partial c_i}{\partial t} = D_i \frac{\partial^2 c_i}{\partial x^2} \qquad 2.6$$

A complete analysis of the derivation of Fick's laws is given by Reed-Hill (1967) [125].

2.7.2 Modifications of Fick's Laws

According to Fick's laws diffusion is expected to occur only down a concentration gradient, but there are many instances (e.g. precipitation of a second phase) where diffusion takes place up a concentration gradient. This anomaly has been overcome by considering that diffusion proceeds down a chemical potential gradient ($\partial\mu_i/\partial x$). Furthermore, the chemical potential (μ_i) of a species i is itself defined in terms of the activity (a_i) of the species in a system. Finally the activity (a_i) of the species in a system. Finally the activity (a_i) of a species is proportional to the concentration (c_i) or atomic fraction (N_i) through the activity coefficient (γ_i) according to the relation:

$$a_i = \gamma_i N_i \qquad 2.7$$

Fick's first law can be rewritten in terms of activities to give:

$$j_i = - D_i \left(\frac{\partial a_i}{\partial x}\right) \qquad 2.8$$

And differentiating w.r.t. time and substituting from equation 2.7 gives an alternative statement of Fick's second law:

$$\frac{\partial c_i}{\partial t} = \frac{\partial N_i}{\partial t} = \frac{\partial}{\partial x}\left[D_i\left(\gamma_i + N_i \frac{\partial \gamma_i}{\partial N_i}\right) \frac{\partial N_i}{\partial x} \right] \qquad 2.9$$

The expression of equation 2.9, derived by Birchenall & Mehl (1947) [11], reduces to the simple statement of Fick's second law (equations 2.5 and 2.6) when the diffusing system is an ideal solution ($\gamma_i = 1$).

It can also be shown that the atom flux j_i is dependent upon the diffusing atom mobility G_i and that Fick's first law then becomes [28, 100]:

$$j_i = - G_i\, kT \left[1 + \left(\frac{\partial \log \gamma_i}{\partial \log N_i}\right) \right] \frac{\partial N_i}{\partial x} \qquad 2.10$$

Comparing equations 2.4 and 2.10 shows that:

$$D_i = G_i kT \left[1 + \left(\frac{\partial \log \gamma_i}{\partial \log N_i}\right) \right] \qquad 2.11$$

It is apparent from equation 2.11 that the diffusion coefficient (D_i) is a function of the mobility of the diffusing species (G_i) but it is also a function of the ideality (γ_i) of the solution

Finally, equation 2.10 can be differentiated with respect to time for non-steady state conditions to give:

$$\frac{\partial N_i}{\partial t} = \frac{\partial}{\partial x}\left[G_i kT \left(1 + \frac{\partial \log \gamma_i}{\partial \log N_i}\right) \frac{\partial N_i}{\partial x} \right] \qquad 2.12$$

This expression only reduces to the simple statement of Fick's second law (equation 2.6) if the solution is both thermodynamically ideal ($\gamma_i = 1$) and the mobility G_i is not a function of position [28, 100].

It is apparent then that the diffusion coefficient is not merely a

measure of the mobility of the diffusing species but depends upon the ideality of the solution, which in turn is a function of the type and strength of the various interatomic bonds within the solution (diffusing system). The mobility of the species is itself dependent on such factors as the lattice parameter, jump frequency and correlation factor.

2.7.3 Diffusion Coefficients

Fick's first law can be used to define a number of diffusion coefficients, the nature and significance of which depend upon the conditions in which the equation is applied.

The simplest case is that of tracer diffusion in a homogeneous crystal where diffusion occurs purely as the result of the vanishingly small concentration gradient of the tracer itself. The coefficient D_i^* is termed the tracer diffusion coefficient. In the special case of the tracer and crystal matrix atoms being of the same species the concentration gradient vanishes and self-diffusion occurs by random mixing because of the change in free energy of the system from the change in entropy upon mixing.

A second diffusion coefficient may be derived when a driving force imparts a drift velocity (v_F) to the diffusing species which contributes an additional mass flux of $c_i(v_F)$ to the diffusive flux. If the driving force and hence the drift velocity are proportional to the concentration gradient it can be shown that:

$$D_i^I = D_i^* - \frac{c_i(v_F)}{(\partial c_i/\partial x)} \qquad 2.13$$

where D_i^I is the new (intrinsic) diffusion coefficient.

Furthermore, if D_i^* is equal to the tracer diffusion coefficient irrespective of driving forces and the mobility of the species at any

given composition is the same irrespective of the concentration gradient then the intrinsic diffusion coefficient D_i^I is related to the tracer diffusion coefficient D_i^* by the expression [29] :

$$D_i^I = D_i^* \left(1 + \frac{\partial \log \gamma_i}{\partial \log N_i}\right) \qquad 2.14$$

A third diffusion coefficient, namely the interdiffusion coefficient $\bar{D}$ can be defined to measure the rate at which two species (A and B) of atoms intermingle. The interdiffusion coefficient can be expressed in terms of the intrinsic diffusivities D_A^I and D_B^I and the atomic fractions N_A and N_B of the two species to give the Darken equation [29] :

$$\bar{D} = N_B D_A^I + N_A D_B^I \qquad 2.15$$

If the component B is an isotope of A there is effectively only one species (A) and the interdiffusion coefficient $\bar{D}$ becomes equal to the intrinsic coefficient D_A^I . Furthermore since the isotope and matrix are now the same species the interdiffusion coefficient $\bar{D}$ (equal to D_A^I) is also equal to the tracer diffusion coefficient D_A^* for self-diffusion.

Of the three diffusion coefficients considered so far the tracer diffusion coefficient may be most readily evaluated theoretically in terms of such factors as jump frequencies, lattice parameters and correlation factors [see section 2.8] .

2.7.4 Partial Diffusion Coefficients

In multicomponent systems Fick's first law yields a diffusion coefficient dependent not only on the concentration of the diffusing species i, temperature and pressure but also on the concentration gradients of other species present. The atomic flux j_i can then be

expressed as:

$$j_i = -\sum_k D_{ik} \frac{\partial c_k}{\partial x} \qquad 2.16$$

Equation 2.16 allows for the possibility that the flux j_i of the species i may depend on the concentration gradient $(\partial c_k / \partial x)$ of a species k through the constant D_{ik} termed the partial diffusion coefficient. Normally the constant D_{ik} for i not the same species as k is small compared with i identical to k and are often considered zero (so that the diffusion of i does not depend on the concentration of k except when k = i).

Non-zero values of the cross terms D_{ik} $(i \neq k)$ result in a series of phenomenological equations to describe the diffusion behaviour. Such equations are of particular significance when the diffusion of a given species is correlated to another species and the diffusion mechanism requires the movement of more than one species or of defect complexes. The phenomenological equations of diffusion have been extensively reviewed by a number of authors [124, 74, 28, 97].

2.7.5 The Solution of Diffusion Equations

The differential equations relating the tracer diffusion coefficient to concentration as a function of position and time can be solved for a number of boundary conditions [27].

When the initial distribution of the diffusing species can be represented at time t equals zero by the expression of Fick's second law (equation 2.6) at position x equal zero then the solution of the expression is:

$$c_x = \frac{c_o}{2(\pi D t)^{\frac{1}{2}}} \exp\left(\frac{-x^2}{4Dt}\right) \qquad 2.17$$

where c_o is the original concentration per unit area at the plane x equals zero and D is the tracer diffusion coefficient.

In most diffusion experiments radio-active species are used as the tracer diffusing species. The tracer is applied to the specimen in a sufficiently thin layer for the assumption that diffusion into the specimen surface is instantaneous to be valid and hence Fick's law applies. The concentration of tracer can be related to the radio-active intensity and the diffusion coefficient D can be evaluated by plotting the logarithm of the concentration (or radio-active intensity) against the square of the diffused distance (x^2).

2.8 Theoretical Evaluation of the Tracer Diffusion Coefficient

Atomic flux during self-diffusion originates solely from random atomic movements through the lattice and consequently may be described by the theory of the random walk. The diffusion coefficient may then be evaluated in terms of atomic processes.

In the simplest case of the random walk the jump frequency Γ is independent of the jump direction. The flux j from one plane, containing n_1 atoms of the diffusing species per unit area, to a second plane containing n_2, is given by:

$$j = (n_1 - n_2)\,\Gamma \qquad 2.18$$

The atom concentrations per unit area (n) can be related to the concentration per unit volume (c) by the equation ($n = \lambda c$) where λ is the distance between neighbouring planes. Equation 2.18 can then be written in terms of concentration (c)

$$j = -\lambda^2 \Gamma \frac{c}{x} \qquad 2.19$$

In a cubic system all nearest neighbour jumps are equally likely and all other jumps are unlikely. The total jump frequency ν^1 is thus the product of the individual jump frequency Γ and the number of nearest neighbour sites z. In the simple cubic lattice z is six and equation 2.19 can be written:

$$j = -\frac{1}{6}\lambda^2 \nu^1 \frac{\partial c}{\partial x} \qquad 2.20$$

Comparison with Fick's first law shows that:

$$D = \frac{1}{6}\nu^1 \lambda^2 \qquad 2.21$$

The random jump frequency ν^1 has been expressed as:

$$\nu^1 = n \nu f$$

where n is the total number of independent jumps, each having a probability (frequency) ν and f is the probability that any jump is statistically independent of the previous jump and is called the correlation factor. The diffusion coefficient (D) is then given by [19]

$$D = \frac{1}{6}\lambda^2 n \nu f \qquad 2.22$$

If a specific diffusion mechanism is considered, the jump distance (λ) can be related to the lattice spacing (a) (e.g. for b.c.c. $= (\frac{1}{2})\sqrt{3}\, a$ for nearest neighbour jumps) [98].

Furthermore the correlation factor (f) can be expressed as [4, 20]:

$$f = (1 + \cos\bar{\theta}) / (1 - \cos\bar{\theta})$$

where $\cos\bar{\theta}$ is the average value of the cosine of the angle between successive jumps (θ). The correlation factor has been found to be

unity for interstitial and interchange mechanisms [109] while for vacancy mechanisms it is a function of crystal structure (f = 0·72 for b.c.c; f = 0·78 for f.c.c.) [20] .

In most metal systems diffusion is thought to involve defects (usually vacancies) and so the diffusion coefficient depends upon defect concentration and the jump probability between lattice sites and defect sites. The diffusion coefficient can be expressed as [102] :

$$D = \alpha a^2 / \tau \qquad 2.23$$

where α is a geometric factor depending upon the number of nearest neighbours, a is the lattice parameter and τ is the average time between successive jumps. The factor τ is related to the jump frequency ν by the expression:

$$\frac{1}{\tau} = p \nu \exp(-\frac{\Delta G}{RT}) \qquad 2.24$$

where p is the number of equivalent paths for diffusion. Thus the diffusion coefficient can now be written:

$$D = \alpha a^2 p \nu \exp(-\frac{\Delta G}{RT}) \qquad 2.25$$

where ΔG is the jump activation energy.

If diffusion occurs by a vacancy mechanism it can be shown that [19] :

$$D = \alpha a^2 \, p \, \nu \, f \, \exp(-\frac{\Delta G_F}{RT}) \exp(-\frac{\Delta G_M}{RT}) \qquad 2.26$$

where ΔG_F and ΔG_M are activation energies of vacancy formation and motion respectively and f is the correlation factor. The geometric factor (α) is equal to the reciprocal of the path multiplicity factor (p) and so their product is unity and they may be omitted from equation

2.26 which may be rewritten:

$$D = a^2 \nu f \exp - \left(\frac{\Delta G_F + \Delta G_M}{RT}\right)$$

or $$D = a^2 f \exp\left(\frac{\Delta S_F + \Delta S_M}{R}\right) \exp - \left(\frac{\Delta H_F + \Delta H_M}{RT}\right) \qquad 2.27$$

The jump frequency ν is the frequency with which an atom jumps from an activated complex (i.e. the atomic configuration around an atom at the top of the activation potential barrier) [see Fig. 2.4] to an equilibrium site. It is usually equated to the Debye frequency [102] .

2.8.1 The Temperature Dependence of the Diffusion Coefficient

Over a wide range of temperatures experimentally measured diffusion coefficients are often found to fit the Arrhenius relation:

$$D = D_o \exp\left(-\frac{Q}{RT}\right) \qquad 2.28$$

where both Q, the activation energy of diffusion, and D_o, the frequency factor, are assumed independent of temperature but depend on the identity of the diffusing species and the composition of the matrix crystal.

The Arrhenius relation is found to apply best when the tracer diffusion coefficient is measured. A comparison with LeClaire's expression [103] given in equation 2.27 shows that:

$$D_o = a^2 \nu f \exp\left(\frac{\Delta S_F + \Delta S_M}{R}\right) \qquad 2.29$$

and $$Q = \Delta H_F + \Delta H_M \qquad 2.30$$

Both D_o and Q are usually assumed constant since all the terms from which they are formed are effectively constant, and adherence to the Arrhenius relation is said to characterise 'normal' diffusion. In

FIG. 2.4.
THE ACTIVATED COMPLEX ATOMIC CONFIGURATION

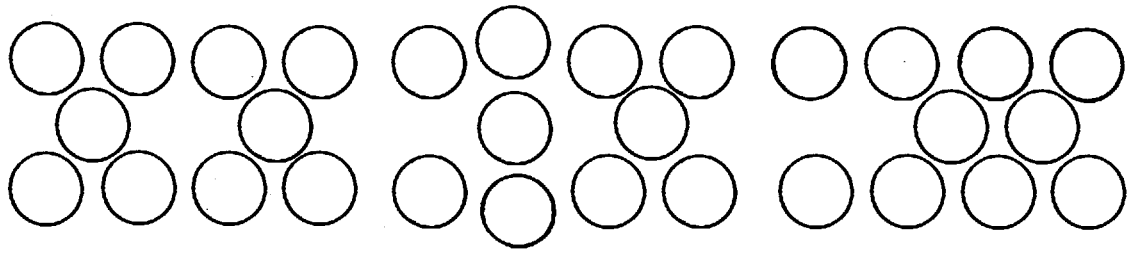

a. EQUILIBRIUM CONFIGURATION

b. ACTIVATED COMPLEX CONFIGURATION

c. EQUILIBRIUM CONFIGURATION

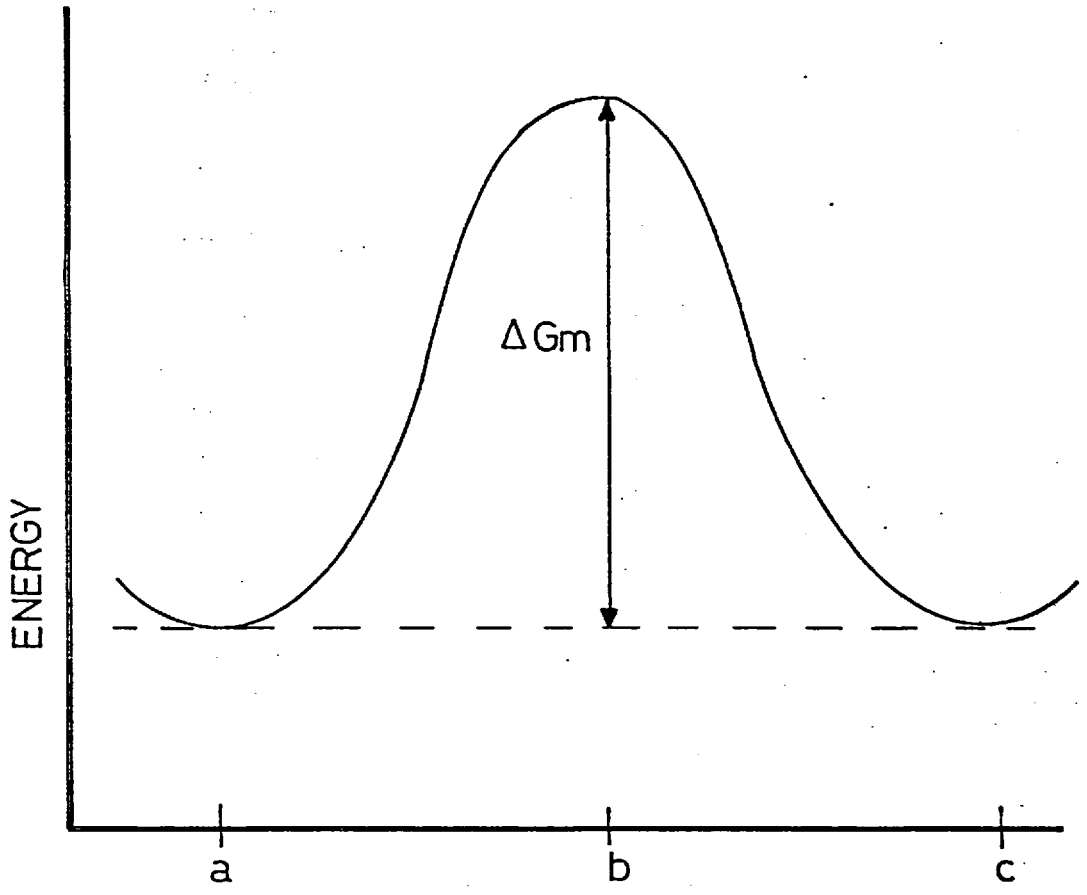

fact both D_o and Q may vary with temperature giving rise to 'anomalous' behaviour.

There are three essential features which are said to characterise 'normal' diffusion:

(i) The temperature dependence of D is accurately described by the Arrhenius relation.

(ii) The activation energy Q is independent of the ambient temperature but is proportional to the melting point T_M of the material, or the solidus temperature in the case of alloys. The empirical correlation for self-diffusion is generally found to be, to within $\pm$ 20%, $Q = 34\ T_M$ (Q in calories/mole, T in ^oK).

(iii) The frequency factor D_o is usually in the range 0·1 to 10·0 cm^2/sec.

Anomalous diffusion behaviour, where the diffusion coefficient does not obey the Arrhenius expression and a curvature is observed in the log D vs ($^1/T$) plot can arise for a number of reasons. Typical examples include the breakdown of the Arrhenius relationship near the ordering temperature T_c [95] seen in CuZn, anomalies linked with the temperature dependence of the elastic constants seen in β-Zr and β-Ti [138, 139] and the general case where more than one independent diffusion mechanism may be operating over the same temperature range (e.g. grain boundary and volume diffusion).

Frequently an analysis of the factors comprising the frequency factor D_o can account for apparently anomalous diffusion behaviour.

2.8.2 Zener's Theory of D_o

Departures from the Arrhenius relation may arise from a temperature dependence of the frequency factor D_o. The most important contribution to such a case is likely to come from the exponential entropy term [see equation 2.29] .

In the case of an interstitial diffusion mechanism where no defects are required ($\Delta S_F = 0$) the term ΔS_M can be evaluated [153, 152,162] .

By definition ΔS_M is given by:

$$\Delta S_M = -\frac{\partial \Delta G_M}{\partial T} = -\Delta G_o \left[\frac{\partial (\Delta G_M / \Delta G_o)}{\partial T} \right]$$ where ΔG_M is the energy of motion and ΔG_o is the value of ΔG_M at absolute zero ($T=0^oK$).

It has been shown that the energy required to move an atom to the top of the potential barrier into the activated complex confugration (i.e. ΔG_M) is given by [162] :

$$\Delta G_M \approx \varepsilon_o^2 \mu$$

where ε_o is a measure of the elastic strain of the lattice around the activated complex and μ is the elastic shear modulus.

The entropy of motion ΔS_M is then given by:

$$\Delta S_M = -\beta \xi \frac{\Delta H_o}{T_M} \qquad 2.31$$

where $\beta = \frac{\partial (\mu/\mu_o)}{\partial (T/T_M)}$ and T_M is the melting point. The enthalpy of motion ΔH_o at 0^oK is equal to ΔG_o. The factor β is usually negative while the factor ξ is a positive constant less than unity to allow for the fact that not all the work done in forming the activated complex goes into straining the lattice.

Since all the factors, β , ξ and T_M are constants for a given solvent the entropy of motion ΔS_M is proportional to the enthalpy of

motion ΔH_M ($\approx \Delta H_o$). Furthermore since β is negative and all other factors are positive the entropy of motion is also positive.

A similar treatment has been applied to the case of vacancy diffusion, where the entropy of formation ΔS_F was assumed proportional to ΔS_M, to give the expression [161] :

$$\Delta S = \Delta S_F + \Delta S_M \approx - \beta \xi \frac{\Delta H}{T_M} \qquad 2.32$$

where $\Delta H = \Delta H_F + \Delta H_M$.

The factor ΔS_F was found to be positive and consequently ΔS was predicted to be positive. Zener's theory is found to be in good agreement with interstitial diffusion mechanisms but in poorer agreement in the case of defect mechanisms where negative activation entropies have been consistently found in some systems.

2.8.3 Anomalous Diffusion Behaviour

In 'anomalous' diffusion curvature is observed in the linear relationship predicted by the Arrhenius relationship and activation energies and frequency factors are often far below values predicted for 'normal' diffusion. Furthermore negative activation entropies are common in such systems.

Zener's theory (of D_o) has been modified to allow negative entropies. The activation entropy ΔS is considered as the sum of two contributions; the first ΔS_1 arises from the reduction in vibrational frequencies near a vacancy and is positive, the second ΔS_2 arises from the increase in frequency in the region of an activated complex and is negative [32, 79] . Thus if $|\Delta S_2| > |\Delta S_1|$ then their sum ΔS is negative.

Negative activation entropies may also occur, even in Zener's

original theory, if the temperature dependence of the shear modulus is not negative and hence the factor β is also not negative [see equations 2.31 and 2.32] . Some b.c.c. transition metals have been found to exhibit an anomalous temperature dependence of the elastic shear modulus [139] in the same temperature range in which anomalous diffusion behaviour is observed [138, 1] .

Finally it has been found that even systems which are usually considered to exhibit normal diffusion behaviour, a curvature in the Arrhenius plot can be detected if the temperature range is sufficiently wide. For example the activation energy for the self diffusion of nickel has been found to increase slowly with temperature. This has been explained in terms of an increasing contribution to diffusion from di-vacancies and multiple vacancies resulting in an increase in the defect entropies [127] . The activation energy varies with temperature because several mechanisms are occuring simultaneously.

In ordered compounds where lattice symmetry imposes constraints on random diffusion and the diffusivities of the component species are likely to be correlated it may be expected that diffusion behaviour may not be straightforward and apparent anomalies may be observed.

2.9 Diffusion Mechanisms in B2 Compounds

One of the principal mechanisms of diffusion in both pure metals and alloys is the vacancy mechanism. In pure metals and random solid solutions diffusion may occur by the random motion of mono-vacancies in nearest neighbour jumps. In ordered alloys and intermetallic compounds such random motion of single vacancies is energetically less favoured because it may result in the disordering of the atomic arrangement.

Many B2 intermetallic compounds are known to contain constitutional defects in off-stoichiometric compositions (see section 2.4.1), which may contribute to diffusion. Furthermore, thermal defects in such compounds are not monovacancies but may involve several lattice sites (see sections 2.4.4 and 2.4.5). In addition thermal defects are not randomly distributed among the available lattice sites.

By virtue of the fact that these compounds contain more than one atomic species, any mechanism which involves the movement of more than one species is likely to impose correlation constraints on the diffusivities of these species. In other words the diffusion coefficient of one species is likely to be related to or include the effect of the diffusion of the other species.

A number of diffusion models, based on vacancy motion have been proposed for B2 intermetallic compounds. As will be seen in the following sub-sections all these models allow atom movements by vacancy mechanisms while retaining the overall order of the structure.

2.9.1 Next Nearest Neighbour Vacancy Jumps

In a B2 compound AB the nearest neighbour sites to a given atom site belong to the opposite sublattice to that of the said atom. Thus a vacancy ($\square_A$) on the A-sublattice has B atoms on the B-sublattice as nearest neighbours. A nearest neighbour jump by such a vacancy would result in the formation of an anti-structure atom B_A. Subsequent jumps would tend to increase the disorder in the structure.

If, however, vacancies may move by next nearest neighbour jumps then both the intial and final lattice site occupied by the vacancy, upon making a jump, is of the same sublattice. Such a mechanism would thus confine motion within the sublattice of origin of the vacancy and would not result in any disordering. Furthermore, since

the atoms on one sublattice are all of the same species (assuming full order and considering the stoichiometric composition) the mechanism would not require the movement of a second species.

There is some support for next nearest neighbour jumps from the kinetics of ordering and disordering in B2 structures. If only nearest neighbour jumps are allowed, equilibrium long range order takes unreasonably long times to achieve, but when next nearest neighbour jumps are also allowed ordering occurs at a more realistic rate [48].

It has been suggested that as nearest neighbour vacancy motion is predominant in pure metals while in certain ionic compounds ions diffuse only along their respective sublattices, intermetallic compounds, whose bonding has both metallic and ionic characteristics, may follow both courses of action [60]. However calculations of energies of migration for various diffusion mechanisms in AgMg have indicated that the energies of migration of silver and magnesium sublattice vacancies by next nearest neighbour jumps (at 216·0 and 179·4 kj/mole respectively) are considerably higher than for nearest neighbour jumps (at 125·3 and 90·7 kj/mole respectively) [158]. This suggests that next nearest neighbour vacancy motion is energetically less favoured than nearest neighbour jumps, at least in AgMg of the B2 compounds.

2.9.2 Divacancy Motion

It is known, from structure symmetry requirements, that thermal vacancies are formed in twos. These thermal vacancies, one on each sublattice, may be associated in pairs and hence constitute a divacancy. However several constraints would arise from the diffusive movement of divacancies.

If divacancies moved by a nearest neighbour exchange mechanism they would introduce disorder into the structure in the same way as

the nearest neighbour movement of mono-vacancies. Furthermore, two vacancies which are nearest neighbours (and so constitute a divacancy) cannot each move into nearest neighbour sites and still remain in their mutual nearest neigbour configuration. In other words the divacancy would dissociate upon making a jump.

A divacancy might however move by next nearest neighbour jumps, in which case it could move without dissociating or causing disorder. Such a mechanism might be favoured, in preference to a next nearest neighbour motion of single vacancies, if a divacancy could move through the saddle point (the activated complex state) between two equilibrium positions more easily than a single vacancy.

Calculations have been made to evaluate the energy of divacancy motion in AgMg. It has been found that magnesium atoms may exchange positions with next nearest neighbour vacancies (on the Mg-sublattice) quite readily. However a silver atom in moving to exchange positions with a next nearest neighbour silver vacancy (of a divacancy) becomes trapped at the saddle point, in the site of the nearest neighbour magnesium vacancy (of the divacancy). In other words the silver atom makes a nearest neighbour jump, onto the magnesium sublattice, in preference to the longer next nearest neighbour jump entirely within the silver sublattice. Only one of the two species can exchange freely with its own vacancy while the other becomes trapped and divacancy motion by mext nearest neighbour jumps is arrested [158] ; diffusion cannot occur by next nearest neighbour divacancy motion.

Finally the trapping of a silver atom at the site of a magnesium vacancy in attempted divacancy motion results in the degeneration of the divacancy into two silver vacancies and a silver anti-structure atom. This triple lattice point (defect) configuration in AgMg is similar to the triple defects postulated in NiAl and NiGa [145, 143] .

2.9.3 Correlated Vacancy Motion Mechanisms

In a highly ordered (B2) structure the number of nearest neighbour jumps possible which can cause disorder greatly exceeeds the number which would result in re-ordering. Hence the probability of a disordering jump occuring is far greater than the probability of an ordering jump if random nearest neighbour vacancy motion is allowed.

Nevertheless nearest neighbour motion can occur under the constraint that the disordering jumps are balanced by order restoring jumps such that the overall degree of order remains unchanged. While the passage of a single vacancy through the ordered structure by nearest neighbour jumps would result in disorder, a second vacancy following in the wake of the first along the same path can restore order. The second vacancy need not be closely associated with the first and may originate from the same or the opposite sublattice to that of the first, in any event order would be restored. Indeed a single specific vacancy may introduce disorder and then restore order by traversing a cyclic path such that a net mass transport would be affected without any change in the overall degree of order.

The simplest case of a cyclic path is that of an atom exchanging with a vacancy, thereby causing disorder, followed by the reverse jump which re-establishes order. In this case no net atomic flow occurs.

One example of a cyclic path where no net disordering occurs but mass transport is affected is the six jump cycle [33, 78] . There are three distinct geometric forms of the six jump cycle possible in the B2 structure [see FIG. 2.5] . One results in a net transport of a vacancy across a $\langle 110 \rangle$ face diagonal and is referred to as a [110] -type cycle. The other two forms result in a net transport of a vacancy across a $\langle 100 \rangle$ cube edge. One of these cycle paths lies entirely in one plane and is known as the straight [100] -type, while the other follows a folded path and is known as the bent [100] -type cycle [158] .

In all three cycles, the first three vacancy jumps displace atoms onto the wrong kind of site with an accompanying disorder and increase in energy of the system. The latter three jumps progressively restore order. The [110] -type site results in a greater net displacement distance of the vacancy than either of the other two varieties. This suggests that unless the activation energies of the three cycles are different the [110] -type cycle which yields the fastest diffusion rate (largest displacement) is likely to be rate controlling.

In AgMg an analysis of the activation energies of the jumps involved in a six jump cycle has shown that the mechanism has a lower activation energy than either the divacancy or mono-vacancy next nearest diffusion mechanisms, despite the high ordering energy of the compound [158] . Furthermore, the activation energy of diffusion for each species was found to depend on the geometric form of the six jump cycle.

The minimum energy for silver diffusion corresponded to a [110] -type cycle, while magnesium diffusion favoured the bent [100] -type cycle. These findings suggest that a complete closed six jump cycle is unlikely in AgMg but that isolated nearest neighbour jumps occur through the compound in such a way that order is maintained. Such jumps can then be idealised as a six jump cycle [158] .

2.9.4 Theories of the Correlation of Diffusivities Arising from Nearest Neighbour Vacancy Motion

Analysis of the jump sequence involved in the six jump cycle [see Fig. 2.5] shows that atoms belonging to the sublattice on which the vacancy originates make two jumps, while those on the other sublattice make four jumps during the course of one complete cycle. Furthermore since the vacancy returns to its sublattice of origin, subsequent six jump cycles would perpetuate the same jump frequency

FIG 2.5.
THREE POSSIBLE FORMS OF
THE SIX-JUMP CYCLE

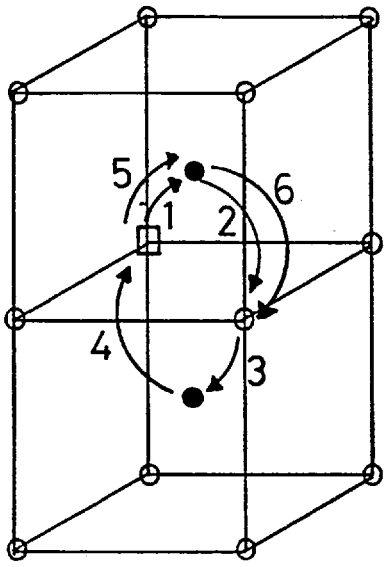

THE {110} CYCLE

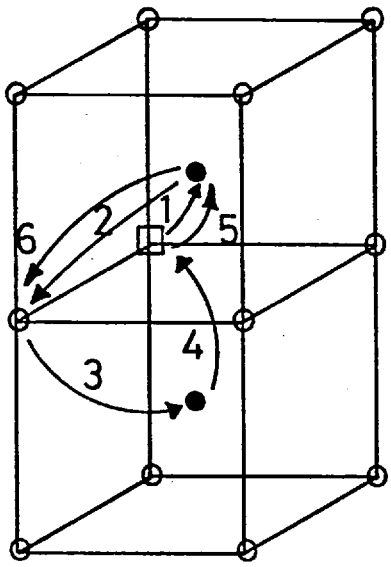

THE BENT {100} CYCLE

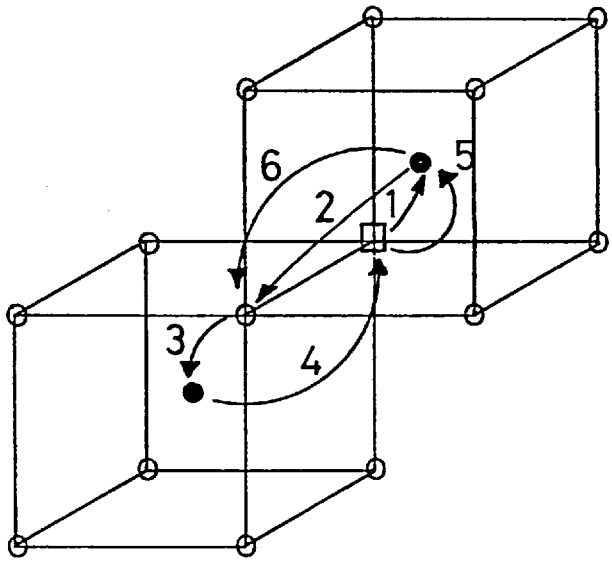

THE STRAIGHT {100} CYCLE

= VACANCY

= A ATOM

= B ATOM

ratio of the two diffusing species. In other words, the species from whose sublattice the vacancy originated would have half the diffusivity of the species on the other sublattice.

In fact, at stoichiometry, equal numbers of thermal vacancies might be expected to exist on either sublattice (the two vacancy defect) and the ratio of the two diffusivities would then tend to unity. However it is known that the constitutional defect structure in B2 compounds (which may include vacancies) varies with the degree of non-stoichiometry [13, 145] . Additionally thermal defect equilibria vary with both composition and temperature [see sections 2.4.4 and 2.4.5] and consequently the assumption of equal numbers of vacancies being present on each sublattice, even at stoichiometry is likely to be invalid. Thus the ratio of the diffusivities of the two species may not be unity and will probably vary with both composition and temperature.

Calculations based on a six jump cycle mechanism have suggested that for the stoichiometric AB alloy the diffusivities ratio should lie in the range [40, 39] :

$$3/2 \geqslant D_A/D_B \geqslant 2/3$$

Diffusivity ratios falling within these limits have been observed in the B2 compounds AgMg [34] , AuCd [78] and CuZn [95] and have been concluded to be indicative of a six jump cycle mechanism being diffusion rate controlling. However the correlated motion required for nearest neighbour vacancy diffusion in B2 compounds makes it difficult to assess the value and significance of an experimentally determined diffusion coefficient of one of the constituent elements in isolation, and to relate it to fundamental atomic motion.

A maximum path probability method has been developed and applied to diffusion in the B2 compound AB [83, 84, 85, 86] . The theoretical model made no assumptions concerning any correlation between the diffusivities of species. The model did assume that diffusion occured exclusively by nearest neighbour atom-vacancy exchanges and considered the motion of four species; A, B and B* (an isotope of B) atoms and vacancies.

The model yielded an expression for a diffusion coefficient change variable ($\hat{D}_B$) which was related to the diffusion coefficient D_B. The importance of $\hat{D}_B$ lay in the fact that it permitted changes in the diffusion coefficient D_B to be expressed in terms of changes in composition and concomittant changes in order, bond energies and defect distributions. The relation between $\hat{D}_B$ and D_B was given by the expression [86] :

$$\hat{D}_B = D_B / c\, W_B \qquad 2.33$$

where the factor c involved such variables as lattice parameter, path probabilities, ordering parameters, bond energies and temperature. The factor W_B in equation 2.33 is the jump probability for a unit jump of a B atom into an adjacent vacancy and was assumed to be inherent to the B atom, independent of surroundings. The jump probability W_B may be expressed in terms of the standard relation:

$$W_B = \Theta_B \exp(-\frac{U_B}{kT}) \qquad 2.34$$

where Θ_B is the vibrational contribution to the jump frequency and U_B is the jump activation energy of a B atom.

The model was then used to calculate the compositional dependence

of the diffusion coefficient $\hat{D}_B$ as a function of three major parameters, Θ, U and T_R which will be considered presently. Additionally thermal vacancy concentrations on either sublattice could be evaluated as a function of compound composition for various values of these three parameters. Two examples, taken from the data of Kikuchi & Sato (1969) [86] are shown in Fig. 2.6, A and B.

The three parameters were defined by the expressions:

$$\text{(i)} \qquad \Theta = \frac{W_B}{W_A} = \frac{\Theta_B \exp(-U_B/kT)}{\Theta_A \exp(-U_A/kT)} \qquad 2.35$$

where W_B has been defined in equation 2.34 and W_A obeys a similar relation.

$$\text{(ii)} \qquad U = (\varepsilon_{BB} - \varepsilon_{AA})/\varepsilon \qquad 2.36$$

where ε is given in turn by the expression

$$\varepsilon = (2\varepsilon_{AB} - \varepsilon_{AA} - \varepsilon_{BB})$$

The factors ε_{AB}, ε_{AA}, ε_{BB} are the bond energies of the (A-B), (A-A) and (B-B) bonds respectively.

$$\text{(iii)} \qquad T_R = T/T_C \qquad 2.37$$

where T is the ambient temperature and T_c the critical ordering temperature.

The effect of these three parameters was detailed as follows:

(a) The effect of Θ

In a disordered binary solid solution, two processes compete in the vacancy mechanism of diffusion: the jumping of an A atom into an adjacent vacancy with the probability W_A and the jumping of a B atom with the probability W_B. The diffusion constant D then depends on

FIG 2.6. A & B CALCULATED VACANCY CONC$^{n.}$ vs. COMPOSITION

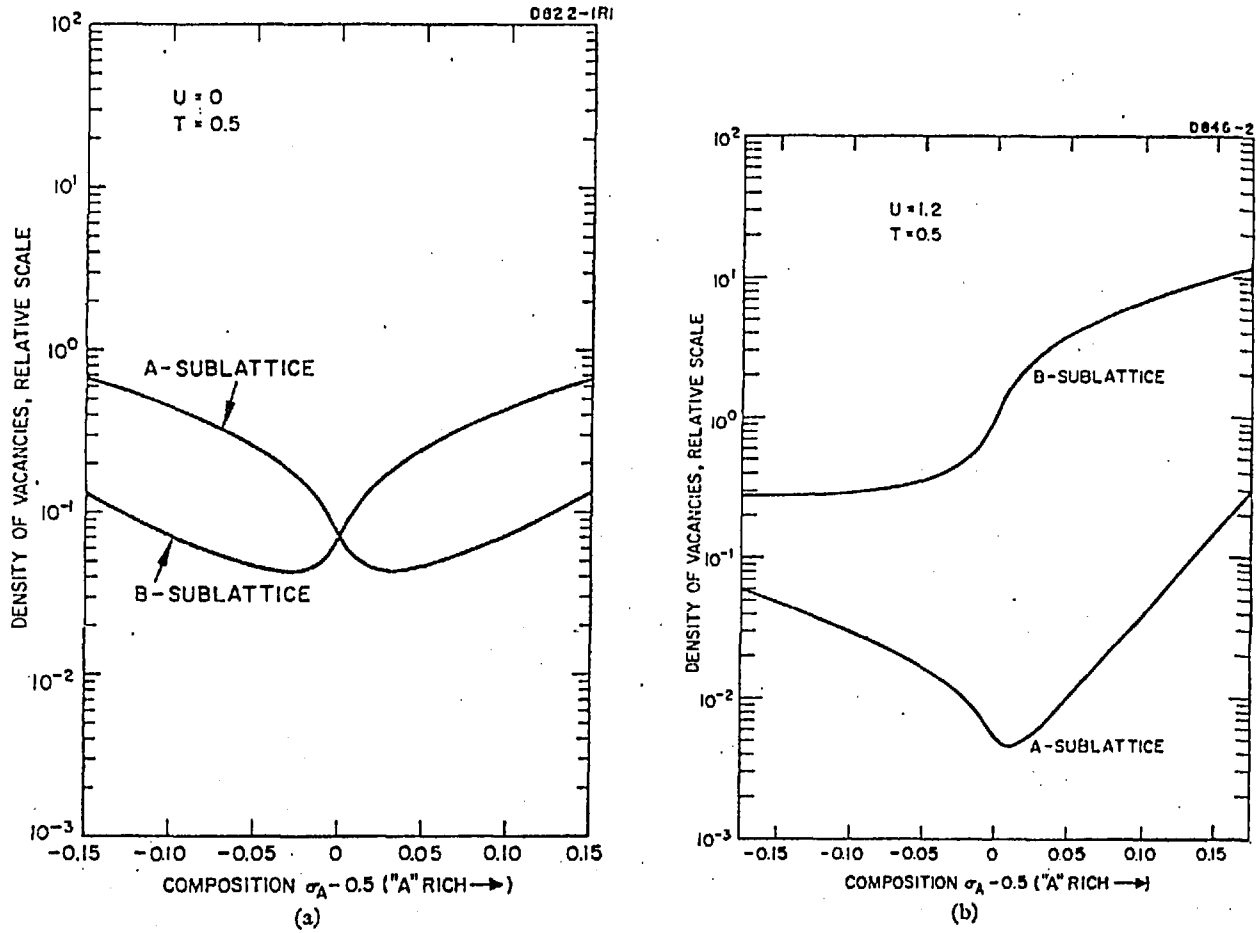

data from ref. 86

FIG. 5. Distribution of vacancies on the two sublattices in an ordered alloy.

these two mechanisms in a rough qualitative manner in the form [86] :

$$D \propto W_A W_B/(W_A + W_B) \qquad 2.38$$

From this expression it was deduced that since both A and B atoms move for diffusion to occur, the slower species determined the rate of diffusion. The diffusion coefficient D_B depends qualitatively on W_A and W_B in a similar manner but the diffusion coefficient change variable $\hat{D}_B$ (see equation 2.33) is a function of D_B divided by W_B. The qualitative dependence of $\hat{D}_B$ should have the form:

$$\hat{D}_B \propto \left(\frac{W_A}{W_A + W_B}\right) = (1 + \theta)^{-1} \qquad 2.39$$

Thus if $\theta \ll 1$, $\hat{D}_B$ is not very dependent upon θ, and for $\theta > 1$, $\hat{D}_B$ decreases as θ increases. The general behaviour of $\hat{D}_B$ as a function of composition for various values of θ is shown in Fig. 2.7, A & B.

(b) The effect of U.

The difference between ε_{AA} and ε_{BB} does not influence the ordering behaviour in the equilibrium state since the latter is a function of only (see equation 2.36). However, the value of U affects kinetic processes very sensitively. The curves in Fig. 2.8 show that as U decreases, (B-B) bonds become easier to break and thus $\hat{D}_B$ increases on the B-rich side of stoichiometry. At the same time, as U decreases the (A-A) bonds become harder to break; the decrease of $\hat{D}_B$ with decrease in U for A-rich compositions reflects the greater number of (A-A) bonds in such compositions.

(c) The effect of T_R

The effect of T_R was primarily on the degree of order present in the structure. In the limiting case of total disorder the diffusion coefficient became dependent upon the jump probability of the slower

FIG 2.7 A & B EFFECT of Θ PARAMETER on DIFFUSIVITY ($\hat{D}_B$)

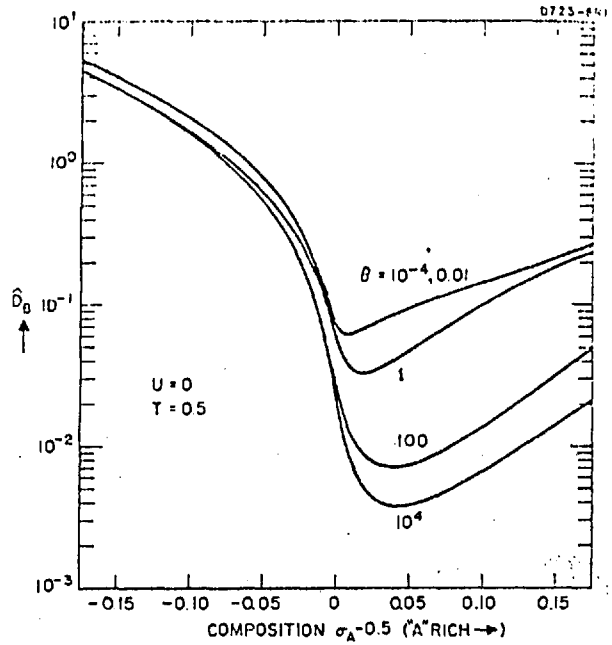

(a)

data from
ref. 86

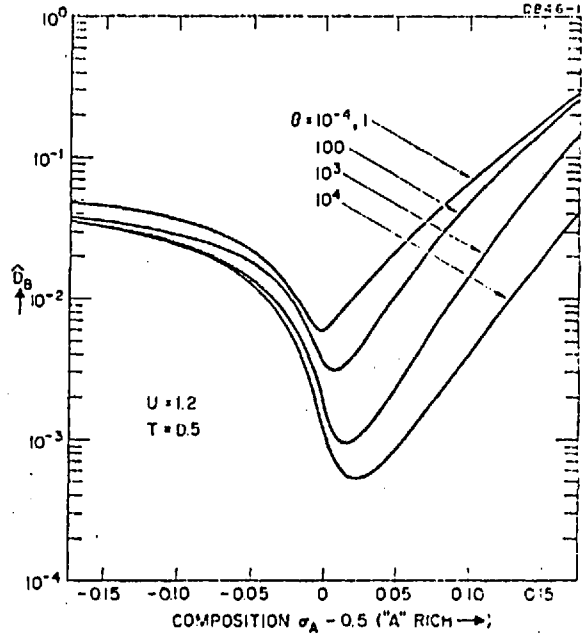

(b)

FIG. 4. Dependence of the isotope diffusion coefficient $\hat{D}_B$ on the parameter θ.

FIG 2.8 EFFECT of PARAMETER U on DIFFUSIVITY ($\hat{D}_B$)

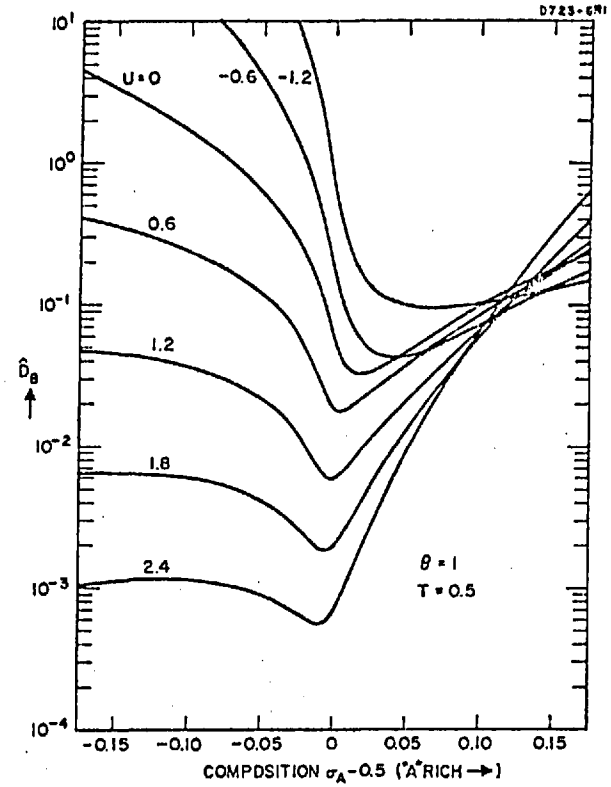

FIG. 7. Dependence of the isotope diffusion coefficient on the parameter U.

data from ref. 86

moving species [see equation 2.38] and did not vary greatly with composition. The curves of Fig. 2.9 (A & B) reflect this trend of a smaller compositional dependence with increasing temperature.

The fact of a compositional dependence of the coefficient $\hat{D}_B$ was explained for the symmetrical case of $\Theta = 1$ (so that $W_A = W_B$) and $U = 0$. The jump of an atom to an adjacent vacancy became harder when more (A-B) bonds had to be broken in the process. In consequence atomic migration was easier in non-stoichiometric compositions which were more disordered and hence contained fewer (A-B) bonds than the stoichiometric compound. The diffusion coefficient $\hat{D}$ had a V-shaped compositional dependence with a minimum at stoichiometry.

In fact the curve was found to be asymmetrical with the minimum occuring to the A-rich side of stoichiometry. This occured because more (A-B) bonds had to be broken on the A-rich side than on the B-rich side of stoichiometry in order for B^* atoms to move. Secondly it was known that fewer vacancies were present on the A-sublattice in A-rich alloys than in B-rich alloys [see Fig. 2.6, A] . Thus the jump of a B^* atom into a vacancy on the A-sublattice was considered to be rate controlling because it required the breaking of more (A-B) bonds than the reverse jump into a B-sublattice vacancy. Consequently the migration of B^* atoms became harder on the A-rich side of stoichiometry.

It is evident that from a similar argument, the migration of A^* atoms will show a minimum in the compositional dependence of $\hat{D}_A$ displaced to the B-rich side of stoichiometry.

Finally the theory was applied to evaluate the diffusivities ratio (D_B/D_A) and examine how much information the ratio may yield concerning the diffusion mechanism. The two diffusion coefficients were expressed by the relations:

FIG 2.9 A&B EFFECT of TEMPERATURE PARAMETER T_R on DIFFUSIVITIES ($\hat{D}_B$ & $\hat{D}_A$)

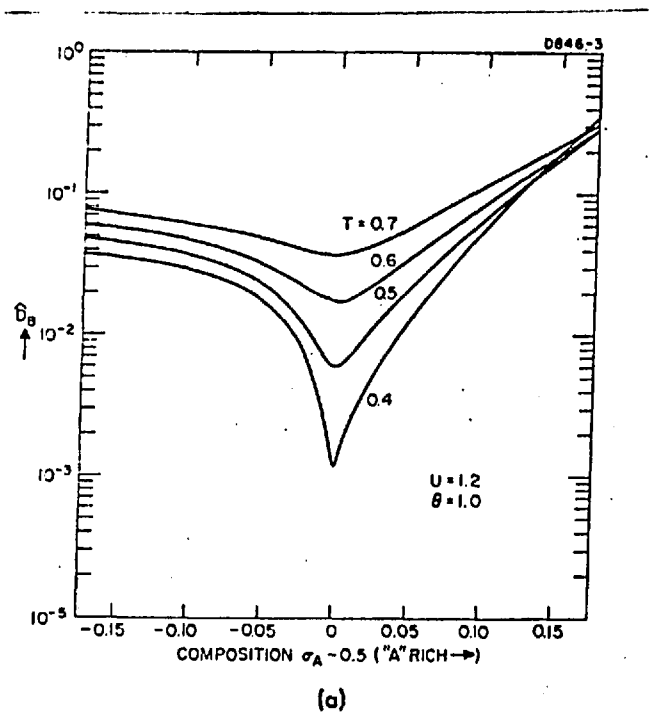

data from

ref. 86

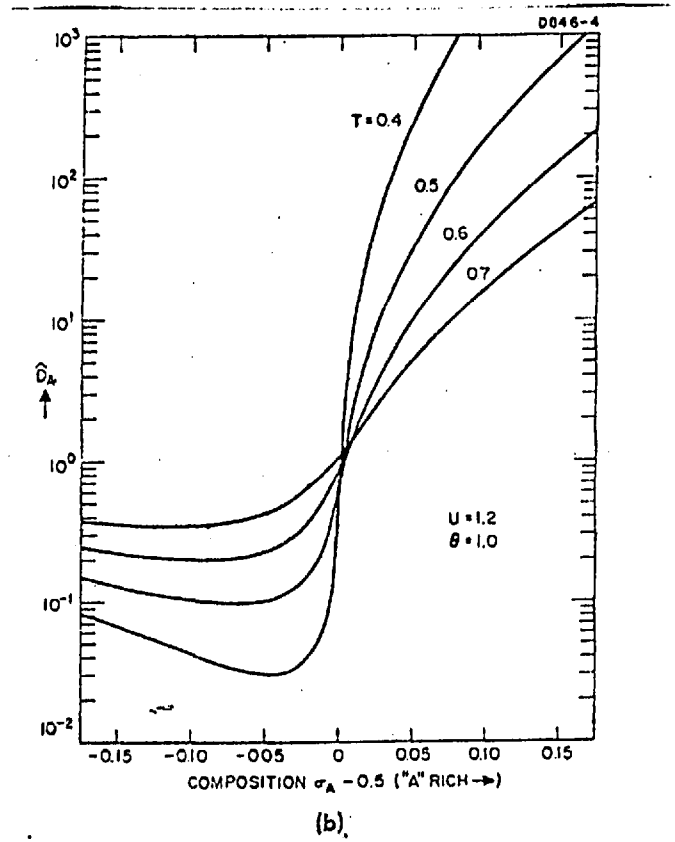

FIG. 8. The isotope diffusion coefficients of (a) B atoms and (b) A atoms in an ordered alloy.

FIG 2.10 RATIO of the DIFFUSION COEFFICIENTS (D_B / D_A) vs. COMPOSITION

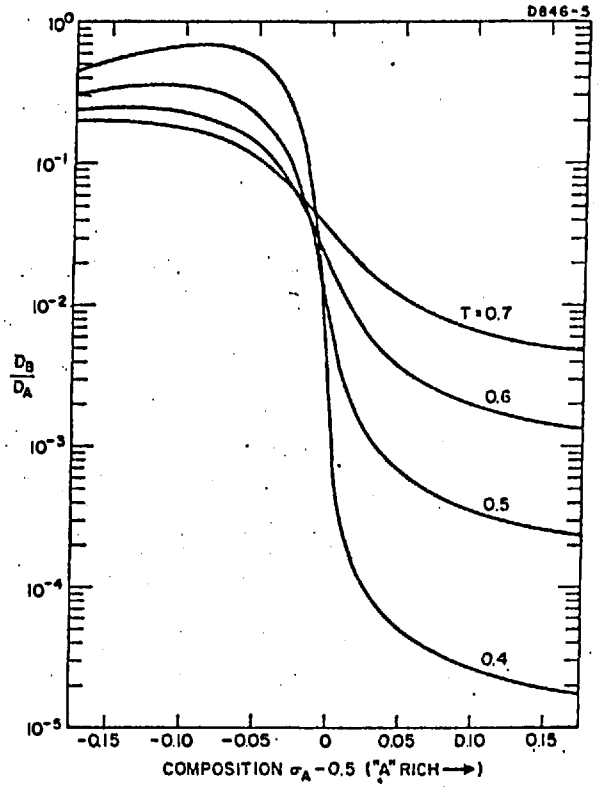

FIG. 9. The ratio of the two diffusion coefficients D_B/D_A derived from Fig. 8.

data from FIG 2.9. A & B

ref. 86

$$D_B = W_B \; f(N_A - N_B,\ U,\ \theta,\ {}^{1}/_{kT})$$

$$D_A = W_A \; f(N_B - N_A,\ -U,\ \theta^{-1},\ {}^{1}/_{kT}) \qquad 2.40$$

where the functions $f(N_A - N_B, \ldots)$ and $f(N_B - N_A, \ldots)$ are equivalent to $(c\hat{D}_B)$ and $(c\hat{D}_A)$ respectively [see equation 2.33] , and N_A and N_B are the concentrations of A and B respectively.

In many experiments it has been found that:

$$D_A/D_B = 1 \quad \text{when } N_A = N_B \qquad 2.41.$$

This relation occurs when U = 0 and θ = 1 which is the condition tacitly assumed in the analyses of Elcock and McCombie (1958) [40] . However, equation 2.41 does not require the assumption of U=0, θ=1 since other combinations of these two parameters may also make the equation valid [86] . In fact it was concluded that the validity of equation 2.41 did not necessarily support any particular diffusion mechanism. The curves of Fig. 2.10 shows the diffusivities ratio $({}^{D}B/D_A)$ as a function of composition for data taken from Fig. 2.9 (A & B).

In conclusion the model was used to predict the compositional dpendence of the diffusion coefficient (D_{Ag}) in AgMg and compared with the experimental data of Domian & Aaronson (1964) [33] and Hagel & Westbrook (1961) [61] and found to be in good agreement.

2.9.5 Correlated Diffusivities - a Summary

Analysis of diffusion by nearest neighbour vacancy motion in B2 compounds has led to the suggestion that diffusivities of the two species will be correlated.

One particular correlated mechanism suggested to be rate controlling in such compounds was the six jump cycle [33, 78] which imposed the

restriction [40, 39] that:

$$3/2 \geqslant D_A/D_B \geqslant 2/3$$

A more rigorous analysis by a path probability method indicated that the diffusion coefficient of either species was dependent largely on three variables; Θ which was a relative jump probability factor, U which was a measure of bond energies and T_R which was a reduced temperature [86] .

The theory predicted that the compositional dependence of the diffusion coefficient $\hat{D}_B$ (or $\hat{D}_A$) varied markedly with the value of the U parameter. Furthermore large differences between the compositional dependencies of the two diffusion coefficients $\hat{D}_B$ and $\hat{D}_A$ were possible especially for values of U and Θ not equal to zero and unity respectively. The theory also indicated that the diffusivities ratio (D_A/D_B) could vary markedly with composition, temperature and the values of U and Θ. It was concluded that particular values of the diffusivities ratio (e.g. in the range predicted by the six jump cycle) were not necessarily indicative of any particular mechanism.

A particular problem not covered by the path probability theory [86] was the case of large numbers of constitutional vacancies since only anti-structure atom defects were considered and the total vacancy concentration was assumed small at all times. It seems likely that constitutional vacancies may result in even less need for diffusivity correlation within the range envisaged for the six jump cycle mechanism.

2.10 Creep

2.10.1 The Phenomenon of Creep

Creep is the continuing plastic deformation of a material when subjected to a constant stress at constant temperature. The rate at which such deformation occurs, known as the creep strain rate ($\dot{\varepsilon}$), may be used as a measure of the performance (creep resistance) of a material under given conditions.

Under constant test conditions the creep strain rate has been found to vary with time. Apart from the instantaneous strain which accompanies initial loading a total of three distinct time dependent regions of the creep rate have been identified between initial loading and the failure of a material. The first region, called primary creep, is generally characterised by a high creep rate which diminishes with time, gradually approaching a constant value. In the second region, called steady state creep, the creep rate is constant and independent of time (and hence also of creep strain). Finally in the third region, called tertiary creep, the creep rate accelerates with time until cracking and subsequent failure of the material occurs. Under real conditions one or more of the time dependent regions described above may be missing, depending upon the stress and temperature.

It has been suggested [36] that since during creep a constant stress does not produce an indefinately increasing creep rate, some internal friction mechanism must operate within the material to limit the deformation rate to a certain value. Three classes of mechanism which could account for creep behaviour have been postulated [36] :

(i) True frictional forces so that the creep rate is controlled by viscous flow.

(ii) Thermally activated processes.

(iii) Quantum tunnelling effects.

The majority of creep experiments indicate behaviour consistent with thermally activated processes, which generally involve the (thermally activated) migration of dislocations, grain boundary shearing and diffusion of vacancies [112] . Furthermore, because of the great versatility of dislocations and the numerous interactions they may undertake with one another, additional lattice defects, and various substructural details, a number of different dislocation mechanisms can control creep.

Much of work done in formulating theories to account for creep behaviour has been concentrated on steady state creep. Many empirical equations have been proposed to describe the dependence of the creep rate ($\dot{\varepsilon}$) on such parameters as stress (τ) and temperature (T) and attempts have been made to rationalise these equations in terms of specific atomic deformation processes.

2.10.2 Variables Affecting Creep

Macroscopically the creep strain rate is known to depend upon both the stress and temperature. On the atomic scale this reflects the mobility of dislocations as a function of stress and temperature. However the stress and temperature dependence of dislocation motion is itself a function of the type and concentration of dislocations present, the planes on which they move and the interactions they undergo among themselves and with other lattice defects.

In other words a primary consideration in evaluating the creep behaviour of a material is a knowledge of its crystal structure and the dislocation mechanisms involved in its deformation.

In pure metals and random solid solutions the dislocations present are unit dislocations. These are known to dissociate into partial dislocations separated by stacking fault in the case of f.c.c.

materials [76, 126]. It has also been reported that the core of a dislocation in a b.c.c. material may be dissociated to a certain extent [76, 92]. The extent of the dissociation of a unit dislocation into partials plus a region of stacking fault is governed by the elastic modulus and the stacking fault energy on the slip plane (in which the unit dislocation lies) [24].

In the case of ordered alloys, superlattice dislocations occur which may dissociate into unit dislocations separated by a region of antiphase domain boundary. The unit dislocations may themselves become extended (dissociated). For example, in an AB_3 (f.c.c.) superlattice the (superlattice) dislocation consists of two extended (unit) dislocations separated by an antiphase domain boundary [110]. The actual equilibrium separation between the four partials depends upon the energy of the stacking fault and the energy of the antiphase domain boundary which in turn depends upon the degree of order.

The importance of extended dislocations in respect of creep properties lies in the fact that such dislocation motion mechanisms as thermally activated cross-slip or diffusion controlled dislocation climb would result in the introduction of additional faulted material unless the extended dislocations were first constricted. Hence the creep activation energy may include a constriction energy term and the creep rate may depend upon the elastic modulus, the stacking fault energy and the ordering energy.

In general, alloying has been found to significantly affect (lower) the creep rate in materials. Three mechanisms have been proposed to account for this [52]:

(i) the reduction of dislocation mobilities

(ii) the 'pinning' of dislocations by solute 'atmospheres'

(iii) the stabilisation of dislocation arrays by slowing climb and

recovery.

Each of the three mechanisms reflect the changes in such factors as bonding energies, stacking fault energies, elastic constants and diffusivities which occur upon alloying.

Another factor which has been found to affect the steady state creep rate is the subgrain size which is developed during testing, and which although independent of temperature, depends upon stress. Consequently, the effect of stress may not be easily separated from the effects of coincident substructural changes [112].

In addition the substructure developed during creep is not an unique function of the creep strain, for the same strain may be produced by a low density of highly mobile dislocations or by large numbers of slow moving dislocations. The substructure developed in either case is unlikely to be the same [36].

Finally the proportion of grain boundary shearing to the total creep strain increases with decreasing stress. Since the former may have a different stress dependence of the strain rate compared to bulk deformation the overall effect would be to produce a stress sensitive stress dependence of the creep rate [36, 112, 52].

It is apparent that many parameters, some external (e.g. stress and temperature) and some intrinsic to the material (e.g. elastic constants) may affect the creep strain rate and that their effects may be inter-related and possibly not separately resolvable.

2.10.3 The General Equation Describing Creep

Experimental evidence shows that creep flow is thermally activated; local thermal activation provides added energy, beyond that supplied mechanically, to dislocations to enable them to overcome barriers to

their movement. The applied stress aids in overcoming these barriers and imparts a direction to the resultant flow.

A generalised function relating the creep rate ($\dot{\varepsilon}$) to the stress (σ), the temperature (T) and the structure (S) for a given deformation mechanism (i) has been developed from the theory of thermodynamic fluctuations. The relation is given by the expression [36, 51] :

$$\dot{\varepsilon} = \sum_i Z_i(\nu, T, S)\, \sigma_i(T, S) \exp\left[- \frac{\Delta H_i(T, S)}{RT} \right] \qquad 2.42$$

where the function Z_i may depend upon the temperature (T) and contains the normal frequency for unit flow (ν), the entropy change upon deformation ($\exp \Delta S_i/R$) and a structure term (S). The stress function σ_i may depend upon temperature and structure. The factor ΔH_i is the activation enthalpy of the i^{th} process governing the creep rate and may be temperature and structure dependent.

In fact it has been found that the same creep mechanism can appear to give rise to a different creep response in different materials. This has led to the normalisation of stresses and temperatures so that creep data for various materials may be more readily compared. Normalised temperature may be defined as the ratio of the test temperature to the melting temperature (T/T_M) while normalised stress is the ratio of the applied stress to the elastic shear modulus (σ/μ). As a result of this development similar creep mechanisms in different materials could be compared under a unified scheme for widely different test conditions.

It has also been found that in general above 0·5 T_M a single deformation mechanism may be rate controlling and an unique activation energy can be evaluated. Below 0·5 T_M several mechanisms may contribute to the creep rate and the apparent activation energy is then a weighted

mean of these contributions and may vary with temperature. This has led to a distinction between high and low temperature creep mechanisms with the former generally diffusion controlled while the latter are not diffusion controlled.

The complementary nature of the relation of stress and temperature in providing the energy required to surmount barriers to creep deformation has also resulted in the idea of high and low stress conditions.

Finally it has been found that particular groups of creep mechanisms predominate in each of the four areas of creep conditions (namely high and low temperatures and high and low stresses) although there is considerable overlap between them [150].

2.10.4 The Stress Dependence of Steady State Creep

The stress dependence of the creep rate can usually be expressed by one of the following three relations [130]:

(i)	The Linear Law	$\dot{\varepsilon} = A\sigma$	
(ii)	The Power Law	$\dot{\varepsilon} = A'\sigma^{n}$	2.43
(iii)	The Exponential Law	$\dot{\varepsilon} = A'' \exp B\sigma$	

In fact all three relationships have been expressed in terms of a single function [50]:

$$\dot{\varepsilon} = A'''(\sinh \alpha\sigma)^{n} \qquad 2.44$$

where various values of the constants A''', α & n result in equation 2.44 reducing to one of the three simple stress laws.

Each of the three stress laws pertains to a different stress level and as applied to high temperature (diffusion controlled) creep it has been found that typically the linear law is valid for low stress levels where $(\dot{\varepsilon}/_{D} < 10^{2})$.

The power law has been found to apply for intermediate stress levels where $(10^2 < \dot{\varepsilon}/_D < 10^9)$, while the exponential law has been found valid for $(\dot{\varepsilon}/_D > 10^9)$ [130]. The factor D is the diffusion coefficient.

As a rule most experimental creep tests comply with the conditions of the intermediate stress level where the power law is valid. The stress exponent n (equation 2.43) is generally substantially constant over a wide range of stress and temperature. The factor A' is independent of stress but is a function of temperature (cf. equation 2.42).

The value of the exponent n generally falls between about 3 and 7 for various solid solutions and pure metals [112]. However values as high as 10·5 have been found, for example, in the intermetallic compound NiAl [159] and even higher values (n = 40) have been reported for the creep of thoriated nickel [156] although the physical significance of such unusually high values is not clear.

The stress exponent (n) has been found to be higher at high stresses than expected from extrapolations of lower stress data, in keeping with the trend towards an exponential stress dependence with increased stress [130]. Additionally it has been found that the transition from a linear stress dependence to a power law is shifted to higher values of $(\dot{\varepsilon}/_D)$ and stress (σ) when the grain size is decreased below $\sim$0·1 mm [130]. Furthermore the stress exponent n has been found to show an increasing trend with increasing grain size [52, 53], which may reflect a higher stress sensitivity in bulk deformation as opposed to grain boundary shearing.

More recent reviews have suggested that the observed variations in n for metals show no systematic relationship with crystal structure, grain size, stacking fault energy or any other known factor [112].

In conclusion, the stress dependence of the creep rate has been found to obey a number of empirical laws, the most widely applicable of which is the stress power law. There is currently no clear relationship between the stress exponent n and other material parameters.

2.10.5 The Temperature Dependence of Steady State Creep

Creep is generally controlled by thermally activated processes and as such the temperature dependence of the creep rate may be expressed [112]:

$$\dot{\varepsilon} = f(\sigma) \exp(-\frac{Q_c}{RT}) \qquad 2.45$$

where the stress function $f(\sigma)$ is assumed independent of temperature and the apparent activation energy of creep Q_c, is independent of both stress and temperature.

Equations 2.43 and 2.45 may be combined to give the general relation:

$$\dot{\varepsilon} = K \sigma^n \exp(-\frac{Q_c}{RT}) \qquad 2.46$$

where K is some constant assumed independent of both stress and temperature.

The apparent activation energy of creep Q_c can be evaluated from equation 2.46 for creep tests carried out at constant stress over a range of temperature. If a single deformation process is rate controlling, a comparison of equations 2.42 and 2.46 shows that a single particular stress function σ^n (equal to σ_i) occurs and that the constant K is equal to the structure factor Z_i (divided by the entropy term). The apparent activation enthalpy of creep ΔH_c (equal to $Q_c - T\Delta S_c$) can then be identified unambiguously with the activation enthalpy ΔH_i of a single mechanism.

However when several mechanisms operate concurrently Q_c cannot be

related to any specific mechanism ΔH_i (see equation 2.42) but becomes some mean value of the activation energies of the mechanisms involved. Under these conditions Q_c is found to be both temperature and stress dependent.

It was mentioned earlier that different creep mechanisms are found to be deformation rate controlling for different temperature ranges; hence the distinction between high and low temperature creep behaviour. This infers that the activation energy of creep will change with temperature, although it may remain constant within the temperature range of a specific rate controlling mechanism.

In pure aluminium, for example, the temperature dependence of the activation energy of creep has been found to fall into three distinct ranges [130] . Between 0·5 and 1·0 T_M the activation energy of creep Q_c increases slightly with increasing temperature, and this is due to the fact that the elastic modulus decreases with increasing temperature (the modulus effect will be considered later). The creep activation energy in this range is found to be nearly equal to that of self-diffusion. Two rate controlling mechanisms have been postulated for this range, dislocation climb [149] and the nonconservative motion of jogs in screw dislocations [6] .

Between 0·3 and 0·4 T_M the activation energy is less than that for self-diffusion and the rate controlling process is believed to involve the cross-slip of dislocations [80] . While below about 0·3 T_M the activation energy of creep has been found to fall almost linearly with decreasing temperature. The rate controlling mechanism in this temperature range is thought to involve dislocation intersection processes [22] .

Similar work in copper [43] , cobalt [44] and tin [149,151] has in each case shown that the activation energy of creep increases with

increasing temperature until at high temperatures ($> 0.5\ T_M$) it becomes effectively independent of temperature and approximately equal to the activation energy of self-diffusion.

Data on both the activation energies of high temperature creep and self-diffusion in pure metals have been collated and compared by Dorn (1956) [35] and Garofalo (1968) [52]. It was found that in most cases there is good agreement between the two quantities. There were however some notable exceptions, usually found in the transition metals and those which exhibit anomalous diffusion behaviour. For example, in α-titanium, the activation energy of diffusion has been reported in the range 129·7 to 205·0 kj/mole (31 to 49 Kcal/mole) [9] while creep data give an activation energy of about 251·0 kj/mole ($\sim$ 60 Kcal/mole) [35].

In the case of alloys and compounds each constituent species has associated with it a diffusivity and diffusion activation energy. Consequently high temperature creep may show more than one diffusion dependent activation energy. Alternatively one species (in a compound) may diffuse by a different mechanism in different temperature ranges so resulting in more than one diffusion activation energy (for the same species). Thus creep may be controlled by the diffusion of one species and yet show more than one diffusion dependent creep activation energy. This has in fact been observed in NaCl [130]. Between 0·5 and 0·75 T_M the activation energy of creep is about equal to that for chlorine ion diffusion in high dislocation density single crystals. Between 0·75 - 0·95 T_M the activation energy for creep is equal to that for chlorine ion diffusion, when not controlled by the presence of divalent cation impurities, and so represents intrinsic behaviour.

Some diffusion and high temperature creep activation energies, for a number of ordered alloys, are shown in TABLE XII. These data will be considered in detail in the discussion (see chapter 5, section 5.4).

TABLE XII Creep(Q_C) & diffusion(Q_D) activation energies in some intermetallic compounds

COMPOUND	DIFFUSING SPECIES	Q_D KJ/Mole	REF	Q_C KJ/Mole	REF
Cu Zn	Cu *	150·6			
	Zn	150·6	95	160	69·73
	Cu †	92·0			
	Zn	78·7	95	97·91	73
Fe Co	Fe *	556·5			
	Co	556·5	164	690·4	73
	Fe †	230·1			
	Co	251·0	164	395·4	73
Ni_3Al	Ni	300·1–306·1	64	686·2	91
$Ni_3(Al\ Ti)$	Ni	295·5–266·7	64	556·5	147
Ag Mg	Ag	138·9–188·7	33,34 61,62		
	Mg	198·7	34	212·5	116
Ni Al	Ni	177·8–307·1	65	231·5–306·0	159
Ni Ga	Ni	143·1–175·3	THIS	194·3–288·6 A	THIS
	Ga	146·5–222·0	STUDY	164·7–262·3 B	STUDY

* = ORDERED ALLOY A = 800K CREEP SERIES
† = DISORDERED ALLOY B = 1000K CREEP SERIES

In summary the temperature dependence of steady state creep may be outlined by the following points:

(i) Creep is a thermally activated process and as such shows an 'Arrhenius relation' temperature dependence. Consequently apparent activation energies of creep may be evaluated.

(ii) Different deformation mechanisms may be creep rate controlling at different temperatures; those with the highest activation energies being rate controlling at the highest temperatures. Consequently the apparent activation energy of creep may be temperature dependent.

(iii) In general at high temperatures ($> 0.5\ T_M$) a single (diffusion controlled) deformation mechanism is creep rate controlling so that the activation energy of creep may be identified with that of a specific flow mechanism.

(iv) In pure metals the activation energy of high temperature creep is found to equal that of self-diffusion. In alloys and compounds there is a multiplicity of diffusion activation energies and diffusion controlled creep may thus have several activation energies.

2.10.6 Effect of Elastic Moduli and Stacking Fault Energies on Steady State Creep

It has been found that the steady state creep rates among various metals and alloys can be more effectively correlated if a normalised stress (σ/G) [see section 2.10.3] is used in place of the applied stress (σ) in the general expression for the creep rate (equation 2.46). The new relation becomes [112] :

$$\dot{\varepsilon} = K' \left(\frac{\sigma}{G}\right)^n \exp\left(-\frac{Q_c}{RT}\right) \qquad 2.47$$

where G is the shear modulus of elasticity.

However equation 2.47 is not dimensionally correct and does not fully reflect the requirements for thermally activated processes. A more appropriate relationship has been suggested, given by the expression [112] :

$$\dot{\varepsilon} = K''\left(\frac{\sigma}{G}\right)^{n-1}\left(\frac{\sigma\Omega}{kT}\right)\exp\left(-\frac{H_c}{RT}\right) \qquad 2.48$$

where the factor $\left(\frac{\sigma\Omega}{kT}\right)$ indicates the fact that the expected exponential stress dependence of the activation energy of creep Q_c reduces to the linear case; Ω is the activation volume and H_c the activation enthalpy of creep.

Good agreement is found between H_c and H_D (the activation enthalpy for self-diffusion) for high temperature creep in pure metals. In fact on the assumption that high temperature creep is invariably diffusion controlled, steady state creep rates may be given by the expression [112] :

$$\dot{\varepsilon} = K''' \left(\frac{\sigma}{G}\right)^{n}\left(\frac{Gb}{kT}\right) D \qquad 2.49$$

where D is the diffusion coefficient and b the Burger's vector.

A second factor which may effect the creep rate is the stacking fault energy (γ). Thus in pure polycrystalline f.c.c. metals the creep rate has been found to follow the expression [7] :

$$\dot{\varepsilon} = A\, D\, \gamma^{3.5}\left(\frac{\sigma}{E}\right)^{5} \qquad 2.50$$

where A is a constant and E is Young's modulus. The exponent of the stress term in equation 2.50 was a mean value of the stress exponent n (assumed to be constant for all metals).

But equation 2.50 has been criticised because of the physically unacceptable implication that creep rates would be infinite for metals with infinite stacking fault energies. A modified version of equation 2.50 has been proposed by A. Mukherjee et al. (1968) [112] :

$$\dot{\varepsilon} = A D \left(\frac{Gb}{kT}\right) \phi \left\{\frac{\gamma}{Gb}\right\} \left(\frac{\sigma}{G}\right)^n \qquad 2.51$$

where A is some constant and $\phi\left(\frac{\gamma}{Gb}\right)$ is a function of the stacking fault energy (γ), the shear modulus (G) and the Burger's vector (b).

Nevertheless, returning to equation 2.50 it has been shown that [130] :

$$Q_c = -\frac{Rd \ln \dot{\varepsilon}}{d^1/T} = -\frac{Rd \ln D}{d^1/T} + \frac{5Rd \ln E}{d^1/T} - \frac{3{\cdot}5\ Rd \ln \gamma}{d^1/T}$$

But the term ($-Rd \ln D/d^1/T$) is equal to Q_D, the activation energy of self-diffusion. Hence:

$$Q_c = Q_D + \frac{5Rd \ln E}{d^1/T} - \frac{3{\cdot}5\ Rd \ln \gamma}{d^1/T} \qquad 2.52$$

It can be seen from equation 2.52 that the apparent activation energy of creep may be dependent upon both the elastic modulus and the stacking fault energy through a temperature dependence of these two parameters. In general the stacking fault energy is assumed independent of temperature while the elastic modulus falls with increasing temperature and hence $Q_c > Q_D$, although the effect is usually small. In ordered materials a further term may occur in equation 2.52 from the contribution of antiphase domain boundaries (and hence ordering energy).

Finally, it is evident that the creep behaviour of a material does not depend merely upon the external variables, stress and temperature. The elastic moduli and stacking fault energies of the material are likely to be of considerable importance. Indeed since creep involves the

the movement of dislocations, any of the multitude of factors which affect their movement must be considered in evaluating creep behaviour.

2.10.7 High Temperature Creep Mechanisms

In pure metals Q_c at high temperatures ($> 0{\cdot}5\ T_M$) has been found to be nearly equal to the activation energy of self-diffusion Q_D [130, 35] while in alloy systems it is usually found to be nearly equal to the activation energy of the element exhibiting the lowest diffusivity [52].

A number of diffusion controlled mechanisms have been suggested as rate determining for high temperature creep. They include dislocation climb [149], the nonconservative motion of jogs in screw dislocations [6, 49], viscous glide [149] and diffusion creep [70, 157]. The various mechanisms plus modifications thereof have been extensively reviewed by Dorn (1961) [36], Mukherjee et al. (1968) [112] and more recently by Klahn et al. (1970) [89]. The various models will now be considered briefly in turn.

(i) The dislocation climb model predicts that the steady state creep rate is given by the expression [89]:

$$\frac{\dot{\varepsilon}\, kT}{D_V Gb} = K\left(\frac{\nabla}{G}\right)^{4{\cdot}2 \text{ to } 6{\cdot}7} \qquad 2.53$$

where D_V is the volume diffusivity and K is some constant. The model is found to be in good agreement with experimental data and is further supported by the observation that typically most of the dislocations within subgrains and subgrain boundaries are in edge orientation [107].

(ii) The nonconservative motion of jogs in screw dislocations yields several relationships, depending on the vacancy model used. The vacancy

absorbing jog model gives [112] :

$$\dot{\gamma}_a = \rho_S \, 6D \left\{ 1 - \exp\left(-\frac{\tau l_j b^2}{kT}\right) \right\} \qquad 2.54$$

where $\dot{\gamma}_a$ is the steady state shear strain rate (based on the vacancy absorbing jog model), τ is the shear stress and ρ_S, l_j and D refer to the density of mobile screw dislocations, the mean distance between jogs and the volume diffusivity respectively. The jog models are found to require untenably high densities of screw dislocations in order to predict the observed stress sensitivity [112] .

(iii) The viscous glide model predicts that [89] :

$$\frac{\dot{\varepsilon}\, kT}{D_S\, G\, b} = K\left(\frac{\tau}{G}\right)^{3.0 \text{ to } 3.5} \qquad 2.55$$

where D_S is the solute atom interdiffusivity. This model suggests that dislocations have solute atmospheres associated with them which hence control their motion by viscous drag. The model is thought to apply at intermediate and low stresses [36] .

(iv) The diffusion creep model, which is thought to apply only at very high temperatures and low stresses predicts that [89] :

$$\frac{\dot{\varepsilon}\, kT}{D_V G b} = 5\left(\frac{b}{d}\right)^2 \left(\frac{\tau}{G}\right) \qquad 2.56$$

where D_V is the volume diffusivity and d is the mean grain size.

In conclusion, current theoretical models of high temperature creep have been largely developed from the creep behaviour of pure metals and dilute alloys. The observed steady state creep rate has been most accurately paralleled on the basis of a diffusion controlled dislocation climb model.

2.11 Creep in Ordered Alloys

Investigations into the creep behaviour of CuZn [16, 69, 15, 55] have shown that the formation of long range order is accompanied by a decrease in the steady state creep rate and an increase in the creep activation energy (calculated from the expression of equation 2.46). Tracer diffusion data for CuZn [95] have been obtained for both the ordered and disordered conditions. It has been found that there is good agreement between the activation energy of creep and the activation energy of diffusion (of copper) for both the ordered and disordered alloys.

Other studies on Ni_3Fe [90, 30], Fe_3Al [96], FeCo [92, 73] and MgCd [133] have all confirmed the findings in CuZn in that the creep rate decreased and the activation energy of creep increased upon ordering, but diffusion data are not available for comparison. However both high temperature creep activation energies and diffusion activation energies are available for a number of intermetallic compounds, which remain ordered up to their respective melting points.

Diffusion and creep activation energies are shown in TABLE XII for the compounds AgMg [61, 33, 34, 116], NiAl [65, 159], Ni_3Al and $Ni_3(AlTi)$ [64, 91, 147] and NiGa [present study] together with the data for CuZn [95, 16, 69] in both the fully ordered and disordered state. In general the reported creep activation energy is found to be appreciably greater than that of diffusion. However usually the diffusion activation energy of only one species is known while the creep rate may well be controlled by the diffusion of the other species, which may have a higher activation energy.

Few high temperature creep models have been proposed specifically for ordered alloys and in general they assume creep to be diffusion

controlled with the creep activation energy equal to that of diffusion.

One model [47] proposed that climb of the antiphase boundary in a superlattice dislocation, biased by stress, is rate controlling. However the creep activation energy Q_c shows an abrupt change at T_c and is not a continuous function of the degree of order (S). Consequently it has been shown that the model could apply only if an alloy remained ordered up to its melting point or if the character of the superlattice dislocations did not change with the degree of order [134].

A second model, which does not depend upon the character of the dislocations present, proposed that the climb rate controlling mechanism is the thermal creation of wrong bonds, biased by stress, ahead of a dislocation. This model predicted that [96]:

$$\dot{\varepsilon} = \frac{A\,D}{E_{APB}} \qquad 2.57$$

where A is a (stress dependent) constant, D is the diffusivity and E_{APB} is the antiphase boundary energy. But since E_{APB} is proportional to the long range order parameter squared (S^2), the creep rate should vary continuously with S and the model cannot account for the abrupt discontinuity observed at T_c.

However it has been suggested that on the compression side of the stress field of an edge dislocation a high degree of order may be maintained (since unlike bonds have smaller interatomic distances) even close to T_c. Thus for dislocation climb, the thermal creation of wrong bonds may require the same energy as diffusion in the fully ordered lattice [134] until T equals T_c.

In conclusion, the mechanisms which determine high temperature creep in ordered alloys and intermetallic compounds are thought to be diffusion controlled. However the limited data available for diffusion and creep activation energies in ordered alloys indicates that agreement

between the two energies is less good than that found in pure metals.

The theoretical models developed specifically to describe creep behaviour in ordered alloys have been based on diffusion controlled (extended) dislocation climb. But they have been unable to account fully for the abrupt change in the creep activation energy observed at T_c, purely on the basis of a change in diffusivity.

As a rule the general theories of creep, developed for pure metals and disordered alloys [36, 112, 149, 89, 25] (see also section 2.10.7) have been used to interpret creep data in ordered alloys [140, 96, 55, 115, 72] . Finally, high temperature creep data, which have been normalised according to the expression:

$$\frac{\dot{\varepsilon} T}{D} = K\left(\frac{\sigma}{G}\right)^n \qquad 2.58$$

where D is the diffusivity (see equations 2.49, 2.53 and 2.55), have been collated and compared for a number of ordered alloys by Strutt & Dodd (1969) [135] .

2.11.1 Creep in B2 Intermetallic Compounds

Among the B2 intermetallic compounds, the creep behaviour of AgMg [89, 116,115,117, 114] and NiAl [140, 159, 72, 136, 137, 82] have been most extensively studied.

In AgMg several different deformation mechanisms have been found to be rate controlling, depending on the stress and temperature. At low temperatures ($T \leqslant 300^{\circ}K$) the behaviour has been found to obey a thermally activated Peierls mechanism [117,114] . The activation energy is that for the nucleation of a pair of kinks and is equal to 39·54 kj/mole (0·41 eV) [114] .

In the intermediate temperature range ($300^{\circ} \leqslant T \leqslant 650^{\circ}K$) a different thermally activated mechanism has been found to be rate

controlling [117] . However this mechanism did not have a unique stress dependence of the strain rate; plots of ln $\dot{\varepsilon}$ vs ln Γ proved to have an increasing slope with increasing stress. No activation energy was evaluated for this range, and furthermore the data could not be correlated with any of the existing theories of creep [117] .

At high temperatures ($T > 650^{\circ}K$) the creep behaviour in AgMg has been found to conform to the requirements of a thermally activated dislocation climb mechanism [116] (see equation 2.53). The stress dependence of the strain rate follows the power law (equation 2.43) and gives a stress exponent $n \sim 5{\cdot}7$. The activation energy of creep in this temperature range has been evaluated as 212·55 Kj/mole (50·8 Kcals/mole) [116] .

The creep activation energy is somewhat higher than the accepted values for the activation energy of silver diffusion which are in the range 125·5 to 167·4 Kj/mole [61, 33] . However it is in fair agreement with the single determination of the activation energy of magnesium diffusion [34] which gave a value of 198·2 Kj/mole. Unfortunately the value of the activation energy of silver diffusion determined in the same study [34] proved to be high (at 188·7 Kj/mole) in comparison with accepted values. This may reflect on the validity of the magnesium diffusion energy result.

As in AgMg, several different regions of creep behaviour can be distinguished in NiAl, depending upon the stress and temperature. In the intermediate temperature range $748^{\circ} \leqslant T \leqslant 1048^{\circ}K$ creep has been found to be controlled by a thermally activated mechanism whose activation energy is considerably less than that of diffusion [82] . It has also been found that the stress dependence of the creep rate, expressed in terms of the power law (equation 2.43), yields values of the stress exponent n that are temperature dependent [140,159] .

The activation energy of creep in the temperature range where the stress exponent is temperature dependent has been found to decrease both with increasing stress and temperature. This disqualifies such mechanisms as viscous glide and diffusion controlled dislocation climb where the creep activation energy is stress (and temperature) independent [140]. In fact it has been suggested (at least for the stoichiometric alloy) that the creep rate controlling mechanism is that of thermally activated cross-slip [82].

Electron microscope studies on stoichiometric NiAl, for specimens deformed at intermediate temperatures, have revealed the presence of dislocation loops. It has been suggested that these form as the result of double cross-slip of screw dislocations by glide on $\{100\}$ and $\{110\}$ planes with common $\langle 100 \rangle$ Burger's vectors [82]. Comparable studies in CoAl [72] have shown that similar dislocation loops occur, but at higher homologous temperatures. These too, have been interpreted as indicating cross-slip.

At temperatures, where the stress exponent is temperature dependent, it has been found that the general trend is for the stress exponent to increase with decreasing temperature [140, 159]. For example, in the 56 atomic % nickel alloy the exponent n has been found to increase from 4·0 at 1298°K to 7·2 at 1073°K [140]. However, over certain temperature intervals, the stress exponent may decrease with decreasing temperature, within the overall trend of an increasing exponent with decreasing temperature. Thus in the stoichiometric alloy the exponent first rises from a value of 4·9 at 1273°K to 10·4 at 1068°K, then falls to 9·1 at 1023°K before rising again to reach 11·6 at 861°K [136].

At high temperatures, all alloy compositions (of NiAl) have been found to follow a power law stress dependence of the creep rate. Each composition has a constant, stress and temperature independent, stress

exponent. But below some critical temperature (i.e. the boundary of the intermediate temperature range), which is composition dependent, the stress exponent has been found to be temperature dependent [140, 159].

For example, below 1223°K for the stoichiometric alloy, 1123°K for the 51 atomic % nickel alloy and about 973°K for the 49 atomic % nickel alloy the stress exponent (n) is found to be temperature dependent [159]. Above these critical temperatures, the exponent becomes constant and has values of 4·6, 4·7 and 4·5 respectively [159].

For high temperatures (where n is constant) the activation energy of creep has been found to be in good agreement with that of nickel diffusion for alloys in the composition range 48 to 55 atomic % nickel. One alloy containing 46 atomic % nickel was found to have a creep activation energy considerably higher than that of diffusion [159].

The fact that at high temperatures the creep activation energy is not a function of stress has been interpreted as indicating that either viscous glide or dislocation climb must be creep rate controlling [140]. Furthermore since the stress exponent values of about 3·5 were obtained for all compositions it was suggested that Weertman's model of viscous glide [149] which predicts n equal to 3·6, illustrated the rate controlling mechanism [140]. Other workers [159] have found that compositions considerably removed from stoichiometry yielded stress exponent values in agreement with a mechanism of viscous glide. However it has also been found [159, 136] that alloys containing 49, 50 and 51 atomic % nickel respectively yielded stress exponents of about 4·5. It was suggested that the rate controlling process in these alloys was a dipole recovery mechanism [159].

In summary the creep behaviour of ordered (B2) intermetallic compounds, based on observations made in AgMg and NiAl, may be outlined

as follows:

(i) As in the case of pure metals the activation energy of creep depends upon the particular rate controlling mechanism and consequently varies with temperature as different mechanisms become predominant.

(ii) Creep at high temperatures is probably diffusion controlled but the agreement between the activation energies of creep and diffusion are not as good as in pure metals.

(iii) In AgMg the high temperature creep rate controlling mechanism is thought to be that of dislocation climb [116].

(iv) In NiAl, high temperature creep properties have been found to vary markedly with deviation from stoichiometry, suggesting rate controlling mechanisms that are composition dependent [159]. The rate controlling mechanism for compositions far removed from stoichiometry has been suggested as compatible with viscous glide [140, 159]. For near stoichiometric compositions a diffusion controlled glide mechanism, based on dislocation dipole recovery, has been postulated as the rate controlling mechanism [159].

Finally, it is clear from (iii) and (iv) above that one particular (B2) compound cannot be assumed as representative of the creep behaviour of the class. Indeed no particular composition of a given compound is necessarily representative of the creep behaviour of the compound as a whole.

CHAPTER THREE: Experimental Procedure

3.1 Alloy Preparation

3.1.1 Inert Electrode Electric Arc Melting

Weighed quantities of nickel (99·99% pure) and gallium (99·9% pure) were separately melted under a reduced pressure of purified argon in a water-cooled, copper hearth electric arc furnace fitted with an inert tungsten electrode. The metal 'buttons' were then reweighed and examined (visually) for metal losses and contamination respectively. Both the nickel and gallium 'buttons' were found to be clean and bright and weight changes resulting from melting were insignificantly small.

Alloys of any required composition were then prepared by melting together weighed 'buttons' of nickel and gallium. The prepared alloys were melted several times to ensure homogeneity and were then cast into bar form. The 'as cast' alloys were reweighed and estimates of errors in nominal composition were calculated from weight changes [see section 3.2.1] . Total charge weight were about 50g for each alloy prepared.

The 'as cast' ingots were found to be lightly contaminated by a surface oxide scale. One alloy with heavy contamination was rejected. The surface scale was removed from the ingots by grinding before any subsequent treatments were carried out.

All the alloys prepared were in the nominal composition range 43·5 to 54·5 atomic % nickel.

3.1.2 Radio Frequency Induction Melting

Some alloys were required with a large grain size and a uniform ingot cross-section (round) for subsequent diffusion experiments. A high frequency induction furnace arranged as a modified Bridgman apparatus (as designed by McDonnell et al. (1967) [106]) was used to prepare

induction melted ingots.

The ingots were prepared from arc melted alloys. The apparatus was evacuated and outgassed with purified argon. Crystal growth was achieved by passing the crucible containing the alloy charge through the induction coil by means of a mechanical drive. The required operating temperature was maintained by controlling the power supply to the induction coil.

The ingots produced were found to be clean and bright with little oxide scale evident. Some ingots required more than one melting to remove porosity and improve ingot shape. One alloy with 43·5 atomic % nickel (nominal composition) remained persistently porous despite repeated melting and was subsequently used only for powder and metallographic specimens.

All alloys prepared by induction melting were slow cooled under argon in the apparatus.

3.2 Alloy Analysis

3.2.1 Estimation of Nominal Composition from Charge Weight

The nominal atomic composition of the 'as cast' arc-melted alloys was determined from the constituent element charge weights (before alloying). The atomic fraction of nickel F_{Ni} in a given alloy is given by the expression:

$$F_{Ni} = f_{Ni} A_{Ga} \Big/ (f_{Ni} A_{Ga} + f_{Ga} A_{Ni})$$

where f_{Ni} and f_{Ga} are the nominal weight fractions and A_{Ni} and A_{Ga} the atomic weights of nickel and gallium respectively.

The probable errors in the calculated nominal composition were evaluated by assuming that all the weight losses which occured on alloying were attributable to first one element and then the other. New values of the weight fractions f_{Ni} and f_{Ga} were determined for the two limiting cases and hence the likely range of the atomic fraction F_{Ni} was evaluated. It was found that the errors were generally no larger than $\pm$ 0·5 atomic % (nickel).

3.2.2 Chemical Analysis

Small samples were cut, at intervals along the length, from each of the arc melted alloys after surface grinding to remove oxide scale. Generally three sections were taken from each ingot and the total sample weights (for each alloy) were between 0·25 and 1·0 grammes.

All the samples from each alloy were dissolved and duplicate aliquot portions of the stock solutions were analysed using wet chemical and electrogravimetric techniques. The alloys were analysed for nickel, gallium and copper content. Errors in the mean alloy composition were estimated to be $\pm$ 0·1 atomic % nickel. The results of the chemical analysis are shown in TABLE I.

The compositions determined by chemical analysis were equal to those estimated from charge weights within the $\pm$ 0·5 atomic % nickel error estimated for the latter nominal compositions.

3.3 Alloy Metallography

Small transverse sections were taken from each arc melted and each induction melted ingot and prepared for optical metallographic examination in the usual manner. The sections were etched in alcoholic ferric chloride solution to reveal the microstructure.

3.3.1 Arc Melted Alloys

All the alloys were found to be single phase and showed a chill cast grain morphology. Some porosity was evident in most cases, with the alloy of lowest nickel content (43·98 atomic %) showing extensive micro porosity as well as the usual random larger voids.

The grain size was found to decrease with falling nickel content. However the grains were quite large and columnar, with the long axis up to 3 mm and the short axis up to 1 mm for all alloy compositions.

3.3.2 Induction Melted Alloys

All the alloys examined were found to be single phase with exception of the two alloys furthest away from stoichiometry (43·98 and 54·59 atomic % nickel) which were two phase. In the two phase alloys, the second phase in each case consisted of fine precipitate particles dispersed throughout the large matrix grains.

No evidence of porosity was found in the alloys with the exception of the 43·98 atomic % nickel composition which remained porous despite repeated meltings.

The grain morphology of all the alloys was found to consist of very large grains, columnar along the long axis of the ingot and equi-axed in transverse section. The long axis of the grains sometimes extended the entire length of an ingot (up to 5 cm.) particularly in nickel rich alloys. The transverse grain diameter was between 2 and 5 mm. Some grain refinement was observed in going from the base to the top of the ingots (that is in the direction in which the alloy charge was passed through the induction coil). Also the grain size was found to fall with decreasing nickel content.

The metallography of both arc melted and induction melted alloys is summarised in TABLE II.

3.4 X-Ray Techniques

3.4.1 Debye-Scherrer Powder Photographs

Powder samples, prepared by filing, were taken from the arc melted alloys (in the "as cast and surface ground condition") and also from each of the induction melted alloys (surface ground). Any steel file chippings were removed magnetically.

The powder samples were annealed for 1 hour at 1073°K, to remove cold work effects due to filing. For the heat treatment, each powder sample was held in a closed end alumina tube and encapsulated in silica under a reduced pressure of purified argon. After heat treatment, samples were allowed to air cool while still encapsulated.

The annealed filings were sieved (350 mesh) and placed in a thin walled quartz capilliary tube ($\sim$ 0·3 mm O.D.). The tube of filings was then X-rayed, using a standard Debye-Scherrer camera, with monochromatic Cu K_α radiation at 40 K_V and 20 mA. The total exposure time for each sample was two hours and no filters were used either for the incident beam or within the camera.

The films were developed and dried using a standard procedure. The line positions of the diffraction lines on each film were determined (from an arbitrary zero line) using a Vernier-scale ruler. The line patterns were analysed and the structure and lattice parameter determined with the aid of a computer programme [see section 3.4.2].

All the films, both of arc melted and induction melted samples, proved to have single phase CsCl structures, with the exception of the lowest nickel composition (43·98 atomic % Ni) which proved to be two phase in both instances. These results contrast with the metallographic observations, where no second phase was evident in any of the chill cast specimens while both the 43·98 and 54·59 atomic % nickel

alloys were two phase in the induction melted condition.

The discrepancy was thought to arise from the 1073°K annealing treatment the powder samples had received. At these temperatures the phase diagram (see section 2.2) [66] shows that the nickel rich composition (54·59%) is single phase while the nickel deficient composition (43·98%) is two phase. The heat treatment was thought to be long enough to produce the at temperature equilibrium structure. But the subsequent cooling was not sufficiently slow to produce the two phase structure observed in the induction melted 54·59 atomic % nickel composition.

The results of the lattice parameter evaluations are given in the results [see GRAPH G.1] .

3.4.2 Debye-Scherrer Film Computer Analysis

A programme was devised and written to perform all the steps made in a manual computation of the lattice parameter. The data for the programme was in the form of line positions, taken in pairs, for each diffraction angle with the first datum pair corresponding to the {100} line of the superstructure.

The programme was able to select the lines of a given structure from a two phase alloy provided the first datum pair chosen belonged to the structure of interest and the diffraction lines of the two phases were not superimposed.

The programme evaluated a lattice parameter from each pair of lines of the structure. These lattice parameter values were plotted against the Nelson-Riley function and a best straight line was determined using a least squares fit. The best estimate of the lattice parameter was then evaluated from the intercept of the line with the lattice parameter ordinate.

The final computer print out yielded the best estimate of the lattice parameter plus an error in its estimation.

3.5 Alloy Density Determinations

The density of alloy samples was determined by an Archimedes buoyancy technique. Density measurements were carried out on bulk samples cut from induction melted ingots. All the induction melted alloys were used except the 43·98 atomic % nickel composition, which was porous [see TABLE I] .

Prior to sectioning, each ingot was heat treated for 1 hour at 1073°K under the same conditions used for X-ray powder specimens (see section 3.4.1). This was to allow a direct comparison between experimental density values and those calculated from lattice parameter measurements.

Metallographic examination showed that all the alloys remained single phase with the exception of the 54·59 atomic % nickel alloy which was two phase before and after heat treatment. This latter alloy was thought to remain two phase, unlike its powder counterpart, because the larger bulk of the ingot specimens resulted in a slower cooling rate than in the powder specimens, with the consequence that reprecipitation in the nickel-rich alloy could occur.

After heat treatment each ingot was cut into two or three sections of roughly equal length (~1·5 cm). These sections were designated bottom, centre and top, in the order in which the ingot had been passed through the induction coil. This was done to allow a check on any compositional segregation which might have occured during melting.

The sections were then ground and polished to a 1μ (diamond lapping paste) finish. The mirror finish of the entire section surface area

allowed the detection of any porosity (which was not observed) and also minimised the entrapment of air when the section was immersed in liquid.

The buoyancy liquid used was dibromoethane. Its density was determined at a number of temperatures using mercury as a standard of known density.

The procedural sequence for determining the density of alloy sections was:

(i) Weigh the sample container; suspended from the arm of a beam balance, in air (whose density is known from tables).

(ii) Weigh the container plus alloy sample in air.

(iii) Weigh the container plus sample in dibromoethane.

(iv) Weigh the container in dibromoethane.

(v) Repeat steps (i) and (ii).

The entire procedure was repeated several time for each sample while efforts were made to keep ambient temperatures constant, so that the subsequent alloy densities would be known all at the same temperature ($\sim 23^{\circ}C$).

Density values ρ_{NiGa} were then determined by solving the two simultaneous equations:

$$W_{Air} = W\left[\frac{\rho_{NiGa} - \rho_{Air}}{\rho_{NiGa}}\right] \qquad 3.1$$

$$W_{Br} = W\left[\frac{\rho_{NiGa} - \rho_{Br}}{\rho_{NiGa}}\right] \qquad 3.2$$

where W, W_{Air}, W_{Br} are the weight of the alloy sample in a vacuum, in air and in dibromoethane respectively; and ρ_{NiGa}, ρ_{Air} and ρ_{Br} are the densities of the alloy, air and dibromoethane respectively.

Dividing 3.1 by 3.2 and solving for ρ_{NiGa} gives:

$$\rho_{NiGa} = \left[\frac{(W_{Air}\,\rho_{Br} - W_{Br}\,\rho_{Air})}{(W_{Air} - W_{Br})} \right] \qquad 3.3$$

The values of alloy densities calculated from equation 3.3 are given in the results [GRAPH G.2] .

3.6 Diffusion Experiments

3.6.1 Specimen Preparation

A total of nine alloy compositions which had been induction melted and had densities determined were used for the preparation of diffusion specimens [see TABLE I] . The density sections of these alloys were cut into parallel sided disc specimens (of round cross-sections), about 2 mm thick. The relative position of each disc specimen in its respective alloy ingot was noted because alloy density had been found to vary slightly along any given ingot. Compositional segregation was thought to account for this variation in density. But the compositional dependence of the density (GRAPH G.2) suggested that the composition change along the length of any given ingot was probably less than the uncertainty of the chemical analysis (i.e. $\pm$ 0·1 atomic % nickel).

Each disc specimen was set in a cold setting resin (plastic) in a mould which consisted of a metal piston which could move co-axially inside a metal cylinder. The face of the piston and the end of the cylinder thus remained in parallel alignment as the piston was moved inside the cylinder [see FIG. 3.1] . This jig was used to grind both sides of the disc specimens flat and parallel. After grinding each specimen was marked with an identifying number on one face and had

FIG 3.1.A
GRINDING JIG FOR PRODUCING
FLAT, PARALLEL SIDED SPECIMENS
FOR TRACER PLATING

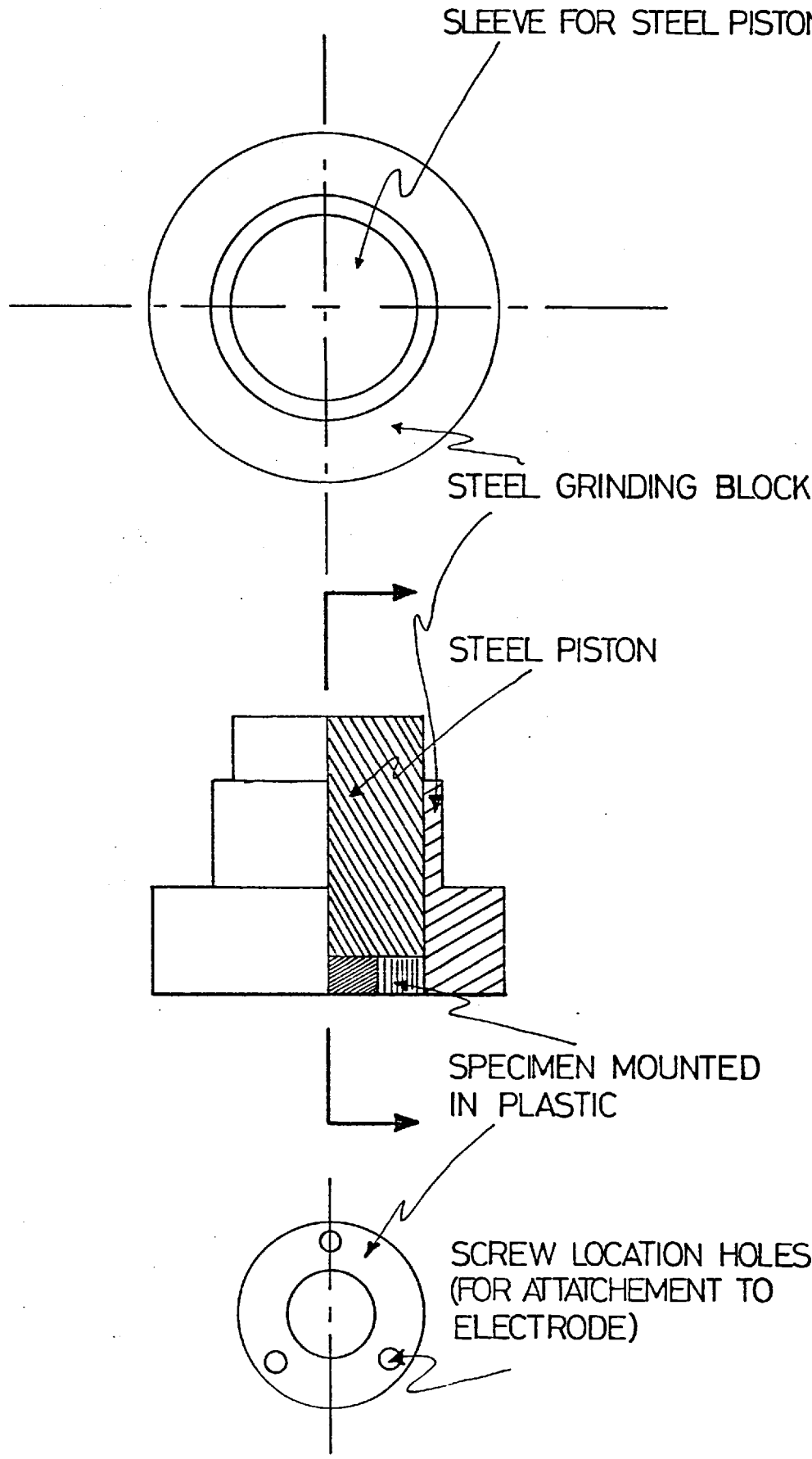

FIG 3.1. B.
GRINDING JIG FOR TRACER
PENETRATION ANALYSIS

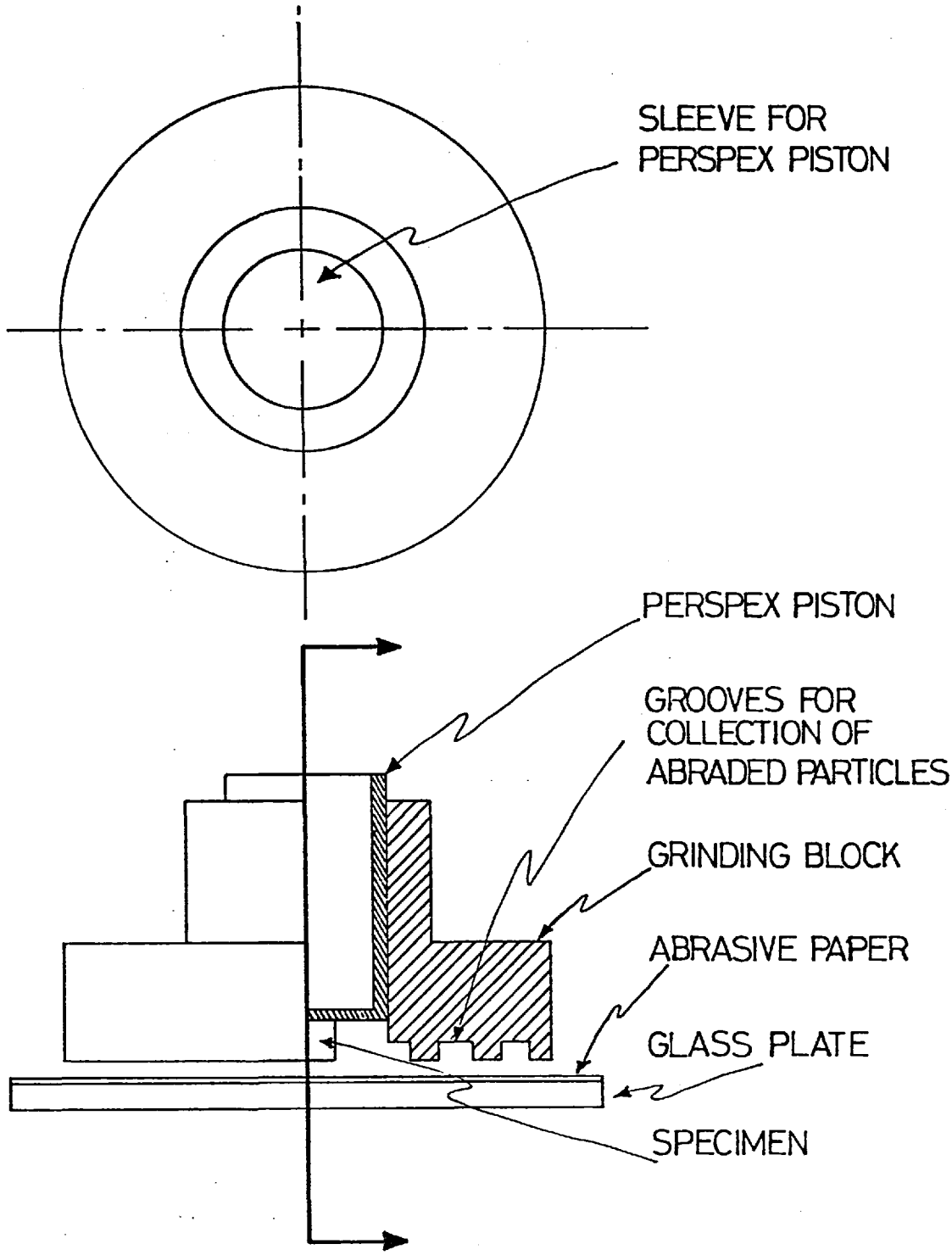

location holes drilled through its plastic mount. The latter operation was to allow mounted specimens to be attached to an electrode for subsequent electroplating of radio-active tracers [see FIG. 3.2] .

The specimens were then polished to a mirror finish on one side. Thus the finished item consisted of a flat, parallel sided disc with one surface highly polished. For the first diffusion experiments the polished surface of specimens was etched in alcoholic ferric chloride solution to remove any remaining deformed material from the surface, prior to tracer deposition. This practice was later discontinued as etching tended to produce an uneven surface finish. Specimens were then plated in the as polished condition.

3.6.2 The Radio-Isotopes of Nickel and Gallium

The isotope of nickel used as a tracer in this study was nickel-63 which decays by the emission of β-particles with an energy of 0·067 MeV. The isotope has a half life of 92 years.

The gallium isotope used was gallium-67 which decays by electron capture and the subsequent emission of γ-rays with an energy spectrum of 0·093 to 0·4 MeV. The isotope has a half-life of 78·1 hours.

The much higher radiation energy and far shorter half-life of the gallium isotope led to a radically different technique being used for gallium diffusion analysis compared with that of nickel.

3.6.3 Electrodeposition of Radio Isotope Tracers

Both nickel and gallium can be electroplated from aqueous solutions but the quantities of tracer actually required on a specimen are very small and in fact it is not possible to plate only active atoms from an 'as-supplied' tracer solution because the dilution is too great. In practice the tracer solution is mixed with a solution containing a non-

FIG 3.2. Electrode for tracer plating

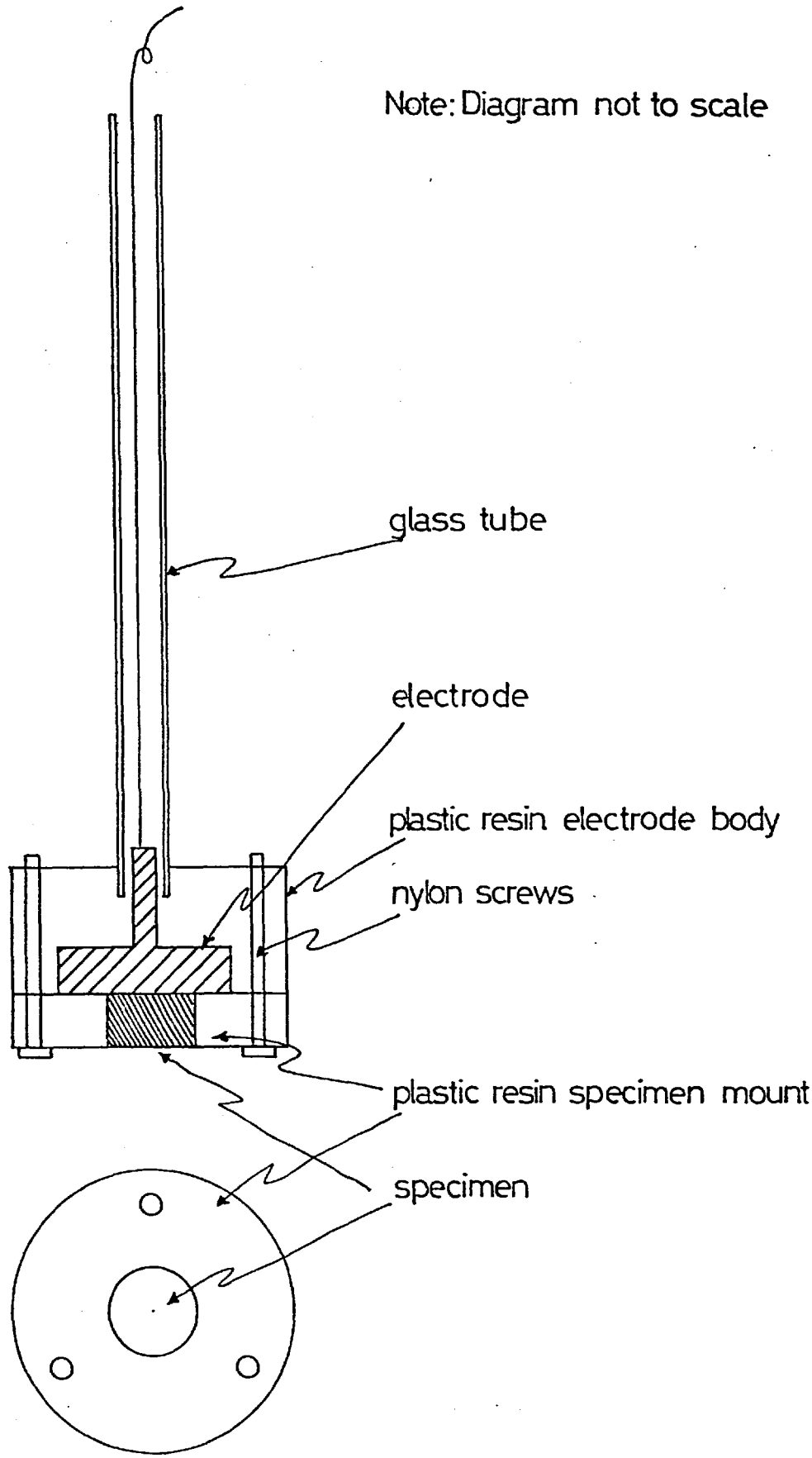

active isotope of the same element and the two isotopes are plated together, with the latter acting as a carrier. The required activity may be plated onto a specimen in the form of a large plating bulk (of active and inactive material).

Nickel-63 was plated from an approximately 1 N solution of nickel sulphate and nickel chloride with added boric acid to act as a buffer agent (this is a standard nickel plating solution). The plating apparatus consisted of a glass container with a platinum anode sealed into the glass at the base. Additions of boric acid or ammonium hydroxide could be made to the plating solution from side reservoirs to neutralise excess acid formed during plating. The entire plating apparatus was held in a water bath to maintain the required deposition temperature of 40 $\pm$ 10°C [see FIG 3.3] .

The specimen to be plated was screwed onto the cathode [see FIG 3.2] . The current density used was approximately 50 mA/sq. cm (of cathode). The deposition time was adjusted to plate a layer of approximately 0·5 to 1·0 μm thick.

Gallium can be electroplated from an aqueous solution of sodium gallate [63, 88] . This was prepared by dissolving gallium metal in a mixture of concentrated nitric and hydrochloric acid and then neutralising the excess acid with $\sim$ 3 N sodium hydroxide solution until a precipitate of gallium hydroxide was produced. Further sodium hydroxide solution was then added to redissolve the precipitate. The final solution consisted of sodium chloride and nitrate, sodium gallate and excess sodium hydroxide. The preparation of the solution can be summarised by the equations:

FIG 3.3 Ni PLATING BATH

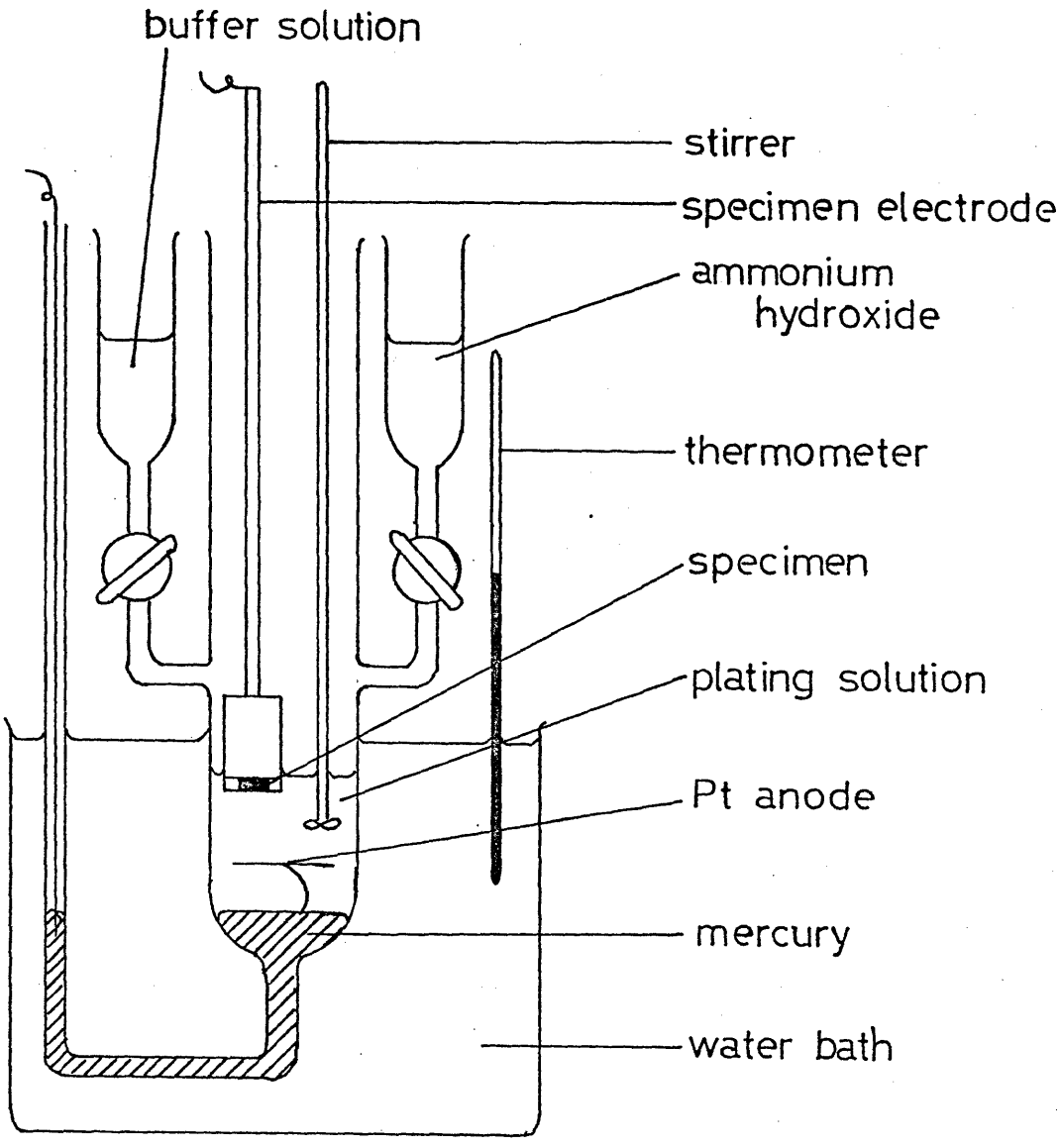

$$2\ Ga + 6\ HCl \longrightarrow 2\ GaCl_3 + 3\ H_2 \qquad \text{(i)}$$

$$GaCl_3 + 3\ NaOH \longrightarrow 3\ NaCl + Ga(OH)_3 \downarrow \text{PPT} \qquad \text{(ii)}$$

$$Ga(OH)_3 + NaOH \longrightarrow Na\,[Ga(OH)_4] \qquad \text{(iii)}$$

The solution was then made up to a standard volume, contained about 4 g of gallium metal per litre, and was $\sim 0{\cdot}25$ N with respect to sodium hydroxide.

The 'as-supplied' (Radio Chemical Centre, Amersham) carrier free gallium-67 tracer was added to about 50 ml of the standard sodium gallate to provide a plating solution of the required specific activity. The plating bath consisted of a glass container with a platinum anode. The diffusion specimens were mounted for plating as in the case of nickel plating. The plating bath was maintained at a temperature of about $10^{\circ}C$ to ensure the deposition of solid gallium. The current density used was about 150 mA/sq cm (of cathode) and the deposition time was adjusted to plate a layer of $< 0{\cdot}5\,\mu m$ thick.

In order to evaluate the required specific activity (in mCi/g of deposited plating) of the plating solution (for both nickel and gallium deposits) a number of assumptions and boundary conditions were used. Firstly, after diffusion, the penetration profile must be sufficiently active to a reasonable depth to allow its shape to be determined and hence the diffusion coefficient to be evaluated.

The method used for determining the penetration profile involved measuring the activity of successive parallel layers removed from the specimen. As a rule these layers were some 10 to $20\,\mu m$ thick and a minimum of ten such layers were required to determine the diffusion penetration profile. Thus a penetration depth of $200\,\mu m$ was chosen to define the limit of diffusion, at which point the tracer activity fell to zero.

The penetration profile was then assumed to be defined by a straight line and the activity at half the limiting penetration depth (of 200μm) I_A was taken as ten times the known background (cosmic) activity. The activity I_A was that of a layer of unit thickness (the unit being the thickness of layers removed during penetration analysis, i.e. 20μm). The total activity under the profile I_{TOT} is thus given by:

$$I_{TOT} = I_A \cdot \frac{x}{l}$$

where x is the total penetration depth (200μm) and l is the thickness of each layer (20μm).

The value I_{TOT} is the activity of the layer that must be plated onto a specimen such that after diffusion the penetration profile is measureable. However this value makes no allowance for the decay in activity during the time of diffusion annealing and it assumes 100% efficiency of the counting apparatus. In general, counter efficiency is usually quite low ($\sim$ 10%), while activity decay is insignificant in the case of nickel-63 but must be allowed for in the case of gallium-67. The activity I_T is the value of I_{TOT} after corrections are made for counter efficiency and activity decay ($I_T > I_{TOT}$).

Thus I_T is the required activity of the layer plated onto a specimen and is related to the total activity I_S in the plating solution by the expression:

$$I_T/I_S = w_1/w_s \qquad 3.4$$

where w_1 is the weight of the plated layer and w_s is the weight of tracer plus carrier in the plating solution.

Finally the plated layer was assumed to be 1μm thick so that its weight per unit area (w_1) was known. Hence, since I_s is the total activity of the solution is equal to the known activity of the as-supplied

tracer, the required specific activity of the plating solution ($^{I}s/w_s$) may be calculated from equation 3.4.

The procedure outlined above was used to determine the amount of carrier which had to be added to the tracer to produce plated layers of the necessary bulk and activity (i.e. specific activity).

Preliminary plating experiments with non-active solutions were done to establish calibration curves of deposit weight against plating time for given current densities. These calibration curves were used to select the plating time required to produce a layer of the necessary thickness on diffusion specimens. The specimens were weighed before and after plating (for both nickel and gallium diffusion experiments) to afford a check on any gross errors which might occur during plating.

After tracer plating, specimens were removed from their plastic mounts and their sides and back surface were lightly abraded to remove any tracer deposits other than on the polished face. The specimens were then ready for annealing.

3.6.4 Diffusion Annealing

In the case of nickel diffusion the long half-life of nickel-63 allowed long diffusion anneals (if required) and plenty of time for subsequent penetration analysis. Consequently batches of specimens, with two of each composition placed with active faces in contact, were wrapped in molybdenum foil and annealed for the required time at given temperatures in a vacuum furnace.

The design of the furnace was that of B.R. McDonnell (1969) [105] and it consisted basically of a resistance heated furnace tube held vertically in an evacuated can [FIG. 34]. The specimens were placed on a platform (in a tray) which could be pushed into the hot zone of

FIG 3.4 VACUUM DIFFUSION ANNEALING FURNACE

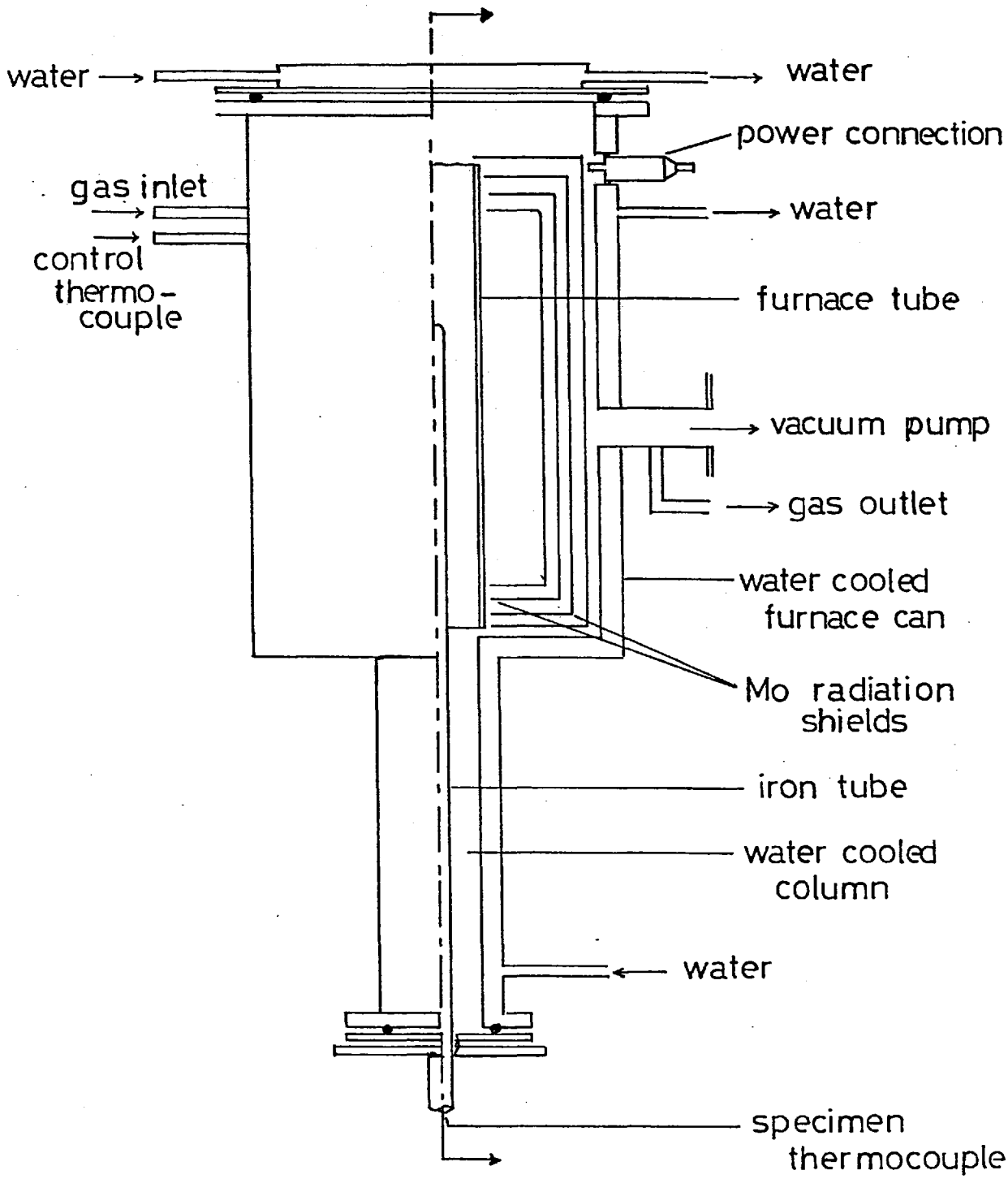

FIG 3.5.
SPECIMEN HOLDING ARRANGEMENT FOR
VACUUM DIFFUSION ANNEALING FURNACE

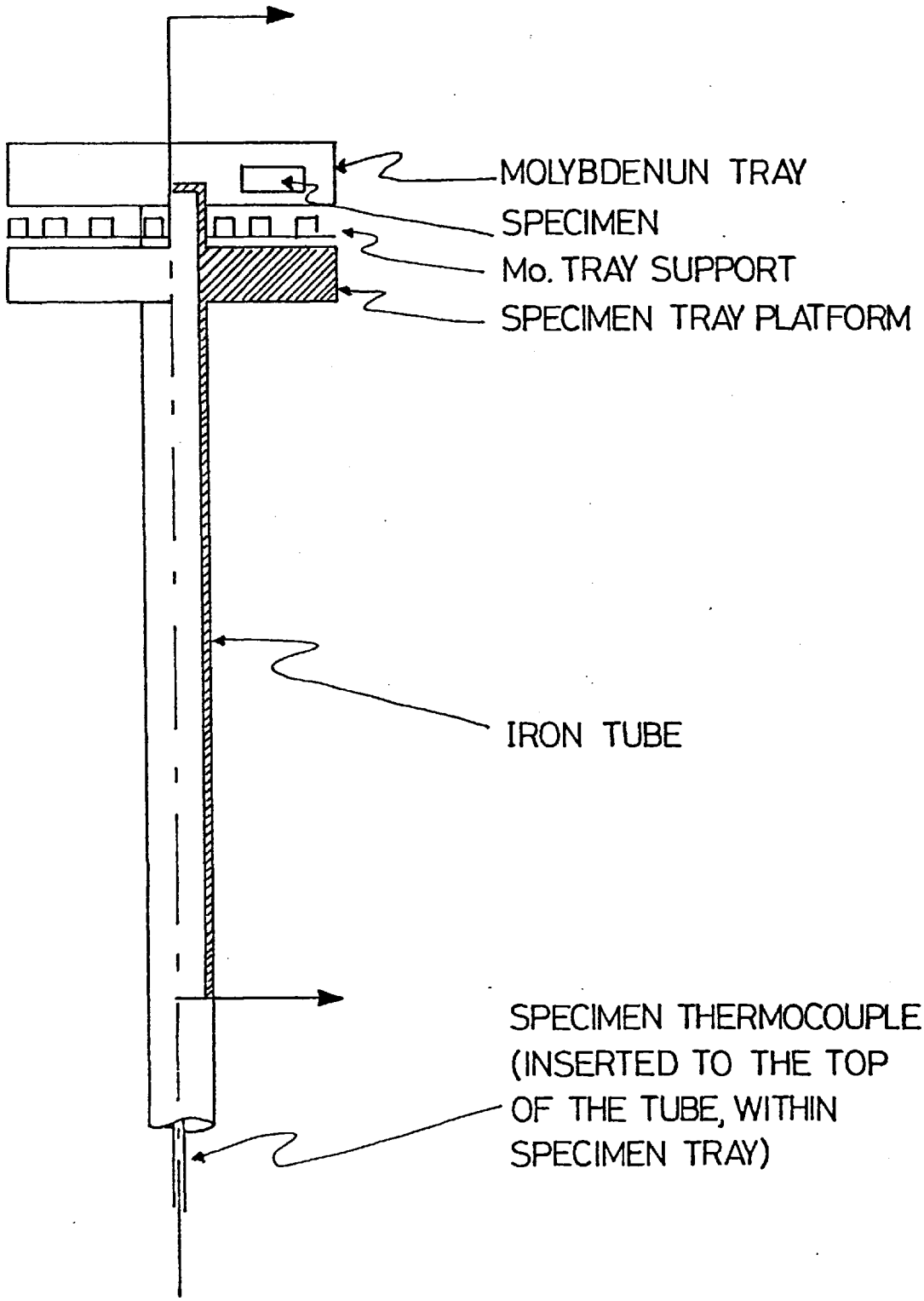

the furnace [FIG 3.5] . This arrangement minimised heating up and cooling down times.

After annealing, the specimens were removed from the hot zone of the furnace and allowed to cool in vacuo before removal for penetration analysis. The use of the vacuum furnace minimised the risk of specimen oxidation. The placing of specimens in pairs, with active faces in contact, was to prevent evaporation losses of plated tracers. But high temperature anneals resulted in specimen welding in some cases and later anneals were carried out with specimens placed singly with active faces uppermost in the tray. The evaporation of nickel tracer for either single or paired specimens has been found to be negligible [131] even at the highest temperatures used in this study. Finally the use of molybdenum foil wrapping was to prevent sticking of specimens to the tray and each other.

The annealed specimens were found to be clean and bright. In the case of paired specimens, oxidation of the active face was negligible but single specimens did show some slight contamination of the active face.

In the gallium-67 diffusion series time was of the paramount importance because of the short half-life of the isotope. Consequently several different furnaces were used so that batches of specimens could be treated, each at a different temperature, over the same period of time.

One batch of gallium-67 plated specimens were annealed in the vacuum furnace in the same manner as the nickel series except that all specimens were paired. All other batches were annealed in conventional tube furnaces. For these latter heat treatments the specimens were placed in pairs with active faces in contact and then wrapped in molybdenum foil. The paired specimens were then stacked in a cylindrical

arrangement and each batch wrapped in molybdenum foil like a tube of sweets. The prepared batches were then sealed in silica under a reduced pressure of purified argon. Each sealed batch was then inserted into the hot zone of the furnaces used and upon completion of the anneal, removed and allowed to air cool while encapsulated.

On the question of tracer evaporation, it had been found that after plating, the gallium film was difficult to remove mechanically, even at hot water temperatures, presumably because of a solid/liquid diffusion interaction which 'fixed' the gallium film on the specimen surface. In consequence it was thought unlikely that the gallium tracer would melt and flow away from the specimen during the annealing treatment. Furthermore gallium does not boil until 2523°K and it was thought that evaporation losses at the highest annealing temperature of $\sim$1373°K would be small. A check on the non-active surfaces of specimens, after annealing, failed to detect any active species suggesting that evaporation losses were probably small.

After annealing, the vacuum furnace specimens were clean and bright with very little contamination. The silica sealed specimens were appreciably more oxidised, especially those annealed at the highest temperatures. Some high temperature specimens were welded and difficult to separate. Occasionally specimens were broken during separation attempts however these could often be salvaged for analysis. In some cases specimens could not be separated and attempts were made at analysis by removal of layers from the back surface towards the active face.

In summary all the nickel diffusion anneals were carried out in a vacuum furnace. The specimens were clean with little oxidation. Welding problems were overcome by using single specimens rather than pairs. One diffusion anneal of gallium specimens in the vacuum furnace yielded clean, uncontaminated specimens. Other batches were annealed

sealed in silica; low temperature anneals yielded good specimens although somewhat more oxidised than their vacuum counterparts, high temperature anneals produced specimens that were welded and often difficult to separate but nevertheless they were useable.

3.6.5 Boundary Conditions for the Solution of the Isotope Penetration Curve

A number of techniques are available for determining the diffusion penetration curve. The most widely used are the sectioning technique and the residual activity technique. In both cases successive parallel layers are removed from the active surface of the specimen. In the former method the activity of the removed layer is measured while in the latter the residual activity of the exposed surface is determined. The major disadvantage of the sectioning technique is the need to retain all the material removed in each layer. The drawback of the residual activity technique is the error introduced by the contribution to the surface activity of atoms below the surface.

The sectioning technique is usually used for intermediate and high energy decay radiations while the residual activity technique is most often used for weak radiations. In fact it may be used for diffusion analysis for three distinct conditions.

(i) The energy of the radiation is so weak that the absorption coefficient (μ) of the material is high and effectively only surface atoms contribute to the activity measured at the surface. The condition describing this case is ($^1/\mu \ll 2\sqrt{Dt}$) where D is the diffusion coefficient and t the annealing time ($2\sqrt{Dt} \approx x$ where x is the total penetration depth). This condition is fulfilled by the weak radiation of nickel-63, and the residual activity technique was used for nickel diffusion analysis.

Errors from below surface intensity contributions can be corrected if these (contributions) originate from depths less than the section thickness removed for each layer [10] .

(ii) When the energy of the radiation is so high that the absorption coefficient is low enough for all the atoms from the entire diffusion zone to contribute to the surface intensity, thus ($^1/\mu \gg 2\sqrt{Dt}$). The activity of a given layer is hence known by difference.

(iii) The diffusion coefficient may be evaluated by the residual activity technique for the intermediate radiation energy condition ($^1/\mu \approx 2\sqrt{Dt}$), which is the case for gallium-67 radiation, but the mathematics are complex [141] . Hence a modified sectioning technique was employed for the analysis of the gallium-67 penetration curves.

3.6.6 Penetration Analysis of Nickel-63 Diffusion

The diffusion specimens were brittle and not machineable and so could neither be turned to produce round disc specimens of known surface area nor to remove successive parallel layers from the active face. Consequently specimens were cut using high speed resin bonded SiC wheels to produce discs of known square cross-section. The cutting operation also removed the former outside surfaces from the sides of each specimen and hence any contributions from surface diffusion.

Each square disc specimen was glued onto the end of a hollow perspex cylinder so that the active face was uppermost and parallel to the end face of the cylinder (and perpendicular to its longitudinal axis). Layers of thickness between 10 and 20 μm were then removed successively from the specimen's active face using a precision grinding block similar to that employed by Einsen & Birchenall (1957) [38] . The grinding arrangement was very similar to that outlined in FIG. 3.1

except that the metal piston was replaced by the hollow perspex piston (cylinder) to which the specimen was permanently attached.

The specimens (plus cylinder) were weighed before and after the removal of each layer and from the weight change and the known density and cross-sectional area the thickness of the layer removed was determined. The residual activity of the ground face of the specimen was counted with a scintillation counter consisting of a phosphor sensitive to β particles, and a photomultiplier tube mounted in a lead shielding castle. The count was recorded on a decade scalar and the activity was calculated from the mean of several fixed time counts. The counting time used depended on the ratio of the specimen activity to that of the background and was adjusted to maintain the same relative error for all activities.

The inside of the lead counting castle was modified to accommodate a jig which consisted of a fixed brass sleeve designed to hold the perspex cylinder and attached specimen coaxially with the photomultiplier tube so that the active face of the specimen was parallel to the phosphor surface (cf. the grinding block arrangement FIG. 3.1). Furthermore, since all specimens did not have the same section area, a window of fixed circular geometry, punched in lead foil, was interposed between the specimen and phosphor. Consequently only the activity from a circular area in the centre of each specimen's active face was counted. Thus the exposed area and geometry of all specimens was kept constant.

The thickness of the lead foil was large enough to ensure that the activity contribution from screened portions of the specimen at the phosphor was $< 5\%$. Care was taken to expose the specimen in exactly the same geometry for every count taken during any one penetration analysis. It has been estimated that the interposition of a foil window reduces the specimen counting geometry from 2π to $1{\cdot}98\pi$ and that such a small reduction does not contribute measurable inaccuracies in specimen counts [105, 17].

3.6.7 Penetration Analysis of Gallium-67 Diffusion

The technique used for the penetration analysis of gallium diffusion specimens was a modification of the standard sectioning technique. The residual activity method was considered unsuitable because of the relatively high energy of the isotope's γ radiation and its short half-life which made speed of operation essential [see section 3.6.5].

As in the case of nickel penetration analysis, square section specimens of known area were first prepared. Each specimen had its active face coated with a thin film of releasing agent (Vaseline) and was placed active face down onto the face of the steel piston of the grinding jig [FIG. 3.1] and cast in cold-setting resin. The back surface of the mount was then ground away to expose the non-active face of the specimen. The releasing agent on the front face of the specimen ensured that while being cast in resin the specimen remained flat and parallel, in contact with the steel piston.

On removal from the grinding jig (mould) each specimen consisted of a square section alloy disc, embedded in plastic, with the ground back surface and the as annealed active front surface exposed and parallel. The plastic mounted specimens then had location holes drilled to allow them to be attached to an electrode for electro-etching (see preparation of diffusion specimens, section 3.6.1).

An electro-etching technique was used to remove successive layers (and simultaneously collect in solution the material removed) from the exposed active surface of the specimen. The plastic mount of the specimen protected the side surfaces from attack by the etchant. The surface of the specimen was firmly in contact with the anode and periodic examination failed to reveal any signs of attack of this surface.

The etching solution used has been described by Seybolt & Westbrook (1964) [129]. It consisted of HCl (15 ml), HIO_3 (10 ml), CH_3COOH (10 ml),

H_2O (35 ml) and a small amount of ferric chloride. This mixture was further diluted in the ratio three parts of mixture to two of water for etching purposes.

Preliminary experiments indicated that a current density of approximately 400 mA/sq cm maintained for about three minutes removed about 20 μm of material and produced a smooth polished finish on the specimen surface. The temperature of the etching solution was kept below 15°C by the use of an ice bath.

The etching bath consisted of a small glass beaker, a platinum cathode and the mounted specimen as an anode. The anode [see FIG. 3.2] was hand held and used as a stirrer. The volume of electro-etch used for each layer removed was 25 ml, measured out with a pipette.

After etching the specimen/anode was removed from the beaker and washed with distilled water. The washings were collected in the beaker. The platinum cathode was similarly treated. The solution was then transferred to a counter container, the beaker was washed and the washings added to the container. The solution in the container was then made up to a standard mark corresponding to 40 ml. The activity of the solution could then be counted.

The solution container consisted of a perspex tube cut and ground so that its ends were flat and parallel and perpendicular to its longitudinal axis. At one end a circular sheet of P.V.C. of uniform thickness ($\sim$20 μm) was glued to form a closed-end tube container.

The activity of the solution was counted with a scintillation counter consisting of a thallium-doped NaI phosphor crystal, sensitive to γ-rays, and a photomultiplier tube mounted in a lead castle shield. As in the case of nickel diffusion a decade scalar was used to record the activity.

Again as in the case of nickel diffusion the inside of the lead castle was modified, in this case to accommodate an aluminium jig designed to hold the perspex solution holder in a fixed aspect, with the P.V.C. window parallel to the phosphor surface. The counter geometry thus remained the same for each section of all specimens. No lead foil windows were used during these analyses since specimen solutions were held in containers of identical cross-sectional area and geometry.

The short half-life of the gallium-67 isotope precluded the use of long count times, but these were unnecessary in view of the high specimen activities. Several short, fixed time counts were made for each section and the activity determined from the mean value. No attempt was made to vary the count time as a function of activity in order to maintain a constant relative error. The time of entry and removal of each solution from the counter was noted, with the start time (zero time) being taken as the time of starting the analysis of the first section of a given specimen. This was to allow for a correction for the decay in intensity of the gallium-67 isotope during counting. The corrected count was then determined from the observed count and elapsed time.

After analysis, a given solution was discarded and the container washed in readiness for the next solution. A periodic check of both the background activity and any residual activity in the solution containers was made.

The mounted specimens were weighed before and after each electro-etching and from weight differences and the known density and cross-sectional area values the thickness of each layer removed was determined. It was found that there was a tendency for the specimen surface to etch more rapidly around the edges of a section producing a convex instead of a flat surface profile. Also some grains were found to etch more

rapidly than others, producing a stepped surface. All such irregularities are known to produce errors in the final estimate of the diffusion coefficient [17] but were unfortunately inherrent to the etching technique.

A few specimens which could not be separated were analysed by removing layers from the non-active surface and approaching the active face. In general for two welded specimens the one (of the pair) analysed from its back surface towards the active face yielded results with very large errors in the estimate of the diffusion coefficient. However the second specimen of the pair which was subsequently analysed from its active face gave good results. Little difficulty was experienced in locating and identifying the interface between two such welded specimens.

3.6.8 Evaluation of Diffusion Coefficients and Activation Energies

The solution to Fick's second law of diffusion may be expressed in terms of the count intensity (I) (replacing the concentration c; see equation 2·17) as a function of diffusion distance (x) by the relation [62]:

$$I - \frac{1}{\mu}\frac{\partial I}{\partial x} = \frac{K}{(\pi Dt)^{\frac{1}{2}}} \exp\left(-\frac{x^2}{4Dt}\right) \qquad 3.5$$

where μ is the linear absorption coefficient, D is the diffusion coefficient, K is a constant and t is the time of isothermal diffusion (annealing time).

For the case of the weak β-radiation of nickel-63 μ is very large and $I \gg (1/\mu)\left(\frac{\partial I}{\partial x}\right)$ thus equation 3.5 reduces to:

$$I = K' \exp - \frac{x^2}{4D't} \qquad 3.6$$

Furthermore in the sectioning technique the activity of the removed layer

is measured directly and consequently the absorption coefficient of the material (μ) does not enter into the expression relating I and x, and equation 3.6 can be applied directly.

The diffusion coefficient (D') can be evaluated from equation 3.6 from the linear plot of lnI against x^2 (both experimentally known). In the case of the residual activity technique a better estimate of D can be made by differentiating equation 3.6 and evaluating the term $(\partial I/\partial x)$ and subsequently plotting $\ln [I - (1/\mu) (\partial I/\partial x)]$ against x^2, to obtain a new value of D. The procedure can then be repeated as required [62].

In this study equation 3.6 was applied directly to experimental values of count intensity (I) as a function of penetration depth (x) for the case of nickel-63 diffusion. No correction for the contribution of the absorption coefficient (μ) was attempted since its value was not known. Values of the diffusion coefficients (D_{Ni}) for the various compositions at given temperatures are shown in the results (TABLE III).

In the case of gallium-67 diffusion two corrections were made to the raw experimental data before applying equation 3.6. These were:

(i) The measured activity values I_t were corrected for isotope decay to a standard base time ($t_d = 0$). The corrected activity $I_o (> I_t)$ may be calculated from the activity observed I_t at time t_d from the expression:

$$I_o = I_t \exp \left[\frac{(\ln 2)\, t_d}{\tau} \right] \qquad 3.7$$

where τ is the isotope half-life.

(ii) After correction for isotope decay the (corrected) measured activity I_o was the total activity within a given layer (of thickness Δx). It was assumed that the activity profile within each layer

removed was linear so that the activity at the mid-position of a given layer I_m was also the mean activity of the said layer. Then I_m can be expressed in terms of the corrected measured activity I_o by the relation:

$$I_m = I_o/\Delta x \qquad 3.8$$

But the depth x defines the penetration depth after the removal of a given layer, therefore the activity I_m refers to a depth $(x - \frac{\Delta x}{2})$. Thus substituting these values into equation 3.6 and substituting for I_m from equation 3.8 gives:

$$\frac{I_o}{\Delta x} = K \exp\left[-\frac{(x - \frac{\Delta x}{2})^2}{4Dt}\right] \qquad 3.9$$

Thus a plot of $\ln (I_o/\Delta x)$, which is the logarithm of the corrected activity of a layer per unit thickness of that layer against $(x - \frac{\Delta x}{2})^2$, the square of the mean penetration position of the layer, yields a straight line from whose slope the diffusion coefficient D_{Ga} can be calculated.

Values of the diffusion coefficients (D_{Ga}) for the various compositions at given temperatures are shown in the results (TABLE IV).

The values of the diffusion coefficients D_{Ni} and D_{Ga} at various temperatures T were then used in the Arrhenius equation to yield the activation energy of diffusion Q_{Ni} and Q_{Ga} respectively. The expression used was (see equation 2.28):

$$D = D_o \exp(-\frac{Q}{kT}) \qquad 3.10$$

The activation energy Q was evaluated from the slope of the linear plot of lnD versus $(1/T)$.

The activation energies of diffusion Q_{Ni} and Q_{Ga} for the various alloy compositions are shown in the results (TABLES III & IV).

3.7 Creep Experiments

The extreme hardness and brittleness of NiGa alloys at room temperature prohibited the use of specimens which required extensive machining; for this reason creep experiments were carried out in compression on simple cuboid polycrystalline specimens.

3.7.1 Preparation of Creep Specimens

Polycrystalline material for compression testing must have a fine grain size, hence chill cast (arc melted) material was selected although even in this condition the grain size was known to be fairly large (see section 3.3.1). Cold working and subsequent recrystallisation to produce a finer grain size (than arc melted samples) was precluded by the brittleness of the material. Other methods of melting and solidification, such as induction melting or resistance heating were found to produce a coarser grain structure than that achieved by arc melting.

The arc melted samples were checked for porosity and remelted until good density was achieved. The ingot bars were then cut into slices to produce transverse sections about 2·5 to 3·0 mm thick. These slices were then further cut to produce cuboid specimens of the approximate dimensions 6 by 3 by 3 mm. The long axis of each specimen was parallel to the columnar axis of the chill cast grains (of the microstructure).

The specimens from each ingot were then mounted in plastic in groups of up to a dozen (all from the same ingot) in the grinding jig [see FIG. 3.1, A] used for the preparation of diffusion specimens in readiness for electroplating. The two faces of each (cuboid) specimen parallel to the surfaces of the mount were then ground flat and parallel to each other. The specimens were then removed from the

mounting plastic and remounted so that a second two faces could be ground. Finally the procedure was repeated to grind the ends of the specimens.

The use of this grinding procedure allowed equal sized specimens with accurately parallel faces to be made in batches. Also the support afforded by the plastic matrix cut down the incidence of specimens being chipped at an edge or corner and thereby rendered useless. The final size of the finished specimens was between 5 and 6 mm for the long axis, and between 2 and 2·5 mm for each of the short axes.

3.7.2 The Creep Testing Apparatus

Specimens were tested in compression using a direct loading apparatus designed by Evans (1967) [42]. Tests were carried out at temperature in air.

The creep apparatus is shown schematically in FIG. 3.6. It consisted basically of a fixed alumina ram located in the hot zone of a water cooled resistance heated furnace. A second alumina ram, above and aligned with the first and co-axial with the furnace tube was allowed to move down into contact with the lower fixed alumina ram. A flat loading platform was attached to the top of the upper ram and both it and the ram were suspended from pulleys and held in position by counterbalance weights.

Specimens were compressed between the two alumina rams under the load placed on the loading platform while at the temperature of the hot zone of the furnace. The deformation strain of a compressed specimen was measured by a transducer which monitored the movement (downwards) of the upper compression ram. The strain data (in fact not strain but deformation, with units of length) was recorded as a continuous function of time on a chart recorder. The recorder was also used to keep a

FIG 3.6.
SCHEMATIC DIAGRAM OF COMPRESSION
CREEP TESTING APPARATUS

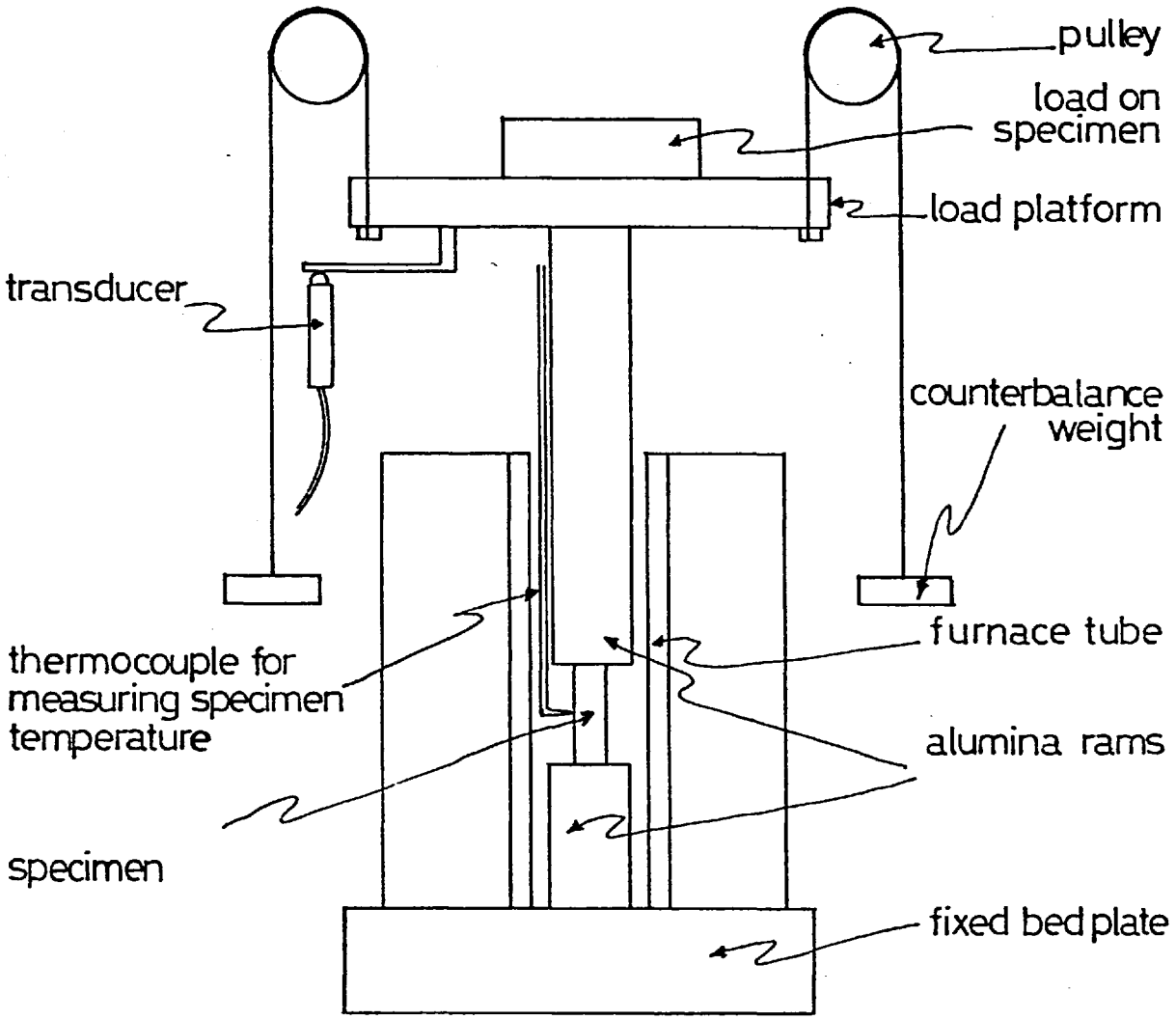

continuous record of the temperature of the specimen as determined by a thermocouple placed close to the specimen [see FIG. 3.6] .

3.7.3 Creep Tests

The specimen to be tested was measured with a micrometer and its dimensions recorded. It was then placed between the two alumina rams of the testing apparatus, with its long axis aligned with the rams. The upper ram and loading platform were counterbalanced so that the specimen was under zero load. A small load was placed on the loading platform and the furnace was switched on and brought up to the required temperature. The purpose of the small load on the specimen was to prevent the possibility of it toppling during the heating up period.

Once the specimen and apparatus had reached equilibrium conditions at temperature, the transducer was adjusted to give a zero reading, the temperature was noted, the required load applied and the chart recorder switched on to commence the creep test.

The chart recorder produced a continuous record of the specimen length change and the specimen temperature. The fixed chart speed allowed the recorded length change of the specimen to be interpreted in terms of a length change per unit time, and knowing the specimen dimensions this in turn yielded the compression creep rate.

During the course of a test the conditions were periodically changed to investigate the effect of changing load at constant temperature and changing temperature at constant load. In all cases of a change in conditions the creep rate was allowed to reach steady state conditions before any further changes were made. The load, temperature and time were noted immediately before and after a change in conditions. In general a test was terminated when a specimen had undergone between 5 and 10% deformation.

On completion of a test the final time, load and temperature were noted, the chart recorder was switched-off, the specimen load was removed, the top ram lifted and the specimen was allowed to cool under zero load by switching off the furnace. After cooling, the specimen was removed from the furnace and its new dimensions were measured and recorded.

Two series of tests, carried out in an air atmosphere, were performed for a number of alloy compositions; in the first series specimen temperature changes were confined to the range 746°K to 887°K and in the second series they were in the range 953° to 1088°K. In general, two specimens of each alloy composition were tested in each creep series (a total of four specimens for each alloy in all).

It was found that upon the start of a test primary creep continued to about 0·3 - 0·5% strain. Thereafter steady state creep was achieved after only a small amount of primary creep whenever the test conditions were changed.

Load changing tests were carried out at constant temperature and as a rule load values were increased and decreased alternately, with the initial loading conditions being repeated at least once during. This was to afford a check on the strain and structure dependence of the stress sensitivity.

Temperature change tests were carried out at constant load and again the initial test conditions were repeated in the course of a test.

In general, it was found that several variable load tests could be carried out at different constant temperatures within the limitation of some 5% total strain before terminating a creep run on a given specimen. Similarly several change of temperature tests could be performed at different constant loads. In practice one variable load test and two or more variable temperature tests were carried out during the course

of a creep run on a single specimen, to yield one stress exponent and several values of the creep activation energy.

3.7.4 Analysis of Creep Data

After a creep test the total deformation strain of a specimen was determined by direct measurement of its dimensions. This value was found to be in good agreement with the total deformation strain calculated from the chart record.

The length change produced by creep under any set of constant test conditions was determined for each part of the test. Hence the specimen length at the beginning (l) and end ($l-2\Delta l$) of a given part of a test, under given conditions of load and temperature, was known. Assuming constancy of volume during deformation and using the mean length ($l-\Delta l$) of the specimen, a mean cross-sectional area of the specimen was calculated for each part of the test. In other words if one set of test conditions prevailed while a specimen deformed from a length (l) to a length ($l-2\Delta l$) then its cross-sectional area was calculated by assuming its true length to be ($l-\Delta l$) and volume constant.

A correction was also applied for the change in specimen dimensions as the result of thermal expansion (when temperature conditions were changed).

The true stress borne by a specimen was then calculated from the known applied load and the calculated true specimen dimensions (i.e. corrected for deformation and thermal strain).

A mean steady state extension rate, for each set of test conditions, was calculated from the slope of the chart recorded data (which printed extension as a function of time). Each steady state extension rate was then expressed as a true steady state creep strain rate on dividing by

the calculated true length $(l-\Delta l)$ pertaining to each set of test conditions.

These calculations thus yielded a series of true creep strain rate values corresponding to test conditions of known true stress and applied temperature. In this form the creep data was then used to evaluate creep stress exponents and creep activation energies.

3.7.5 Calculation of Stress Exponents and Creep Activation Energies

Stress exponents were evaluated from the creep data (true stress, true strain rate and temperature) determined during change of load tests at constant temperature. The creep strain rate $(\dot{\varepsilon})$ is dependent on the stress (σ) according to the relation:

$$\dot{\varepsilon} = K \sigma^n \qquad 3.8$$

where n is the stress exponent. The exponent n was evaluated from the gradient of the linear plot of $\ln \dot{\varepsilon}$ versus $\ln \sigma$, using a least squares best straight line computer programme.

Stress exponents determined by this method for the various alloy compositions and fixed temperatures are given in the results [TABLES V & VII].

The general creep equation relating the creep strain rate with both stress (σ) and temperature (T) is given by (see equation 2.46):

$$\dot{\varepsilon} = K' \sigma^n \exp\left(-\frac{Q_c}{kT}\right) \qquad 3.9$$

where Q_c is the apparent activation energy of creep. But the change of temperature tests were carried out at constant load and not constant stress and hence the stress term is not constant.

However equation 3.9 may be written:

$$\left(\frac{\dot{\varepsilon}}{\sigma^n}\right) = K' \exp\left(-\frac{Q_c}{kT}\right) \qquad 3.10$$

Now at constant load the stress changed because of the change in specimen dimensions due to deformation and temperature changes. However the true stress values correcting for these effects are known [see section 3.7.4] . Also the stress exponent was evaluated experimentally and hence also known. Consequently the activation energy of creep Q_c was calculated by plotting $\ln(\dot{\varepsilon}/\sigma^n)$ versus $(1/T)$ and determining the gradient of the resultant straight line by means of a least squares best straight line fit computer programme.

It was noted that this plot would only yield a linear relationship on the assumption that the stress exponent (n) was not temperature dependent.

Activation energies of creep determined from equation 3.10 for various alloy compositions and constant loads (actually given as nominal stresses) are shown in the results [TABLES VI & VIII] .

CHAPTER 4: Experimental Results

4.1 Alloy Analysis

The chemical compositional analysis of all the alloys used in this study are shown in TABLE I. The same table also includes a schematic outline of the experimental observations carried out on any given alloy.

4.2 Alloy Metallography

All the alloys were metallographically examined under an optical microscope in both the chill cast (arc melted) condition and in the induction melted condition. The findings were reported in the experimental procedure [sections 3.3.1 and 3.3.2].

A number of the alloys were also analysed by Debye-Scherrer X-ray photography and both crystal structure and lattice parameter determined. The results of both X-ray and optical metallography are shown in TABLE II.

4.3 Lattice Parameter Measurements

Alloy powder samples, taken from both arc-melted and induction melted ingots, were X-rayed and lattice parameter values were determined from the resultant diffraction patterns [sections 3.4.1 and 3.4.2]. The variation of the lattice parameter as a function of composition for all X-rayed samples is shown in GRAPH 1 (G.1.).

The observed compositional dependence of the lattice parameter can not be accounted for on the basis of differences in quenched-in thermal

TABLE 1

ALLOY COMPOSITION AT %			USE MADE OF ALLOY	
Ni	Ga	Cu	Arc Melted	Induction Melted
43.98	56.02		M X	M X
47.18	52.82		M X	M X D GA
47.28	52.72		M X	M X D NI
48.76	51.24		M X	M X D NI GA
49.33	50.67		M X	M X D NI
50.01	49.99		M X	M X D NI GA
50.45	49.55		M X	M X D NI
50.73	49.27		M X	M X D NI GA
51.01	48.99		M X	M X D NI GA
52.40	47.60		M X	M X D NI GA
54.59	45.51		M X	M X D
48.96	51.04		M C	
49.03	50.97		M C	
50.17	49.83		M C	
50.37	49.63		M C	
51.00	49.00		M C	
52.27	47.73		M C	

ERROR ± 0.1% IN ALL CASES

ERROR ± 0.2% IN ALL CASES

LESS THAN 0.01% IN ALL CASES

KEY

M = OPTICAL METALLOGRAPHY
X = X-RAY PHOTOGRAPHY
D = EXPERIMENTAL DENSITY
NI = DIFFUSION OF Ni-63
GA = DIFFUSION OF Ga-67
C = COMPRESSION CREEP

TABLE II

Alloy Compn Atomic% Ni	OPTICAL METALLOGRAPHY		X-RAY METALLOGRAPHY	
	Arc Melted	Induction Melted	Arc Melted	Induction Melted
43.98		LGS 2P Porous	Two phase-ordered B.C.C matrix	
47.18				
47.28	SINGLE PHASE	SINGLE PHASE		
48.76			SINGLE PHASE	
49.33	CHILL CAST:	VERY LARGE GRAIN		
50.01				
50.45	COLUMNAR	SIZE. GOOD DENSITY		
50.73	GRAINS		ORDERED B.C.C.	
51.01				
52.40	SOME POROSITY			
54.59		Very LGS 2P Dense		
48.96	IN ALL CASES		NOT X-RAYED	
49.03		NOT		
50.17				
50.37		INDUCTION		
51.00				
52.27		MELTED		

KEY. 2P= TWO PHASE LGS= LARGE GRAIN SIZE

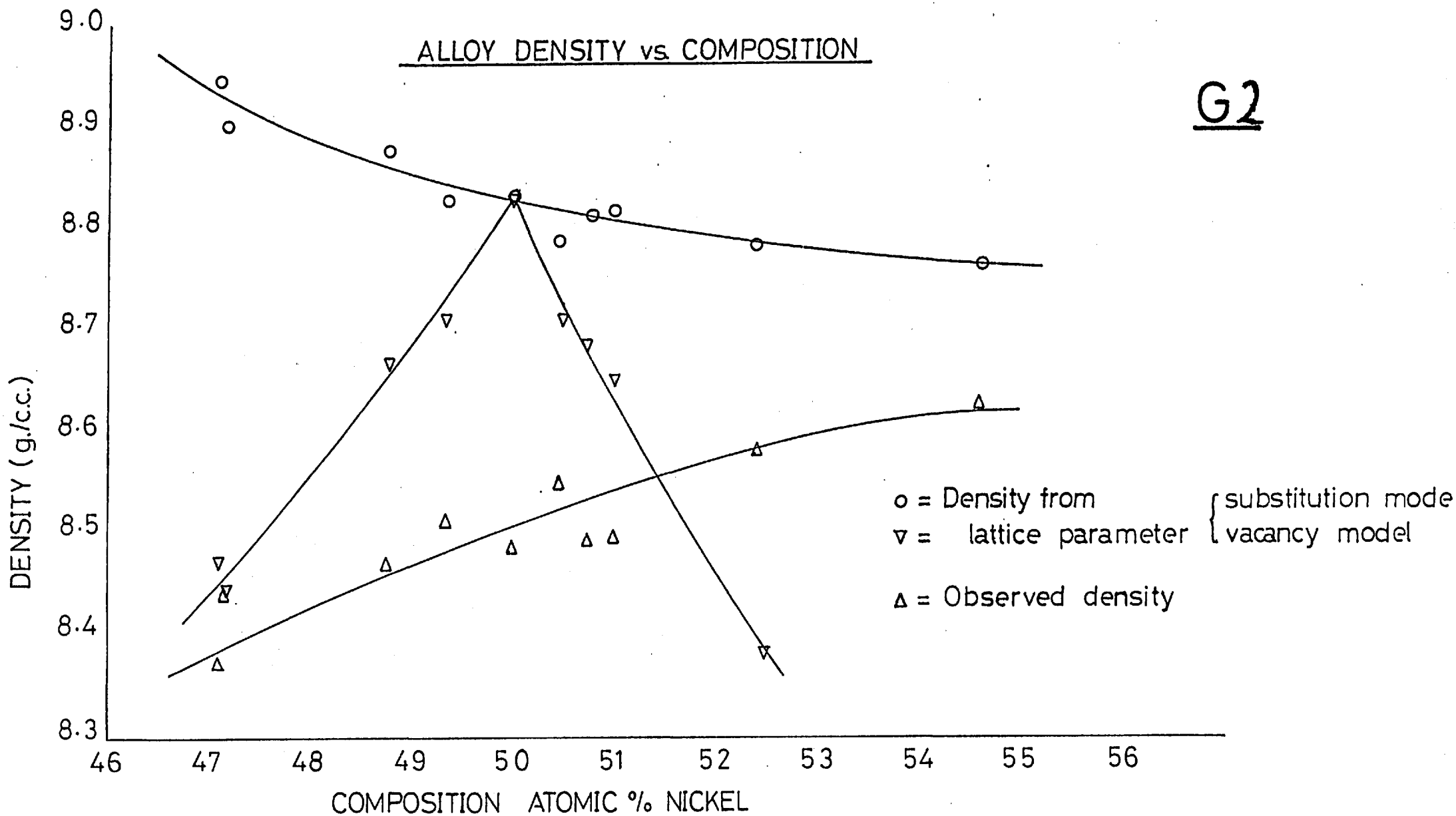
ALLOY DENSITY vs. COMPOSITION
G2
9·0
8·9
8·8
8·7
8·6
8·5
8·4
8·3
DENSITY (g./c.c.)
46
47
48
49
50
51
52
53
54
55
56
COMPOSITION ATOMIC % NICKEL
o = Density from
∇ = lattice parameter
substitution mode
vacancy model
Δ = Observed density

defect concentrations as a function of composition. This is because all the alloy samples were quite slowly cooled after annealing and consequently retained thermal defect fractions are likely to be small. Indeed the same trend in the compositional dependence of the lattice parameter has been observed both for furnace cooled and water quenched powder samples [145] .

Furthermore, although large numbers of quenched-in defects have been reported in NiGa (up to 1% for quench temperatures of 1133°K) [145] even these concentrations are insufficient to account for the compositional dependence of the lattice parameter. Consequently it has been concluded that constitutional defects are responsible for the observed lattice parameter variation.

In order to afford a comparison with the experimental lattice parameter data, a theoretical lattice parameter, based on Vegard's Law, was calculated assuming two atoms per unit structure cell and using the Goldschmidt atomic radii of (r_{Ni} = 1·25 Å) and (r_{Ga} = 1·35 Å) for nickel and gallium respectively. The lattice parameter 'a_v' was then given by:

$$a_v = \frac{4}{3^{\frac{1}{2}}} \left[f_{Ni} \cdot r_{Ni} + f_{Ga} \cdot r_{Ga} \right]$$

where f_{Ni} and f_{Ga} are the atomic fractions of nickel and gallium respectively.

Now Vegard's Law assumes full site occupancy and is hence a direct substitutional model. Consequently the compositional dependence of the lattice parameter predicted by Vegard's Law is that for a direct substitution (constitutional) defect model.

A second theoretical lattice parameter was evaluated for the case of constitutional vacancy defects. It was assumed that no defects were present at stoichiometry and that in the limiting case a vacancy had zero

volume. Then, considering vacancies as a third substitutional species, the maximum variation of the lattice parameter with composition was evaluated from a modification of Vegard's law. Then for the compound $Ni_{(x)}\ Ga_{(1-x)}$ the lattice parameter allowing for vacancies a_v^v was given by:

$$a_v^v = \frac{2}{(3)^{\frac{1}{2}}} \left[r_{Ni} + \left(\frac{1-x}{x}\right) r_{Ga} \right] \qquad x \geqslant 0.5$$

$$a_v^v = \frac{2}{(3)^{\frac{1}{2}}} \left[\left(\frac{x}{1-x}\right) r_{Ni} + r_{Ga} \right] \qquad x \leqslant 0.5$$

(cf. the vacancy density model in Appendix 1)

The compositional dependences of these two theoretical lattice parameters (the substitutional model and the vacancy model) are shown in GRAPH 1 (G.1) for comparison with the observed values.

4.4 Theoretical and Experimental Density Values

Experimental density values were measured for bulk samples taken from induction melted ingots [see section 3.5]. The compositional dependence of the density is given in GRAPH 2 (G.2).

The observed compositional dependence of the density was not due to changes in quenched-in defect concentrations with composition, since the effect of these latter was too small. Furthermore the compositional dependence of the density did not merely reflect a change in the degree of alloy porosity with composition. Although some porosity was observed in all samples there was no evident change in the degree of porosity with composition. In addition the compositional dependence of the density measured in the bulk samples was in good agreement with measurements reported for powder samples, where porosity would be less important [145].

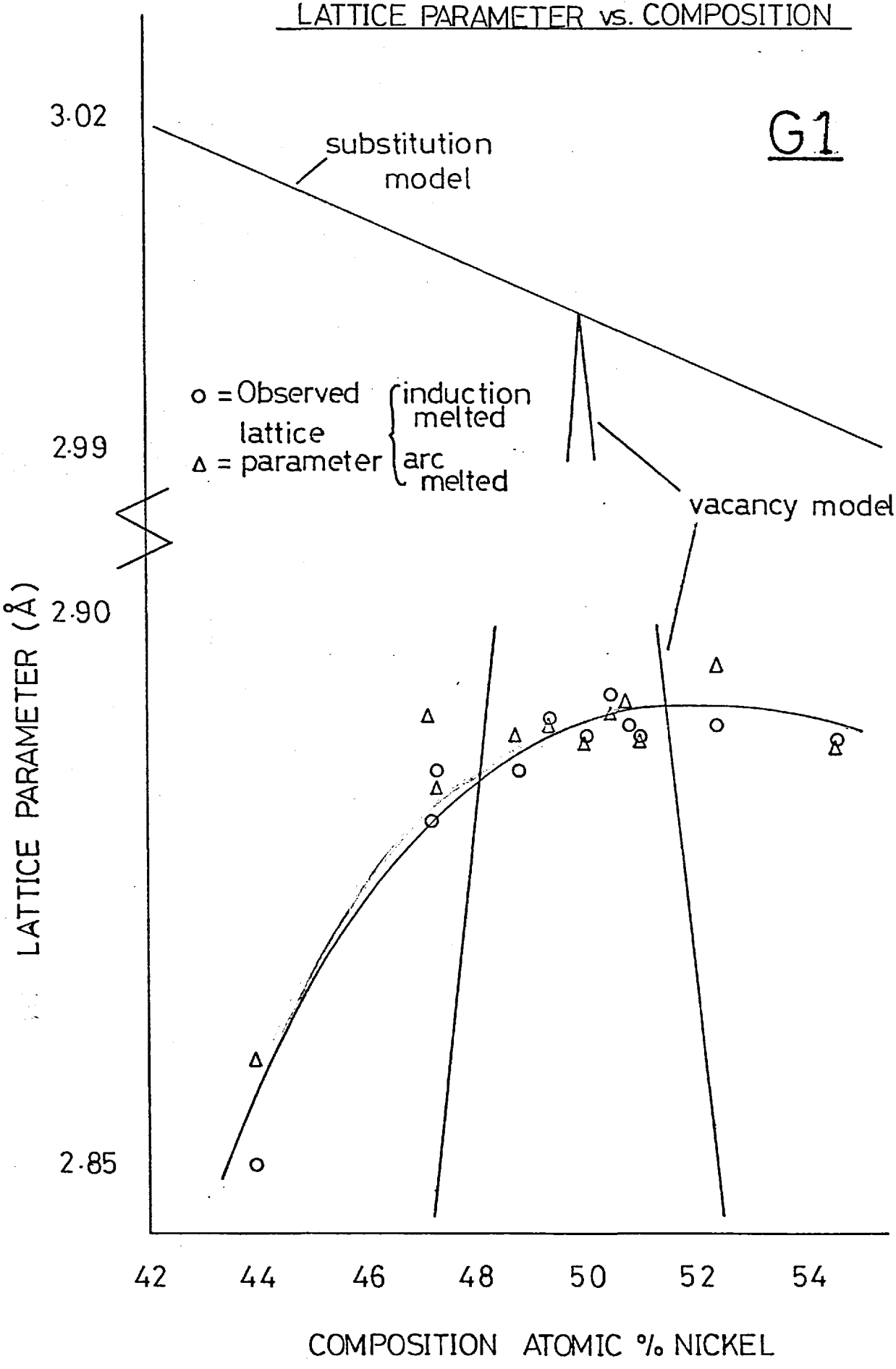
LATTICE PARAMETER vs. COMPOSITION
G1
3·02
2·99
2·90
2·85
substitution model
o = Observed lattice parameter
induction melted
arc melted
vacancy model
LATTICE PARAMETER (Å)
42
44
46
48
50
52
54
COMPOSITION ATOMIC % NICKEL

It was concluded that the observed compositional dependence of the density arose from the presence of constitutional defects.

A theoretical density (ρ_{th}) was calculated from experimental lattice parameter values (a_o) on the assumption of two atoms per unit cell. The theoretical density (ρ_{th}) is given by the expression:

$$\rho_{th} = 2 M_{NiGa} / N_A (a_o)^3 \qquad 4.1$$

where N_A is Avogadro's number and M_{NiGa} is the mean atomic weight of the species occupying the lattice (see Appendix 1).

In the case of the direct substitution model M_{NiGa} is given by the expression (Appendix 1):

$$M_{NiGa} = f_{Ni} \cdot A_{Ni} + f_{Ga} \cdot A_{Ga}$$

where f_{Ni} and f_{Ga} are the atomic fractions and A_{Ni} and A_{Ga} the atomic weights of nickel and gallium respectively.

The experimental density and the theoretical density are shown as a function of composition in graph (G.2).

4.5 Diffusion Results

One example of the diffusion penetration profiles determined by radio-tracer analysis is given for each of the two tracer species used; a penetration profile for nickel-63 is shown in graph G.3 and a penetration profile for gallium-67 is shown in graph G.4. Both profiles were plotted as a count activity (counts/unit time) against the diffused distance (in micro-metres) [see sections 3.6.6 to 3.6.8].

One example of the penetration profile plotted as the log of the count activity (ln I) versus the penetration depth squared (x^2) is shown

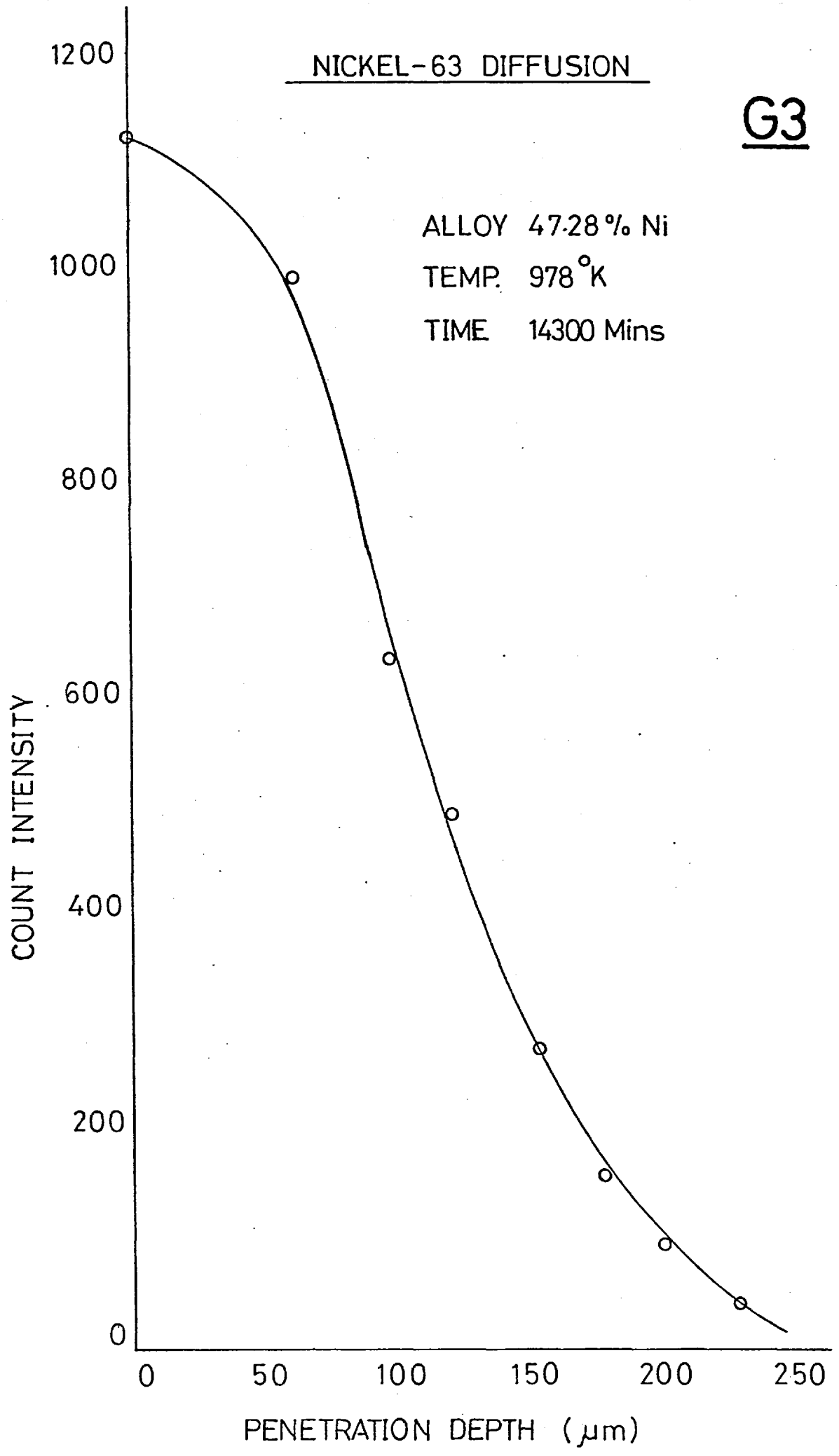
NICKEL-63 DIFFUSION
G3
ALLOY 47·28 % Ni
TEMP. 978 °K
TIME 14300 Mins
COUNT INTENSITY
1200
1000
800
600
400
200
0
0
50
100
150
200
250
PENETRATION DEPTH (μm)

GALLIUM - 67 DIFFUSION

G4

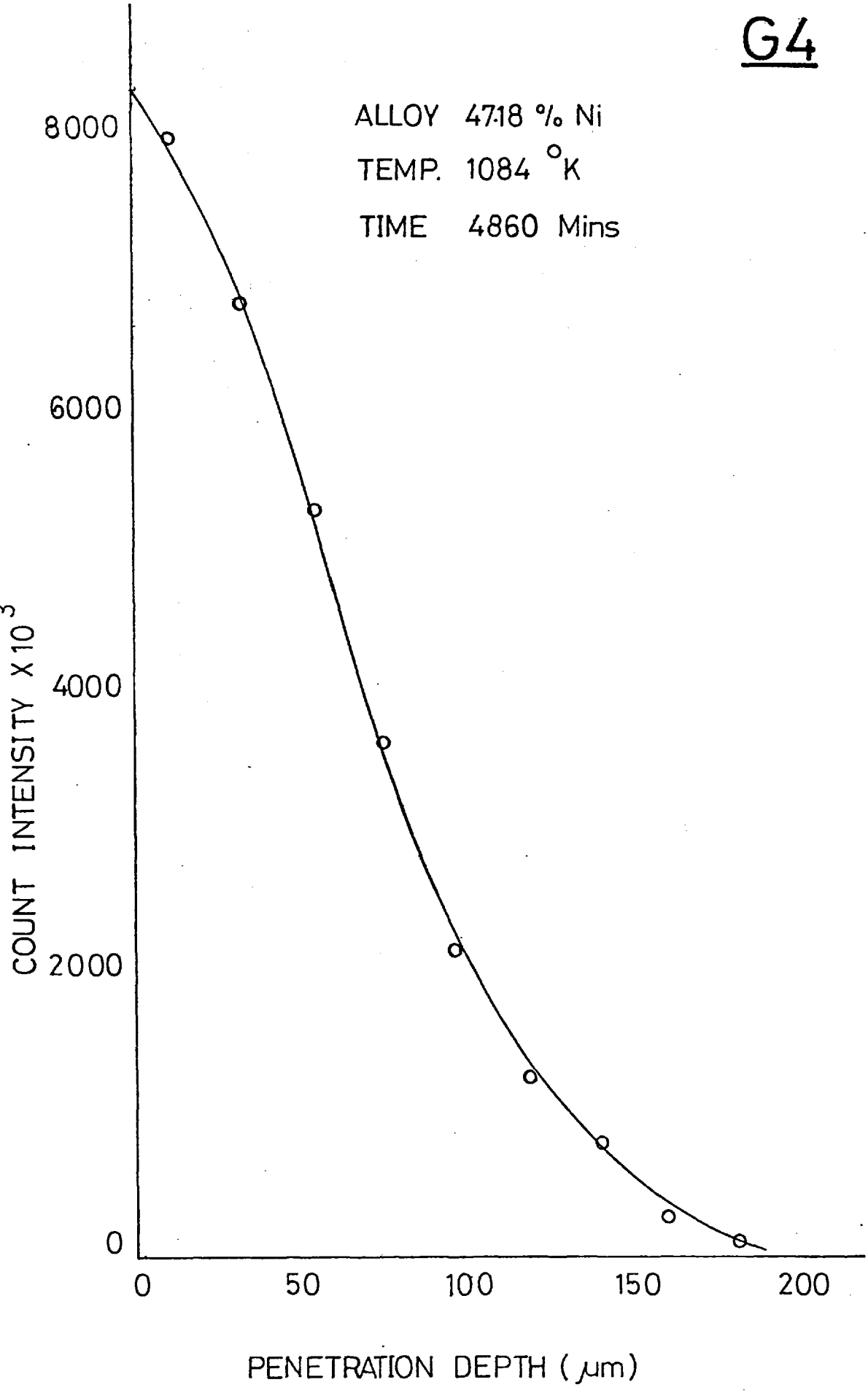

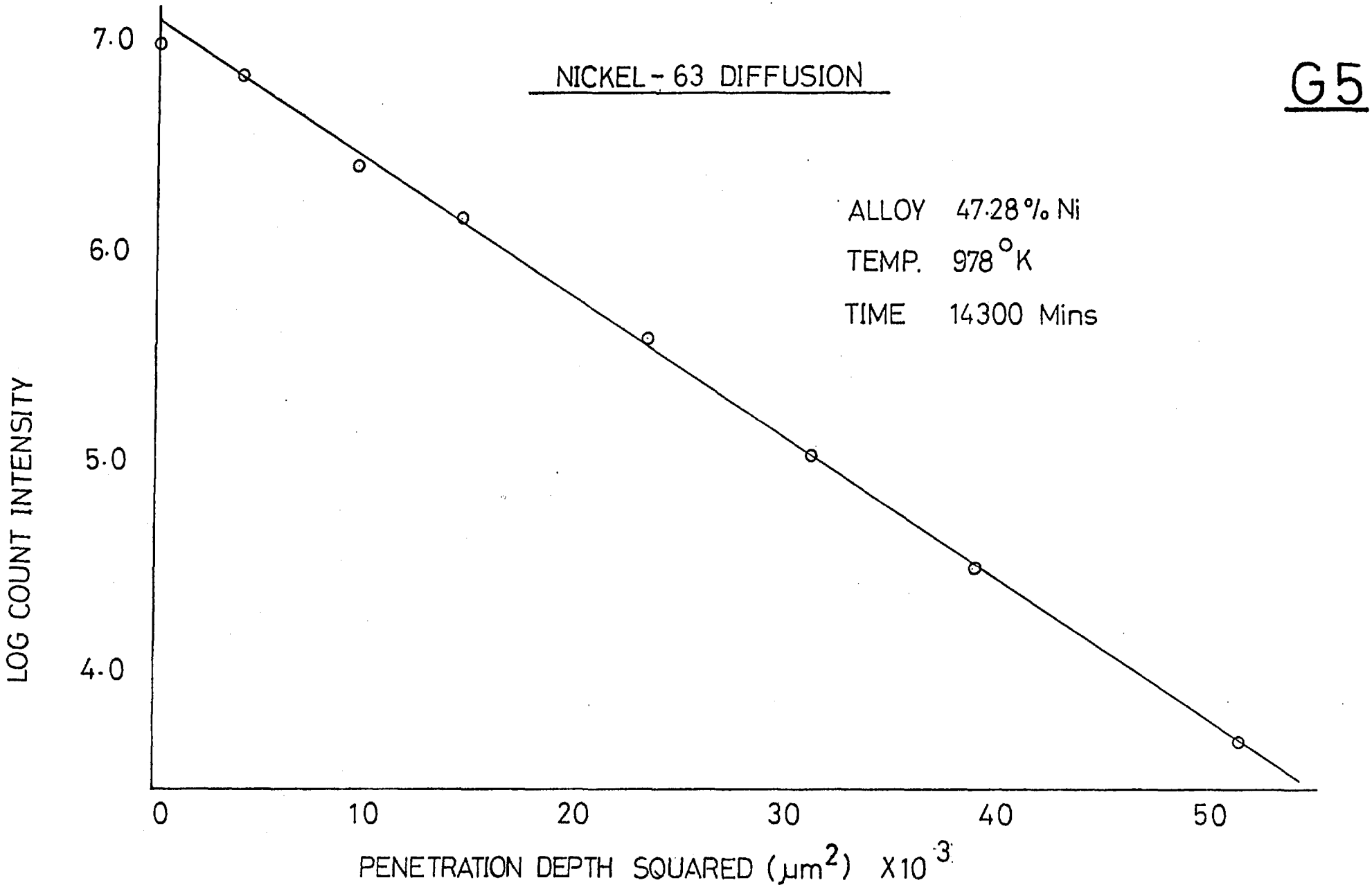
NICKEL - 63 DIFFUSION
G5
ALLOY 47·28 % Ni
TEMP. 978 °K
TIME 14300 Mins
LOG COUNT INTENSITY
7·0
6·0
5·0
4·0
0
10
20
30
40
50
PENETRATION DEPTH SQUARED (μm²) X10⁻³

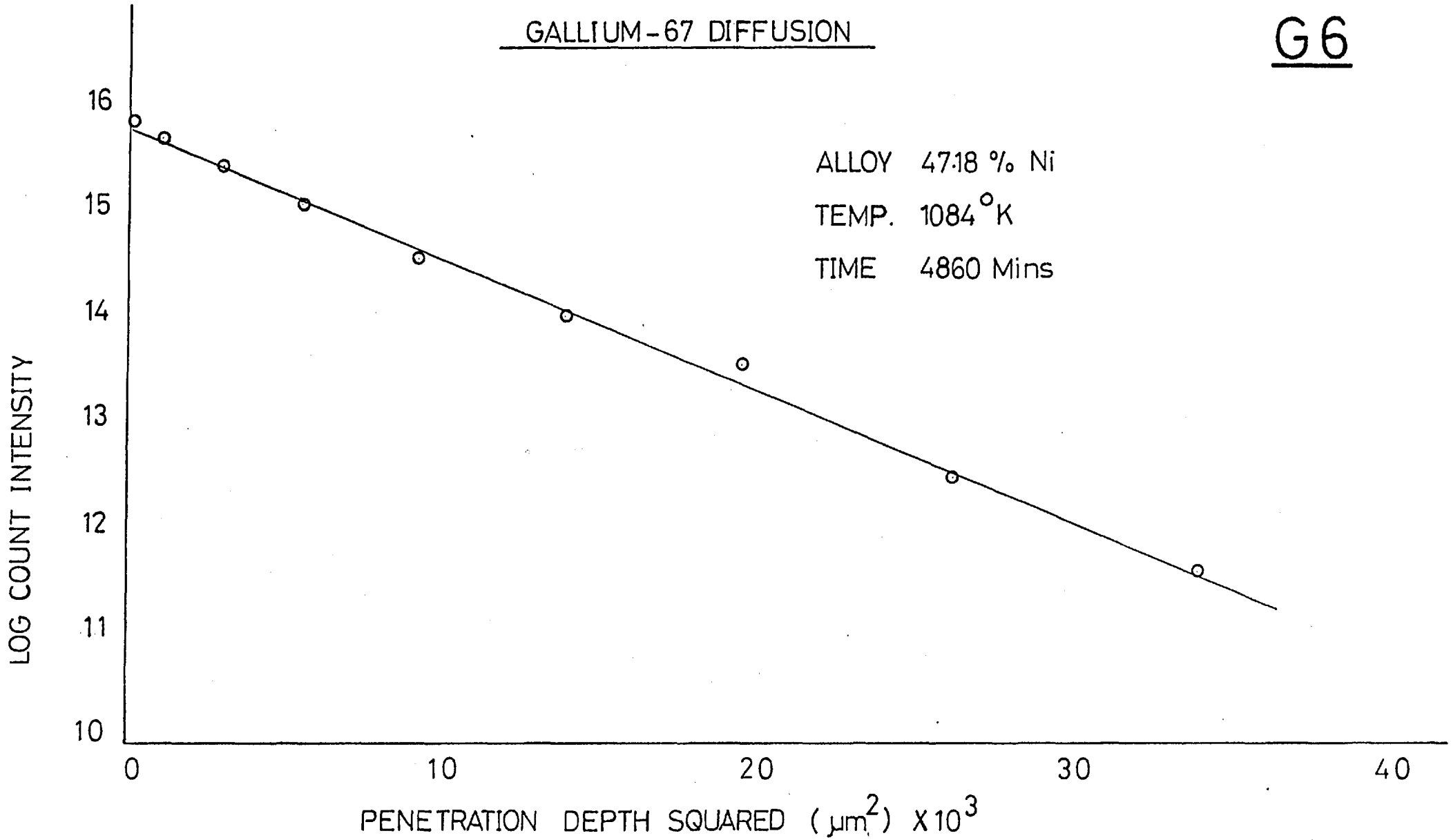
GALLIUM-67 DIFFUSION
G6
ALLOY 47·18 % Ni
TEMP. 1084°K
TIME 4860 Mins
LOG COUNT INTENSITY
16
15
14
13
12
11
10
0
10
20
30
40
PENETRATION DEPTH SQUARED (μm²) X10³

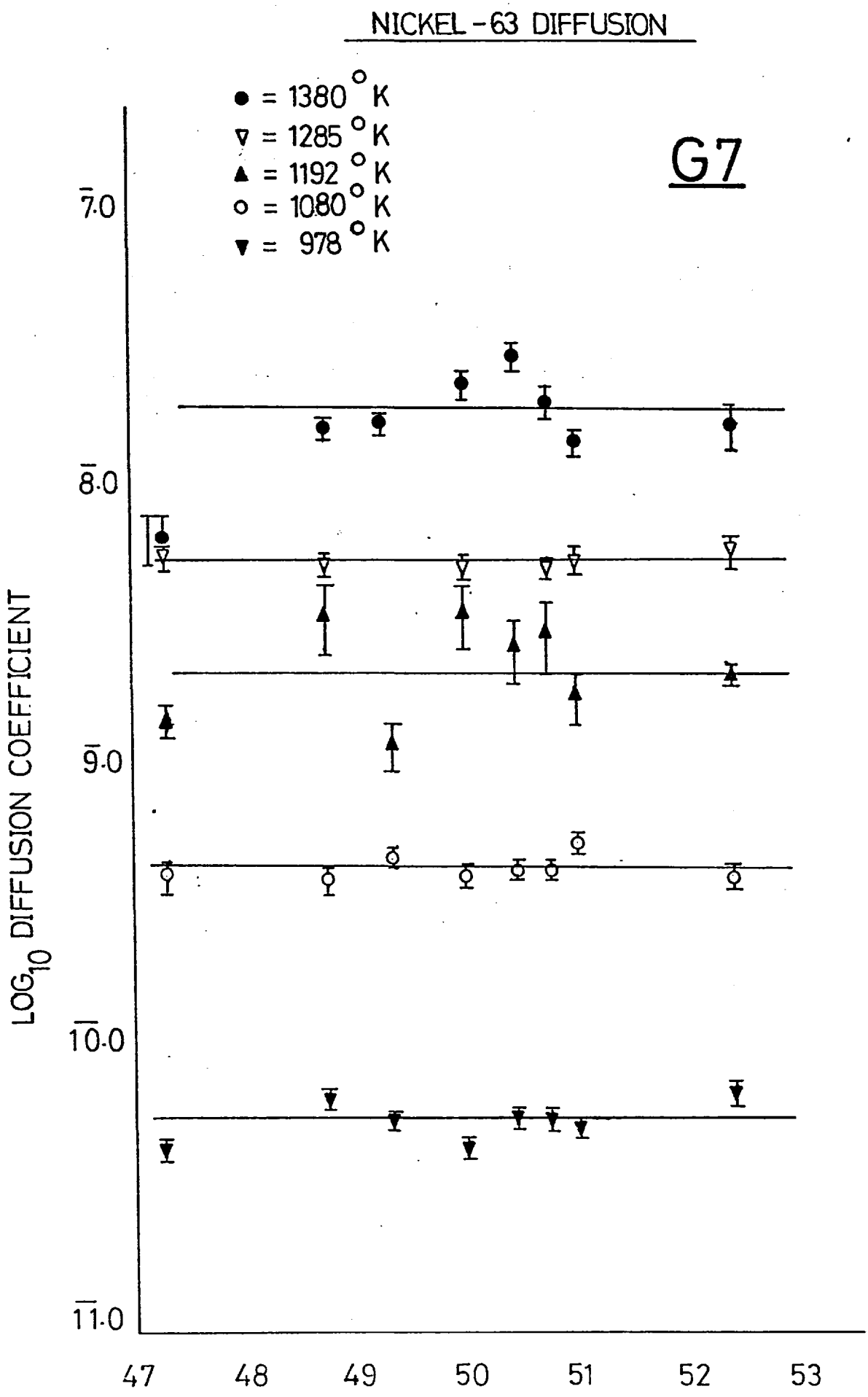
NICKEL - 63 DIFFUSION
● = 1380 °K
▽ = 1285 °K
▲ = 1192 °K
○ = 1080 °K
▼ = 978 °K
G7
$\bar{7}$·0
$\bar{8}$·0
$\bar{9}$·0
$\bar{10}$·0
$\bar{11}$·0
LOG$_{10}$ DIFFUSION COEFFICIENT
47
48
49
50
51
52
53
COMPOSITION ATOMIC % NICKEL

GALLIUM-67 DIFFUSION

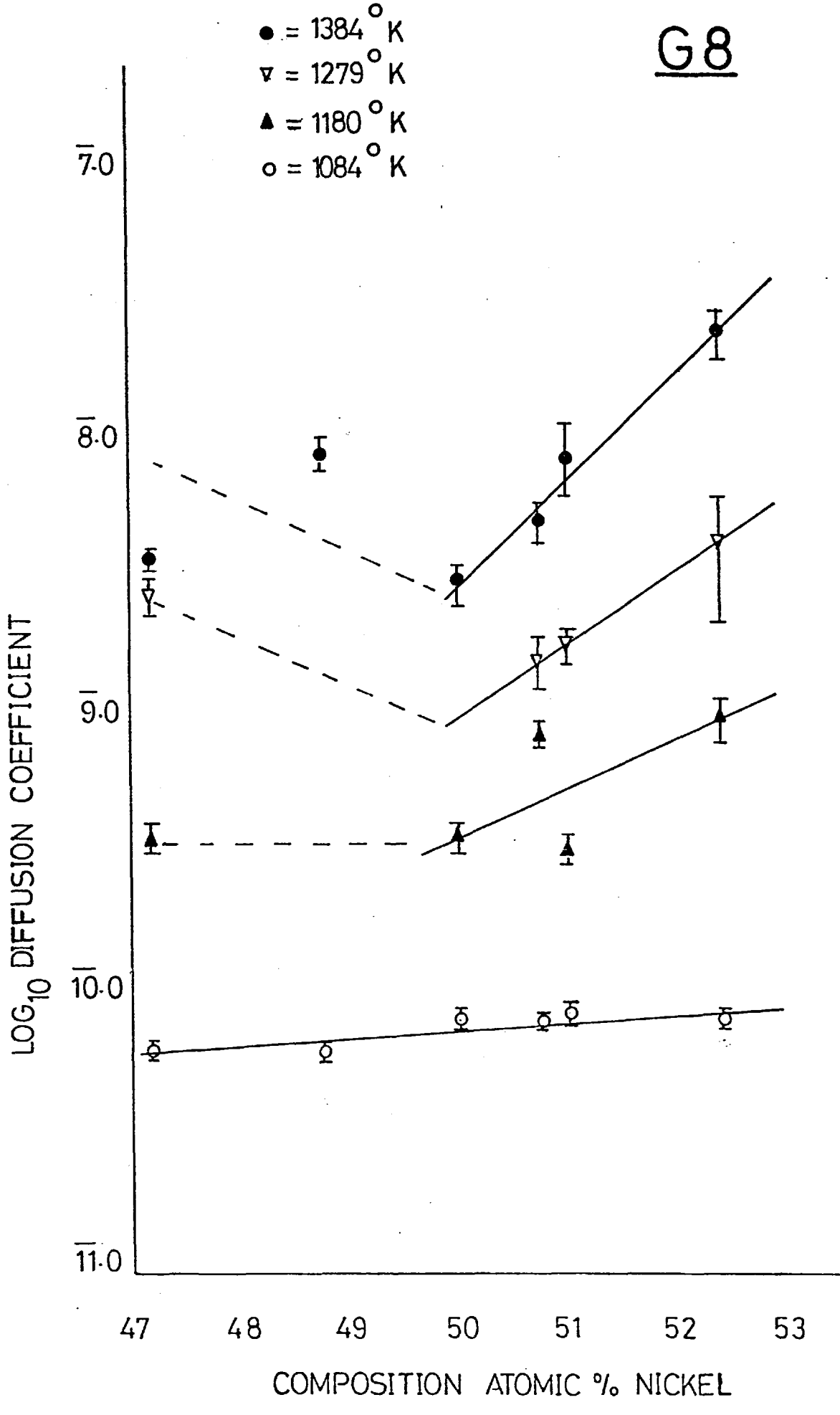

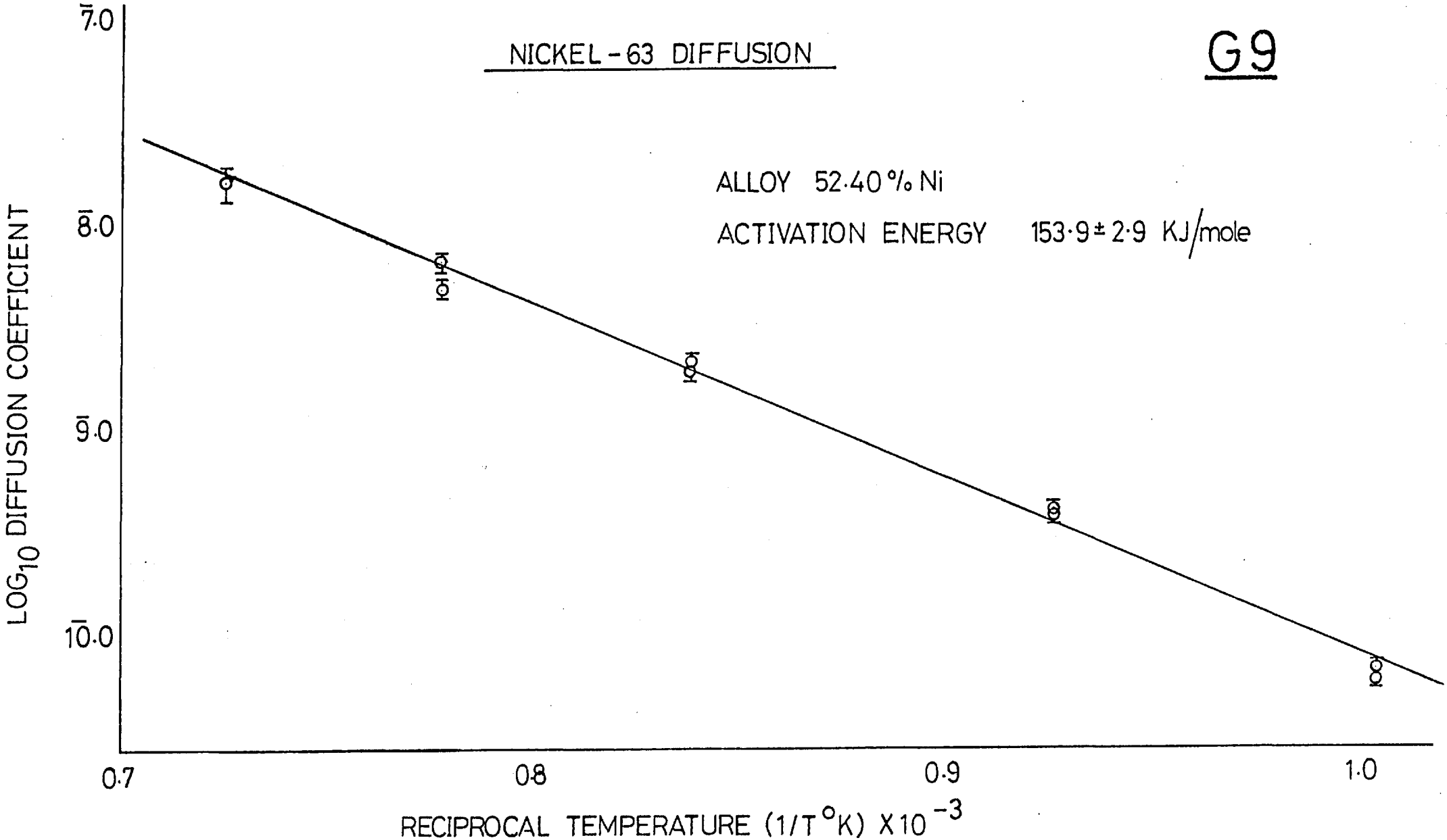
NICKEL-63 DIFFUSION
G9
ALLOY 52·40 % Ni
ACTIVATION ENERGY 153·9 ± 2·9 KJ/mole
$\bar{7}$·0
$\bar{8}$·0
$\bar{9}$·0
$\bar{10}$·0
LOG10 DIFFUSION COEFFICIENT
0·7
0·8
0·9
1·0
RECIPROCAL TEMPERATURE (1/T °K) X10 -3

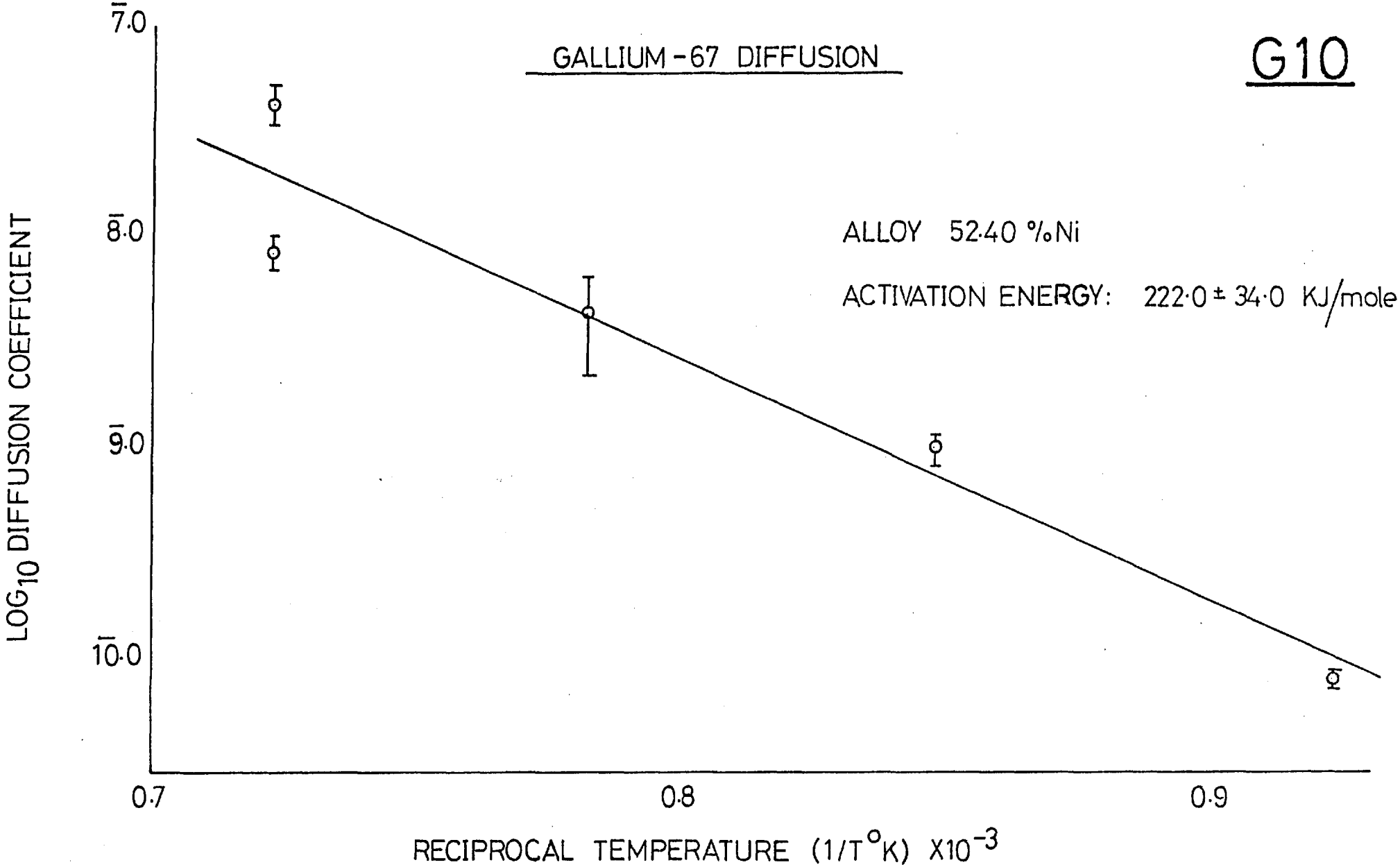
GALLIUM-67 DIFFUSION
G10
ALLOY 52·40 %Ni
ACTIVATION ENERGY: 222·0 ± 34·0 KJ/mole
LOG10 DIFFUSION COEFFICIENT
$\bar{7}$·0
$\bar{8}$·0
$\bar{9}$·0
$\bar{10}$·0
0·7
0·8
0·9
RECIPROCAL TEMPERATURE (1/T °K) X10^{-3}

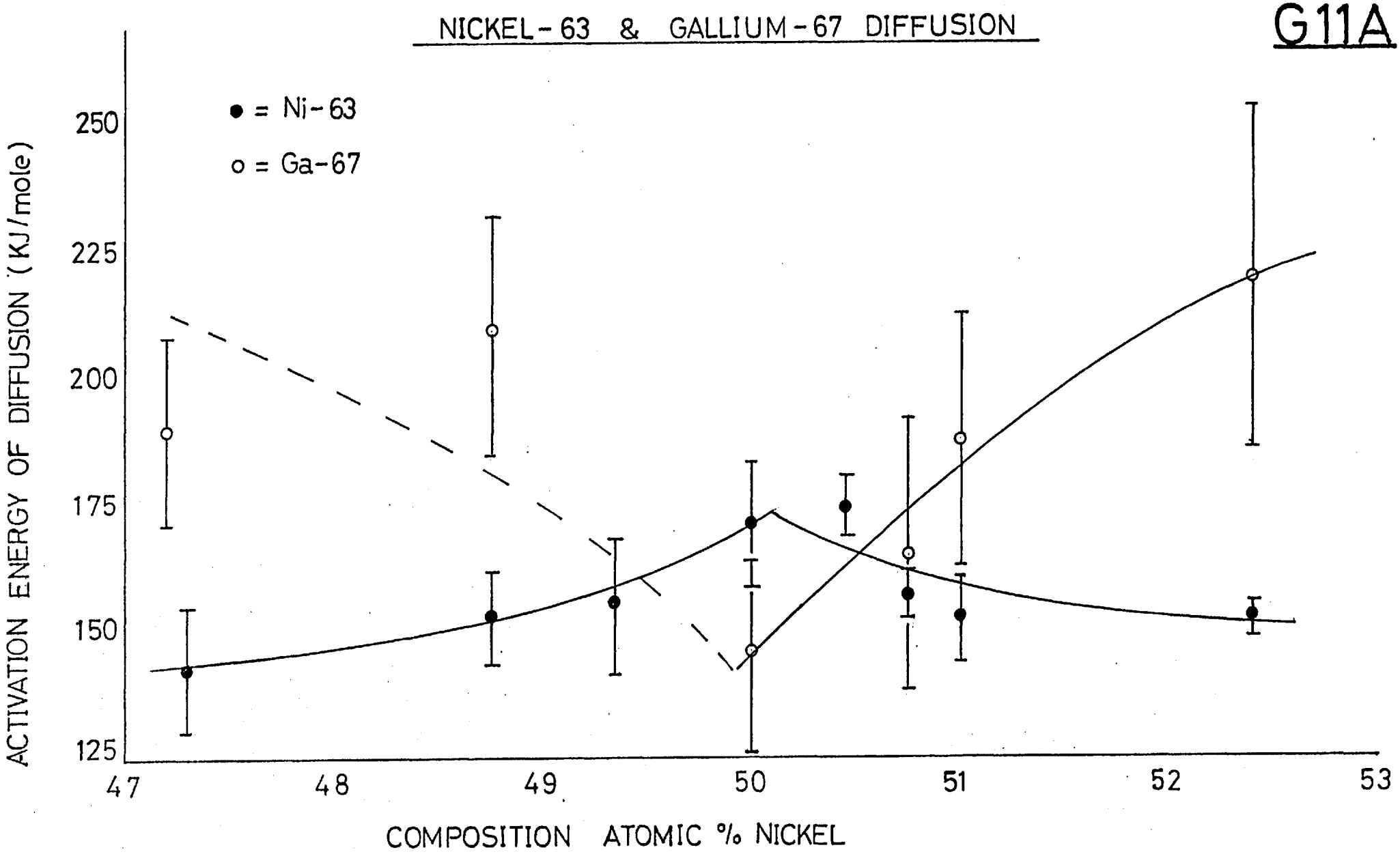
NICKEL-63 & GALLIUM-67 DIFFUSION
● = Ni-63
o = Ga-67
ACTIVATION ENERGY OF DIFFUSION (KJ/mole)
250
225
200
175
150
125
47
48
49
50
51
52
53
COMPOSITION ATOMIC % NICKEL

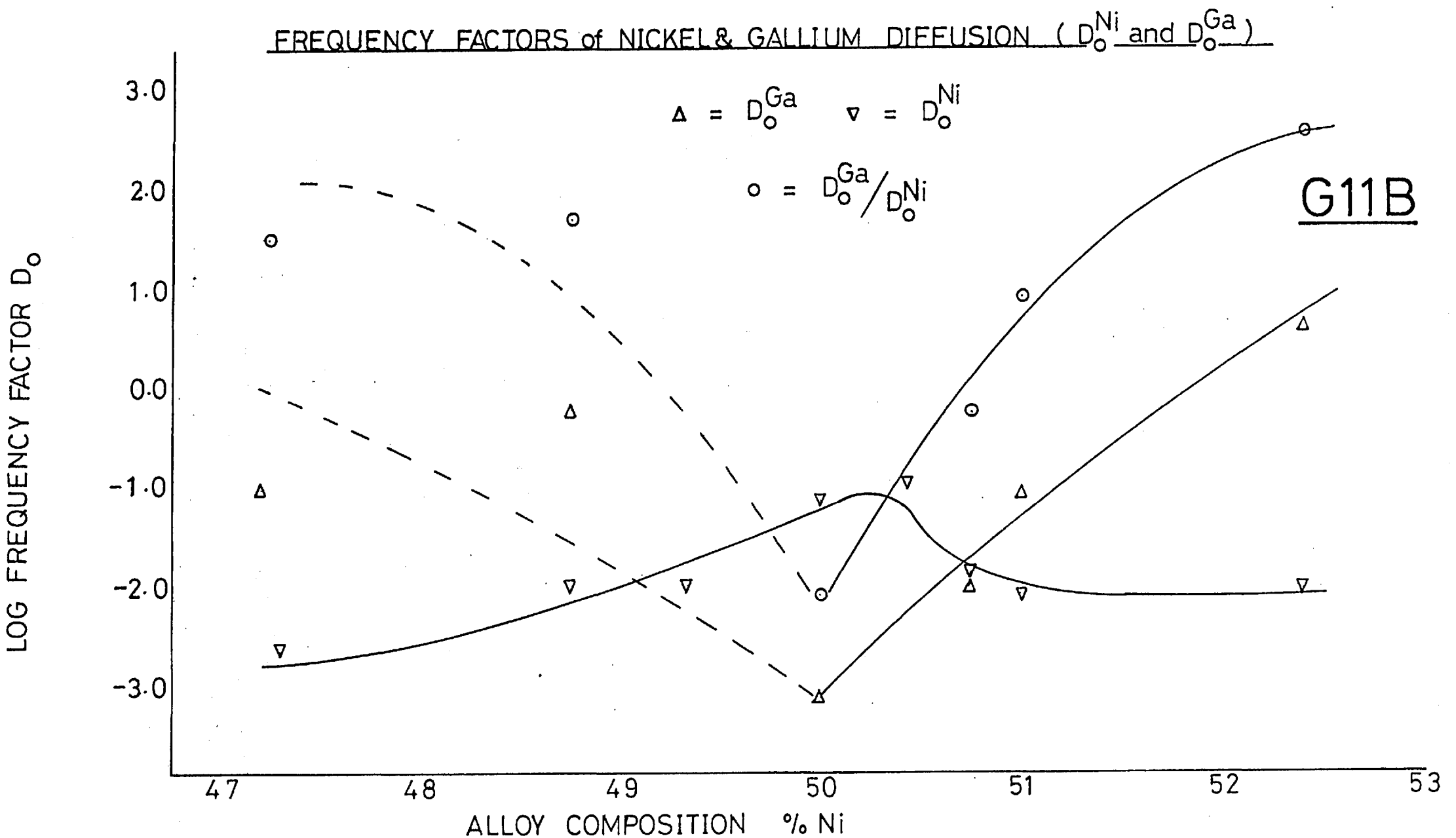
FREQUENCY FACTORS of NICKEL & GALLIUM DIFFUSION (D_o^{Ni} and D_o^{Ga})
Δ = D_o^{Ga}
∇ = D_o^{Ni}
○ = D_o^{Ga}/D_o^{Ni}
G11B
LOG FREQUENCY FACTOR D_o
3·0
2·0
1·0
0·0
-1·0
-2·0
-3·0
47
48
49
50
51
52
53
ALLOY COMPOSITION % Ni

TABLE III DIFFUSION OF NICKEL-63

ALLOY COMP^{n} % Ni	DIFFUSION COEFFICIENT AS FN. TEMPERATURE X10^{-11}										Q	EQ	D_o	ED_o
	978° K		1080° K		1192° K		1285° K		1380° K					
	D	ED	D	ED	D	ED	D	ED	D	ED	KJ/mole	KJ/mole		
47·28	4·46	0·07	43·55	3·34	154·68	18·44	612·45	75·10	712·81	139·94	143·1	12·7	0·0029	0·0038
48·76	6·71	0·27	42·14	3·30	374·05	102·13	567·32	61·59	1812·56	71·28	154·3	8·9	0·0126	0·0117
49·33	5·72	0·04	50·08	1·99	128·46	26·32	——	——	1864·98	97·49	156·0	13·8	0·0130	0·0192
50·01	4·54	0·05	43·66	1·62	383·78	92·92	558·13	55·56	2573·36	204·11	172·5	12·5	0·0936	0·1220
50·45	5·88	0·07	46·09	2·83	288·28	70·49	——	——	3223·16	362·78	175·3	8·2	0·1353	0·1187
50·73	5·82	0·10	45·93	3·15	323·90	94·36	554·46	32·50	2206·66	275·72	158·2	4·6	0·0174	0·0084
51·01	5·28	0·07	57·28	3·52	192·11	37·39	582·70	65·21	1603·13	90·28	153·7	8·7	0·0107	0·0095
52·40	7·23	0·08	43·78	3·84	229·03	16·23	650·82	45·49	1834·19	325·32	153·9	2·9	0·0121	0·0037

KEY: Q = ACTIVATION ENERGY D = DIFFUSION COEFFICIENT D_o = FREQUENCY FACTOR

EQ = ERROR IN Q ED = ERROR IN D ED_o = ERROR IN D_o

TABLE IV DIFFUSION OF GALLIUM - 67

ALLOY COMP^{n} % Ni	DIFFUSION COEFFICIENT AS FN. OF TEMPERATURE, X 10^{-11}								Q	EQ	D_o	ED_o
	1084°K		1180°K		1279°K		1384°K					
	D	ED	D	ED	D	ED	D	ED	KJ/mole	KJ/mole		
47·18	6·56	0·11	38·14	3·57	294·26	45·04	398·23	33·21	191·5	12·7	0·1230	0·2317
48·76	6·39	0·03	—	—	—	—	983·19	134·16	209·4	—	0·7874	—
50·01	8·46	0·29	38·91	3·28	—	—	324·40	54·31	146·5	18·8	0·0010	0·0019
50·73	8·41	0·25	93·99	7·10	172·79	25·84	558·74	87·64	166·4	27·4	0·0122	0·0329
51·01	9·07	0·21	35·73	3·37	191·01	24·38	949·17	312·40	189·6	25·3	0·1087	0·2656
52·40	8·59	0·12	107·66	13·40	465·94	229·12	2776·31	559·96	222·0	34·0	5·1430	20·9524

KEY: Q = ACTIVATION ENERGY D = DIFFUSION COEFFIENT D_o = FREQUENCY FACTOR

EQ = ERROR IN Q ED = ERROR IN D ED_o = ERROR IN D_o

for nickel-63 and gallium-67 diffusion in graphs G.5 and G.6 respectively. The diffusion coefficients D_{Ni} and D_{Ga} were evaluated from the slopes of the resulting straight lines [see section 3.6.8] .

The compositional dependence of the diffusion coefficient D_{Ni} of nickel-63 is shown for the various annealing temperatures in graph G.7. The corresponding data for the diffusion coefficient D_{Ga} of gallium-67 is shown in graph G.8.

The activation energy of diffusion Q was determined for each alloy composition from the gradient of the straight line plot of ln D versus $(^1/T)$. One example of this plot is shown for nickel-63 and gallium-67 diffusion in graphs G.9 and G.10 respectively.

The compositional dependence of the activation energy of nickel diffusion Q_{Ni} and gallium diffusion Q_{Ga} is shown in graph G.11.

Finally the diffusion data, diffusion coefficients and activation energies of the various alloys, for nickel diffusion are summarised in TABLE III while the corresponding data for gallium diffusion are summarised in TABLE IV.

4.6 Compression Creep Results

Two series of compression creep test were carried on specimens cut from arc melted alloys [see TABLE I] . In the first series, hereafter termed the 800°K series, tests were conducted within the temperature interval 746° to 887°K and in the second series, hereafter termed the 1000 K series, tests were conducted in the temperature interval 953°K to 1038°K.

In both series of tests, constant temperature variable load tests were used to evaluate stress exponents from equation 3.8 (see section 3.7.5). Similarly constant load variable temperature tests allowed the

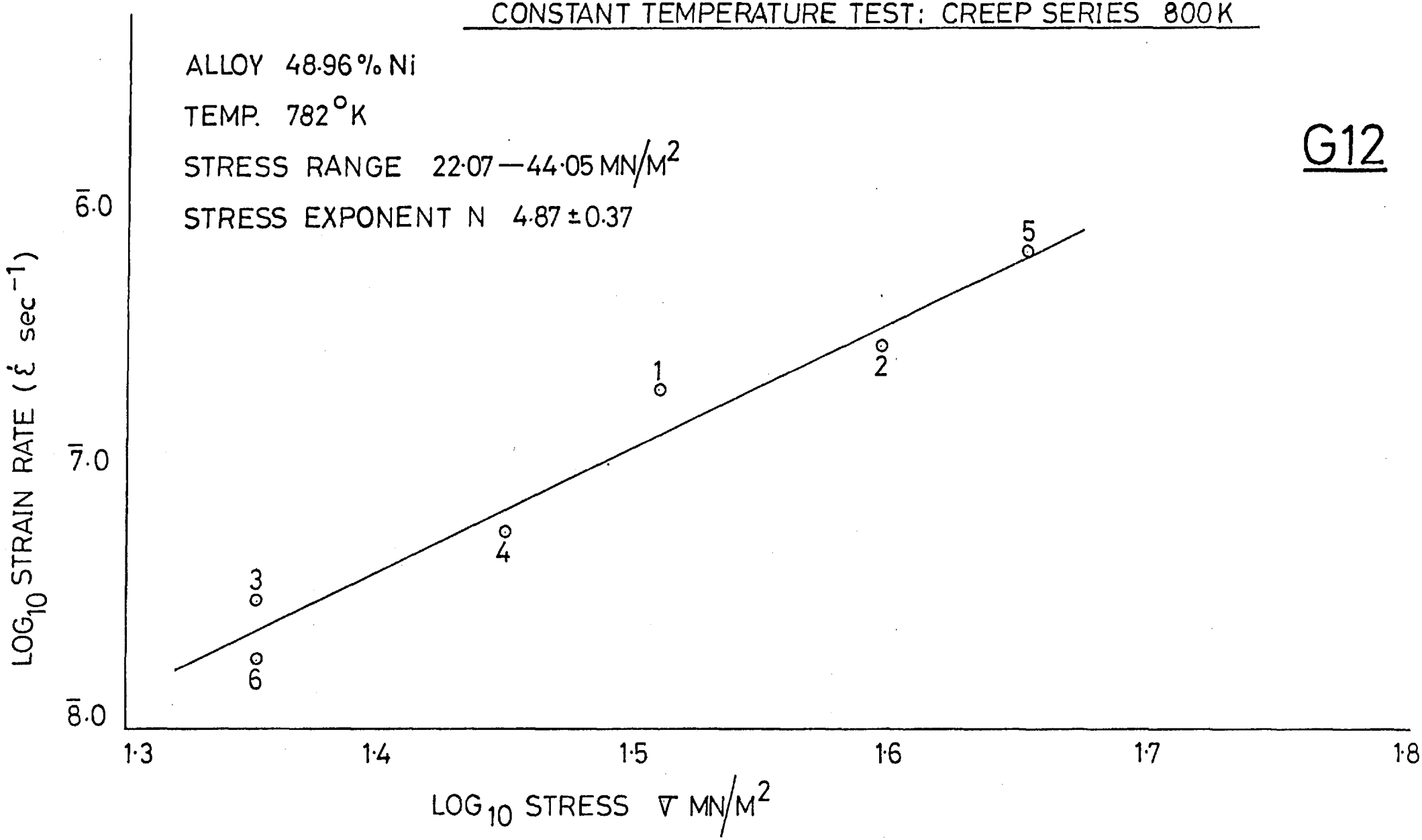
CONSTANT TEMPERATURE TEST: CREEP SERIES 800K
ALLOY 48·96% Ni
TEMP. 782°K
STRESS RANGE 22·07—44·05 MN/M²
STRESS EXPONENT N 4·87 ± 0·37
G12
LOG10 STRAIN RATE (ε̇ sec⁻¹)
6·0
7·0
8·0
1·3
1·4
1·5
1·6
1·7
1·8
LOG10 STRESS σ MN/M²
1
2
3
4
5
6

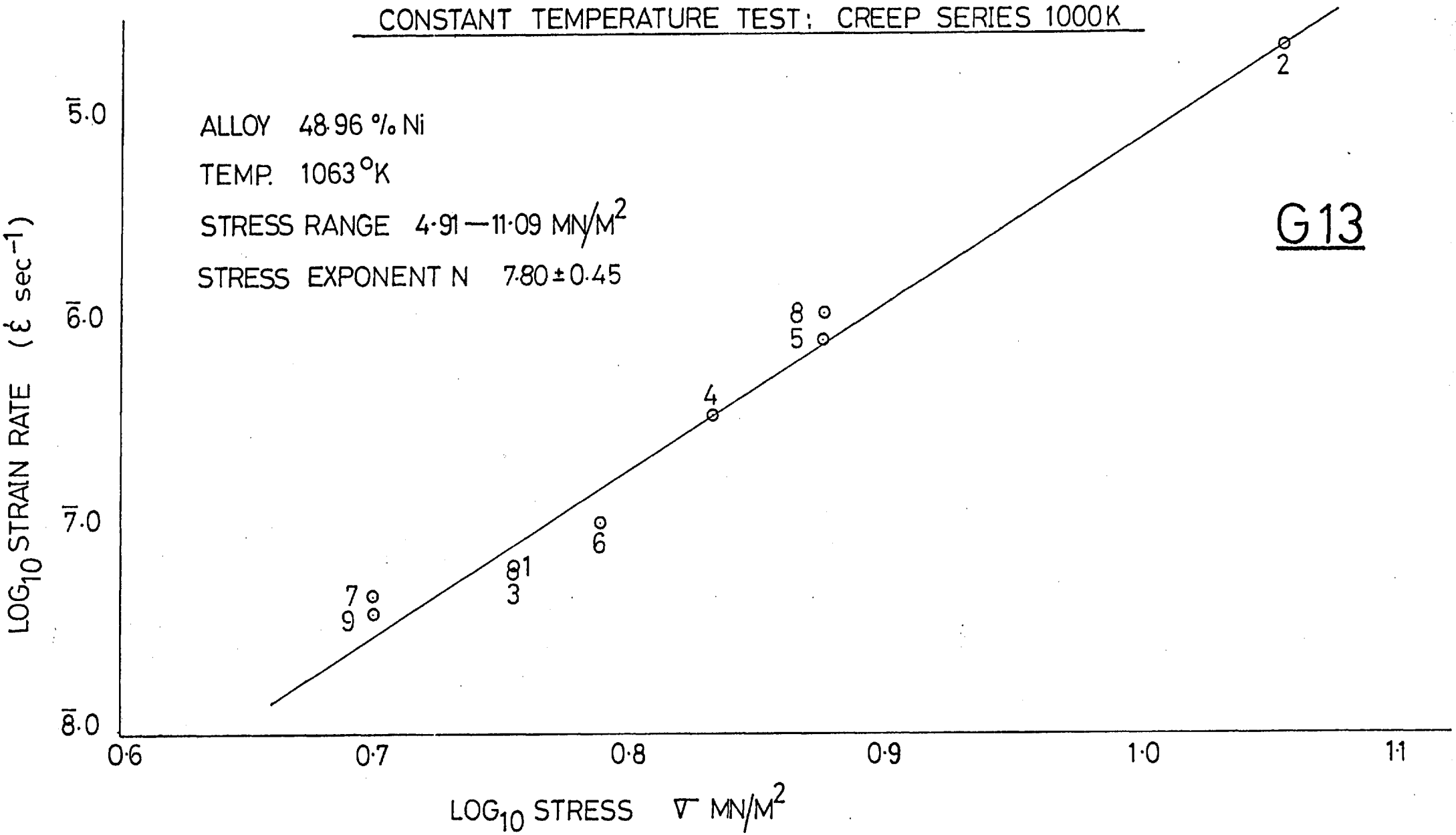
CONSTANT TEMPERATURE TEST: CREEP SERIES 1000K
ALLOY 48·96 % Ni
TEMP. 1063 °K
STRESS RANGE 4·91 — 11·09 MN/M²
STRESS EXPONENT N 7·80 ± 0·45
G13
LOG10 STRAIN RATE (ε̇ sec⁻¹)
5·0
6·0
7·0
8·0
0·6
0·7
0·8
0·9
1·0
1·1
LOG10 STRESS σ MN/M²
1
2
3
4
5
6
7
8
9

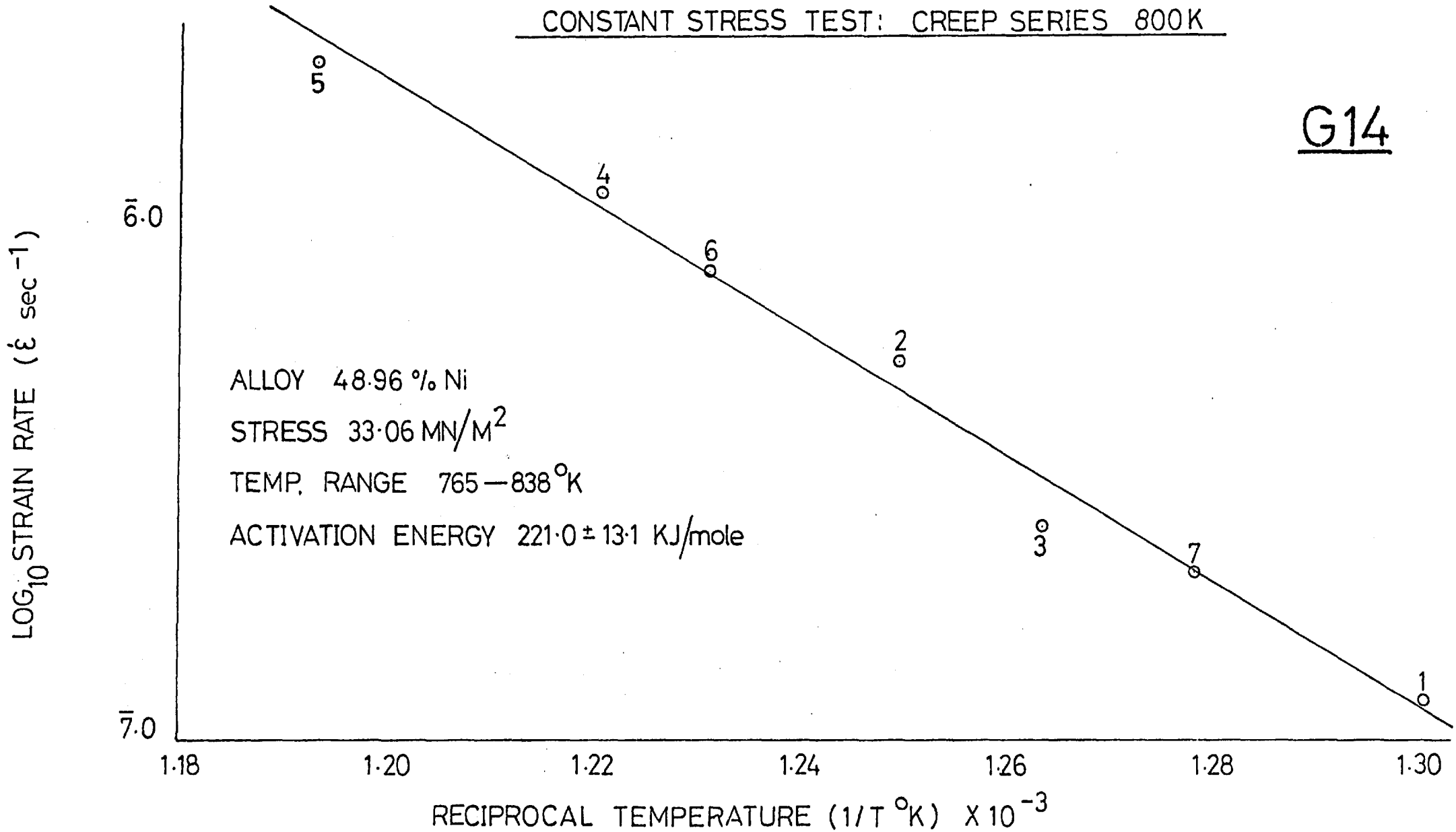
CONSTANT STRESS TEST: CREEP SERIES 800K
G14
ALLOY 48·96 % Ni
STRESS 33·06 MN/M²
TEMP. RANGE 765 — 838 °K
ACTIVATION ENERGY 221·0 ± 13·1 KJ/mole
LOG10 STRAIN RATE (ε̇ sec⁻¹)
6·0
7·0
1·18
1·20
1·22
1·24
1·26
1·28
1·30
RECIPROCAL TEMPERATURE (1/T °K) X 10⁻³
1
2
3
4
5
6
7

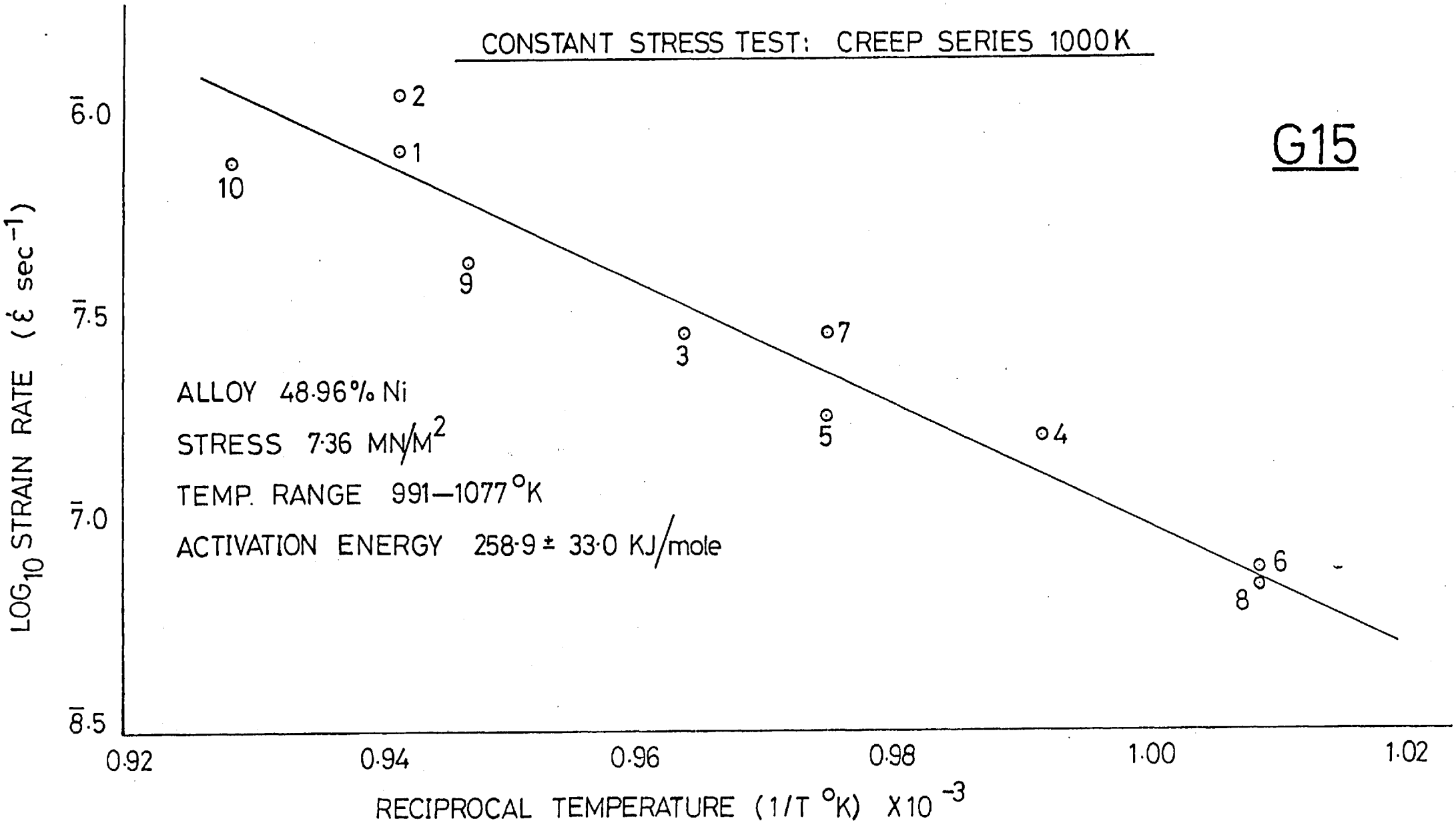
CONSTANT STRESS TEST: CREEP SERIES 1000K
G15
ALLOY 48·96% Ni
STRESS 7·36 MN/M^2
TEMP. RANGE 991—1077 °K
ACTIVATION ENERGY 258·9 ± 33·0 KJ/mole
$\bar{6}$·0
$\bar{7}$·5
$\bar{7}$·0
$\bar{8}$·5
LOG$_{10}$ STRAIN RATE ($\dot{\varepsilon}$ sec^{-1})
0·92
0·94
0·96
0·98
1·00
1·02
RECIPROCAL TEMPERATURE (1/T °K) X10^{-3}
1
2
3
4
5
6
7
8
9
10

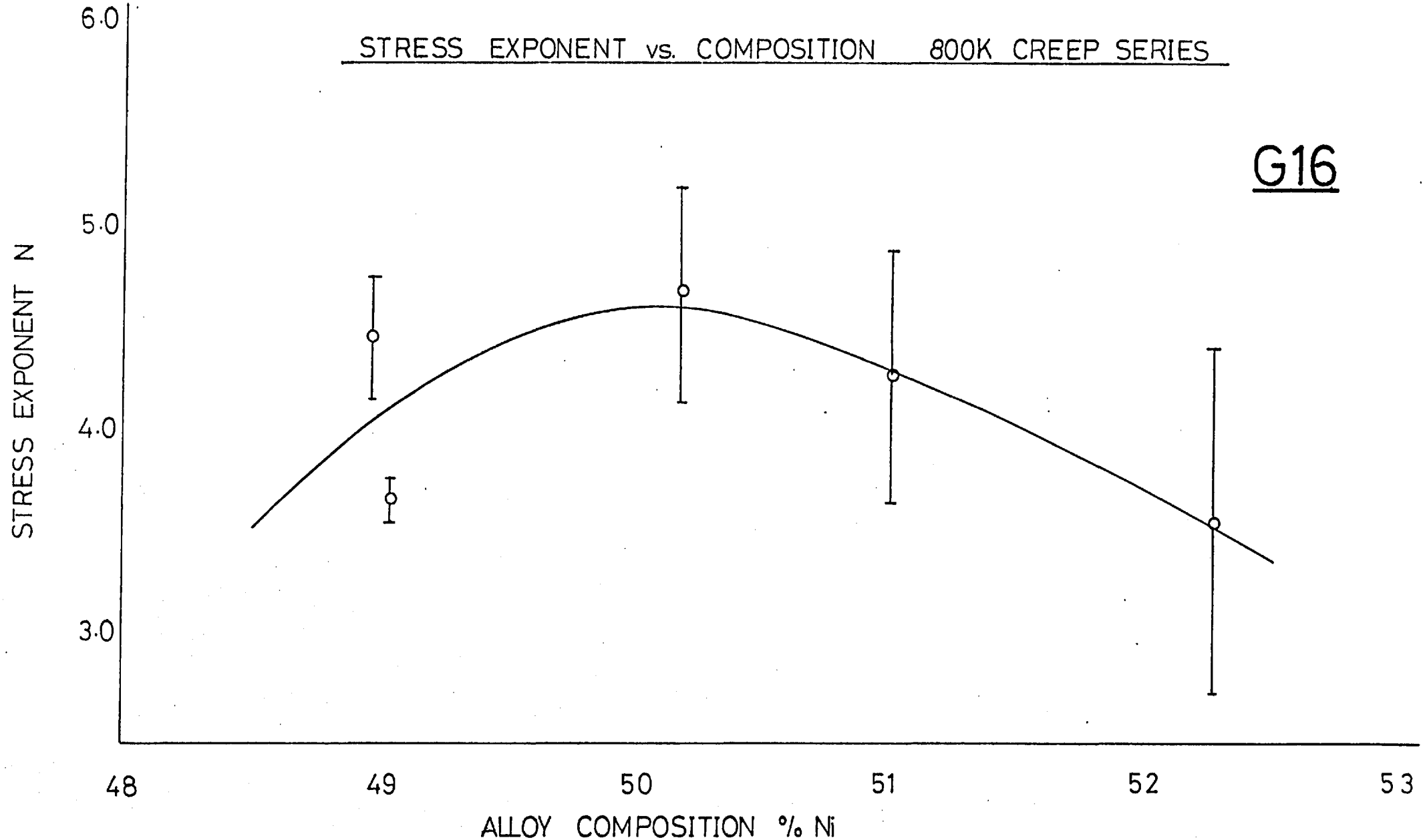
STRESS EXPONENT vs. COMPOSITION 800K CREEP SERIES
G16
STRESS EXPONENT N
6·0
5·0
4·0
3·0
48
49
50
51
52
53
ALLOY COMPOSITION % Ni

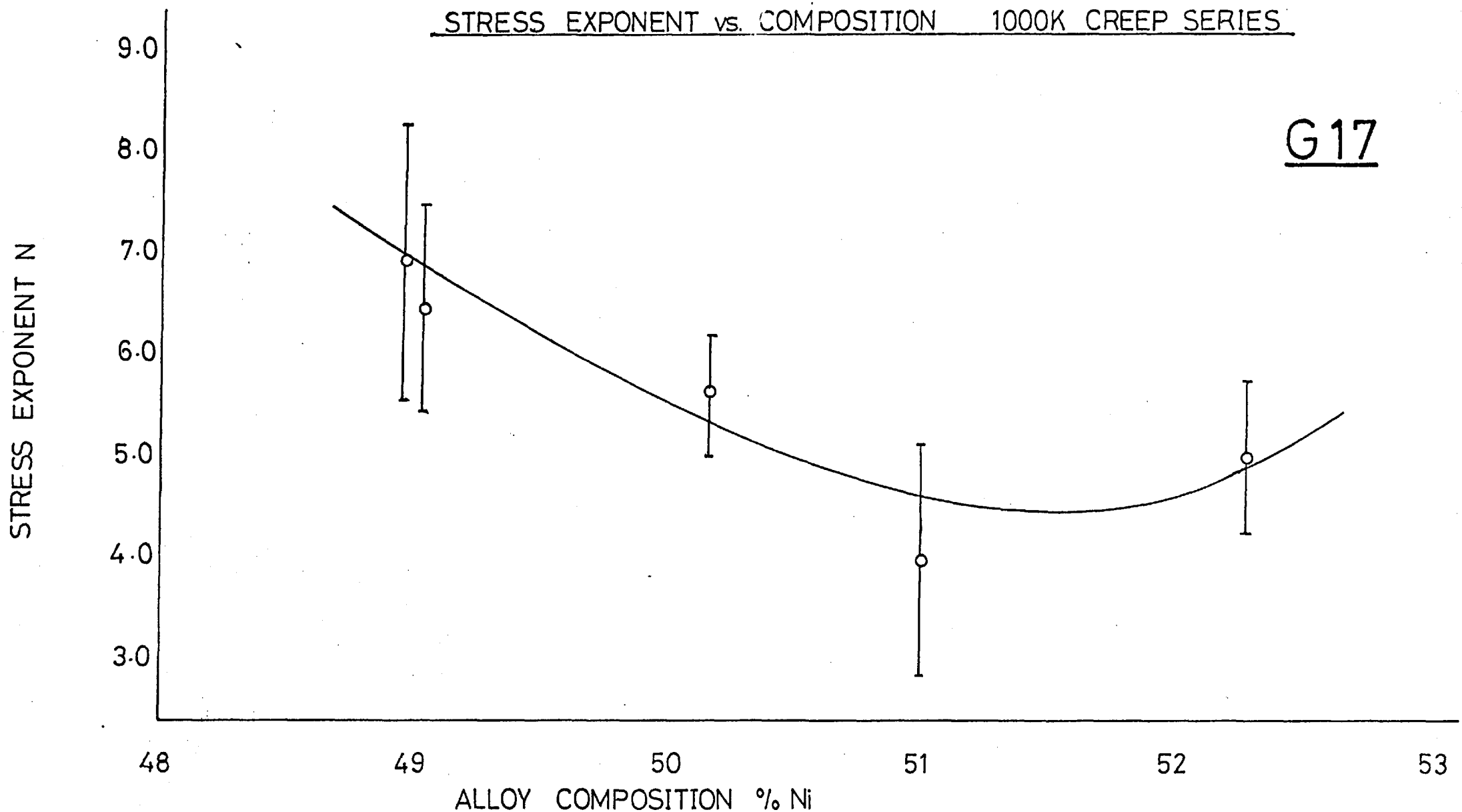
STRESS EXPONENT vs. COMPOSITION 1000K CREEP SERIES
G17
STRESS EXPONENT N
9.0
8.0
7.0
6.0
5.0
4.0
3.0
48
49
50
51
52
53
ALLOY COMPOSITION % Ni

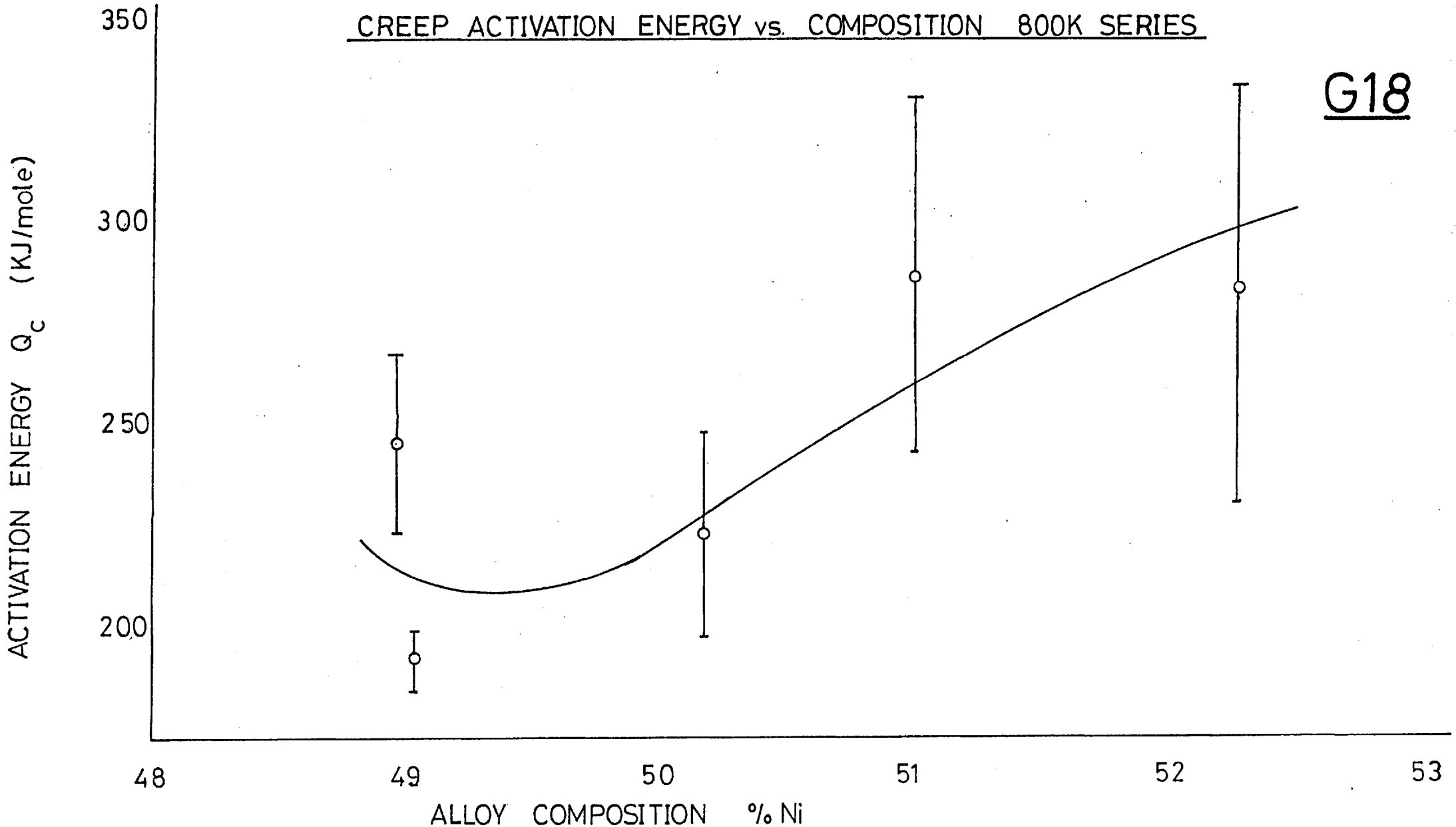
CREEP ACTIVATION ENERGY vs. COMPOSITION 800K SERIES
G18
ACTIVATION ENERGY Q_c (KJ/mole)
350
300
250
200
48
49
50
51
52
53
ALLOY COMPOSITION % Ni

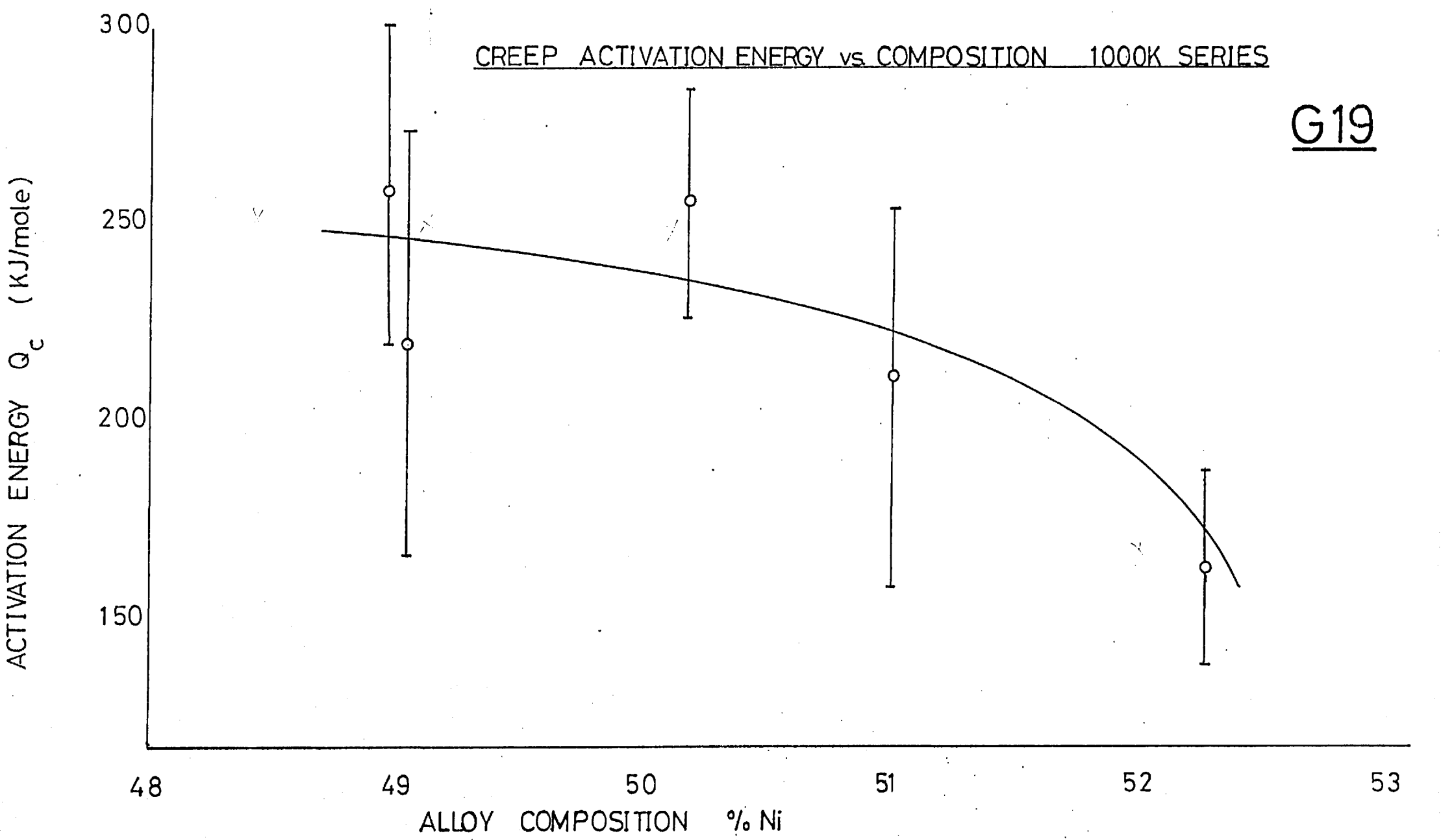
CREEP ACTIVATION ENERGY vs COMPOSITION 1000K SERIES
G19
ACTIVATION ENERGY Q_c (KJ/mole)
300
250
200
150
48
49
50
51
52
53
ALLOY COMPOSITION % Ni

TABLE V Stress Exponents as a function of Comp^n 800K creep series

Alloy Comp^n % Ni	Exponent N	Error EN	Temp °K	Stress Range MN/M^2	Mean N & error
48·96	4·09	0·41	779	32·1 — 47·7	4·5 ± 0·3
	4·73	0·38	782	20·1 — 40·1	
	4·69	0·11	814	10·9 — 43·4	
49·06	3·71	0·10	766	25·1 — 43·8	3·7 ± 0·1
	1·37*	—	798	5·4 — 49·1	
50·17	3·59	0·15	763	35·2 — 49·9	4·7 ± 0·5
	5·93	0·48	769	20·3 - 30·6	
	4·66	1·06	791	31·7 — 47·2	
51·0	3·51	1·03	753	20·4 — 55·3	4·3 ± 0·6
	4·03	0·20	759	45·8 —102·8	
	5·41	0·62	771	33·5 — 93·6	
52·27	11·50†	0·30	772	105·2 —196·2	3·6 ± 0·9
	3·59	0·85	781	18·7 — 37·6	

*: only 2 data points — value not used in calculating mean N

†: high stresses — " " " " " " "

TABLE VI Creep Activation Energies Q_c as a function of composition. 800 K series

Alloy Comp^n % Ni	Q_c KJ/mole	Error Q_c KJ/mole	Stress MN/M^2	Temp Range °K	Mean Q_c & error
48·96	175·3	32·5	20·3	782 — 854	247·2 ± 22·9
	232·3	15·0	35·4	765 — 838	
	333·8	21·2	33·2	756 — 824	
49·03	171·8	6·02	25·1	746 — 855	194·3 ± 9·3
	213·3	11·2	32·7	747 — 840	
	197·8	10·8	34·6	751 — 828	
50·17	164·9	26·2	32·2	751 — 852	225·1 ± 25·0
	232·0	13·1	38·9	765 — 842	
	278·3	35·7	49·9	759 — 783	
51·0	244·8	50·6	20·8	753 — 835	288·6 ± 43·4
	332·4	36·2	33·5	771 — 805	
52·27	280·1	56·3	28·9	770 — 887	284·2 ± 51·9
	315·0	23·6	30·2	781 — 852	
	257·5	75·8	126·7	732 — 831	

TABLE VII Stress Exponents as a function of composition 1000K series

Alloy Comp^n % Ni	Exponent N	Error EN	Temp °K	Stress Range MN/M^2	Mean N & error
48·96	7·54	2·75	1005	8·14— 9·42	7·0 ± 1·4
	6·28	1·14	1002	4·91 — 8·34	
	6·59	1·06	1063	4·91 —10·40	
	7·66	0·53	1063	4·71 —10·89	
49·03	6·43	0·84	965	5·00— 9·22	6·6 ± 1·0
	5·75	1·45	1014	5·40 — 8·63	
	7·55	0·68	1041	5·10 — 7·65	
50·17	5·64	0·91	991	4·12 — 8·73	5·7 ± 0·6
	5·67	0·62	1005	3·04 — 5·79	
	5·81	0·26	1051	5·30 —10·40	
51·0	3·12	1·07	1008	4·41 — 8·04	4·1 ± 1·2
	5·07	1·27	1017	4·41 — 6·47	
52·27	5·09	0·77	1027	3·24 — 5·98	5·1 ± 0·8

TABLE VIII Creep Activation Energies Q_c as a function of composition 1000K series

Alloy Comp^n % Ni	Q_c KJ / mole	Error Q_c KJ / mole	Stress MN/M^2	Temp Range °K	Mean Q_c & error
48·96	380·7	92·8	4·92	1022 — 1063	262·3±40·9
	236·7	73·1	5·56	1020 — 1075	
	258·5	28·4	7·13	991 — 1077	
	296·8	17·0	8·38	940 — 1061	
	257·1	44·9	9·41	989 — 1049	
49·03	285·1	77·6	5·16	965 — 1053	221·9 ± 52·9
	214·6	74·1	5·45	989 — 1068	
	188·0	47·4	6·94	1014 — 1088	
	199·8	12·6	7·44	953 — 1051	
50·17	311·8	37·6	4·35	970 — 1066	257·0 ± 28·3
	180·4	13·9	5·75	967 — 1053	
	266·3	46·8	7·77	965 — 1068	
	269·5	14·8	10·36	979 — 1075	
51·0	238·5	50·0	4·55	963 — 1068	213·2 ± 42·1
	187·9	34·1	6·45	965 — 1068	
52·27	151·9	18·7	4·51	974 — 1063	164·7 ± 24·0
	177·5	29·2	5·97	974 — 1063	

activation energy of creep Q_c to be evaluated from equation 3.10 (see section 3.7.5).

One example of the linear plot of the logarithm of the strain rate ($\log \dot{\varepsilon}$) versus the logarithm of the stress ($\log \sigma$) at constant temperature is given for each of the two creep series in graphs G.12 and G.13 for the 800 K and 1000 K series respectively.

Similarly one example of the straight line relation between ($\log \dot{\varepsilon}$) and the reciprocal temperature ($^1/T$) at constant load (corrected for varying stress) is shown in graphs G.14 and G.15 for the 800 K and the 1000 K creep series respectively.

The compositional dependence of the (mean) stress exponent n for both the 800 K and the 1000 K creep series is shown in graphs G.16 and G.17. The compositional dependence of the (mean) activation energy of creep is shown in graph G.18 for the 800 K series and graph G.19 for the 1000 K series.

Finally the creep data for all the creep experiments is summarised in TABLES V, VI, VII and VIII.

CHAPTER 5: Discussion

5.1 Constitutional Defects in NiGa

The fact that the compound NiGa can exist at non-stoichiometric compositions indicates that constitutional defects must occur in the compound. Furthermore the number and type of such defects must vary with the composition of the compound.

Four constitutional defect types may occur in NiGa; vacancies $\square_{Ni}$ and $\square_{Ga}$ on the nickel and gallium sublattices respectively and substitutional atoms Ni_{Ga} and Ga_{Ni} on the gallium and nickel sublattices respectively. Furthermore these defects may be divided into two groups; those which affect the nickel sublattice ($\square_{Ni}$ and Ga_{Ni}) and those which affect the gallium sublattice ($\square_{Ga}$ and Ni_{Ga}).

Now the two defects, $\square_{Ni}$ (which indicates a deficiency of nickel) and Ga_{Ni} (which indicates an excess of gallium) can account only for an extended phase field on the gallium-rich side of stoichiometry. This is because structure symmetry demands that the number of Ni-sublattice sites equal the number of Ga-sublattice sites and since thetwo defects ($\square_{Ni}$ and Ga_{Ni}) do not affect the latter sublattice, it will always be filled by gallium atoms. Hence the atomic fraction of gallium cannot fall below 50% as the result of these defects being present.

Similarly the two defects $\square_{Ga}$ and Ni_{Ga} affect only the Ga-sublattice and can account only for nickel-rich compounds.

It can be seen that for the compound NiGa to exist at compositions on either side of stoichiometry at least two constitutional defects, one affecting each sublattice, must occur. If, for the moment, only two defects are assumed to occur, then there are four possible combinations which could account for the entire phase field of NiGa. These defect

combinations are; Ni_{Ga} plus Ga_{Ni} (direct substitution), $\square_{Ni}$ plus $\square_{Ga}$ (two vacancy defects), $\square_{Ni}$ plus Ni_{Ga} and finally $\square_{Ga}$ plus Ga_{Ni}.

The first combination results in direct substitution throughout the phase field while the second in constitutional vacancies on either side of stoichiometry. The third and fourth combinations are complex models.

5.1.1 The Direct Substitution Model (Ni_{Ga} plus Ga_{Ni})

In this model, neglecting thermal vacancies, both sublattices are entirely full throughout the phase field and the unit (structure) cell contains two atoms for all compositions.

The model predicts that the compositional dependence of the lattice parameter should follow Vegard's law [see section 4.4] . Thus with increasing nickel content the cell size should fall, since the nickel atom is smaller than the gallium atom.

In fact it is found that the experimentally determined lattice parameter increases with increasing fraction of the smaller nickel species, on the gallium rich side of stoichiometry. In nickel rich alloys the lattice parameter continues to increase with increasing nickel content but in compositions well removed from stoichiometry a reverse in the trend is suggested with the lattice parameter beginning to fall with further excess of nickel [see graph G.1] .

It can be seen then that the substitutional model predictions and experimental values are entirely at variance in gallium-rich compositions and consequently gallium anti-structure atoms Ga_{Ni} are unlikely to be the predominant constitutional defect in these alloys. In nickel-rich alloys theoretical and observed lattice parameter values are in poor agreement, except in very nickel-rich compositions. It is not clear whether nickel anti-structure atoms are the predominant constitutional

defects in these alloys. However in view of the limited agreement between model and experiment this defect cannot be rejected.

Theoretical densities were calculated assuming direct substitution and using the experimental values of the lattice parameter (see Appendix 1). The theoretical density was found to fall continuously with increasing nickel content throughout the phase field although in nickel-rich alloys the density became almost constant. The experimental density was however found to increase continuously with nickel content [see graph G,2] .

Thus the theoretical density and experimental density show entirely different compositional trends in gallium-rich alloys. Once more Ga_{Ni} defects are suggested to be unlikely. In nickel-rich alloys the predicted and observed compositional dependence of the lattice parameter begin to correlate. Again Ni_{Ga} defects may occur.

In conclusion, model and experiment do not agree in gallium-rich alloys, suggesting that Ga_{Ni} defects are not the predominant constitutional defect type in gallium rich alloys. However there is some inconclusive correlation between model and experiment in nickel-rich alloys. Thus it seems likely that Ni_{Ga} defects do occur but may not be the only constitutional defect type in nickel-rich alloys.

5.1.2 The Direct Vacancy Model ($\square_{Ni}$ plus $\square_{Ga}$)

In this model the unit cell does not contain two atoms, except at the stoichiometric composition. The nickel sublattice is full only in nickel-rich alloys while the gallium sublattice is full only in gallium rich alloys.

The model predicts that the lattice parameter will be a maximum at stoichiometry; an excess of nickel results in a fall of the parameter

as does an excess of gallium. The limiting case in which the vacancies are assumed to have zero volume (in other words complete lattice relaxation) has been used to evaluate the maximum variation in the lattice parameter with composition (see section 4.3). The resultant compositional dependence of the theoretical lattice parameter is shown in graph G.1.

It can be seen that the compositional trend in the theoretical lattice parameter and the observed lattice parameter are in good agreement in gallium-rich alloys. This suggests that the predominant constitutional defect type in these alloys may well be ($\square_{Ni}$) vacancies on the nickel sublattice.

In nickel-rich compositions the model and experiment are entirely at variance with the former suggesting that the lattice parameter should fall rapidly from a maximum at stoichiometry while the latter shows that the lattice parameter in fact increases continuously with increasing nickel content. This suggests that the constitutional defects $\square_{Ga}$ postulated by the model probably do not occur in any great numbers.

A theoretical density was evaluated on the basis of the constitutional vacancy model (see Appendix 1) and plotted as a function of composition as shown in graph G.2.

Again it can be seen that in gallium-rich alloys both the theoretical and observed density increases with increasing nickel content up to the stoichiometric composition. However although the trend in the compositional dependence is the same for both model and experiment the absolute values yielded by the model are not in good agreement with those observed.

This suggests that although the constitutional defects $\square_{Ni}$ postulated by the model for gallium rich alloys are likely to be present they may not be the only constitutional defects to occur in these alloys.

In nickel-rich alloys it can be seen that the theoretical density

falls rapidly with increasing nickel content whereas the observed density in fact increases continuously with excess of nickel. This difference between model and experiment infers that the defects $\square_{Ga}$ suggested by the model probably do not occur constitutionally to any great extent.

In conclusion, both lattice parameter and density measurements indicate that the gallium sublattice vacancies $\square_{Ga}$ are not the predominant constitutional defects in nickel rich alloys. On the other hand nickel sublattice vacancies $\square_{Ni}$ do occur in gallium rich alloys but may not be the sole constitutional defects present in these alloys.

5.2 The Proposed Constitutional Defect Model in NiGa

It can be seen from sections 5.1.1 and 5.1.2 that the predominant constitutional defects which account for non-stoichiometric compositions in NiGa whilst conforming to the observed compositional dependence of the lattice parameter and density are nickel vacancies $\square_{Ni}$ in gallium rich alloys and nickel anti-structure atoms Ni_{Ga} in nickel rich alloys. This defect combination was one of the four mentioned in section 5.1 and is the one generally reported for NiGa [145] . However this does not mean that the other constitutional defects, gallium vacancies $\square_{Ga}$ and gallium anti-structure atoms Ga_{Ni} do not occur, but simply that they probably occur only in very small concentrations and are therefore of lesser importance.

While the two constitutional defects $\square_{Ni}$ and Ni_{Ga} are said to account for the phase field of NiGa [145] it has also been tacitly assumed that there is a sharp transition from one defect type to the other on crossing the stoichiometric composition. Furthermore it is assumed that the concentration of either constitutional defect tends to

zero at stoichiometry. But, although the two defects $\square_{Ni}$ and Ni_{Ga} are able to account for the observed trend in the compositional dependence of both the lattice parameter and density, the detailed agreement between the model and experiment is poor.

Especially significant is the fact that both the observed lattice parameter and density do not show the sharp discontinuity at stoichiometry predicted by the model. Additionally the rate of change of both of these quantities as a function of composition is found to be far less rapid than indicated by a defect model which consists of only one defect on one side of stoichiometry, no defects at stoichiometry and then a second different defect on the other side of stoichiometry.

It would seem reasonable to suppose that both the defects $\square_{Ni}$ and Ni_{Ga} are present simultaneously in varying proportions throughout the phase field (on either side of stoichiometry). There is then no abrupt change from one constitutional defect type to another at stoichiometry. The trend would still be, as in the simple model [145], that in gallium-rich alloys nickel vacancies predominate, but a small fraction of nickel anti-structure atoms would also be present, while in nickel-rich alloys nickel anti-structure atoms predominate although a small number of nickel vacancies also occur.

In this new model, the stoichiometric composition contains both nickel vacancies $\square_{Ni}$ and nickel antistructure atoms Ni_{Ga} and furthermore it need not be the composition which contains the minimum constitional defect fraction. This latter composition will depend upon the variation of the two defect fractions as a function of composition.

The first consequence of this new defect model, that an intermetallic compound may contain more than one constitutional defect type in a given composition is not new in that it has already been put forward in the case of NiAl. In this latter compound aluminium rich

compositions have been found to contain both aluminium anti-structure atoms and nickel vacancies [13, 23] . Furthermore the idea of mixed defects has been analysed in some detail for the case of thermal defects and defect equilibria [142, 41] and their interaction with constitutional defects.

Also the new constitutional defect model indicates that the stoichiometric composition in NiGa contains constitutional defects. In fact a similar situation has been found in Fe_2Nb where iron anti-structure atoms were identified by Mössbauer spectroscopy in the stoichiometric composition [132] . Furthermore the present study and earlier work on NiGa [145] has indicated that the unit cell does not contain two atoms at stoichiometry, which suggests constitutional vacancies are still present (and hence from structure symmetry so too are anti-structure atoms).

Having established that a mixed constitutional defect model for NiGa is feasible the detailed structure of the model has been developed as follows. The only constitutional defects which are assumed to be present are $\square_{Ni}$ and Ni_{Ga}, the other two defect types Ga_{Ni} and $\square_{Ga}$ are assumed not to occur [see sections 5.1.1 and 5.1.2] . It can then be shown (see Appendix 1) that the number of nickel vacancies N^{V}_{Ni} and the number of nickel anti-structure atoms N^{Ni}_{Ga} in $N_{(x)}$ lattice sites at the composition x (equal to the atomic fraction of nickel) are given by the expressions:

$$N^{V}_{Ni} = \left(\frac{X-x}{x}\right) N_{(X)} \qquad 5.1$$

$$N^{Ni}_{Ga} = (2X-1)\ 0{\cdot}5\ N_{(X)} \qquad 5.2$$

where $N_{(X)}$ is the value of $N_{(x)}$ at the composition X (atomic fraction of nickel) which contains no (constitutional) vacancies.

Theoretical densities were calculated for any alloy composition (x) from the known defect fractions (given by equations 5.1 and 5.2) predicted by the model, using arbitrary values of X and the experimental lattice parameter values. This yielded a series of curves (of different fixed X) for the compositional dependence of the theoretical density [see graph G.20] .

It was then assumed that, at the composition where a theoretical density curve of given X intersected the experimental density curve, the defect (structure) fractions of the two constitutional defects $\square_{Ni}$ and Ni_{Ga} defined by X were identical to the actual defect structure present. Thus X could be determined for several different compositions (x) and then the compositional dependence of X was evaluated by the Legrange method (see Appendix 1).

The defect fractions f^{v}_{Ni} and f^{Ni}_{Ga} of nickel vacancies and nickel anti-structure atoms were then expressed solely in terms of the composition x (equal to atomic fraction of nickel). The two relevant expressions are:

$$f^{v}_{Ni} = Z = 6{\cdot}95x^2 - 7{\cdot}81x + 2{\cdot}20$$

$$f^{Ni}_{Ga} = \emptyset = 2{\cdot}91x^2 - 2{\cdot}30x + 0{\cdot}44$$

The compositional dependence of these two functions (and hence of nickel vacancy and nickel anti-structure atom concentrations) are shown in graph G.21. It can be seen that the atomic fraction of nickel vacancies decreases continuously with increasing nickel content throughout the phase field (the Z function in the graph) but does not show a discontinuity at stoichiometry. Furthermore the fraction of vacancies does not fall to zero even in nickel-rich compositions. It is still of the order of 1% in very nickel-rich alloys (~54-55 atomic % nickel).

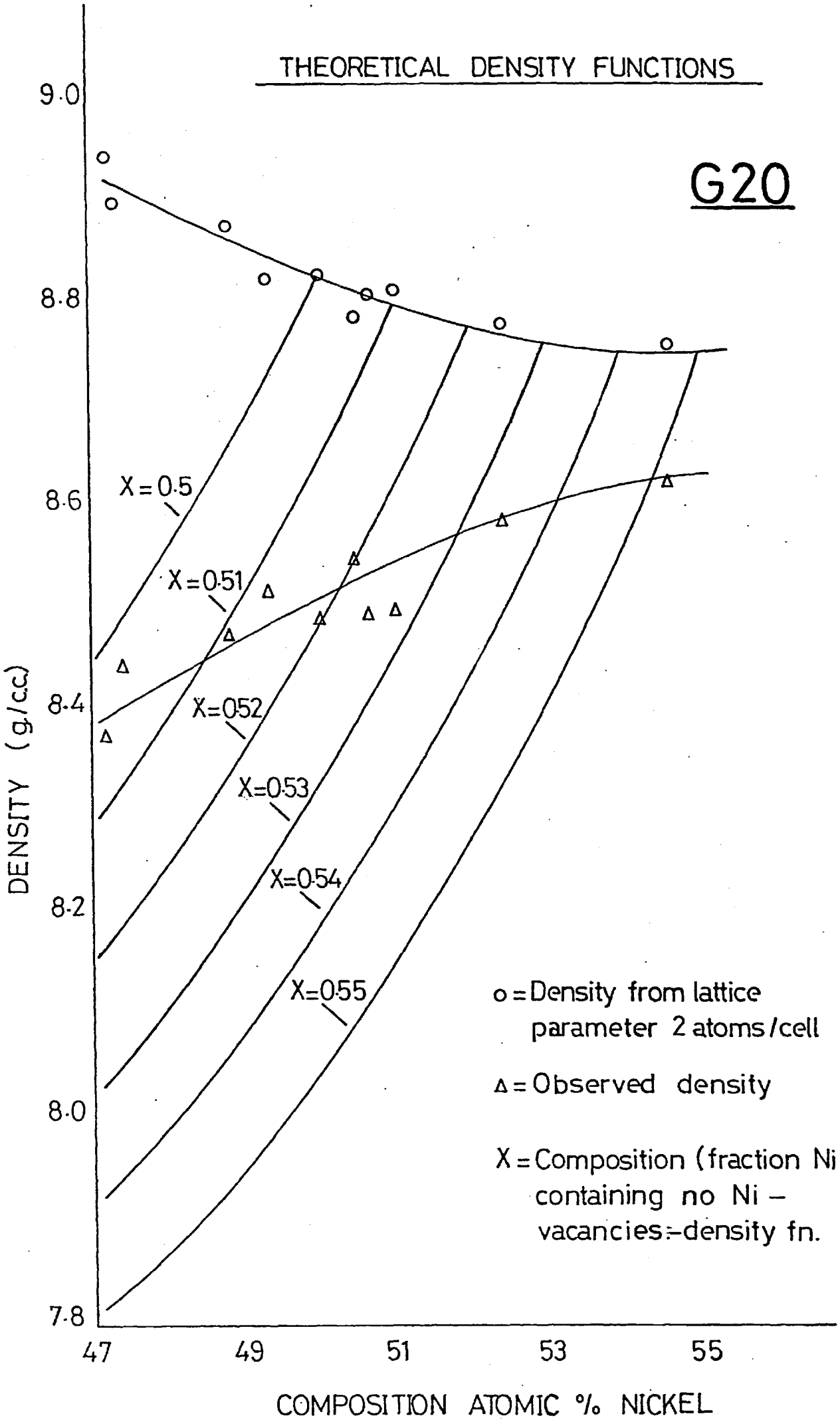
THEORETICAL DENSITY FUNCTIONS
G20
9.0
8.8
8.6
8.4
8.2
8.0
7.8
DENSITY (g/cc)
X = 0.5
X = 0.51
X = 0.52
X = 0.53
X = 0.54
X = 0.55
o = Density from lattice parameter 2 atoms/cell
Δ = Observed density
X = Composition (fraction Ni) containing no Ni – vacancies:-density fn.
47
49
51
53
55
COMPOSITION ATOMIC % NICKEL

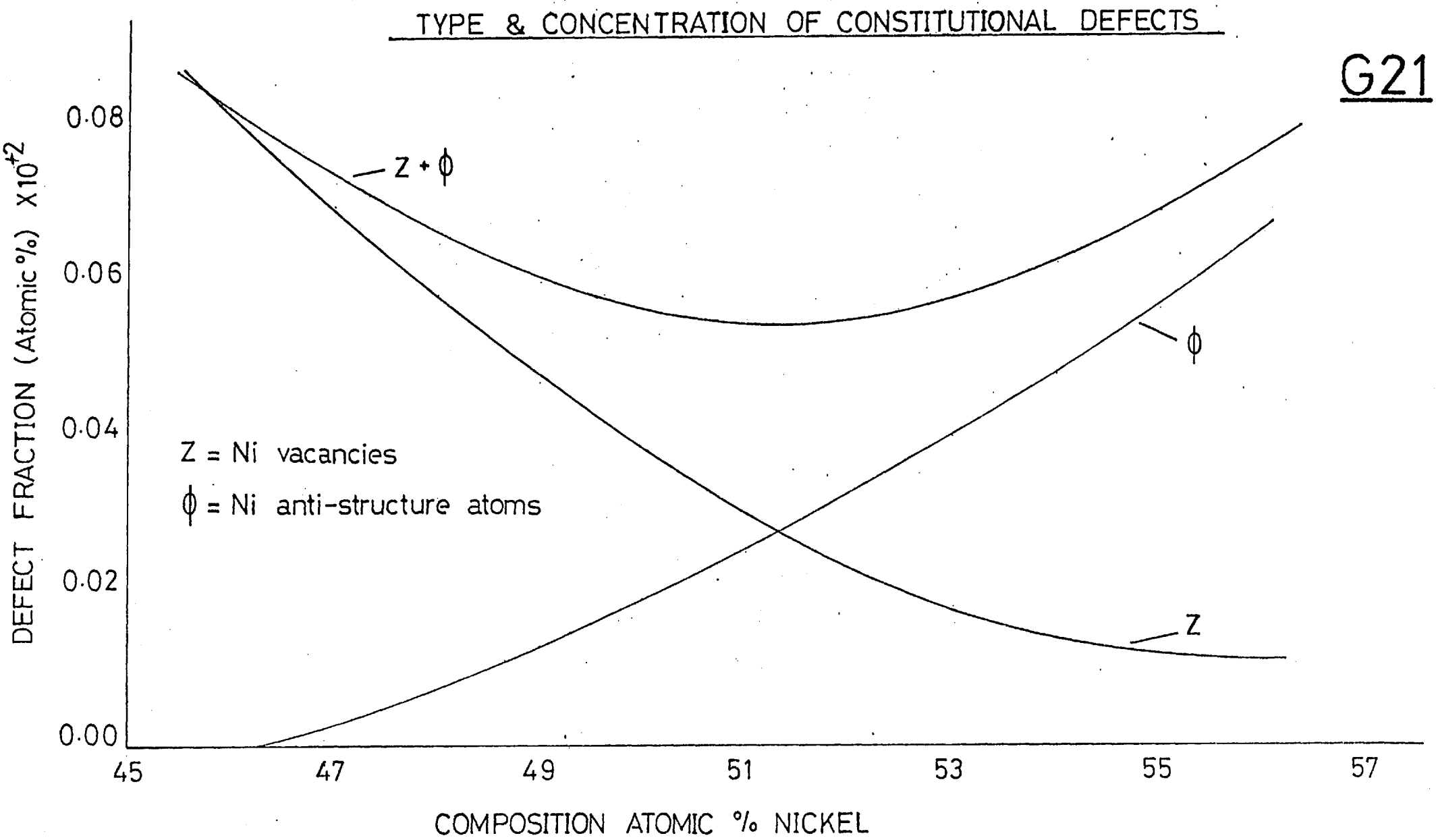
TYPE & CONCENTRATION OF CONSTITUTIONAL DEFECTS
G21
DEFECT FRACTION (Atomic %) X10+2
0·08
0·06
0·04
0·02
0·00
Z + ϕ
ϕ
Z
Z = Ni vacancies
ϕ = Ni anti-structure atoms
45
47
49
51
53
55
57
COMPOSITION ATOMIC % NICKEL

Similarly the predicted variation in the fraction of nickel anti-structure atoms is a continuous decrease with increasing gallium content, again with no discontinuity at stoichiometry (the $\emptyset$ function in the graph). The fraction of anti-structure atoms does not fall to zero at stoichiometry, in fact the model suggests that anti-structure atoms remain present up to a composition of 46·3 atomic % nickel.

The total constitutional defect concentration, ζ, given by the sum of the Z and $\emptyset$ curves, as a function of composition is also shown in graph G.21. The minimum total constitutional defect concentration is found to occur not a stoichiometry but in the 51·25 atomic % nickel composition.

In summary, a constitutional defect model which contains the defects $\square_{Ni}$ and Ni_{Ga} has been proposed for the intermetallic compound NiGa. The compositional dependence of the two defect types was determined empirically from experimental values of the lattice parameter and density. The details of the model may be outlined as follows:

(i) Nickel vacancies $\square_{Ni}$ and nickel anti-structure atoms Ni_{Ga} are the two predominant constitutional defects which account for the extended phase field of the compound NiGa. This is in agreement with the findings of Wasilewski et al. (1968) [145].

(ii) Since there is no discontinuity in the compositional dependence of either the lattice parameter or the density of the compound at stoichiometry it was concluded that there is no discontinuity in the change from vacancy to anti-structure atom defects with composition.

(iii) Thus both vacancies and anti-structure atoms occur simultaneously throughout the phase field of the compound. On increasing the nickel content from the extreme gallium rich limits of the phase field through

to nickel-rich alloys the fraction of nickel vacancies decreases continuously while that of anti-structure atoms increases continuously [see Z and $\emptyset$ functions of graph G.2] . The existence of a mixed constitutional defect structure has already been proposed in aluminium-rich NiAl [13, 23] .

(iv) The stoichiometric composition in NiGa contains both vacancy and anti-structure atom defects. A similar situation has been found in Fe_2Nb where the stoichiometric composition contains iron anti-structure atoms [132] .

Furthermore the stoichiometric composition in NiGa does not contain the minimum total constitutional defect concentration. On this point, it has been found that in both NiAl [65] and NiGa [145] the composition in which the minimum overall total defect concentration (constitutional plus thermal) occurs does not coincide with stoichiometry but varies with temperature. Thus depending on the change in the compositional dependence of the thermal defect concentration with changing temperature a non-stoichiometric composition containing no thermal defects and hence only constitutional defects may be found to contain the minimum total defect concentration.

Finally the present constitutional defect model was derived empirically from experimental values of lattice parameter and density. Now it is known that quenched-in thermal defects may affect the former and these defects and alloy porosity may also affect the latter quantity. However it was concluded that the variation of both lattice parameter and density with composition resulted from the presence of constitutional defects [see sections 4.3 and 4.4] . Consequently the form of the constitutional defect model proposed for NiGa is justified.

Nevertheless while porosity was considered not to affect the shape

of the compositional dependence of the density it undoubtedly does affect the actual values determined for the density. Therefore the absolute values of defect fractions predicted by the defect model are likely to be somewhat high.

5.3 Diffusion Behaviour of NiGa

In the course of the following discussion the diffusion behaviour of NiGa will be compared with that of other B2 intermetallic compounds of the type AB. The diffusion coefficients of the A elements (e.g. nickel in NiGa, silver in AgMg, etc.) will be compared with one another as will the diffusion coefficients of the B elements (e.g. gallium in NiGa, magnesium in AgMg, cadmium in AuCd).

Furthermore all data will be compared at homologous temperatures T_H (equal to the ratio of the measured temperature T and the melting temperature T_M). Finally since it is known that the diffusion behaviour in these compounds is dependent upon composition, any comparison between the diffusion coefficients of species in different compounds will be made for compositions of equivalent deviation from stoichiometry.

The particular variation of the diffusion coefficients of both nickel (D_{Ni}) and gallium (D_{Ga}) in NiGa as a function of alloy composition will be discussed in detail in the following sections. Suggestions concerning possible diffusion mechanisms will be outlined.

5.3.1 The Compositional Dependence of Ni-63 Diffusion in NiGa

With the possible exception of the highest diffusion annealing temperature 1384°K ($T_H = 0{\cdot}99$), the diffusion results of this study indicate that the diffusion coefficient of nickel D_{Ni} does not change

markedly with composition in NiGa [see graph G.7] . This behaviour is in marked contrast with data for the diffusion of nickel in NiAl [65] , silver in AgMg [61, 33, 34, 62] and gold in AuCd [57, 78, 56] where the diffusion coefficient is found to fall to a minimum at or near stoichiometry.

The compositional change in the diffusion coefficient of nickel in NiAl, for example, may approach two orders of magnitude; it increases from approximately $1{\cdot}0 \times 10^{-12}$ at stoichiometry to about $5{\cdot}0 \times 10^{-11}$ (cm^2/sec) in the 58 atomic % nickel composition, for a temperature of $1273^{\circ}K$ ($T_H = 0{\cdot}67$) [65] .

The diffusion coefficient of nickel D_{Ni} in NiGa has been compared with that of nickel in NiAl, gold in AuCd and silver in AgMg for various alloy compositions and homologous temperatures. For the comparison the phase field of each alloy was divided into A-rich compositions, stoichiometry and B-rich compositions. Selected data are shown in TABLE IX. Each portion of the phase field will now be considered in turn.

(i) In A-rich alloys, the diffusion coefficient of nickel in NiGa is larger than that of nickel in NiAl and gold in AuCd for all temperatures in the range $0{\cdot}7 \leqslant T_H \leqslant 1{\cdot}0$. The difference is most marked at low temperatures but becomes progressively smaller with temperature. The diffusion coefficient of silver in AgMg is about an order of magnitude smaller than that of the A elements in the other three compounds [see TABLE IX] .

(ii) At stoichiometry the situation is much the same with the diffusivity of nickel in NiGa again being the most rapid. But in this case the difference between the diffusion coefficient in NiGa and those found in the other compounds is considerably greater than in A-rich alloys, although again this difference becomes less marked with

TABLE IX A comparison of the diffusivities (D_A & D_B) in various B2 alloys as a function of normalised temperature T_H (equal T/T_M)

Compound & Comp^n % A element		Normalised Temperature T_H 0·7		0·77		0·85		0·91		0·99	
		D_A	D_B	D_A	D_B	D_A	D_B	D_A	D_B	D_A	D_B
† Ni Ga	52·4	7·23xE-11	—	4·38xE-10	8·59xE-11	2·29xE-9	1·08xE-9	6·51xE-9	4·66xE-9	1·83xE-8	2·78xE-8
x Ni Al	53·2	1·3 x E-11	—	1·2 x E-10	—	1·1 x E-9	—	—	—	—	—
° AuCd	52·5	4·62xE-11	—	2·60x E-10	1·7 x E-10	2·29x E-9	1·35x E-9	6·85xE-9	6·85x E-9	—	—
Δ AgMg	54·2	3·01x E-12	—	3·6 x E-11	—	2·85x E-10	—	7·0 x E-10	—	—	—
† Ni Ga	50·01	4·54xE-11	—	4·37x E-10	8·46x E-11	3·84xE-9	3·89x E-10	5·58xE-9	1·14x E-9	2·57x E-8	3·24xE-9
x Ni Al	50·0	4·6 x E-12	—	4·5 x E-11	—	5·7x E-10	—	—	—	—	—
° AuCd	50·0	2·57x E-11	3·0xE-11	2·2 x E-10	3·0 x E-10	1·46x E-9	2·0x E-9	5·0xE-9	7·0 x E-9	3·08x E-8	6·17x E-8
Δ Ag Mg	50·2	9·2 x E-13	—	8·0 x E-12	1·0 x E-11	6·51x E-11	1·0x E-10	4·0x E-10	8·0x E-10	—	3·36xE-9
† Ni Ga	48·76	6·71 x E-11	—	4·21x E-10	6·39x E-11	3·74x E-9	4·39x E-10	5·67x E-9	2·53x E-9	1·81 x E-8	9·83xE-9
x Ni Al	48·6	7·0 x E-12	—	3·4 x E-11	—	1·7 x E-10	—	—	—	—	—
° AuCd	49·5	—	—	4·0x E-10	6·0 x E-10	2·0 x E-9	3·0 x E-9	8·4x E-9	1·3 x E-8	—	—
Δ AgMg	48·0	2·78x E-12	—	1·8 x E-11	—	9·46xE-11	—	7·0xE-10	—	—	—

Powers written in E format eg. 10^{-11} = E-11

† = Data from this study
x = Data from ref. 65
° = Data " " 57, 78
Δ = Data " " 33, 34, 61, 62

increasing temperature.

(iii) In B-rich alloys the situation is a repeat of the A-rich case with nickel diffusion in NiGa being the most rapid but less markedly so than at stoichiometry.

These data suggest that in comparison with the other three compounds the diffusivity of nickel in NiGa is large, while its compositional dependence (graph G.7) shows that it is effectively constant and independent of composition.

In general the compositional dependence of the diffusion coefficient in B2 compounds has been explained in terms of the compositional change of the bonding energy and in terms of a change in atomic jump frequencies [86]. For example the jump frequency (of nearest neighbour vacancy jumps) may be greater in non-stoichiometric compositions because a greater degree of intrinsic disorder (due to constitutional defects) already exists in such compositions. Furthermore the presence of constitutional defects, especially vacancies as in aluminium rich NiAl [13, 23], will almost certainly contribute directly to an increase in the diffusion coefficient.

The fact that D_{Ni} in NiGa is both large, in comparison with similar compounds, and compositionally invariant may be accounted for by three possibilities, namely:

(i) little change in bond energies as a function of alloy composition,
(ii) a high concentration of thermal vacancies across the phase field,
(iii) constitutional vacancies occur at all compositions and take part in diffusion.

These possibilities will now be considered in more detail.

The first condition is unlikely in view of the fact that NiGa is

far from a thermodynamically ideal solution. The activity of gallium a_{Ga} is found to change markedly with composition [128]. For example a_{Ga} has the values 0·02, 0·05 and 0·12 in the compositions containing 48·4, 50·4 and 59·0 atomic % nickel respectively. Thus bonding energies may be expected to change appreciably with composition in the compound, and consequently the diffusion coefficient of nickel D_{Ni} would be expected to show a compositional dependence.

The fact that the diffusivity of nickel is found to be independent of composition suggests that the bonding configuration around a diffusing nickel atom cannot affect the unit atomic jumps of the diffusion mechanism. A more realistic supposition would be that the bonding configuration before and after a unit jump remains the same and so its net effect on diffusion is zero.

Such a situation can be realised for the case of next nearest neighbour diffusion; nickel diffusion may take place entirely within the nickel sublattice. Thus the diffusivity of nickel may be independent of any compositional changes in bonding energy.

The second consideration is that large concentrations of thermal vacancies may occur throughout the phase field of NiGa. This has been found to be the case. Quenching experiments have shown that the thermal vacancy concentrations at 1133°K are as high as 1·53, 1·68 and 1·73% in alloys containing 48·25, 50·0 and 52·40 atomic % nickel respectively. Furthermore extrapolation of these data has indicated that the corresponding fractions at the solidus temperature would be 3·2, 3·1 and 3·5% respectively [145].

Additionally it has been postulated that thermal defect equilibria occur in B2 compounds and that thermal triple defects, consisting of two vacancies on one sublattice and an anti-structure atom on the other sublattice, may predominate at high temperatures [143, 145, 41] (see

sections 2.4.4 and 2.4.5). These defects arise when thermal vacancies on one sublattice have a high energy of formation and may degenerate into a vacancy on the opposite sublattice plus an anti-structure atom (on the first sublattice) with a saving in energy.

In NiGa triple defects of the type $2V_{Ni}\ Ni_{Ga}$, formed by the degeneration of gallium sublattice thermal vacancies, have been postulated as predominant at high temperatures. This together with the high thermal defect fractions found in the compound suggests that very large concentrations of thermal vacancies occur, the bulk of which are present on the nickel sublattice while on the gallium sublattice the predominant thermal defects are nickel anti-structure atoms.

The fact that the thermal vacancy concentration in NiGa is large throughout the phase field of the compound and also largely confined to the nickel sublattice would favour rapid diffusion and may account for the absence of a compositional dependence of the diffusion coefficient of nickel (D_{Ni}).

The third factor which was considered as having a bearing on the diffusion of nickel in NiGa was the presence of constitutional defects. It was suggested earlier [see section 5.2] that NiGa contains nickel sublattice vacancies and nickel anti-structure atoms and that both types of constitutional defect occur throughout the phase field of the compound. The high constitutional vacancy concentrations present, even in nickel-rich alloys (see graph G.21), may well account for the high observed values of the nickel diffusion coefficient (D_{Ni}).

Both the thermal vacancy and constitutional vacancy models in isolation explain the observed high value of D_{Ni} but in each case the vacancy concentration is known to vary with composition; consequently some compositional dependence in D_{Ni} might be expected. However the constitutional vacancy fraction decreases with increasing nickel content

(see graph G.21) whereas quenching experiments have shown that the thermal vacancy fraction increases with nickel content [145]. The two factors complement each other so that the overall vacancy concentration (largely confined to the nickel sublattice) becomes less composition dependent than would otherwise be expected. Consequently nickel diffusion, assuming that vacancies are involved, may be both rapid and compositionally invariant.

Finally both constitutional and thermal nickel anti-structure atoms Ni_{Ga} may well play a significant role in the diffusion of nickel, by facilitating nearest neighbour and next nearest neighbour vacancy jumps. (This consideration will be dealt with later.)

5.3.2 The Compositional Dependence of Ga-67 Diffusion

Unlike the diffusion of nickel in NiGa the results of the diffusion of gallium do show a compositional dependence. With the exception of the lowest diffusion temperature 1084°K (T_H = 0·77), where the diffusion coefficient of gallium D_{Ga} remains effectively constant throughout the phase field, D_{Ga} follows the more usual compositional dependence [see graph G.8] ; the coefficient passes through a minimum value close to stoichiometry.

Again, as in the case of nickel, the diffusion coefficient of gallium D_{Ga} in NiGa has been compared with that of cadmium in AuCd and magnesium in AgMg for various alloy compositions and homologous temperatures [see TABLE IX] . For the purposes of comparison the phase field of each alloy was divided into A-rich compositions, stoichiometry and B-rich compositions. Each portion of the phase field will now be considered in turn.

(i) In A-rich alloys, the diffusion coefficient of gallium is smaller than that of cadmium in AuCd for all temperatures in the range

$0{\cdot}77 \leqslant T_H \leqslant 0{\cdot}91$. The difference is greatest at the lower temperatures but decreases with increasing temperature. There are no appropriate diffusion data available for further comparison with other B2 compounds.

(ii) At stoichiometry the diffusion coefficient of gallium is found to be smaller than that of cadmium in AuCd but larger than that of magnesium in AgMg over the temperature range $0{\cdot}77 \leqslant T_H \leqslant 0{\cdot}99$. The difference between D_{Ga} and D_{Cd} increases with temperature while the difference between D_{Ga} and D_{Ag} falls with increasing temperature. This indicates that the diffusivity of gallium is less sensitive to temperature than the diffusivities of cadmium or silver in their respective stoichiometric alloys.

(iii) Finally in B-rich alloys the situation is again similar to the A-rich case with gallium diffusion being slower (in NiGa) than that of cadmium in AuCd. Also, as in A-rich alloys, the difference between the two diffusivities decreases with increasing temperature indicating that gallium diffusion is more temperature sensitive than cadmium diffusion in their respective alloys.

These data show that gallium diffusion in NiGa is relatively slow particularly for the stoichiometric composition. Non-stoichiometric compositions are far more temperature sensitive than the stoichiometric composition. The effect of departure from stoichiometry on D_{Ga} is far less marked in gallium rich alloys than in nickel rich alloys [see graph G.8 and TABLE IV].

In other words the diffusion of gallium in NiGa is slow in the stoichiometric composition for all temperatures. In non-stoichiometric alloys D_{Ga} is small at low temperatures but increases rapidly with increasing temperature.

In the case of nickel diffusion, three possibilities were put forward to account for the absence of a compositional dependence in D_{Ni}. It was concluded that nickel diffusion may not require the breaking of unlike bonds (A-B) and hence will not vary with composition. Alternatively (or additionally) the large defect fractions (thermal and constitutional) present throughout the phase field might account for the observed diffusion behaviour.

The fact that gallium diffusion is composition dependent and slow may arise for two reasons:

(i) The large concentrations of thermal and constitutional vacancies known to occur on the nickel sublattice are not involved in the diffusion mechanism of gallium.

(ii) Alternatively if they are involved the over-riding factor in the case of gallium atom-nickel vacancy (nearest neighbour) exchanges is the making and breaking of unlike bonds (Ni-Ga). In other words the diffusivity of gallium will depend upon bonding energy and hence will vary with composition (see also section 2.9.3 and reference [86]).

5.3.3 A Comparison of D_{Ni} with D_{Ga} in NiGa

It is generally recognised that diffusion in pure metals and alloys occurs by random vacancy motion. In ordered alloys and intermetallic compounds the requirement that the material remains ordered precludes simple random vacancy motion and imposes correlation restrictions on diffusion paths. A number of suggestions have been made as to the mechanism of diffusion in CsCl type intermetallic compounds.

One such mechanism is the six jump cycle [see FIG. 2.5] which allows diffusion to occur exclusively by nearest neighbour jumps [78, 79]. The first three jumps result in disorder while the latter

three jumps restore atoms to their correct sites. It has been suggested that the ratio of the diffusivities of the two elements in a stoichiometric CsCl (B2) Compound AB, in which diffusion occurs by the six jump cycle, should fall within the limits $^{3}/_{2} \geqslant {}^{D_A}/_{D_B} \geqslant {}^{2}/_{3}$ [40, 39].

However it has also been pointed out that the six jump cycle is merely an idealised geometrical representation of nearest neighbour vacancy motion in a B2 compound and that in fact the only correlation restriction on such motion is that the overall degree of order is maintained during diffusion. A detailed theoretical analysis of nearest neighbour vacancy motion by Kikuchi et al. (1969) [86] indicated that a particular diffusivity ratio ($^{D_A}/_{D_B}$) was not necessarily indicative of any particular diffusion mechanism [see FIG. 2.10].

Nevertheless diffusion data for CuZn [95], AgMg [34] and AuCd [57] have all been found to comply with the suggested limits proposed for the six jump cycle.

An alternative mechanism proposed for diffusion in B2 compounds is that of next nearest neighbour vacancy jumps [48, 60]. Such a mechanism involves no disordering since atom movements are confined within one sublattice. Furthermore this mechanism does not impose any correlation between the diffusivities of the two elements.

A comparison of the diffusivities of nickel and gallium in NiGa shows that the ratio ($^{D_{Ga}}/_{D_{Ni}}$) does not fall within the limiting values proposed for the six jump except at very high temperatures and large deviations from stoichiometry. In fact for the stoichiometric composition the ratio does not exceed 0·2 even at the highest diffusion temperature ($T_H = 0{\cdot}99$) [see TABLE XIII].

The variation of the diffusion ratio with both composition and temperature may reflect a compositional dependence of the factors θ and U which represent atomic vibrational frequencies and bond energies

TABLE XIII The variation of the diffusivity ratio D_{Ga}/D_{Ni}

Alloy Composition	Values of the diffusivity ratio D_{Ga}/D_{Ni} as a function of temperature			
% Ni	1082°K	1186°K	1282°K	1382°K
47·2	0·15	0·25	0·48	0·56
48·76	0·15	—	—	0·54
50·01	0·19	0·10	—	0·13
50·73	0·18	0·29	0·31	0·25
51·01	0·16	0·19	0·33	0·59
52·40	0·20	0·47	0·72	1·51

respectively [86] (see section 2.9.3). Alternatively the diffusion mechanisms responsible for nickel and gallium diffusion may change (with composition and temperature). A change in the diffusion mechanism across the phase field of the compound has been suggested to account for diffusion behaviour in NiAl [65].

It seems likely, in view of the large difference between the diffusivities of nickel and gallium together with their radically different compositional and temperature dependencies that nickel and gallium diffusion may occur by separate and uncorrelated mechanisms.

In the case of nickel diffusion, the absence of a compositional dependence in D_{Ni} in spite of changes in bonding energy suggests that the atomic configuration around a diffusing atom either has no bearing on diffusivity or does not change. The latter condition was suggested as being satisfied by next nearest neighbour vacancy motion (of nickel) entirely within the nickel sublattice. Such a mechanism would be favoured by the large vacancy concentrations known to be present on the nickel sublattice.

An alternative possibility which may account for the rapid diffusion of nickel in NiGa is an uncorrelated nearest neighbour vacancy mechanism. This could arise because both nickel sublattice vacancies $\square_{Ni}$ and nickel anti-structure atoms Ni_{Ga} can be present simultaneously (as the result of thermal defect equilibria and from the constitutional defect model of NiGa [see section 5.2]). In such a case nickel atoms may diffuse by successive nearest neighbour jumps involving the exchange of nickel anti-structure atoms and nickel sublattice vacancies without any movement of gallium atoms. Such a mechanism has been postulated for B2 compounds for compositions containing a high concentration of anti-structure atoms [26].

This mechanism cannot by itself account for the large diffusivity

of nickel in NiGa because its unit jump requires that a nickel anti-structure atom and a nickel sublattice vacancy are nearest neighbours. The probability of this configuration occurring is a function of the product of the two respective defect fractions and consequently remains quite low even for high defect fractions. Thus the diffusion rate resulting from this mechanism alone is likely to be low. However it may contribute to nickel diffusion by acting in parallel with other mechanisms.

The uncorrelated nearest neighbour nickel anti-structure atom - nickel vacancy exchanges may act together with the six jump cycle mechanism, acting as a short circuit for the latter. The nickel diffusion coefficient may then be larger than expected purely from the diffusivity of gallium and the usual diffusivity ratio imposed by the six jump cycle. But the contribution of the former mechanism is unlikely to be large enough to account for values of the diffusivity ratio ($^{D}Ga/D_{Ni}$) as low as those observed.

On the other hand nickel anti-structure atoms and the uncorrelated nearest neighbour nickel diffusion mechanism may be important operating in parallel with a next nearest neighbour vacancy mechanism. This combination of nearest and next nearest vacancy jumps has been suggested to account for the relatively rapid diffusion observed in some B2 compounds [60].

Compared with nickel the diffusion of gallium is slow, particularly in compositions near to stoichiometry and at low temperatures. Also, unlike nickel the diffusivity of gallium is very composition dependent. Hence, it seems likely that the two species diffuse by different types of mechanism.

The fact that the gallium sublattice contains very few vacancies suggests that gallium diffusion by a next nearest neighbour vacancy

mechanism, entirely within the gallium sublattice, is unlikely. Consequently a nearest neighbour mechanism may be favoured. Furthermore, the large concentrations of vacancies on the nickel sublattice are available for the initial nearest neighbour gallium atom-vacancy exchanges and so support the suggestion of a nearest neighbour (gallium) diffusion mechanism. However subsequent jumps by gallium atoms (on the nickel sublattice) into vacancies on the gallium sublattice would merely reverse the initial jumps and result in no net diffusive flux unless vacancies on the gallium sublattice are permitted to move by exchanges with nickel atoms. In other words gallium diffusion by nearest neighbour jumps requires the correlated movement of nickel atoms, effectively the condition of the six jump cycle.

Assuming that a nearest neighbour mechanism is responsible for gallium diffusion the reason for the observed low diffusivity of gallium cannot lie in a lack of nearest neighbour (nickel sublattice) vacancies nor in the co-operative diffusivity of nickel atoms which is large. Consequently it seems that the breaking of unlike bonds (Ni-Ga) required in nearest neighbour exchanges must be the rate determining factor.

In such a case, the diffusion of gallium may then be more rapid in non-stoichiometric compositions because the general disordering of the lattice due to constitutional defects means that fewer unlike bonds need to be broken during diffusion in such compositions. The compositional dependence of the diffusion coefficient will then show a characteristic V-shaped curve with a minimum at or close to stoichiometry [86].

If a nearest neighbour motion, specifically the six jump cycle, is the gallium diffusion rate controlling mechanism and since nickel sublattice vacancies are in plentiful supply, it is reasonable to suppose that cycles start with vacancies originating on the nickel sub-

lattice. This infers that four jumps in each complete cycle will involve gallium atom-vacancy exchanges and only two will involve nickel atom jumps [see FIG. 2.5] . Thus the resultant diffusivity ratio ($^{D}Ga/D_{Ni}$) should lie towards the top of the range suggested by Elcock & McCombie (1958) [40] . But the observed ratio is below the bottom of the suggested range in some of the alloys investigated in this study [see TABLE XIII] .

The observed diffusion data cannot be explained by the operation of a six jump cycle mechanism in isolation. Gallium diffusion may well occur exclusively by nearest neighbour jumps (the six jump cycle) and consequently be closely correlated with nearest neighbour diffusion jumps made by nickel atoms. However nickel is probably able to diffuse by next nearest neighbour jumps, which are not correlated with gallium jumps, as well as by nearest neighbour jumps. Consequently the overall correlation between the diffusivity of the two species is not evident. In effect the correlation factor becomes decomposed into two components each related to only one sublattice (and hence largely to one species).

It has been found in the course of a theoretical derivation of a diffusion coefficient in a binary (B2) ordered alloy that precisely this situation occurs, namely that the correlation factor decomposes into two components related to the two sublattices [87] .

In summary, the diffusivities of nickel and gallium D_{Ni} and D_{Ga} respectively together with their ratio may be accounted for as follows:

(i) The diffusion of nickel is rapid and compositionally insensitive probably because a next nearest neighbour diffusion mechanism is predominant.

(ii) Nickel is also likely to diffuse in part by nearest neighbour atom-vacancy exchanges. These jumps may involve either only nickel antistructure atoms and nickel sublattice vacancies and so be uncorrelated with gallium atom jumps or they may be part of a six jump cycle sequence and so be correlated with gallium diffusion.

(iii) Gallium diffusion probably occurs exclusively by a nearest neighbour

(six jump cycle) mechanism and as such is closely correlated with nearest neighbour nickel atom jumps.

(iv) The independence of nickel diffusion from that of gallium diffusion allows the diffusivity ratio to take on values well outside the range predicted when a six jump cycle is considered as the sole diffusion rate controlling mechanism. In effect the diffusion correlation factor decomposes into two components related to the two sublattices [87].

5.3.4 The Compositional Dependence of the Activation Energies and Frequency Factors of Diffusion in NiGa

The activation energies Q_{Ni} and Q_{Ga} and the frequency factors D_o^{Ni} and D_o^{Ga} of nickel and gallium diffusion show markedly different compositional dependencies [see graphs G.11, A & B]. This difference in behaviour offers support to the earlier suggestion that the two species may diffuse by separate (different) mechanisms.

The compositional dependence of Q_{Ni}^{Ga} shows a minimum close to stoichiometry but there are insufficient data in gallium-rich alloys to determine the composition of minimum diffusion activation energy with any confidence [see graph G.11]. The minimum does however appear to lie somewhere to the gallium-rich side of stoichiometry. This behaviour does not parallel in any way the compositional dependence of the activation energy of cadmium in AuCd [57], which shows a maximum close to stoichiometry. No data are available in other B2 compounds to allow further comparison.

Both the activation energies of nickel and gallium diffusion conform reasonably well with the general empirical relationship $Q = 34\ T_M$ ($\pm$ 20%), where Q, the activation energy, is in calories per mole and T_M, the solidus temperature, is in degrees Kelvin [58]. However, the compositional dependence of the activation energy of either species cannot be directly attributed to the variation of the solidus temperature, which falls continuously with increasing gallium content throughout the

phase range of NiGa.

It has been suggested that the compositional dependence of the elastic constants, which influence the activation energy of motion E_M of point defects may account for the variation of the diffusion activation energy observed in compounds. Calculations based on the variation of elastic constants have been used to predict the compositional dependence of the diffusion of zinc in CuZn [95] with some success. But similar calculations in AuCd [57] did not correlate particularly well with the observed compositional dependence of the activation energy.

The explanation of the observed compositional dependence of both Q_{Ni} and Q_{Ga} found in NiGa must lie in the changes in the formation and motion energies of the vacancies which take part in the diffusion rate controlling mechanisms.

As was reviewed earlier the energies of formation of thermal defects in B2 intermetallics are based not on monovacancies but on defects involving two or even three lattice sites. Furthermore the energies of motion determined from resistivity experiments have been found to depend upon the fraction of defects annealed out, because of defect equilibria [120, 146, 145].

The energy of formation E_F of thermal defects (assumed to be two vacancy defects) has been determined in NiGa as a function of composition and has values of 63·2, 70·1 and 63·2 kj/mole for the compositions containing 47·4, 50·0 and 52·4 atomic % nickel respectively [145]. However it was also found earlier that the formation of vacancies on the gallium sublattice was difficult while on the nickel sublattice it was easy. It is evident then that the measured defect formation energy, assuming a vacancy is formed on either sublattice, is the sum of the formation energy of a (single) nickel sublattice vacancy (E^V_{Ni}) and the formation energy of a gallium sublattice vacancy (E^V_{Ga}), and that

$E^V_{Ga} \gg E^V_{Ni}$.

Thus in the case of nickel diffusion, which has been postulated to occur predominantly by a next nearest neighbour mechanism involves only nickel sublattice vacancies, the energy of vacancy formation contribution to the activation energy of nickel diffusion Q_{Ni} is likely to be small. Furthermore constitutional vacancies occur on the nickel sublattice throughout the phase field of NiGa [see section 5.1.2]. Consequently nickel diffusion may occur without requiring the formation of thermal vacancies. In such an event the compositional dependence of the diffusion activation energy of nickel Q_{Ni} may reduce to the dependence of the activation energy of motion E_M.

A similar argument has been put forward for the diffusion of nickel in nickel-deficient NiAl [8]. The vacancy formation energy was assumed zero and consequently the activation energy of diffusion Q_{Ni} (in NiAl) became equal to that of vacancy motion E_M and did not vary greatly with composition in these aluminium-rich alloys.

In the case of gallium diffusion no constitutional vacancies are present on the gallium sublattice, and so the diffusion activation energy Q_{Ga} may contain an energy of vacancy formation term. Furthermore this contribution may be quite large because gallium sublattice vacancies are difficult to form (i.e. E^V_{Ga} is high). However if gallium diffusion occurs by a six jump cycle mechanism which involves (constitutional) nickel vacancies the thermal formation of further vacancies may not be required for gallium diffusion. Consequently, the activation energy of gallium diffusion may not contain an energy of vacancy formation term.

The second factor contributing to the activation energy of diffusion is that of the energy of vacancy motion. Values of the activation energies of motion E_M have been determined in NiGa as a function of composition [145]. They were found to vary with the residual

fraction of defects $[f = {}^{n(t)}/_{n(o)}]$. For example in the stoichiometric composition values obtained were: E_M, (f = 0·8) 179·9 kj/mole, (f = 0·5) 146·6 kj/mole and (f = 0·2) 125·5 kj/mole.

Now at a given diffusion temperature diffusive motion will occur within a structure containing the equilibrium defect structure characteristic of the said temperature. In order to determine the energy of motion a high temperature defect structure is retained at low temperatures by quenching. The retained defects are subsequently annealed out at some intermediate temperature (T_A) while changes in resistivity are measured as a function of time. The activation energy of motion is then evaluated from the rate of change of resistivity as a function of annealing temperature (T_A). But this energy is found to change with remaining defect fraction.

The true energy of motion will be that measured in a structure containing the equilibrium number of defects characteristic of the quench temperature. In other words it will be equal to the measured activation energy of motion for the limiting condition of the remaining defect fraction being equal to unity (i.e. no defects annealed out). Thus the energy of motion (during diffusion) will equal the upper limiting value of the energy of motion evaluated from quenching and subsequent annealing experiments. But the value of E_M so determined will be characteristic only of the particular quench temperature used. In fact E_M will vary with quench temperature because of its dependence on defect fractions and hence also defect equilibria.

Values of E_M (for f = 1) have been determined in NiGa for a quench temperature of 923°K for a number of alloy compositions; E_M was found to have a value of 179·9 kj/mole at stoichiometry and in gallium rich compositions, in nickel rich alloys it had values of 136·2 and 95·9 kj/mole for the compositions containing 51·25 and 52·4 atomic % nickel

respectively [145] .

The energies of defect formation E_F and motion E_M taken from the data of Wasilewski et al. (1968) [145] have been evaluated as a function of alloy composition in NiGa. These and their sum $(E_F + E_M)$ are tabulated with the activation energies of diffusion Q_{Ni} and Q_{Ga} for comparison in TABLE X. The compositional dependence of the sum $(E_F + E_M)$ shows a small maximum near stoichiometry. This trend is similar to that found for Q_{Ni} of nickel diffusion but the agreement between the absolute values is poor and the correlation may be fortuitous. There is no apparent agreement between the sum $(E_F + E_M)$ and Q_{Ga} either in compositional dependence or in absolute values.

The generally poor correlation between the sum $(E_F + E_M)$ and the two diffusion activation energies is not unexpected in view of the difficulty in evaluating appropriate values for the activation energies of vacancy formation and motion from quenching and annealing experiments.

In fact the model, based on the theory of absolute reaction rates, used to express the activation energy of diffusion Q in terms of defect formation and motion energies entailed a number of simplifying assumptions. The diffusion coefficient D was given by [153, 99, 101] :

$$D = \gamma a^2 p_d \nu_j \qquad 5.3$$

where γ is a numerical constant a is the lattice parameter, p_d is the probability that a defect exists adjacent to a diffusing atom and ν_j is the jump frequency (see section 2.8 and 2.8.1). The probability p_d was then evaluated, assuming that the defects (vacancies) were randomly distributed throughout the lattice in thermal equilibrium, from the expression

$$p_d = \exp(-\frac{\Delta G_F}{RT}) \qquad 5.4$$

where ΔG_F is the activation energy of defect formation.

TABLE X A comparison of the energies of formation (E_F) & motion (E_M) of thermal defects in Ni Ga with the energies of diffusion $(Q_{Ni}$ & $Q_{Ga})$ & creep (Q_C)

Alloy Compⁿ % Ni	E_F * KJ/mole	E_M * KJ/mole	E_F & E_M * KJ/mole	Q_{Ni} † KJ/mole	Q_{Ga} † KJ/mole	Q_C (800K) † KJ/mole	Q_C (1000K) † KJ/mole
47·2 ± 0·2	63·18	179·91	243·09	143·1	191·5	—	—
48·5 ± 0·5	69·04	179·91	248·95	154·3	209·4	—	—
49·3 ± 0·1	71·13	179·91	251·04	156·0	—	220·7	242·1
50·1 ± 0·1	70·08	179·91	249·99	172·5	146·5	225·1	257·0
51·1 ± 0·2	68·83	136·19	205·02	153·7	189·6	288·6	213·2
52·3 ± 0·1	63·18	95·94	159·12	153·9	222·0	284·2	164·7

* Data from ref 145

† Data from this study

Also the jump frequency ν_j was evaluated by assuming that the diffusional jump was equivalent to the reversible motion of an atom across a potential barrier of height W (equal to ΔG_M) in thermal equilibrium, while the atom vibrating with a constant frequency ν_o, was constrained to a plane perpendicular to the direction of motion. The jump frequency was then given by:

$$\nu_j = \nu_o \exp(-\frac{\Delta G_M}{RT}) \qquad 5.5$$

Equations 5·4 and 5·5 were substituted into 5·3 which was then compared with the Arrhenius relationship to give:

$$Q = \Delta H_F + \Delta H_M \qquad 5.6$$

$$D_o = \gamma a^2 \nu_o \exp(\frac{\Delta S_F + \Delta S_M}{R}) \qquad 5.7$$

where ΔH_F (equal to E_F) and ΔH_M (equal to E_M) are the activation enthalpies of defect formation and motion.

In NiGa thermal vacancies are known to be largely confined to the nickel sublattice and consequently the equation (5·4) from which the probability p_d was derived is not applicable. Also diffusion is not in fact a thermodynamically reversible process [99] and consequently equation 5.5 for the jump frequency ν_j does not strictly apply. It can be seen then that there is no fundamental reason for an equality between the activation energy of diffusion Q and the sum of the defect formation and motion energies $(E_F + E_M)$. Consequently the activation energy of nickel diffusion Q_{Ni} and that of gallium diffusion Q_{Ga} need not follow the compositional dpendence of the sum $(E_F + E_M)$.

In the case of nickel diffusion the plentiful supply of constitutional nickel sublattice vacancies present in all alloy compositions studied may mean that the activation energy of nickel diffusion is equal to that of vacancy motion (and contains no E_F term). It was also

suggested earlier that nickel diffusion probably occurs largely by next nearest neighbour jumps together with some nearest neighbour jumps. The compositional dependence of Q_{Ni} may then reflect the compositional dependences of the energies of motion of the two jump types and will depend upon any relative changes in their contributions to diffusion as a function of composition.

If particular values of the diffusivity ratio $(^{D}Ga/D_{Ni})$ are indicative of a correlation between the diffusion mechanisms of the two species rather than merely the ratio of two independent diffusion coefficients, a number of inferences and conclusions may be drawn with respect to diffusion mechanisms in NiGa.

For example the ratio $(^{D}Ga/D_{Ni})$ is found to tend to fall within the limits predicted by the six jump cycle for off-stoichiometric compositions. This suggests that nickel nearest neighbour jumps become more prevalent (compared with next nearest neighbour jumps) in these compositions. But in general a nearest neighbour jump may be expected to have a lower activation energy than a next nearest neighbour jump. This in turn would result in a decrease in the activation energy of diffusion Q_{Ni} as nearest neighbour jumps became more prevalent (i.e. in going to off-stoichiometric compositions).

If in fact two mechanisms are operating in the diffusion of nickel then the frequency factor D_o^{Ni} may be expected to show a compositional variation in keeping with compositional changes in diffusion mechanism. It can be seen (graph G.11, B) that close to stoichiometry where largely next nearest neighbour jumps are considered to account for nickel diffusion the frequency factor falls within the limits $10{\cdot}0 \geqslant D_o^{Ni} \geqslant 0{\cdot}1$ associated with 'normal' diffusion (that is diffusion controlled by a single thermally activated mechanism). Away from stoichiometry nearest neighbour jumps begin to contribute to diffusion and two

mechanisms are thus operative. The frequency factor correspondingly becomes anomalously low [see graph G.11, B and TABLE III] .

Unfortunately the frequency factor data are subject to very large errors and suggestions based upon them are necessarily speculative. Furthermore if nickel diffusion does in fact become correlated with that of gallium in a six jump cycle then both species will have the same barriers to diffusion and hence will have the same (or at least similar) activation energies and compositional dependences thereof. Since in fact the activation energies of nickel and gallium are not similar and their compositional dependences are totally unalike it must be concluded that their respective diffusion mechanisms are not closely correlated. Consequently particular values of the diffusivity ratio ($^{D}Ga/D_{Ni}$) merely reflect the relative values of the activation energies of diffusion Q_{Ni} and Q_{Ga} and the temperature at which diffusivities were determined.

In the case of gallium diffusion the frequency factor D_o^{Ga} is found to fall within the limits $10{\cdot}0 \geqslant D_o^{Ga} \geqslant 0{\cdot}1$ for all compositions, conforming to the conditions of 'normal' diffusion [see graph G.11.B and TABLE IV] . This supports the suggestion that gallium diffusion occurs entirely by one mechanism, possibly nearest neighbour jumps (in a six jump cycle).

If in fact gallium diffusion is considered to occur by the six jump cycle mechanism the observed compositional dependence of the gallium activation energy may be rationalised as follows. First of all, cycles may start with the motion of constitutional vacancies originating on the nickel sublattice so that the activation energy of gallium diffusion might not contain a contribution from the energy of defect formation (E_F) and hence will equal that of the activation energy of motion.

Now diffusion by a six jump cycle can be viewed in two separate ways. In the first case all six jumps of a cycle must be completed in a correlated sequence before diffusion is effected and hence the diffusion energy is that required to move through a complete sequence. Alternatively the six jump cycle may be considered simply as a resultant geometrical representation of the (six) various jump types under the boundary condition that disordering jumps are balanced by an equal number of re-ordering jumps [86] (see sections 2.9.3 and 2.9.4). In this case the slowest jump of the six will be rate controlling and the activation energy of gallium diffusion will equal the activation energy of this rate controlling jump.

In the first instance the activation energy of diffusion will vary with composition in the same manner as the compositional dependence of the activation energy for traversing a complete cycle. It has been calculated in AgMg that the different geometric forms of the six jump cycle [see FIG. 2.5] have different activation energies. Hence it may be that the compositional dependence of the activation energy of diffusion (by a six jump cycle) arises from a change from one geometric form of the cycle to another as a function of composition. Certain cycles can occur only in non-stoichiometric compositions [33, 34].

It seems, however, more probable that a particular nearest neighbour jump (which occurs in a cycle) may be diffusion rate controlling and then the activation energy of diffusion will vary as a function of composition in the same way as the energy of that jump. Alternatively other jumps with different activation energies may become rate controlling as composition is changed.

A recent theoretical derivation of the diffusion coefficient in B2 compounds [87] suggests that nearest neighbour jumps depend on a particular vacancy availability factor which is not the same for all jumps

(see the probability factor p_d in equation 5.3). Furthermore, different jumps were suggested to have different jump frequency factors and consequently each different nearest neighbour jump had a unique activation energy. This analysis favours the supposition that a single jump rather than a sequenc of jumps (such as the six jump cycle) is probably diffusion rate controlling.

In NiGa there are four possible nearest neighbour atom-vacancy exchanges:

$$\square_{Ni} + Ga_{Ga} \longrightarrow Ga_{Ni} + \square_{Ga} \qquad 5.8$$

$$\square_{Ga} + Ni_{Ni} \longrightarrow Ni_{Ga} + \square_{Ni} \qquad 5.9$$

$$\square_{Ga} + Ga_{Ni} \longrightarrow Ga_{Ga} + \square_{Ni} \qquad 5.10$$

$$\square_{Ni} + Ni_{Ga} \longrightarrow Ni_{Ni} + \square_{Ga} \qquad 5.11$$

where $\square_{Ni}$, Ni_{Ni} and Ga_{Ni} are a vacancy, a nickel atom and a gallium atom on the nickel sublattice respectively and $\square_{Ga}$, Ni_{Ga} and Ga_{Ga} are the equivalent species on the gallium sublattice. In the case of a complete six jump cycle which starts with the movement of a nickel sublattice vacancy the jumps 5·8 and 5·10 occur twice.

In attempting to determine which of these four jumps may be diffusion rate controlling several factors need to be considered:

(i) The availability of an adjacent vacancy with which a diffusing atom may exchange positions. This factor will be termed F for further reference.

(ii) The change in energy between the two equilibrium states at the beginning and end of a jump. This term will be called ΔE (equal to

$E_1 - E_2$) where E_1 and E_2 are the free energies of state of the equilibrium conditions at the beginning (E_1) and end (E_2) of a jump.

(iii) The activation energy barrier to motion for the jump. This factor E_{MOT} will be assumed for the purposes of the current analysis to be proportional to the ratio of the projected area of the diffusing atom (πr_A^2 where r_A is the A atom radius) to the area in the $\{111\}$ plane between the three B atoms comprising the saddle point for diffusion in a $\langle 111 \rangle$ direction [see FIG. 5.1] . The saddle point area SA is given by:

$$SA = \tfrac{1}{2} (3^{\frac{1}{2}} a_o^2 - \pi r_B^2)$$

where a_o is the experimental lattice parameter of NiGa and r_B is the atomic radius of the B atom. When a nickel atom is diffusing ($r_A = r_{Ni}$ and $r_B = r_{Ga}$) when a gallium atom is diffusing ($r_A = r_{Ga}$ and $r_B = r_{Ni}$) assuming perfect order (i.e. an A atom moving between three B atoms). When anti-structure atoms occur r_B is altered proportionally to account for the possibility of the saddle point atoms containing an atom of the same species as that which is diffusing. Thus for perfect order:

$$E_{MOT} \text{ (A atom)} \quad \propto \quad 2 \pi r_A^2 / (3^{\frac{1}{2}} a_o^2 - \pi r_B^2)$$

and similarly:

$$E_{MOT} \text{ (B atom)} \quad \propto \quad 2 \pi r_B^2 / (3^{\frac{1}{2}} a_o^2 - \pi r_A^2)$$

These energies of motion are then normalised to give a ratio E according to the expression:

$$E_B = \frac{E_{MOT} \text{ (B atom)}}{E_{MOT} \text{ (A atom)}}$$

B = gallium

A = nickel

FIG 5.1. The Saddle Point Geometry for ⟨111⟩ Diffusion in Ni Ga

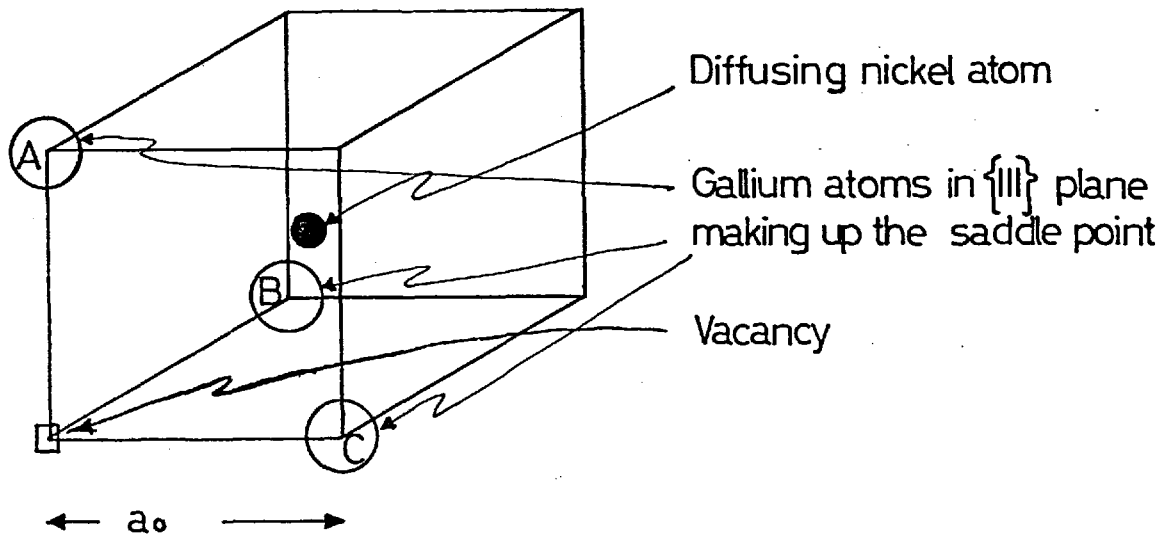

{111} plane

$AB=BC=CA=\sqrt{2}a_o$ (≡4·06units)

a_o=lattice parameter≈2·9 "

Gallium atoms radius (r_{Ga}) =1·35 units

Diffusing nickel atom radius (r_{Ni}) =1·25 units

Area of {111} plane ≡ $\triangle ABC \equiv \frac{\sqrt{3}}{2} a_o^2$

projected area occupied by Ga atoms ≡ $\frac{1}{2}\pi r_{Ga}^2$

projected area occupied by Ni atom ≡ πr_{Ni}^2

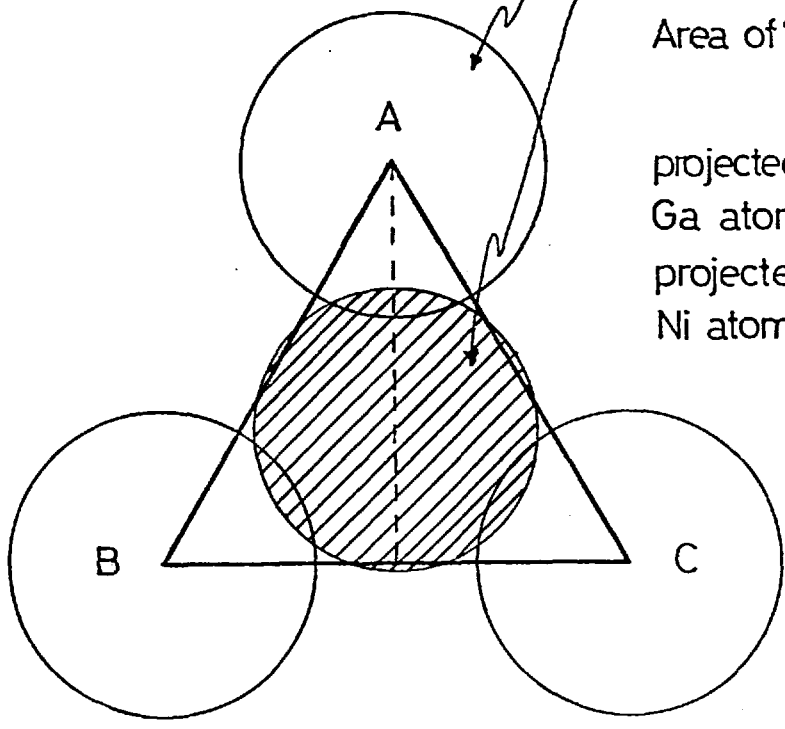

The three factors F, Δ E and E can be qualitatively evalued for the four types of diffusion jump and their compositional dependence estimated. The values expressed as a fraction of their value at stoichiometry are shown in TABLE XI for stoichiometry, nickel rich gallium rich alloys. The energy terms Δ E and E have been expressed using the convention that if energy must be supplied for a reaction the value is positive (thus E, the energy of motion, is always positive). Note that E_B the energy to move a gallium atom is greater than E_A the energy to move a nickel atom.

TABLE XI

Qualitative estimates of the factors F, ΔE & E

(normalised w.r.t. the value at stoichiometry)

Reaction Equation	Frequency Factor F	Energy of State ΔE	Energy of Motion E
(i) Stoichiometry			
5·8 (Ga_{Ga})	Large (L)	Large positive (L)	E_B ($> E_A$)
5·9 (Ni_{Ni})	Small (S)	Small negative (-S)	E_A
5·10(Ga_{Ni})	Small (S)	Large negative (-L)	E_B ($> E_A$)
5·11(Ni_{Ga})	Large (L)	Small positive (+S)	E_A
(ii) Nickel Rich			
5·8	Less large ($<$L)	Larger positive ($>$L)	$> E_B$
5·9	Larger ($>$S)	Less negative ($>$-S)	$< E_A$
5·10	Larger ($>$S)	Less large negative ($>$-L)	$> E_B$
5·11	Less large ($<$L)	Smaller positive ($<$S)	$< E_A$
(iii) Gallium Rich			
5·8	Larger ($>$L)	Less large positive ($<$L)	$< E_B$
5·9	Smaller ($<$S)	Larger negative ($<$-S)	$> E_A$
5·10	Smaller ($<$S)	More large negative ($<$-L)	$< E_B$
5·10	Larger ($>$L)	Larger positive ($>$S)	$> E_A$

TABLE XI can be used to suggest which of the diffusion jumps may be rate controlling for nearest neighbour gallium diffusion. Thus while the diffusion jump of a gallium atom into a nickel vacancy (5·8) has a large availability frequency factor F at stoichiometry its large activation energy ($\Delta E + E$) may make it the rate controlling step.

In nickel-rich compositions the frequency factor of jump (5·8) has fallen while its activation energy has increased suggesting that it is even more likely to be the rate controlling step than at stoichiometry. Thus the diffusion activation energy Q_{Ga} may be expected to increase in nickel rich compositions.

In gallium-rich compositions the situation is less clear but it would appear that the gallium diffusion step (5·8) becomes easier and may no longer be rate controlling. It is likely that reaction 5·11 may become rate controlling in preference to 5·8 because while both reactions produce the high energy defect $\square_{Ga}$, the latter (5·8) also results in the formation of gallium anti-structure atoms which may now be favoured in gallium rich compositions.

In conclusion the compositional dependence of both the nickel and gallium activation energies of diffusion in NiGa may be summarised as follows:

(i) The activation energy of nickel diffusion in NiGa is low throughout the phase field and not very sensitive to composition. This is because constitutional nickel vacancies occur throughout the phase field and hence the diffusion activation energy does not require an energy of vacancy formation term.

In comparison with NiAl [145] the activation energy of nickel diffusion in NiGa is very low (about half) in nickel rich alloys (where the former compound contains no constitutional vacancies) but roughly com-

parable in nickel deficient alloys (where both NiAl and NiGa contain constitutional vacancies).

(ii) Nickel diffusion in NiGa probably involves more than one mechanism, namely nearest and next nearest neighbour vacancy jumps. The latter is postulated to be predominant throughout the phase field of the compounds.

(iii) Gallium diffusion is suggested to occur exclusively by the various types of nearest neighbour atomic jumps. These are considered to be interdependent but not closely correlated in the geometrical sense of a six jump cycle path.

(iv) The compositional dependence of the activation energy of gallium diffusion is very marked in comparison with that of nickel. It may be qualitatively explained in terms of the compositional dependence of the activation energy of the particular rate controlling nearest neighbour jump or alternatively in terms of a change from one rate controlling jump to another with composition.

5.4 Creep in the Intermetallic Compound NiGa

Experimental data obtained from steady state compression creep tests were used to evaluate two creep parameters, namely the stress exponent n and the apparent activation energy of creep Q_c.

Specimens tested over the temperature interval 732 - 887°K (0·52 - 0·63 T_M) belonged to one series called the 800K series. In a second series 1000K tests were carried out in the temperature interval 953 - 1077°K (0·68 - 0·77 T_M).

The equations used and the corrections applied to the experimental

data when evaluating the stress exponents and activation energies of creep are detailed in section 3.7.5. The values obtained for n and Q_c are tabulated as a function of alloy composition for both the 800 K and the 1000 K creep series in the results [see TABLE V to VIII].

5.4.1 The Stress Dependence of Creep in NiGa

In a given creep series individual values of the stress exponent were determined over the same stress ranges at various constant temperatures for all alloys. Consequently any variation of the exponent as a function of composition did not reflect a stress sensitivity of the stress exponent.

Furthermore the constant temperatures used during the stress change tests from which stress exponents were evaluated were roughly equal for all the alloys tested within a particular creep series. Therefore it was assumed that changes of the exponent as a function of composition did not reflect a temperature sensitivity of the stress exponent.

Hence the variation of the stress exponent determined a number of times for a given alloy in a given creep series was attributed to random scatter. Consequently, a mean stress exponent was evaluated from the individual values determined for each alloy composition for both the 800 K and 1000 K creep series. The compositional dependence of this mean stress exponent is shown for both the 800 K and 1000 K creep series in graphs G.16 and G.17 respectively.

In the 800 K ($\sim$0·6 T_M) series the stress exponent reaches a maximum of 4·7 in the nickel rich composition 50·17 atomic % nickel [see graph G.16] . A similar compositional dependence of the stress exponent has been observed in NiAl (at the homologous temperature 0·6 T_M) where a maximum in the value of the stress exponent occurs at compositions close to stoichiometry (i.e. between 49 & 51 atomic % nickel) [136, 140,

159] .

The compositional dependence of the stress exponent in NiGa for the 1000 K ($\sim$0·73 T_M) shows a curve which passes through a minimum of 4·1 at the 51·0 atomic % nickel composition [see graph G.17] . Data for the compositional dependence of the stress exponent in NiAl show that the maximum observed at T($\sim$0·6 T_M) becomes progressively less pronounced with increasing temperature [159] . Furthermore at very high temperatures ($\sim$0·91 T_M) the data of Vandervoort et al. (1966)[140] exhibit a minimum value for the exponent n near stoichiometry (in NiAl).

The markedly different compositional dependencies of the stress exponent in NiGa as determined for the 800 K and 1000 K creep series suggest that the stress exponent varies with temperature (as well as composition). In fact a comparison of the values of the exponent (n), for a fixed composition, for the 800 K and 1000 K series indicates that the stress exponent (n) increases with increasing temperature.

In most materials the stress exponent shows a decreasing value with increasing temperature until at very high temperatures and low stresses the linear law (n = 1) is followed. The creep strain rate is then linearly proportional to the stress and 'diffusion creep' is rate controlling [119, 70] .

In NiAl the overall trend is one of a decreasing stress exponent with increasing temperature, until at high temperatures the exponent becomes constant and temperature insensitive [140, 159] . The temperature at which the stress exponent reaches a constant value is dependent on alloy composition.

However, it has also been found in NiAl that over a restricted temperature range the stress exponent may increase with temperature. In the stoichiometric composition, for example, the exponent increases from a value of 9·1 at 1023°K ($\sim$0·54 T_M) to 10·4 at 1068°K ($\sim$ 0·56 T_M)

[136]. It was also reported by the same authors that the same effect has been observed in AuZn and that it has been attributed to the presence of structural (constitutional) lattice defects [136].

It would seem reasonable to suppose that the compositional dependence of the stress exponent may depend on the defect structure in NiGa. But the defect structure (constitutional plus thermal) in the compound is known to vary with temperature as well as composition [145]. Consequently the stress exponent may be expected to be temperature dependent and its temperature sensitivity may be determined by the defect equilibria which occur in the compound.

In summary the stress dependence of the creep rate in NiGa as defined in terms of the stress exponent may be outlined as follows:

(i) The stress exponent varies with composition. The compositional dependence shows a small maximum near stoichiometry for the 800 K ($\sim 0.6\ T_M$) creep series. At higher temperatures ($\sim 0.73\ T_M$) in the 1000 K series the compositional dependence of the exponent shows a minimum at the 51·0 atomic % nickel composition.

(ii) The stress exponent is also temperature dependent and is found to increase with temperature over the range spanned by the two creep series ($0.53 \leqslant T/T_M \leqslant 0.77$).

(iii) Both the compositional and temperature dependence of the stress exponent are probably due to the presence of constitutional and thermal defects, and defect equilibria.

5.4.2 The Apparent Activation Energies of Creep in NiGa

Values of the apparent activation energy of creep Q_c were determined from steady state, change of temperature, creep tests conducted at constant load and corrected for changes in stress (see section 3.7.5).

A mean activation energy of creep was evaluated from the individual values determined for each given alloy composition in both the 800 K and 1000 K creep series. The compositional dependence of the mean activation energy of creep is shown for both the 800 K ($\sim 0{\cdot}6\ T_M$) and 1000 K ($\sim 0{\cdot}73\ T_M$) creep series in graphs G.18 and G.19 respectively.

It was seen in the previous section that the stress exponent n was found to vary with temperature, at least over the limited temperature range covered by the two creep test series. Consequently the stress factor of equation 3.9 cannot be assumed independent of temperature. The equation may be reformulated as:

$$\frac{\dot{\varepsilon}}{\sigma^n} = A \exp\left(-\frac{Q_c}{kT}\right) \qquad 5.7$$

hence

$$\ln \dot{\varepsilon} - n \ln \sigma = \ln A - \frac{Q_c}{kT} \qquad 5.8$$

where $\dot{\varepsilon}$ is the creep strain rate, σ the stress, A is some constant and k is Boltzman's constant.

Now if the stress exponent n increases with temperature then the term ($n \ln \sigma$) will also increase with temperature. Hence as the temperature T increases ($\propto 1/T$ falls) the true value of the left hand side of equation 4·4 (i.e. $\ln \dot{\varepsilon} - n \ln \sigma$) is smaller than the value expected if the stress exponent is assumed constant. Qualitatively the slope of the Arrhenius plot is reduced because of the temperature dependence of the stress exponent. Consequently the true activation energy of creep Q_c is lower than that computed when assuming the stress exponent is constant (when it is in fact varying).

When this correction was attempted it resulted in Arrhenius plots which curved rapidly with temperature and consequently a true activation

energy could not be determined. This curvature may have occured because the estimate of the temperature dependence of the stress exponent (assumed to vary linearly between the values determined for the 800 K and 1000 K creep series) was incorrect. Alternatively (and more significantly) the stress factor, as written in equation 5·8, varies in magnitude depending upon the units used to express the stress. In fact the stress would be better expressed in dimensionless units (divided by the elastic modulus for example).

The Arrhenius plots from which the activation energies of creep were initially determined (e.g. graphs G.14 and G.15) did not reveal any apparent curvature, which suggests that the error in assuming the stress exponent was temperature invariant was small. On this basis the uncorrected 'as determined' values were used for comparison with other data (such as diffusion activation energies, etc.). Nevertheless, the analysis outlined above does suggest that these creep activation energies may be somewhat high.

5.4.3 The Compositional Dependence of the Activation Energy of Creep in NiGa

The compositional dependence of the activation energy of creep in NiGa for the 800 K ($\sim 0{\cdot}6\ T_M$) series [see graph G.18] shows a minimum to the gallium rich side of stoichiometry. The data in gallium rich alloys suggest that the composition of minimum creep activation energy lies between 49·0 and 50·0 atomic % nickel.

The compositional trend of the activation energy of creep (in the 800 K series) closely parallel that of gallium diffusion Q_{Ga} [see graphs G.11, A and G.18] . But the creep energy values are somewhat higher than values for the activation energy of gallium diffusion, with the difference reaching a maximum of 30% at the stoichiometric composition.

The compositional dependence of the activation energy of creep in the 1000 K ($\sim 0{\cdot}73\ T_M$) series [see graph G.19] shows a continuously decreasing value of Q_c with increasing nickel content. The variation of Q_c with composition does not parallel the compositional dependence of either the activation energy of nickel or gallium diffusion. In general the activation energy of creep is considerably higher than that of diffusion of the two species (nickel and gallium), although in the composition containing 52·27 atomic % nickel the activation energies of creep and nickel diffusion become nearly equal.

It is however interesting to note that the compositional dependence of the activation energy of creep for the 1000 K creep series follows precisely the same trend as the sum activation energy of thermal vacancy formation and motion ($E_F + E_M$) determined from quenching and resistivity experiments (for quench temperatures of 950°K) [145] (see section 5.3.4 and TABLE X). Furthermore agreement between the two values Q_c and ($E_F + E_M$) is excellent over the phase range studied (i.e. 48·96 to 52·27 atomic % nickel). The possible reason for this correlation will be considered presently.

In NiAl it has been found for nickel rich alloys that the activation energy of high temperature creep is equal to the activation energy of nickel diffusion [159] but in aluminium rich alloys the creep activation energy is somewhat higher than that of nickel diffusion [140, 159]. This may indicate that, in aluminium rich NiAl where constitutional vacancies occur, and in NiGa where similar vacancies are present throughout the phase field, the creep rate is not controlled simply by self-diffusion and that the creep activation energy may contain an additional term.

It has been suggested that a diffusion controlled glide mechanism is creep rate controlling in compositions close to stoichiometry in

NiAl [159]. The microstructure in these alloys (after creep) has been found to consist primarily elongated dislocation loops and dipoles with sub-boundary networks at higher temperatures. Consequently a dipole recovery mechanism via their dissolution to form loops which then shrink in size [159, 149] was postulated as the particular creep mechanism.

This mechanism predicted a stress exponent of 4·0 [159] which is in reasonable agreement with the observed values of 4·7, 4·6 and 4·5 at 0·6 T_M for the NiAl alloys containing 51·0, 50·0 and 49·0 atomic % nickel respectively.

In non-stoichiometric compositions, both in Ni-rich and Al-rich alloys, the stress exponent has been found to be about 3·6 and a viscous glide mechanism has been suggested as rate controlling [140, 159]. However, the micro-structures observed in nickel rich alloys were markedly different to those found in aluminium rich alloys.

For example in the 55 atomic % nickel alloy both the microstructure and dislocation density were found to vary with temperature at a given constant stress. Thus at 973°K ($\sim$ 0·51 T_M) the microstructure consisted of long screw dislocations, at 1073°K ($\sim$ 0·56 T_M) dipoles were observed and elongated loops were also present and at 1173°K ($\sim$0·61 T_M) high densities of dislocation loops were observed emanating from large jogs in the screw dislocations. In aluminium rich alloys on the other hand the structure was characterised by prolific faulting [159].

Now comparison between the creep behaviour of NiAl and NiGa may be used to offer suggestions as to the creep rate controlling mechanisms in the latter. For instance at the homologous temperature of 0·6 T_M the compositional dependence of the stress exponent in NiAl ($T \approx 1150°K$) shows a small maximum near stoichiometry having values of 3·7, 4·6 and 3·6 in the alloys containing 48·0, 50·0 and 55·0 atomic % nickel respectively [159]. Similarly in NiGa at about 800°K (0·6 T_M) the exponent

rises to a maximum near stoichiometry; it has values of 4·1, 4·7 and 3·6 for the alloys containing ~49·0, 50·17 and 52·27 atomic % nickel.

Furthermore at these temperatures (0·6 T_M) the creep activation energy in NiAl is equal to that of nickel diffusion in all but very aluminium rich alloys [159]. Likewise in NiGa the creep activation energy Q_c follows the compositional dependence observed of the activation energy of gallium diffusion Q_{Ga} although the absolute values of Q_c are somewhat higher than those of Q_{Ga}.

It would be reasonable to postulate that the creep rate controlling mechanism in NiGa at these temperatures (0·6 T_M) is the same as that found in NiAl, namely viscous glide in compositions well removed from stoichiometry and dipole recovery for near stoichiometric compositions. Furthermore the micro-structural details may well be similar for the two compounds.

However, in NiAl the stress exponent has been found to become constant and independent of temperature above 0·6 T_M [140, 159, 136] whereas in NiGa it remains temperature sensitive in the range $0{\cdot}54 \leqslant T/T_M \leqslant 0{\cdot}78$. Furthermore the activation energy of creep and its compositional dependence is markedly different in the 1000 K series (~0·73 T_M) in comparison with the 800 K series. This suggests that the creep rate controlling mechanism changes over the temperature interval covered by the two creep series.

Nevertheless in NiAl the stress exponent and activation energy of creep have been found to be temperature dependent in the range $0{\cdot}48 \leqslant T/T_M \leqslant 0{\cdot}61$ for near stoichiometric and nickel rich alloys and the micro-structure has been found to change with temperature [159]. Thus it may be possible to evaluate the likely creep behaviour of NiGa at higher temperatures (~0·73 T_M) by extrapolating the trend in the change in micro-structure (observed in NiAl) to higher temperatures and

applying it to NiGa.

At intermediate temperatures ($0{\cdot}4 \leqslant T/T_M \leqslant 0{\cdot}54$) thermally activated double cross-slip has been postulated as the rate controlling mechanism of creep in NiAl [159, 72, 82]. It has also been postulated for CoAl at somewhat higher temperatures [72]. Such a mechanism is known to result in the formation of jogs in the screw dislocations [76].

But it has been shown that the motion of jogged screw dislocations can be divided into three distinct classes dependent upon the height of the jog. For very small jogs with heights of one or two atom spacings, the screw dislocation may drag the jog along creating point defects (either vacancies or interstitials). For very large jogs, where the distance between the two (screw) dislocation segments is large enough to prevent their mutual interaction, the dislocations will behave separately as single ended sources. In the intermediate case of medium sized jogs, dislocation dipoles will be formed [54].

The situation becomes more complicated when the jog segment of the dislocation can lower its energy by dissociating into partial dislocations, because the jog will have to constrict before it can glide. In the case of vacancy producing jogs all the energy required for constriction must be supplied by thermal activation [76, 71]. At high temperatures, vacancy jogs leave a trail of vacancies which can diffuse away and therefore the movement of the dislocation involves essentially the creation of individual vacancies which is assisted by thermal activation [76].

Now at high temperatures in NiAl ($\geqslant 0{\cdot}6\ T_M$) the microstructure has been found to contain both dipoles, indicating jogs of intermediate height, and loops emanating from large jogs [159]. Consequently small jogs can be expected to be present as well. Furthermore, the non-conservative motion of dislocations containing these small jogs requires

the thermal formation and movement of vacancies. Therefore if the non-conservative motion of screw dislocations containing vacancy producing jogs is rate controlling, the creep activation energy Q_c will be equal to the energy of vacancy formation and motion ($E_F + E_M$). This in turn is normally assumed equal to the activation energy of diffusion.

But it was suggested earlier that in NiGa the diffusion activation energies of nickel Q_{Ni} and probably gallium Q_{Ga} as well do not contain a vacancy formation energy term because of the presence of constitutional vacancies. Thus the activation energy of creep, for the non-conservative motion of jogged screw dislocations, may be greater than that of the activation energy of diffusion in NiGa.

The fact that the compositional dependences of the activation energy of creep Q_c for the 1000 K ($\sim 0{\cdot}73\ T_M$) series and the sum ($E_F + E_M$) are very similar, together with the close agreement between the absolute values of the two energies (see TABLE X) suggests that the non-conservative motion of jogged screw dislocations may be the creep rate controlling mechanism.

5.4.4 The Creep Behaviour of NiGa - a Summary

The creep behaviour of NiGa over the temperature interval $0{\cdot}53 \leqslant T/T_M \leqslant 0{\cdot}78$ may be outlined as follows:

(i) In the temperature range $0{\cdot}53 \leqslant T/T_M \leqslant 0{\cdot}64$ (the 800 K series) the compositional dependence of the stress exponent in NiGa shows a small maximum near stoichiometry; the exponent has values of 4·1, 4·7 and 3·6 for the alloys containing 49·0, 50·17 and 52·27 atomic % nickel respectively.

These data are very similar to both the compositional dependence and the absolute values of the stress exponent found in NiAl at $0{\cdot}6\ T_M$ [159].

(ii) The compositional dependence of the creep activation energy Q_c for this temperature range follows the trend observed for the activation energy of gallium diffusion in NiGa. In NiAl at comparable temperatures (0·6 T_M) the creep activation energy was equal to that of nickel diffusion for all but aluminium rich alloys [159].

(iii) By comparison with the creep behaviour of NiAl at 0·6 T_M it was suggested that the creep rate controlling mechanisms in NiGa may be viscous glide for compositions well removed from stoichiometry and a dipole recovery mechanism in near stoichiometric alloys.

(iv) In the temperature range $0{\cdot}68 \leqslant T/T_M \leqslant 0{\cdot}78$ (the 1000 K series) the compositional dependence of the stress exponent shows a minimum to the nickel-rich side of stoichiometry.

Stress exponent data in NiAl at very high temperatures ($> 0{\cdot}9\ T_M$) suggest that the exponent may fall to a minimum value in near stoichiometric alloys [140].

(v) The activation energy of creep Q_c in the temperature range $0{\cdot}68 \leqslant T/T_M \leqslant 0{\cdot}78$ shows a markedly different compositional dependence than either of the diffusion activation energies Q_{Ni} and Q_{Ga} in NiGa. Furthermore the values of Q_c are generally higher than either Q_{Ni} or Q_{Ga}. However the compositional dependence of Q_c is very similar to that for the sum $(E_F + E_M)$, the energy of formation and motion of a thermal vacancy. Also the absolute values of Q_c and $(E_F + E_M)$ are in good agreement.

(vi) It is tentatively suggested that the non-conservative motion of jogged screw dislocations may be the creep rate controlling mechanism in NiGa.

CHAPTER SIX: Conclusions and Suggestions for Future Work

6.1 Conclusions

Lattice parameter and density measurements have suggested that the compound NiGa contains defects whose type and number vary as a function of composition. But it is known that thermal vacancies may affect both the lattice parameter and density values so the influence of these defects was analysed. It was concluded that constitutional nickel anti-structure atoms and nickel sublattice vacancies were responsible for the observed compositional dependence of the lattice parameter and density.

Furthermore detailed analysis suggested that the constitutional defect structure included both defect types within any given composition. The relative proportions of the two defects changed with composition and even the stoichiometric composition contained constitutional defects.

In diffusion experiments it was found that high standards of atmosphere control were required to prevent specimen oxidation during diffusion anneals.

The short half-life and relatively high radiation energy of gallium-67 required the use of short diffusion anneals and an electro-etching technique for subsequent penetration analysis. Both these limitations resulted in increased errors in the estimates of gallium diffusion coefficients compared with the data for nickel diffusion. Nevertheless results of the log D versus $^{1}/T$ plots indicated that the simple Arrhenius-type relationship applied to the diffusion of both species.

A comparison of the diffusivities and activation energies of the two species suggested each may diffuse by a different separate mechanism. The diffusivity ratio ($^{D}Ga/D_{Ni}$) did not fall within the limits suggested for a correlated six jump cycle diffusion mechanism.

It was concluded that the apparently independent behaviour of the diffusivities of the two species (in relation to each other) was a consequence of the presence of constitutional vacancies throughout the phase field of the compound. Furthermore the diffusion activation energies of both species did not contain a thermal energy of vacancy formation term. Consequently the activation energy of diffusion Q_D does not equal the sum of the energies of vacancy formation and motion.

Compression creep experiments indicated that both the stress exponents and creep activation energies were temperature sensitive over the temperature range investigated ($0{\cdot}53 \leqslant {}^{T}/_{T_M} \leqslant 0{\cdot}78$). It was concluded that this arose as the result of a change in creep rate controlling mechanism with changing temperature.

In the temperature range $0{\cdot}53 \leqslant {}^{T}/_{T_M} \leqslant 0{\cdot}64$ a comparison of the creep activation energy with those of nickel and gallium diffusion indicated that creep deformation was controlled by the diffusion of gallium.

At higher temperatures, $0{\cdot}68 \leqslant {}^{T}/_{T_M} \leqslant 0{\cdot}78$ the creep activation energy was not equal to that of diffusion of either species but appeared to depend on the formation and motion of thermal vacancies ($E_F + E_M$).

6.2 Suggestions for Future Work

The usual trends observed for the diffusion and creep behaviour in other B2 compounds have not been closely reproduced in this study on NiGa. However both the diffusion and creep behaviour of NiGa are dependent on the unusual constitutional defect structure of the compound. Consequently it is felt that further study of this compound could most usefully be concentrated in a re-evaluation of the defect structure in NiGa.

X-ray data could usefully be extended to higher temperatures to establish whether the compound remains ordered up to the solidus temperature. While analysis of superlattice line intensities at low temperatures, in terms of atomic scattering factors, along the lines of Bradley and Taylor's analysis (1937) [13] in NiAl, may reveal the presence of constitutional nickel anti-structure atoms in gallium-rich alloys (as suggested by the empirical defect model).

It may also be possible to identify nickel antistructure atoms in NiGa by Mössbauer spectroscopy. This technique has already shown that iron anti-structure atoms occur at stoichiometry in Fe_2Nb [132].

It is unlikely that a repetition or extension of the diffusion behaviour of NiGa would be necessary or desirable until the appropriate defect model is firmly established. But the creep data of the present study are not conclusive and would bear both repetition and extension.

Hence detailed evaluation of both the stress exponent and activation energy of creep and their variation with temperature would be of interest, particularly if coupled with electron microscope studies of the resulting deformed microstructures. Such data could then establish or refute the observation that the creep activation energy is generally higher than that of the diffusion of either nickel or gallium in NiGa.

Furthermore creep studies might be usefully extended to include a re-examination of the creep behaviour of aluminium rich NiAl alloys where the creep activation energy has also been reported to exceed that of (nickel) diffusion [159].

7. ACKNOWLEDGEMENTS

The author would like to thank both his supervisor, Dr. R.D. Rawlings, and Dr. G.F. Hancock, for their valuable advice and assistance throughout the investigation.

The provision of laboratory facilities in the Department of Metallurgy by Professor J.G. Ball and the financial support of the Science Research Council are also gratefully acknowledged.

The author would further like to thank Mr. P. Burrell for his assistance in the course of the investigation of gallium diffusion during this study.

And finally grateful thanks to my brother Mark for his assistance with the artwork of the diagrams and tables in this thesis.

APPENDIX ONE

The Derivation of a Constitutional Defect Model in NiGa

The following defect model is based upon experimental lattice parameter values and chemical composition value, from which theoretical densities may be calculated. A comparison of theoretical density values, which assume particular constitutional defects are present, with experimental density values then allows the actual defect structure present to be identified.

Theoretical density values ρ_{th} are computed from the relation:

$$\rho_{th} = \frac{2\, M_{NiGa}}{N_A (a_o)^3} \qquad (1)$$

where M_{NiGa} is the mean atomic weight (per lattice site) of the species occupying the lattice sites in the compound NiGa; N_A is Avogadro's number and a_o is the measured lattice parameter.

Since both N_A and a_o are known the problem in evaluating the theoretical density reduces to one of determining M_{NiGa} for various defect structures.

The mean atomic weight per lattice site is given by:

$$M_{NiGa} = \frac{N_{Ni}}{N} \cdot A_{NISITE} + \frac{N_{Ga}}{N} \cdot A_{GASITE} \qquad (2)$$

where N_{Ni} and N_{Ga} are the number of sublattice sites, and A_{NISITE} and A_{GASITE} are the mean atomic weight per sublattice site of the Ni-sublattice and the Ga-sublattice respectively; N is the total number of lattice sites.

Since NiGa is a B2 compound then from structure symmetry:

$$N_{Ni} = N_{Ga} = 0{\cdot}5\, N \qquad (3)$$

Equation 2 may now be re-written:

$$M_{NiGa} = 0{\cdot}5\ A_{NISITE} + 0{\cdot}5\ A_{GASITE} \tag{4}$$

Now the effective atomic weight per sublattice site on the Ni-sublattice is given by:

$$A_{NISITE} = f_{Ni}^{Ni} A_{Ni} + f_{Ni}^{Ga} A_{Ga} + f_{Ni}^{V} A_{V} \tag{5}$$

where f_{Ni}^{Ni}, f_{Ni}^{Ga} and f_{Ni}^{V} are the fraction of Ni-sublattice sites occupied by nickel and gallium atoms and vacancies respectively. The subscripts refer to the sublattice on which the species reside and the superscripts refer to the identity of the species. The factors A_{Ni}, A_{Ga} and A_{V} are the atomic weights of nickel and gallium atoms and vacancies respectively.

Similarly for the Ga-sublattice:

$$A_{GASITE} = f_{Ga}^{Ga} A_{Ga} + f_{Ga}^{Ni} A_{Ni} + f_{Ga}^{V} A_{V} \tag{6}$$

where the same nomenclature convention is used as before.

Now the site fractions occupied by the various species on the Ni-sublattice may be expressed in terms of the number of sublattice sites occupied by each species:

$$f_{Ni}^{Ni} = \frac{N_{Ni}^{Ni}}{N_{Ni}},\quad f_{Ni}^{Ga} = \frac{N_{Ni}^{Ga}}{N_{Ni}},\quad f_{Ni}^{V} = \frac{N_{Ni}^{V}}{N_{Ni}} \tag{7}$$

where N_{Ni}^{Ni}, N_{Ni}^{Ga} and N_{Ni}^{V} are the number of Ni-sublattice sites occupied by nickel and gallium atoms and vacancies respectively.

Again similarly for the Ga-sublattice:

$$f_{Ga}^{Ga} = \frac{N_{Ga}^{Ga}}{N_{Ga}}, \quad f_{Ga}^{Ni} = \frac{N_{Ga}^{Ni}}{N_{Ga}}, \quad f_{Ga}^{V} = \frac{N_{Ga}^{V}}{NG_a} \tag{8}$$

Substituting for N_{Ni} and N_{Ga} from equation 3 into equations 7 and 8 and then using the results in equations 5 and 6 gives:

$$A_{NISITE} = \frac{1}{0{\cdot}5N}\left[N_{Ni}^{Ni} A_{Ni} + N_{Ni}^{Ga} A_{Ga} + N_{Ni}^{V} A_{V}\right]$$

$$A_{GASITE} = \frac{1}{0{\cdot}5N}\left[N_{Ga}^{Ga} A_{Ga} + N_{Ga}^{Ni} A_{Ni} + N_{Ga}^{V} A_{V}\right] \tag{9}$$

Consider now the compound $Ni_{(x)}\ Ga_{(1-x)}$, where x is the atomic fraction of nickel.

(i) Let direct substitution be the consitutional defect model throughout the phase field such that no vacancies occur ($N_{Ni}^{V} = N_{Ga}^{V} = 0$). The general expressions of equation 9 become:

$$A_{NISITE} = \frac{1}{0{\cdot}5N}\left[N_{Ni}^{Ni} A_{Ni} + N_{Ni}^{Ga} A_{Ga}\right]$$

$$A_{GASITE} = \frac{1}{0{\cdot}5N}\left[N_{Ga}^{Ga} A_{Ga} + N_{Ga}^{Ni} A_{Ni}\right] \tag{10}$$

Now the atomic fraction of nickel (x) is defined by the expression

$$x = \frac{N_{Ni}^{Ni} + N_{Ga}^{Ni}}{N_{Ni}^{Ni} + N_{Ni}^{Ga} + N_{Ga}^{Ga} + N_{Ga}^{Ni}} = \frac{N_{Ni}^{Ni} + N_{Ga}^{Ni}}{N} \tag{11}$$

Similarly:

$$1-x = \frac{N_{Ga}^{Ga} + N_{Ni}^{Ga}}{N} \qquad (12)$$

Substituting from 11 and 12 into 10 gives:

$$A_{NISITE} = \frac{1}{0{\cdot}5N}\left[N_{Ni}^{Ni} A_{Ni} + (\overline{1-xN} - N_{Ga}^{Ga}) A_{Ga}\right]$$

$$A_{GASITE} = \frac{1}{0{\cdot}5N}\left[N_{Ga}^{Ga} A_{Ga} + (xN - N_{Ni}^{Ni}) A_{Ni}\right] \qquad (13)$$

Substituting from equation 13 into 4 and simplifying gives:

$$M_{NiGa} = \left[xA_{Ni} + (1-x) A_{Ga}\right] \qquad (14)$$

(ii) Consider the case of a direct vacancy mechanism such that no substitution occurs ($N_{Ga}^{Ni} = N_{Ni}^{Ga} = 0$). The general expressions of equation 9 become:

$$A_{NISITE} = \frac{1}{0{\cdot}5N}\left[N_{Ni}^{Ni} A_{Ni} + N_{Ni}^{V} A_{V}\right]$$

$$A_{GASITE} = \frac{1}{0{\cdot}5N}\left[N_{Ga}^{Ga} A_{Ga} + N_{Ga}^{V} A_{V}\right] \qquad (15)$$

As before:

$$x = \frac{N_{Ni}^{Ni}}{N_{Ni}^{Ni} + N_{Ga}^{Ga}} \qquad \therefore \; N_{Ga}^{Ni} = N_{Ni}^{Ga} = 0$$

and $$1-x = \frac{N_{Ga}^{Ga}}{N_{Ni}^{Ni} + N_{Ga}^{Ga}}$$

But

$$N_{Ni}^{Ni} + N_{Ga}^{Ga} = N - N_{Ni}^{V} - N_{Ga}^{V} \qquad (16)$$

Assuming that the two vacancy types cannot occur together in the same composition the equation 16 becomes:

$$\begin{aligned} N_{Ni}^{Ni} + N_{Ga}^{Ga} &= N - N_{Ni}^{V} \qquad x \leqslant 0{\cdot}5 \\ N_{Ni}^{Ni} + N_{Ga}^{Ga} &= N - N_{Ga}^{V} \qquad x \geqslant 0{\cdot}5 \end{aligned} \qquad (17)$$

Considering the case of $x \leqslant 0{\cdot}5$ and using the equations defining x gives:

$$N_{Ni}^{Ni} = \left(\frac{x}{1-x}\right) N_{Ga}^{Ga} \qquad (18)$$

But for $x \leqslant 0{\cdot}5 \qquad N_{Ga}^{Ga} = 0{\cdot}5N$

Substituting from 18 into 17 gives:

$$0{\cdot}5N \left[\left(\frac{x}{1-x}\right) + 1\right] = N - N_{Ni}^{V}$$

$$\therefore \qquad N_{Ni}^{V} = 0{\cdot}5N \left[1 - \left(\frac{x}{1-x}\right)\right] \qquad (19)$$

Substituting into 15 from 18 and 19 gives:

$$A_{NISITE} = \frac{1}{0{\cdot}5N} \left[0{\cdot}5N \left(\frac{x}{1-x}\right) A_{Ni} + 0{\cdot}5N \left(\frac{1-2x}{1-x}\right) A_{v}\right]$$

$$A_{GASITE} = \frac{1}{0{\cdot}5N} \left[0{\cdot}5N\, A_{Ga}\right] \qquad (20)$$

Because $N^{V}_{Ga} = 0$ for $x \leqslant 0{\cdot}5$.

But the atomic weight of a vacancy A_V is zero.

Substituting from equation 20 into 4 and simplifying gives:

$$M_{NiGa} = 0{\cdot}5\left[\left(\frac{x}{1-x}\right) A_{Ni} + A_{Ga}\right] \quad \text{for } x \leqslant 0{\cdot}5. \tag{21}$$

Similarly

$$M_{NiGa} = 0{\cdot}5\left[A_{Ni} + \left(\frac{1-x}{x}\right) A_{Ga}\right] \quad \text{for} \quad x \geqslant 0{\cdot}5 \tag{21}$$

Equations 14 and 21 define the change in the effective atomic weight per lattice site with composition (x). Hence from equation 1 the change in density with composition, for the case of direct substitution (equation 14) and for the case of the direct vacancy model (equation 21) can be evaluated.

(iii) Consider now the case where nickel vacancies and nickel anti-structure atoms are the only constitutional defects present (thus $N^{Ga}_{Ni} = N^{V}_{Ga} = 0$ for all compositions). The general relations of equation 9 become:

$$A_{NISITE} = \frac{1}{0{\cdot}5N}\left[N^{Ni}_{Ni} A_{Ni} + N^{V}_{Ni} A_{V}\right]$$

$$A_{GASITE} = \frac{1}{0{\cdot}5N}\left[N^{Ga}_{Ga} A_{Ga} + N^{Ni}_{Ga} A_{Ni}\right] \tag{22}$$

Consider now the compound $Ni_{(x)}Ga_{(1-x)}$ and let $X = x(> 0{\cdot}5)$ be some nickel rich composition which contains only nickel anti-structure atoms; the lattice is then entirely full.

Let N_{Ni}^{Ni} and N_{Ga}^{Ni} be constant for all $x \leqslant X$. Thus the number of nickel atoms on the Ni-sublattice and the number on the Ga-sublattice are fixed and compositions ($x < X$) are achieved by the introduction of equal numbers of vacant Ni-sublattice and gallium filled Ga-sublattice sites. Hence for a fixed number of nickel filled lattice sites the total number of all lattice sites increases with increasing gallium content.

Let the total number of lattice sites at $x = X$ be $N_{(X)}$ (equal to the sum $N_{Ni}^{Ni} + N_{Ga}^{Ni} + N_{Ga}^{Ga}$). From structure symmetry:

$$\begin{aligned} N_{Ni}^{Ni} + N_{Ni}^{V} &= 0{\cdot}5N_{(X)} \\ N_{Ga}^{Ga} + N_{Ga}^{Ni} &= 0{\cdot}5N_{(X)} \end{aligned} \tag{23}$$

But $N_{Ni}^{V} = 0$ from the definition of X. Then by definition:

$$x = \frac{N_{Ni}^{Ni} + N_{Ga}^{Ni}}{N_{Ni}^{Ni} + N_{Ga}^{Ni} + N_{Ga}^{Ga}} = \frac{N_{Ni}^{Ni} + N_{Ga}^{Ni}}{N_{(X)}} \tag{24}$$

Rearranging 24 and substituting from 23 gives for $x = X$:

$$\begin{aligned} N_{Ni}^{Ni} &= 0{\cdot}5N_{(X)} \\ N_{Ga}^{Ni} &= (2X-1)\ 0{\cdot}5N_{(X)} \\ N_{Ga}^{Ga} &= (1-X)\ N_{(X)} \end{aligned} \tag{25}$$

Consider now compositions $x < X$, thus $N_{Ni}^{V} \neq 0$. The total number of lattice sites $N_{(x)}$ containing the fixed number of sites occupied by nickel atoms has changed because new sites have been added in going from composition (X) to (x). Equation 23 now reads:

$$N_{Ni}^{Ni} + N_{Ni}^{V} = 0{\cdot}5N_{(x)}$$

$$N_{Ga}^{Ga} + N_{Ga}^{Ni} = 0{\cdot}5N_{(x)} \qquad (26)$$

But $$N_{Ni}^{Ni} + N_{Ga}^{Ni} = X\ N_{(X)} \qquad (27)$$

Substituting 27 into 24 and rearranging gives:

$$N_{Ga}^{Ga} = \left(\frac{1-x}{x}\right) X\ N_{(X)} \qquad (28)$$

Substituting 28 into 26 and rearranging gives:

$$N_{(x)} = \left(\frac{2X-x}{x}\right)\ N_{(X)} \qquad (29)$$

Using the results of 27, 28 and 29 and substituting into 26 gives:

$$N_{Ni}^{V} = \left(\frac{X-x}{x}\right)\ N_{(X)} \qquad (30)$$

Summarising:

$$N_{Ni}^{Ni} = 0{\cdot}5\ N_{(X)} \qquad \text{A}$$

$$N_{Ga}^{Ni} = (2X-1)\ 0{\cdot}5N_{(X)} \qquad \text{B}$$

$$N_{Ga}^{Ga} = \left(\frac{1-x}{x}\right) X\ N_{(X)} \qquad \text{C}$$

$$N_{Ni}^{V} = \left(\frac{X-x}{x}\right)\ N_{(X)} \qquad \text{D}$$

$$N_{(x)} = \left(\frac{2X-x}{x}\right)\ N_{(X)} \qquad \text{E}$$

Using equations A to D in equation 22 and putting A_V (the atomic weight of a vacancy) equal to zero gives:

$$A_{NISITE} = \frac{1}{0{\cdot}5N_{(x)}} \left[0{\cdot}5N_{(X)}\ A_{Ni}\right]$$

$$A_{GASITE} = \frac{1}{0{\cdot}5N_{(x)}} \left[\left(\frac{1-x}{x}\right) XN_{(X)}\ A_{Ga} + (2X-1)\ 0{\cdot}5N_{(X)}\ A_{Ni}\right]$$

Substituting for $N_{(x)}$ from E and simplifying gives:

$$A_{NISITE} = \left(\frac{x}{2X-x}\right) A_{Ni}$$

$$A_{GASITE} = \left(\frac{x}{2X-x}\right) \left[2X\left(\frac{1-x}{x}\right) A_{Ga} + (2X-1)\ A_{Ni}\right] \qquad (31)$$

Substituting 31 into 4 and simplifying gives:

$$M_{NiGa} = \left(\frac{X}{2X-x}\right) \left[x\ A_{Ni} + (1-x)\ A_{Ga}\right] \qquad (32)$$

It can be seen that equation 32 simplifies to the case of simple substitution (equation 14) at x = X, which is consistent with an original boundary condition of the model (that $N^V_{Ni} = 0$ at $x = X$).

Finally equation 32 can be used in conjunction with equation 1 to determine theoretical density values for given values of X. Note that only if X is equal to 0·5 is the condition that vacancies and anti-structure atoms do not occur simultaneously, observed.

Densities calculated for fixed values of X are plotted as a function of alloy composition in graph . It is assumed that the composition at which a given fixed X plot and the measured density coincide, the defect structure defined by the X plot is the one actually present at

the composition of coincidence. The Legrange method was then used to determine X as a function of the composition (x).

The defect fractions of nickel vacancies and antistructure atoms were then evaluated as a function of composition from equations B and D. The specific functions Z and $\emptyset$ defining the variation of the defect fractions with composition are thus known [see discussion: defect structure in NiGa] .

9. REFERENCES

1. P.E. Armstrong & H.L. Brown 1964 Trans. AIME, 230 p. 962
2. A. Ball 1969 Phil.Mag., 20, p. 113
3. A. Ball & R.E. Smallman 1966A Acta Met., 14, 11, p. 1349.
   1966B Acta Met., 14, 11, p. 1517
4. J. Bardeen & C. Herring 1951 Atom Movements. A.S.M. Cleveland
5. C.R. Barrett 1954 J. of Metals (Trans. AIME) p. 1003
6. C.R. Barret & W.D. Nix 1965 Acta Met., 13, 12, p. 1247
7. C.R. Barret & O.D. Sherby 1965 Trans. AIME, 233, p. 1116
8. A.E. Berkowitz, F.E. Jaumot & F.C. Nix 1954 Phys.Rev., 95, 5, p. 1185
9. D.N. Beshers 1965 ASM Conference, Gatlinburg, 9, p. 149
10. C.E. Birchenall & R.J. Borg 1960 Trans. AIME, 218, 982
11. C.E. Birchenall & R.F. Mehl 1947 Trans. AIME, 171, p. 143
12. A.J. Bradley 1951 J. Iron & Steel Inst., 168, 233
13. A.J. Bradley & A. Taylor 1937 Proc. Roy. Soc. (Lond.) A159, 56
14. W.L. Bragg & E.J. Williams 1935 Proc.Roy.Soc.(Lond.) A151, 540
15. N. Brown 1968 ASM Trans.Quart., 61, 4, p. 700
16. N. Brown & D.R. Lenton 1969 Acta Met., 17, 5, p. 669
17. F.S. Buffington, K. Hirano & M. Cohen 1961 Acta Met., 9, p. 434
18. S.R. Butler, J.E. Hanlon & R.J. Wasilewski 1969 J.Phys.Chem.Solids, 30, p. 1929
19. S. Chandrasekhar 1943 Rev.Mod.Phys., 15, 63
20. K. Compaan & Y. Haven 1956 Trans.Farad.Soc., 52, 6, p. 786
21. K. Compaan & Y. Haven 1957 Disc.Farad.Soc., 23, p. 105
22. H. Conrad 1964 J. Metals, p. 582
23. M.J. Cooper 1963A Phil.Mag., 8, p. 805
    1963B Ibid p. 811
24. A.H. Cottrell 1953 'Dislocations & Plastic Flow in Crystals' Oxford Univ. Press

25. A.H. Cottrell 1958 Trans. AIME 212 p. 192

26. J. Cost 1964 Reported by Domian & Aaronson, Trans. AIME 1964 230, 1, p.44

27. J. Crank 1956 'Mathematics of Diffusion' Oxford Univ. Press, New York

28. J. Crank 1957 Disc.Farad.Soc., 23, p. 99

29. L.D. Darken 1948 Trans. AIME, 175, p. 184

30. R.G. Davies 1963 Trans. AIME, 227, p. 227
Ibid p. 665
Ibid p. 22

31. P. Delavignette, H. Richel & S. Amelinckx 1972 Phys.Stat.Sol. (a) 13, 2, p. 545

32. G.J. Dienes 1953 Phys.Rev. (ii) 89, 1, p. 185

33. H.A. Domian & H.I. Aaronson 1964 Trans AIME, 230, 1, p. 44

34. H.A. Domian & H.I. Aaronson 1965 ASM Conf. Gatlinburg, 14, p. 209

35. J.E. Dorn 1957 ASM Conf. Cleveland, p. 255

36. J.E. Dorn 1961 'Mechanical Behaviour of Materials at High Temperatures' McGraw-Hill

37. J.E. Dorn & J.B. Mitchell 1967 'Recent Prog. in App. Mechanics' Ed. B. Borberg, J. Hult & F. Niordson

38. F. Einsen & C.E. Birchenall 1957 Acta Met., 5, p. 265

39. E.W. Elcock 1959 Proc.Phys.Soc., 73, p. 250

40. E.W. Elcock & C.N. McCombie 1958 Phys.Rev. (ii) 109, 2, p. 605

41. M. Ettenberg, K.L. Komarek & E. Miller 1969 AIME 3rd Bolton Landing Conf.

42. A.G. Evans 1967 Ph.D. Thesis, Imperial College, London

43. P. Feltham & J.D. Meakin 1959 Acta Met., 7, p. 614

44. P. Feltham & T. Myers 1963 Phil.Mag., 8, p. 203

45. A. Fick 1885 Poggendorf's Annalen, 94, p. 59

46. J.C. Fisher, R.E. Hoffman 1950 U.S. Atomic Energy Commission Rep., S.O. 2001, p. 6

47. P.A. Flinn 1960 Trans. AIME, 218, 145.

48. P.A. Flinn & G.M. McManus 1961 Phys.Rev., 124, p. 54

49. J. Friedel 1957 'Dislocations & Mech. Props. of Solids', Pub.: Wiley, N.Y.

50. F. Garofalo 1963 Trans. AIME, 227, p. 351

51. F. Garofalo 1965 Fundamentals of Creep and Creep Rupture in Metals, Pub.: Macmillan

52. F. Garofalo 1968 See F. Garofalo 1965

53. F. Garofalo, W. Domis & F. Gemmingen 1964 Trans. AIME, 230, p 1460

54. J.J. Gilman & W.G. Johnston 1962 Solid State Physics, 13, p. 147

55. L.A. Girifalco 1964 J.Phys.Chem. Solids, 25, 323

55A. A. Gittins & R.C. Gifkins 1968 Acta Met., 16, 1, p. 81

56. D. Gupta 1961 Ph.D. Thesis, Univ. Illinois

57. D. Gupta, D. Lazarus & D.S. Lieberman 1967 Phys.Rev., 153, 3, p. 863

58. D. Gupta & D.S. Lieberman 1969 AIME 3rd Bolton Landing Conf.

59. L.N. Guseva 1951 Doklady Akad.Nauk.SSSR, 73, 3, p. 415

60. W.C. Hagel 1963 GEC Lab.Rep. No. 63-RL-3320 M

61. W.C. Hagel & J.H. Westbrook 1961 Trans.AIME, 221, p. 951

62. W.C. Hagel & J.H. Westbrook 1964 ASM Conf. Gatlinburg, 13, p. 197

63. C.A. Hampel 1964 'Encyclopedia of Electrochemistry' Pub: Chapman Hall, Lond.

64. G.F. Hancock 1971 Phys.Stat.Sol. (a) 7, p. 535

65. G.F. Hancock & B.R. McDonnell 1971 Phys.Stat.Sol. (a) 4, 1, p. 143

66. M. Hansen 1958 'Constitution of Binary Alloys' McGraw-Hill

67. E. Hellner 1950 Z.Metallkunde 41, 12, p. 480

68. E. Hellner & F. Laves 1947 Z.Naturforsch. A 2, 3, p. 177

69. M. Herman & N. Brown 1965 Trans. AIME, 206, p. 604

70. C. Herring 1950 J.App.Phys., 21, p. 437

71. P.B. Hirsch 1962 Conf.Proceedings 'Radiation Damage to Solids' Academic Press, N.Y.

72. L.A. Hocking, P.R. Strutt & R.A. Dodd 1971 J.Inst.Met., 99, p. 98

73. J.A. Hren & O.D. Sherby 1965 App. Materials Research, 4, p. 41

74. S.M. Hu 1970 Scripta Met., 4, 7, p. 513

75. T. Hughes, E.P. Lautenschlager, J.B. Cohen & J.O. Brittain 1971 J.App.Phys., 42, 10, p. 3705

76. D. Hull 1968 'Introduction to Dislocations' Pergamon Press

77. W. Hume-Rothery & G.V. Raynor 1962 Institute of Metals: 'The Structure of Metals and Alloys'

78. H.B. Huntington, N.C. Miller & V. Nerses 1961 Acta Met., 9, 8, p. 749

79. H.B. Huntington, G.A. Shirn & E.S. Wajda 1955 Phys.Rev., 99, p. 1085

80. N. Jaffe & J.E. Dorn 1962 Trans AIME, 224, p. 1167

81. T.L. Johnston, R.G. Davies & N.S. Stoloff 1965 Phil.Mag., 12

82. W.R. Kanne, P.R. Strutt & R.A. Dodd 1969 Trans AIME, 245, 6, p. 1259

83. R. Kikuchi 1960 Analytical Phys., 11, p. 306

84. R. Kikuchi 1961A J.Phys.Chem.Solids, 20, 17

85. R. Kikuchi 1961B J.Phys.Chem.Solids, 20, 35

86. R. Kikuchi & H. Sato 1969 J.Chem.Phys., 51, 1, p. 161

87. R. Kikuchi & H. Sato 1972 J.Chem.Phys., 57, 11, p. 4962

88. Kirk-Othmer Encyclopedia of Chemical Technology, 10, p. 315

89. D. Klahn, A.K. Mukherjee & J.E. Dorn 1970 ASM Conf. Pacific Grounds 'Strength of Metals & Alloys'

90. I.I. Kornilov 1960 Mechanical Properties of Intermetallic Compounds Ed: Wiley, N.Y.

91. I.I. Kornilov, A. Ya Shinayev & Ye.N. Pyloyev 1963 Izvest Akad. Nauk. SSSR Russian Metallurgy & Mining No. 5, p. 67

92. Y.G. Koylu, G.F. Hancock & R.D. Rawlings 1973 Phys.Stat.Sol. (a) 16, p. 73

93. F.A. Kröger & H.J. Vink 1956 Solid State Phys., 3, p. 310

94. L.A. Kucherenko & V.A. Troshkina 1971 Izvest Akad. Nauk. SSSR Metally, 1, p. 170

95. A.B. Kuper, D. Lazarus, J.B. Manning & C.T. Tomizuka 1956 Phys. Rev., 104, p. 1536

96. A. Lawley, J.A. Coll & R.W. Cahn 1960 Trans. AIME, 218, p. 166

97. D. Lazarus, 1960 Solid State Phys., 10, p. 71

98. D. Lazarus, 1962 Energetic, 1, p. 1

99. D. Lazarus, 1965 ASM Conf. Gatlinburg, 10, p. 155

100. A.D. LeClaire 1949 Prog. in Metal Phys., 1, p. 306

101. A.D. LeClaire 1953 Acta Met., 1, 4, p. 438

102. A.D. LeClaire 1953 Prog. in Metal Phys., 4, p. 265

103. A.D. LeClaire 1965 ASM Conf. Gatlinburg, 1, p. 3.

104. H. Lipson & A. Taylor 1939 Proc.Roy.Soc., A173, p. 232

105. B.R. McDonnell 1969 Ph.D. Thesis, Imperial College, London

106. B.R. McDonnell, R.T. Pascoe, G.F. Hancock & C.W.A. Newey 1967 J.Mat.Sci., 2, p. 365

107. H.J. McQueen 1968 J. Metals, 20, 31

108. W. Mahler 1950 Reported by Schubert et al., 1959 Z.Metalkunde, 50, p. 534

109. J.R. Manning 1958 Phys.Rev. Letters, 1 , p. 365

110. M.J. Marcinkowski, N. Brown & R.M. Fisher 1961 Acta Met., 9, p. 129

111. M.J. Marcinkowski & D.E. Campbell 1969 AIME 3rd Bolton Landing Conf., Ch. 26, p. 331

112. A.K. Mukherjee, J.E. Bird & J.E. Dorn 1968 Univ.of Calif.Lab.Report UCRL 18526

113. A.K. Mukherjee, J.E. Bird & J.E. Dorn 1969 ASM, 62, p. 155

114. A.K.Mukherjee & J.E. Dorn 1963 Univ.of Calif.Lab.Report UCRL 10916

115. A.K. Mukherjee & J.E. Dorn 1964 Trans. AIME, 230, 5, p. 1065

116. A.K. Mukherjee & J.E. Dorn 1965 J.Inst.Met., 93, 11, p. 397

117. A.K. Mukherjee, W.G. Ferguson, W.L. Barmore & J.E. Dorn 1965 Univ.Calif.Lab.Report, UCRL 16433

118. A.K. Mukherjee, D.S. Lieberman & T.A. Read 1965 J.App.Phys., 36, p. 857

119. F.R.N. Nabarro 1948 Conf.Proc. 'Strength of Solids', Physical Soc., p. 75

120. N. Nakanishi, K.M. Thein & C.M. Wayman 1963 J.App.Sci., 34, 9, p. 2847

121. J.C. Norvell & J. Als-Nielsen 1970 Phys.Rev. B Solid State, 2, 2, p. 277

122. W.B. Pearson 1958 Handbook of Lattice Spacings & Structure of Metals, Pergamon Press

123. G.M. Pound, W.R. Bittler & H.W. Paxton 1961 Phil.Mag., 6, p. 473

124. S. Prussin 1969 Scripta Met., 3, p. 827
1970 Scripta Met., 4, 7, p. 515

125. R.E. Reed-Hill 1967 'Physical Metallurgy Principles', Pub: Van Nostrand

126. A. Seeger 1957 'Dislocations & Mechanical Properties of Crystals', Pub: Wiley

127. A. Seeger, G. Schottky & D. Schumacher 1965 Phys.Stat.Sol., 11, 1, p. 363

128. A.U. Seybolt 1964 J.Electro.Chem.Soc., 11, p. 671

129. A.U. Seybolt & J.H. Westbrook 1964 Acta Met., 12, p. 449

130. O.D. Sherby & P.M. Burke 1967 Prog. in Mat. Sci., 13, 7, p. 325

131. A. Ya Shinayev 1961 Inst. of Met. in Baykova, Akad.Nauk., SSSR

132. A.W. Smith & R.D. Rawlings 1974 Phys.Stat.Sol.

133. A.J.R. Soler-Gomez & W.J. McG. Tegart 1964 Acta Met., 12, p. 961

134. N.S. Stolóff & R.G. Davies 1966 Prog. in Mat.Sci., 13, 1, p. 3

135. P.R. Strutt & R.A. Dodd 1969 AIME 3rd Bolton Landing Conf., 34, p. 475

136. P.R. Strutt, R.A. Dodd & G.M. Rowe 1970 ASM Conf. Pacific Grounds, 3, p. 1057

137. P.R. Strutt, G.M. Rowe, J.C. Ingram & Y.H. Choo 1972 Proc. of 5th Int.Mat.Conf., UCLA, Ed: G. Thomas, p. 722

138. G.P. Tiwari & B.D. Sharma 1967 Acta Met. 15, p. 155

139. G.P. Tiwari & B.D. Sharma 1967 Scripta Met., 1, p. 131

140. R.R. Vandervoort, A.K. Mukherjee 1966 ASM Trans. Quart., 59, 4, p. 930

141. G.H. Von Frischat & H.J. Ogel 1966 Zeitschrift fur angewandte Physik, XX Band, Heft 3.

142. R.J. Wasilewski 1966 Trans. AIME, 236, p. 455

143. R.J. Wasilewski 1968A J.Phys.Chem.Solids, 29, p. 39

144. R.J. Wasilewski 1968B J.Phys.Chem.Solids, 29, p. 51

145. R.J. Wasilewski, S.R. Butler & J.E. Hanlon 1968 J.App.Phys., 39, 9, p. 4234

146. C.M. Wayman, K.M. Thein & N. Nakanishi 1963 J.App.Sci., 34, 9, p. 2842

147. G.A. Webster & B.J. Piearcey 1967 Met.Sci.J., 1, p. 97

148. M.S. Wechsler 1957 Acta Met., 5, 3, p. 150

149. J. Weertman 1957 J.App.Phys., 28, p. 362

Ibid p. 1185

150. J. Weertman 1968 ASM Trans.Quart., 61, 4, p. 681

151. J. Weertman & P. Shahinian 1956 Trans AIME, 206, 1123

152. C. Wert 1950 Phys.Rev., 79, p. 601

152. C. Wert & C. Zener 1949 Phys.Rev., 76, p. 1169

154. J.H. Westbrook 1969 AIME 3rd Bolton Landing Conf., 1, 1

155. A. Westgren & A. Almin 1929 Z.phys.chem., B, 5, 14

156. B.A. Wilcox & A.H. Clauer 1966 Trans.AIME, 236, p. 570

157. R.O. Williams 1957 Acta Met., 5, p. 55

158. P. Wynblatt 1967 Acta Met., 15, p. 1453

159. W. Yang & R.A. Dodd 1973 Met.Sci.J., 7, p. 41

160. C. Zener 1950 Acta Cryst., 3, p. 346

161. C. Zener 1951 J.App.Phys., 22, p. 372

162. C. Zener 1952 'Imperfections in Nearly Perfect Crystals'
Pub: Wiley, N. York

Addenda

163. J. Snoek 1939 Jour.Physica, 6, p. 591

164. S.G. Fishman, D. Gupta & D.S. Lieberman 1970 Phys.Rev.B, 2, 6
P. 1451